UNIVERSITY OF NOTTINGHAM
Department of Electrical and Electronic Engineering

Modeling of Rotor Defects in Squirrel Cage Induction Motors Using the Time stepping Numerical Field Analysis

by

Abdelkader TAMI,
Ingenieur d'Etat, M.Sc.

Thesis submitted to the University of Nottingham

for the Degree of Doctor of Philosophy,

December 1995

ABSTRACT

The arrival of cheap and fast microcomputers has stimulated the development of machine condition monitoring systems. Such systems measure one or more machine performance parameters, with a view to detecting the early signs of failure and initiating some form of action. To help developing these systems, a thorough knowledge of the behaviour of the machine in its post-fault condition must be well known and well understood. With this view in mind, a simple, yet reasonably accurate method of analysing the induction machine magnetic circuit under normal and abnormal conditions at moderate cost has been developed.

Numerical field analysis is applied to the calculation of induction motors. It is based on a very simple Magnetic Network Technique (MNT) solution of the magnetic field. The field is assumed to be two-dimensional. The three-dimensionality of the machine is taken into account within the two-dimensional model. The general time-dependence of the field and the motion of the rotor are modelled correctly in a step-by-step solution. The model uses relatively small amount of computation time when compared with the previous methods of analysis. This technique is used for the evaluation of the broken bars effects on the machines performance and magnetic field variation. A series of experimental tests have been carried out. The results obtained are directly compared with the computed ones and they showed a good correlation. Finally, suggestions for suitable methods for the detection of broken bars are given along with some suggestions for future work.

ACKNOWLEDGEMENT

The author wishes to express his sincere gratitude to Dr. K.J. Bradley for his advice, encouragement and helpful discussions throughout this course.

Thanks are also due to the staff of the machines and drives laboratory of the Department of Electrical and Electronics Engineering, who have given their assistance in the experimental part of this work.

The author is also indebted to the Algerian Higher Ministry of Education for their financial support.

Finally, my deepest thanks and sincere gratitude go to my wife for her help, encouragement, limitless patience and understanding, to my beloved sons Aimene and Anas, and my daughters Sarah and Bushra.

TABLE OF CONTENT

LIST OF SYMBOLS

a	number of parallel paths
B	flux density
β	overlap angles
D	damping moment
f	supply frequency
F_b	branch mmfs
F_n	nodal mmfs
H	magnetic field strength
I_s	Stator current per phase (r.m.s.)
I_r	Rotor current per phase (r.m.s.)
I_0	No-load current per phase (r.m.s.)
I_m	Magnetising current per phase (r.m.s.)
i_a, i_b , i_c	instantaneous stator phase currents
i_A, i_B, i_C	instantaneous rotor phase currents
J	current density
J_m	total moment of inertia
K_g	Carter's factor
K_{ws}	stator winding factor
K_{wr}	rotor winding factor
L	inductance

L_{inc}	incremental inductance
L_{cs}	stator core element length
L_{cr}	rotor core element length
L_{st}	stator tooth length
L_{rt}	rotor tooth length
L_{stt}	stator tooth-tip length
L_{rtt}	rotor tooth-tip length
L_g	airgap length
L_s	stator stack length
L_r	rotor stack length
m_s	number of stator phases
m_r	number of rotor phases
μ_{cs}	stator back iron permeability
μ_{cr}	rotor back iron permeability
μ_{ts}	stator tooth permeability
μ_{tr}	rotor tooth permeability
μ_{stt}	stator tooth-tip permeability
μ_{rtt}	rotor tooth-tip permeability
NCPS1	number of conductors per stator slot
NCPR1	number of conductors per rotor slot
N_s	number of stator slots
N_r	number of rotor slots

N_T	number of turns in series in a coil
P	number of pole pairs
q	number of slots per pole per phase
$R_2^{'}$	rotor resistance referred to the stator
R_1	stator winding resistance per phase
R_2	rotor winding resistance per phase
R_b	equivalent rotor bar resistance
R_a	airgap mean radius
RSO	rotor slot opening
SSO	stator slot opening
T_{av}	steady state average torque
T_e	electromagnetic torque
T_m	load torque
T_{cog}	cogging torque
T_{max}	maximum torque
T_{min}	minimum torque
$\omega_r t$	rotor position
v_a, v_b, v_c	stator instantaneous voltages
v_A, v_B, v_C	rotor instantaneous voltages
W_m	stored magnetic energy
W_{cs}	stator core element width

W_{cr}	rotor core element width
W_{ts}	stator tooth width
W_{tr}	rotor tooth width
W_{stt}	stator tooth-tip width
W_{rtt}	rotor tooth-tip width
ω_r	rotor angular frequency
ω_s	supply angular frequency
ω_f	field angular frequency
λ_s	stator slot pitch
λ_r	rotor slot pitch
Λ_s	total stator slot permeance
Λ_r	total rotor slot permeance
Λ_{sc}	stator core element permeance
Λ_{rc}	rotor core element permeance
Λ_{r1}	rotor slot body permeance
Λ_{r2}	rotor slot opening permeance
Λ_{s1}	stator slot body permeance
Λ_{s2}	stator slot opening permeance
Λ_{st}	stator tooth permeance
Λ_{rt}	rotor tooth permeance

Λ_{stt}	stator tooth-tip permeance
Λ_{rtt}	rotor tooth-tip permeance
Λ_{rso}	equivalent permeance of Λ_{r2} in parallel with Λ_{rtt}, Λ_{r1} and Λ_{rtt}
Λ_{sso}	equivalent permeance of Λ_{s2} in parallel with Λ_{stt}, Λ_{s1} and Λ_{stt}

CHAPTER ONE

INTRODUCTION

1. INTRODUCTION

1.1 BACKGROUND

Squirrel-cage induction motors are the most commonly used of electrical machines. They are robust, reliable and they are of a simple technology. With the advances in power converter technology and control, induction machines are also finding increasing use in variable speed drives. Squirrel-cage rotors for low volume production are often manufactured with copper rotor bars and endrings, while machines for mass production are die-cast. Both forms of construction are subject to winding failure on occasion.

For many years, the manufacturers of induction motors have been optimising the design of the squirrel cage rotor to achieve the highest reliability. This process has become more important in recent years because of the use, by industry, of motors with much higher ratings in a given frame size.

As with other electrical machines, induction motor behaviour is governed by the electromagnetic fields within them. The fields obey Maxwell's equations. Thus, in order to be able to predict performance characteristics, it is necessary in the design of the machine to solve in some way Maxwell equations governing the fields. The differential form (or integral as appropriate) of Maxwell's equations has traditionally made electromagnetics a heavily mathematically oriented discipline. Machine design has traditionally reduced

the complex mathematics to a much simpler form by means of equivalent circuits and examination of parts of the field problem at a time.

Before the advent of the computer, recourse to elaborate mathematics had to be made to solve some of the equations of electromagnetics, using such solution concepts as series expansions, separation of variables, Legendre Polynomials...etc. By these methods, the solution of the electromagnetic field inside an electrical machine under design is a lengthy and laborious process. Indeed it is frequently the case that no close form solution is possible without making drastic simplifying assumptions as to the machines geometry, current distribution, the nonlinearity due to saturation in the iron core and so on. As a consequence of these assumptions, the ensuing solution is not completely reliable but is engineered to provide sufficient accuracy in most cases.

The first part of this chapter is concerned with examining the aspects of machine design and construction which would need to be incorporated into a full model of the operation of the induction machines. Some of the causes of rotor asymmetries and their effects are discussed. A comparison between the existing analytical techniques is then described. In the light of this information the problem to be tackled in this thesis is outlined. Chapter two is devoted to an examination of published work and the contributions of other researchers in this field. In the following two chapters, the method of analysis and logic of

computation are described. In chapter five the validity of the model is proved through comparison of prediction with experimental results taken on a specially designed test motor. Next, in chapter six, the application of the model to the simulation of the problem of broken rotor bars is demonstrated. Finally, in chapter 7, general conclusion are made with some suggestions for further work to be carried out.

1.2 FACTORS INFLUENCING MACHINES PERFORMANCE

When studying the performance of an electrical machine it is very important to take into consideration the effect of slot-openings, relative movement of stator and rotor, slot combinations, saturation, winding arrangement, electromagnetic asymmetry and skew effect since they are the source of many undesirable phenomena during starting and running conditions. In particular, determination of losses, torque pulsations, current and voltage waveforms and noise are all dependent on these features of design. The performance of an induction machine may be determined accurately only if all the machine parameters are known at all instances during its operation.

1.2.1 SATURATION

It is often assumed that the airgap so predominates in a magnetic circuit as to absorb the whole mmf, implying that the ferromagnetic parts have infinite permeability: this is not true. It might be alternatively assumed that the airgap

absorbs a constant fraction of the total mmf. This again is not true, for the permeability μ of ferromagnetic materials varies with the flux density B. However, μ differs for individual specimens of the same ferromagnetic material, and varies even from point to point within a given specimen.

The actual magnetic conditions in a circuit as a whole are exceedingly complex. The waveform shape of flux density as a function of time and space is usually distorted by magnetic saturation of the teeth and core of both stator and rotor. Generally, tooth saturation leads to a flattened curve with a consequent introduction of additional flux harmonics known as "saturation harmonics", while core saturation leads to peaked curve.

The effect of saturation is a function of the working flux density, the magnetisation characteristic of the magnetic material and the machine configuration [17].

About the best that can be done is to construct for a given iron-air magnetic circuit, by careful estimate or by test, a relation between the total flux Φ and the total mmf F, for which Figure 1.1 is a typical result; Φ is proportional to F for low mmf and the relation follows the air line because the airgap reluctance is predominant. For higher mmfs the iron saturation makes increasing

demands and the initial proportionality fails. The per unit inductance, $L = \Phi/F$, is seen to fall markedly at higher excitations.

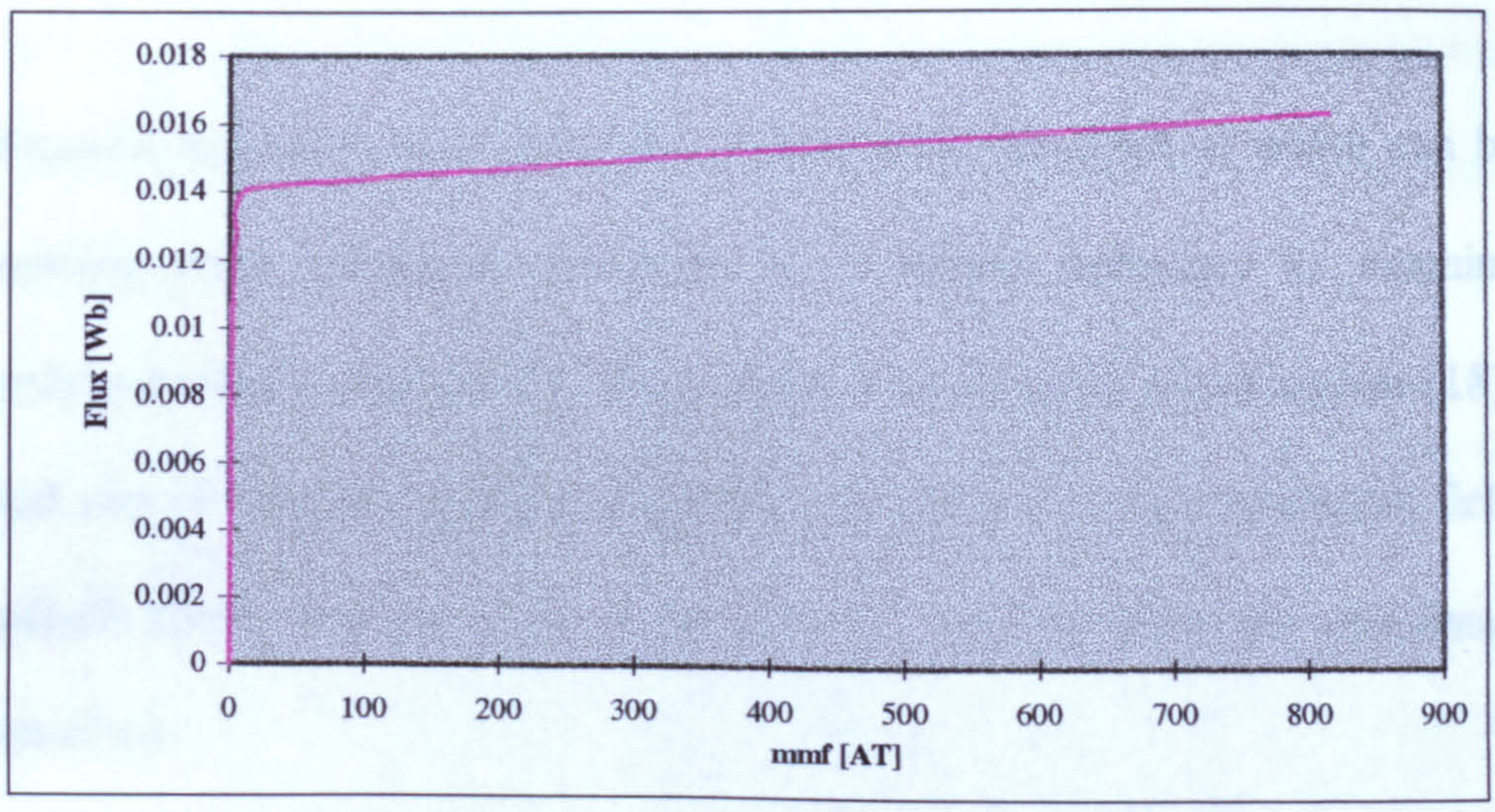

***Figure 1.1** Flux-MMF curve*

Saturation has a considerable effect on both magnetising and leakage inductance coefficients. When the inductance is also a function of the position angle Θ_r, which is the case for the induction machine with small airgaps, the analysis becomes very difficult.

The measurement of the inductance of a machine winding must be taken under current conditions corresponding to those in which analysis is to be applied; otherwise there may be gross resulting errors. This is one of the chief reasons why very poor correlation is sometimes found between machine analysis and practical test. To overcome this problem, one practical method is

to separate the variations of L with i and with Θ_r by considering

$\frac{\partial L}{\partial i}$ and $\frac{\partial L}{\partial \Theta_r}$ independently.

Magnetic saturation is an awkward non-linearity, the effect of which can be anything from trifling to dominant. It is always necessary to examine analytical results critically for the possible consequences of saturation [18]. And one of the most powerful analytical methods is to use numerical field analysis (finite element or finite difference,... etc.) to solve the non-linear equations.

1.2.2 SLOT OPENINGS

The use in electrical machines of cores with slots to put the coils of a distributed winding in is a practice of such a general application that it might lead to the misunderstanding that slots are natural and even essential elements of a magnetic circuit with iron. However, the slots can do much harm to many aspects of machine performance, especially if there are two slotted surfaces along the airgap, as is the case in induction machines. There is abundance of literature reporting on annoying harmonics in voltages and currents, on parasitic losses affecting the conversion efficiency and the machine temperature, on parasitic torques causing cogging effects (at standstill) and crawling effects (at low speed), on bearing currents, on radial and torsional

vibrations, on noise problems, and a common cause of all these phenomena is the slotted core [81].

The introduction of slots in the magnetic cores of electrical machines and of the distributed windings put into these slots, has two distinct electromagnetic consequences:

1) the iron surface along the airgap is no longer smooth, but interrupted by zones of high reluctance;

2) the magnetomotive force (m.m.f.) across the airgap is not changing smoothly but instead in a step-wise mode.

The airgap flux varies spacially as a consequence of the non-uniform airgap permenance. These regular variations produce harmonic components called tooth or slot harmonics. Slot harmonics occur at frequencies set by the spacing between adjacent slots and are given by:

$$\nu_k = K \cdot \frac{N_s}{P} \pm 1 \qquad (1.1)$$

where ν_k : number of harmonic component

N_s : number of stator slot

P : number of pole pairs

K : an integer

K = 1 yields the lowest frequency slot harmonics, which are also the most troublesome ones.

Since these harmonic components are set by the spacing between adjacent coil slots, variations in coil pitch and distribution cannot reduce their effects. Regardless of a coil's pitch, it must begin and end in a slot, and therefore the coil's spacing is an integral multiple of the basic spacing causing slot harmonics in the first place.

Slot effects are often harmful in more than one respect and a universal remedy may not exist; then a compromise on the basis of priority is necessary. Two of the design choices limiting slotting effects in the induction machine are the choice of the number of rotor slot and the skew of the rotor conductors [19].

1.2.3 SKEW

For almost the whole history of electrical machines, skewing of slots has been used to mitigate harmful slot effects, and has often been applied, though not always with success [81]. Skew is an imperfect solution, because it does not take away the cause, and its use may involve the introduction of additional annoying effects. For each case the positive and the negative factors should be weighed against each other.

Skewing affects the stray load and no-load losses, it creates additional flux components, which are loss producing and leads to an increase in leakage reactance. It also causes a loss of efficiency particularly when rotor-bar insulation is absent. Slots are skewed to reduce the cogging tendency and synchronous and asynchronous harmonic torques [19], this remedy increases the magnetic saturation of the machines [20]. Skew gives rise to changes in the field distribution for 3 reasons:

1) The stator and rotor mmfs have a phase difference varying along the axial length. Hence the resultant airgap mmf is a function of the axial length.

2) The permeance of the magnetic circuit changes along the axis, owing to the variation in the relative position of stator and rotor teeth.

3) The axial flux produced by the peripheral component of the rotor current strengthens the main flux under a pole on one end of the core and weakens it at the other end, leading to an axial variation of flux. This effect increases with increasing rotor current. On the other hand, there is a gradual change of phase in the inductance variation as one moves axially along the airgap.

Another advantage claimed for skewing is reducing the vibration and noise levels. This is because skewing either the stator or the rotor slots would make

the radial forces acting on one stator lamination at a given axial position different from the forces acting on the other core laminations situated at other axial positions [82].

1.2.4 WINDING ARRANGEMENT

The magnetic flux is dependent upon the winding arrangement of both stator and rotor. The distributed winding fed with a perfect sinusoidal current produces space harmonics in the mmf waveform of the airgap. The use of a 5/6 pitch winding is sometimes recommended to minimise these harmonics.

Larger machines, particularly those of the medium-voltage type, often cannot be designed but with a larger number of parallel paths. Although with machines having several parallel paths stress is laid on an absolute symmetry of the individual paths, a certain asymmetry may always occur in the manufacture and cause a non-uniform current distribution and thus a generation of higher magnetomotive force harmonics [21].

1.3 ROTOR FAILURE CAUSES AND CONSEQUENCES

In addition to those factors discussed above, and despite the optimum design, from time to time, damage can occur in a rotor cage which progressively worsens and may lead eventually to catastrophic failure of the machine. As a result, the failure of induction machines has become a significant problem in large industrial drives particularly those used in continuous process industries.

The desire to improve the reliability of industrial drive systems has led to concerted research activity of investigating the causes and consequences of rotor bar failure and to the development of diagnostic techniques monitoring the stator current, vibration, leakage flux and/or the rotor speed of a machine to detect failure.

In order to be able to develop diagnostic techniques which differentiate between normal and abnormal conditions, a thorough understanding of the electric and electromagnetic behaviour of the machine under normal and in post-fault conditions is required. In the following sections some of the causes that can lead to a rotor failure and the consequences of these faults are examined.

1.3.1 CAUSES

The majority of rotor failures are caused by a combination of various stresses which act on the rotor. Some of these stresses can be minimised during design, manufacturing and testing followed by correct installation and commissioning. But this necessitates expertise and resources in a wide variety of fields, including electromagnetic analysis, mechanical design, insulation, ventilation, thermal performance...etc. Satisfactory service will then depend on the implementation of appropriate operational routines and maintenance procedures.

In general terms, the most important stresses can be classified as follows

[1, 2, 3 , 4]:

i. Thermal stresses.

ii. Electromagnetic stresses.

iii. Environmental stresses.

iv. mechanical stresses.

1.3.1.1 THERMAL STRESSES

These stresses are mainly due to three factors which are:

1) thermal overload.

2) thermal unbalance.

3) rotor sparking.

1) THERMAL OVERLOAD

The thermal overload can occur under all conditions be it acceleration, running or stalling. From a thermal standpoint, some motors are stator-limited whereas others are rotor limited. While running at full load speeds, most motors are stator-limited. The stall condition has the greatest potential for rotor damage in the shortest time period. As most thermal sensing devices are installed in the stator, by the time they sense the heat generated in the rotor, it is too late.

The most common causes of thermal overload failures are:

i. Abnormal number of consecutive starts causing excessive temperature to bar or endring.

ii. Locked rotor stalling due to high breakaway loading.

iii. Failure to accelerate to full speed due to intersect between the load and motor speed-torque curve caused by overloading.

iv. Rotor rubbing the stator probably due to bearing failure.

v. Unbalanced phase voltages and corresponding negative sequence currents with associated rotor surface heating.

2) THERMAL UNBALANCE

Thermal unbalances can arise from either starting or running conditions.

The most common causes of thermal unbalance failures are:

i. Frequent starts causing temperature differential in the rotor bars due to the skin effect.

ii. Unequal heat transfer between the rotor bars and rotor core.

3) ROTOR SPARKING

In the case of rotor sparking, not all cases are of a destructive nature. This depends on whether the motor is under starting or normal operating conditions. At full load speed sparking is not usually observed for two reasons: first, centrifugal force at full load speed is greater than the electromagnetic force acting on the bar keeping the bar in permanent contact

with the rotor core. Secondly, the rotor frequency is very low resulting in a low impedance rotor cage circuit thus confining all rotor current to the cage itself.

However, at starting, the current in the rotor cage is 5 to 6 times normal. This high current combines with high cage impedance will cause a voltage drop along the length of the bar in excess of 6 times the normal running value. It is this voltage that tends to send current through the lamination. During start-up, there are actually two parallel circuits: one through rotor bar and another through laminations. The magnetic forces created by the high current flow during start-up cause the rotor bars to vibrate at a decaying frequency, which produces a vibration of twice that frequency. This radial vibration causes intermittent interruptions of the current flow between the bars and various portions of the laminations with resultant visible arcing. The sparks observed in the airgap are actually very small particles of bar and/or core iron, heated to incandescence by current passing through the iron-bar boundary.

1.3.1.2 MAGNETIC STRESSES

The action of the slot linkage flux, resulting from bar current, generates electrodynamic forces. They are proportional to I^2 and are unidirectional. They tend to displace the bar radially towards the bottom of the slot. These forces vibrate the bar at twice the rotor current frequency. Hence, they

produce deflection or a bending stress in the bar if it is not adequately wedged into the slot. If the deflection is high enough, a fatigue failure in the bar will result.

1.3.1.3 ENVIRONMENTAL STRESSES

Environmental stresses can be defined as any other condition which affects the life of the rotor. Such stresses are chemicals or moisture which could attack and breakdown the basic rotor materials. Alternatively they may be foreign materials which can cause abrasion or clog the ventilation paths.

1.3.1.4 MECHANICAL STRESSES

Rotor-cage faults may arise during manufacture. This may be due to defective casting in the case of die-cast rotors, or poor jointing in the case of brased or welded endrings. Generally, such faults can be detected before installation [5], and an appropriate remedial action taken.

Faults may develop in rotors where the rotor bars are the sole means of support for the endrings. Here the bars must provide the braking and accelerating forces on the endring when the motor changes speed. If the motor speed fluctuates because of changing load, or as part of the normal duty cycle, the fatigue failures can occur at the joints between bars and ring [6].

1.3.2 CONSEQUENCES

Faults which develop in service are not easily identified, although detection methods based on measurement of the consequent changes in machines performance have been described in literature [9-15].

1.3.2.1 ESCALATING FAILURE

In service, an undetected fault produces a higher resistance bar or joint, which may lead to eventual failure. Current overloading of adjacent bars has an adverse effect on the durability of the cage. In the overloaded bars, the electrodynamic force and the thermal stresses increase and so does the probability that the bars will be damaged. This phenomenon is the so-called avalanche propagation [7, 8]. Eventually the motor becomes unserviceable or the stator burns out.

1.3.2.2 ECONOMIC FEATURE

The sudden and unexpected failure of an electrical machine may be expensive not only in terms of the cost of the repair itself, or in the transportation costs to suitable places of repair but also by virtue of the disruption it causes to the industrial process. In continuous process industries the stopping of the process to replace the motor or repair it would result in considerable cost in terms of lost production. In addition restarting some motors would incur a further period of stress on other motors.

It is very clear that the conventional models are not able to cope with those phenomena and asymmetries that occur in the machine without drastic assumptions and simplifications. So there are pretty good reasons to look for other alternatives. Among these reasons are:

1) In the conventional design of an induction motor the field is known only approximately. The dimensioning of the iron core and the evaluation of the machine characteristics are based on a rough idea of the field distribution in the core. These dimensions are chosen to give specified peak flux densities in the motor teeth and core backs. The flux density waveform is assumed to be sinusoidal in the back core and containing a third harmonic in the teeth. These methods usually give satisfactory results for steady-state operation near the synchronous speed of the machine, but for locked-rotor or transient operation the results are unreliable. The lumped parameter circuit models are based on drastic assumptions. Although developed from fundamental laws on the behaviour of the magnetic fields, they were derived with a view to obtaining terminal (input/output) characteristics of the machine and not for getting detailed information on what happens inside the machine. As such, the computation involved is very simple and typically deals with six or fewer unknowns governed by linear equations. Another advantage here is that the lumped constants of the model may often be experimentally derived, so that for a given machine, the model would be found quite

accurate over the usual operating range of parameters (such as currents, speed, etc.) in that machine.

2) Conventional calculation routines have usually been designed for the analysis of cage or wound-rotor induction motors supplied by sinusoidal voltages. They are not directly applicable to the analysis of motors supplied by static frequency converters.

3) More reliable calculation methods are needed especially in the design of large machines, as it is very expensive to construct full-size prototypes to test the validity of the design. It is also important to know the transient and steady state performance of high-power induction motors accurately, e.g. in starting, in order to be able to determine the requirements imposed on the power supply.

4) In addition to what has been said, the designer should know the behaviour of the designed machine under abnormal conditions so that to minimise the stresses that are emanent from these faults such as negative torques during transients.

Therefore, to obtain an accurate picture of the variation of the magnetic flux distribution in time and space within a machine, all the important parameters affecting the field distribution should be considered. The complete machine flux must be evaluated for the differing positions of the rotor relative to the stator at each instant of time. A model capable of dealing with saturation,

skew and the distorted current waveforms, which occur in a practical machine needs to be developed. And this cannot be achieved but with the numerical field analysis.

In the following section the most important and well known numerical methods are compared against each other.

1.4 COMPARISON BETWEEN EXISTING NUMERICAL METHODS

Numerical field analysis has progressed rapidly in the last two decades. The development of solution methods and the growth of computer capacities have made it possible to solve more and more involved magnetic field problems. In general, the numerical solution of the field equations was achieved through one of the following methods:

1) Finite difference method [56, 68, 69].

2) Finite element method [51-55, 57-66, 71].

3) Nodal analysis method [70].

4) Reluctance matrix method[71,72,73].

1.4.1 FINITE DIFFERENCE METHOD

The finite difference method is essentially expressing the Poisson's equation in difference form. The domain of the solution is divided into rectangular elements and by applying the difference equation to each of the nodes, a set of

linear equations in terms of the potentials at the nodes is obtained; the potentials at the boundary being all known.

Elderlyi et. al [68, 69] used the finite difference method to study the flux distribution in a d.c. machine. Andresen & Muller [56] assumed sinusoidal time variation and used the same method to solve the field equations. The field solution was used for obtaining the locked-rotor current and torque of an induction motor. The effects of different slot shapes on the locked-rotor characteristics were studied.

The limitations of the method is that when studying the flux distribution and the torque at different rotor positions, all the nodes and elements on the rotor need to be reorganised. Moreover, for relatively small dimensions, such as stator and rotor teeth, a fine mesh may be required but to use the same mesh throughout the machine may be expensive since it would result in an unnecessary large number of nodes for solution.

1.4.2 FINITE ELEMENT METHOD

The finite element method is essentially based on the minimisation of the Poisson's equation which is expressed in functional form. The potentials at the nodes are described by describing function. By substituting this describing function into the functional equation a set of simultaneous equations are obtained.

The finite element method is more flexible than the finite difference method. It can simulate almost any shape of the boundary because the elements can be of virtually any shape, such as triangular, polygon, etc. The number of elements also will be less than for the case of finite difference for a desired accuracy to be attained. For this reason it is one of today's best-accepted methods. The method as a result is highly amenable to automation. In view of the method's importance, we shall devote some extra space to it.

In the late 60's many efforts have been made to solve magnetic field problems by the finite element method. The first application of the finite element method to the field problem was probably due to Zienkiewicz et. al [71].

In the analysis of electrical machines the finite element method was first applied to synchronous machines [51] and dc machines [52] because the operation of these machine types can be approximately modelled by stationary fields. Even nowadays most of the research work concerning the magnetic field analysis of electrical machines deals with the modelling of synchronous machines. They have been analysed by using step-by-step methods to solve the time-dependence [53] and by three-dimensional finite element formulations [54].

The field of an induction motor has to be solved with a method that takes the time-dependence into account. Probably the difficulties connected with the solution of time-dependent non-linear fields have postponed the numerical analysis of induction motors. To the author's knowledge, the first publications dealing with this problem appeared at the beginning of the 1980's. For the present only two-dimensional formulations have been used.

Ito et al. [55] computed the non-linear field of an induction motor using an eddy-current formulation and assuming sinusoidal time variation. The method was used to study various properties of induction motors and some suggestions were made to improve the design of motors. Bill et al. [79] thinks that the magnetic field in the region with non-linear characteristic can be solved by finite element method (FEM) whereas in the case of the region described by linear characteristic the boundary element method (BEM) is very well suited. Therefore he resorted to a combination of both methods (FEM and BEM) in the analysis of induction motors.

Williamson & Ralph [57, 58] have connected conventional calculation methods and numerical field analysis in their work. They assumed sinusoidal time variation and skin effect neglected when solving the field equations. The rotor currents are solved from the airgap flux (vector potential) induced by the stator currents with the aid of rotor bar impedances. The method is quite

versatile. The effects of harmonic components and skewed rotor slots are taken into account. A drawback of the method is the time consumption in the iterations needed in the solution of the winding currents. The method was used to compute the properties of a shaded pole motor.

Bouillault & Razek [59] and Brunelli et al. [60] used time-stepping methods to calculate the time variation of magnetic fields in induction motors. Both papers deal with solid rotor induction motors.

The voltage equations of the windings of an induction motor are coupled to the field equation. In earlier publications the currents of the stator winding have been taken as the sources of the field e.g. [56] or the solution is obtained in a double iteration process in which the voltage equations of the stator winding are solved in an outer iteration and the solution of the field equation forms an inner iteration. A more efficient method is obtained if the discretized field and voltage equations are solved in the same iteration loop. Brandl et al. [61] computed steady state operating characteristics of a synchronous machine by solving the coupled field and voltage equations together in the same matrix equation. Nakata & Takahashi [62] and Lindfors et al. [80] used the method to analyse an induction motor in steady-state and Brunelli et al. [60] used a related method in the step-by-step solution of a solid rotor induction motor.

Strangas & Theis [63] have computed the field of an induction motor using a method in which the field equation and the voltage equations of the stator and rotor windings are solved together. They present a quite general two-dimensional step-by-step formulation for the evaluation of the operating characteristics of a shaded pole motor. Later, Strangas [64] applies the formulation to the analysis of a cage induction motor. No computed results of the operating characteristics are presented, but the method seems to be quite generally applicable to the analysis of induction motors. For instance the possibility to rotate the rotor is included in the method.

Shen et al. [65] and Shen & Meunier [66] present a formulation for sinusoidally varying field quantities that is very similar to that given by Strangas for general time-dependence. The voltage equations of the stator and rotor windings are written in matrix form. In recent papers Preston et al. [74] and Arkkio [75] have used a finite element time-stepping technique for the analysis of a cage induction motor. In a subsequent paper, Arkkio [76] applied the same method to a cage induction motor fed by a PWM inverter.

Smith et al. [77] used the same method for modelling transient torques and currents in a slip ring induction motor. The method is based on a coupled fields and circuit equation approach. The numerical solution incorporates a moving rotor to account for slotting and saturation. Some experimental

results were given. Williamson et al. [78] analysed the cage induction motor using two-dimensional finite element. in their analysis they used the decomposition of rotor currents into harmonics distributions and the use of auxiliary circuit equations to take the time-stepping into account.

In particular, the finite element method has proven to be efficient when dealing with complicated geometries. The solution of three-dimensional time-dependent magnetic field of an induction motor is, however, still too large a task. The problem must be simplified by assuming the magnetic field to be two-dimensional, independent of the coordinate parallel to the shaft of the machine.

1.4.3 NODAL METHOD

The nodal method is essentially a finite element method but without using the minimisation of the functional to obtain the solution. The set of simultaneous equations in terms of potentials at the nodes are obtained by substituting directly the describing function in the Amperes equation. The rest of the calculation follows as for the finite difference method.

Hanalla and MacDonald [70], applied the nodal method to the solution of the field problem of an alternator. This method which is based on Amperes law is simpler, when compared to the finite element method, in obtaining the simultaneous equations of the node potentials.

1.4.4 RELUCTANCE METHOD

The other category of numerical methods for the solution of the field is the reluctance matrix method. This method, as the nodal method, is also based on the Amperes law. Elements of rectangular shape are used to simulate the iron geometry. F.M. Abdel-Kader et, al [67, 72] devised a technique to represent the airgap to take into account the constant changing of the airgap reluctance due to the movement of the rotor. From their investigation, it was found that the method was able to handle the saturation satisfactorily. The solution of the field and hence the torque was done virtually at any rotor position and hence simulates the actual running condition of the machine. The main assumption was that the input current was sinusoidal. This is true as long as the iron does not saturate severely [57]. Amin [73] used the same method to predict the performance of induction machines incorporating the full inductance matrix. The computed results showed good agreement with the experimental results.

1.5 CONCLUSION AND PROBLEM DESCRIPTION

From the foregoing discussion the following points are implied:

1. The existing techniques for modelling the induction motor can be classified into two categories; either very fast but first order methods or very accurate but with very long computational time techniques.

2. The vulnerability of the induction motor to asymmetrical faults in the rotor due to the causes outlined earlier makes its modelling very difficult for the first category and almost unpractical for the second category.

The first three methods are both accurate and detailed but are acknowledged to absorb a large amount of computer time to predict the field picture at one instant of time. Obviously the repeated use of such techniques to determine the variation of the field pattern with time would also use an impractical amount of computer time.

The best method for a particular problem depends on the purpose of the application itself. If it is for confirming results obtained from approximate methods and it is to be used for only a few calculations, then the finite element method is the best candidate. However if repeated solutions are required, such as for a torque-speed curve or the analysis of asymmetries in a multipole machine then obviously, a simplified model accounting for all the necessary factors affecting the machine's performance would be better suited.

The aim of this project is to develop a model suitable for routine use during the design of induction machines and the analysis of their performance and behaviour during operation with perfect and asymmetrical rotor circuit. Therefore, a compromise between high accuracy, computationally slow models such as the finite element method and lower accuracy,

computationally fast models such as equivalent circuit has to be made. Sufficient magnetic circuit elements to reflect all properties of a machine, but not so many elements which could unnecessarily slow down the computation without a significant gain in accuracy are required. The reluctance mesh technique offers the prospect of a suitable compromise.

CHAPTER TWO

LITERATURE REVIEW

2. PREVIOUS WORK

2.1 INTRODUCTION

The problem of broken bars and rotor asymmetries in induction machines has received considerable attention [22-50] both in predicting the effects analytically and in determining those effects experimentally.

Many authors have made contributions aimed at improving the techniques for detecting and analysing the effect of broken bars or in general terms, the effect of rotor asymmetries on the performance of the machine. Some authors have concentrated on the derivation of equivalent circuits whereas others have based their analysis on rotating field theory.

A review of published work in all of these areas would cover a great deal of that which has been written about squirrel cage induction machine defects which is the aim of this chapter.

2.2 LITERATURE REVIEW

To the authors knowledge, Georges [22], in 1896, was the first to study the operation of three-phase induction motors with an asymmetrical rotor circuit. In 1941, Jordan and Schmitt [23] applied transmission line theory to analyse the squirrel cage motor with asymmetrical rotor circuit, wherein the case of a broken rotor bar was discussed. In 1955, Mishkin [24] presented an analysis

for machines with broken endrings but he did not consider the more common (and, therefore, more important) case of broken bars.

Later, in 1962, Heller [25] applied the same theory as that of Jordan and Schmitt [23]. He assumed that the effect of a broken bar could be simulated by superimposing a second set of rotor currents on those normally found with a healthy rotor. This second set was obtained by inserting a current generator in place of the broken bar to feed the normal bar current back into the endrings. The resulting current distribution was determined by solving a transmission line equation for the cage. This approach entirely neglected the effect that the stator has on such a current distribution, and although extension to more complex failure would be possible, only a simple single bar fault was discussed [41]. Using the same theory as Heller [25], Deleroi [26] assumed, in his analysis, the stator currents to be imposed and, therefore, no influence upon or from the stator current distribution is possible. The stator having been decoupled (due to this assumption), he considered the behaviour of the squirrel cage in the airgap only.

In 1969, D'Alessandro and Pagono [27] developed an analysis based on multiphase symmetrical component theory to study machines with broken bars, following the successful application of three-phase symmetrical

components to unbalanced slip-ring motors by Gabriano [28] in 1950 and Barton [29] in 1955.

Vera [31], in 1969, applied the symmetrical component theory for analysing the behaviour of such a three-phase squirrel cage induction motor, where some of the rotor bars, which were situated adjacent to each other, were broken. The coupling network in the derived equivalent circuit, which connects the positive and negative sequence impedances of the machine holds only for symmetrical types of rotor asymmetries. Symmetrical component impedances other than the zero, positive and negative sequence ones were not taken into consideration. In a general m-phase problem, m symmetrical component impedances must appear.

In 1975, Vas [32] extended the foregoing theory for such cases where rotor bars situated beside each other have different impedances. One year later, Toke and Vas [33] derived all the symmetrical component impedances of the m-phase rotor machine with endring faults and derived a steady-state equivalent circuit, which is particularly simple if only one endring is broken. In the same year, operational characteristics of a star connected slip-ring induction motor with rotor asymmetries were discussed by J.Vas and P.Vas [34], using symmetrical components. A new equivalent circuit for steady state and constant speed transient operation was derived; equations of currents and

power were given in a ready-to-calculate form. In 1977, J.Vas and P.Vas [35, 36] and P.Vas [37] discussed transient and steady state operation of induction motors with general stator asymmetries, where new general steady-state equivalent circuits were also derived. Differential equations of asymmetrical machines were given in state variable form [27].

In 1978, Juffer and Abdelaziz [38] developed a versatile analysis based on a two-axis rotor model, which could include both types of fault. Once again, however, restrictions were imposed on the distribution of faults on a multibar failure, so reducing the range of applicabilities of the method. Experimental results were given for the stator current pulsation in a two-pole motor with a single bar fault, and showed good agreement with the theoretical predictions.

In the following year, that is 1979, P.Vas and J.Vas [39] applied symmetrical component theory [35-37] to the analysis of three-phase and single phase induction motors, for the case of general squirrel cage asymmetries. P.Vas [40], in 1982, extended the work done by Desai [30] for the transient operation of single-phase squirrel cage induction motors with rotor asymmetries to the case of three-phase slip-ring induction motors with asymmetrical resistances in the rotor circuit. A.Patyk [8], in 1986, used the symmetrical components transformation to study an asymmetry caused by partial fracture of bars of the starting cage of the double squirrel cage motor.

Although the techniques outlined so far represent a progressive improvement from the case of only one endring fault, to symmetrical multibar faults and to general rotor asymmetries, they did not take into account important factors such as saturation, skew and slotting. In addition, the derivation of equivalent circuits to represent particular special cases is of limited use, and a general purpose approach is preferable.

Towards this purpose, Williamson and Smith [41] used an analysis based on rotating-field theory using a mesh model of the rotor described by Poloujadoff [42]. In an other publication [43] using the same model [41], they computed the unbalanced magnetic pull in induction motors with asymmetrical rotor cages. However, in their model they assumed an ideal stator winding excited from a balanced three phase supply (i.e. the stator produces no harmonic fields and is impervious to those produced by the rotor). In the model they developed, the size of the impedance matrix, will increase considerably as each additional stator current time harmonic increases the dimension of this matrix by 1 and as each rotor time harmonic increases it by Nr+1. Another significant assumption is that the rotor speed remains constant. If the rotor speed fluctuates under the influence of the twice slip frequency torque pulsations, then a (1+2s)f component is produced in the stator current. In 1987, Williamson extended this model [41] to accommodate double-cage machines [44]. Clearly, this model is more general than equivalent circuit

theories but still the effect of saturation, skew and slotting effects have been neglected except that saturated values for resistances and reactances may be incorporated.

It is very clear from the foregoing discussion that a more detailed investigation of the field in electrical machines is needed considering nonlinearities of the material and skew effect. Many restrictions may be eased by the numerical solution of the field equations. However, several authors examining this problem have stuck to such assumptions as slotless machines with uniform airgap and stator and rotor saturation neglected.

In 1980 Motya Ito and et al [45] used the complex-valued finite element method to analyse the magnetic field distribution around the rotor of a cage-type three-phase induction motor in order to calculate the unbalanced magnetic pull and torque taking into account the influences of the magnetic saturation of rotor and the skin effect of the rotor whereas the influences of magnetic saturation of stator core and harmonic components of rotor flux on the stator current were neglected.

Recently, in 1989 , Amin [48] used exactly the same method as Motya [45] without reference to his work. As usual, saturation, slotting and skew effect were neglected.

Clearly, saturation is a significant feature which must be considered in machine performance analysis. The techniques outlined so far have either neglected completely the effect of saturation or have been based upon determining saturation factors for the component leakage fluxes and main flux of the machine. This has been necessary because the means of performance evaluation consider all these elements separately in the determination of the inductances. In practice, however, a winding itself cannot differentiate between fluxes resulting from various sources, it merely develops an emf as a result of the net flux which links it. Saturation is a spatial phenomenon - it varies from tooth to tooth and from one to another part of the yoke. It reflects itself in different ways on inductances in one phase compared to another, so it cannot be taken into account correctly by just varying machine equivalent circuit parameters. In the method proposed by Ito [45] and Amin [48], if the number of broken bars is large, the stator core would be saturated so much that accurate analysis would become difficult. This method would give then a larger U.M.P. than that actually occurring.

El Kasabgy et al [46, 47] in 1988, based their work on rotating-field theory but they too used finite element as the numerical tool to analyse the effects of broken bars in the cage rotor of an induction machine. In their analysis they assumed the stator currents to be a sinusoidal function of time. They have shown that the perturbation in airgap field due to one or more broken bars is

of sufficient magnitude to allow detection of the fault condition. They also provided some experimental results from internal stator tooth tip and yoke search coils and external search coil placed against the frame of the motor. They examined the spectrum of the stator current and the harmonic content of the shaft torque. The drawback of this method is the computational time, especially, in the case of broken bars where no symmetry conditions exist. That is the entire cross section of the machine must be analysed.

In the same year, S. Elder, J.F. Watson and W.T. Thomson [49] attempted to develop a technique allowing detection of faults in induction machines during the starting transient. Their research was conducted in two ways. One path involved the capture of the line current waveforms from a laboratory test rig. These waveforms are then examined in the time domain and processed by both spectral and cepstral analysis on industry standard analysers. The signal processing has also been extended to the use of speech processing algorithms.

The other parallel path is in induction motor simulation. This model of the induction motor produces waveforms (line current etc.) which can be processed as with the real motor. In their simulation they used the equivalent two axis D-Q model. The two phase currents i_d and i_q of the stator were then transformed back to the three line currents i_a, i_b and i_c. Then a three phase model has been developed because of the limitation of the two axis D-Q model (a balanced magnetic circuit is necessary and at least one winding must

be completely balanced). In this way individual rotor bars cannot be represented. Saturation was approximated by varying the leakage inductance in both stator and rotor from a saturation characteristic curve derived from tests on the machine.

The calculation of leakage reactance of a machine is a three-dimensional electromagnetic problem of immense complexity, further complicated by the nonlinearity of iron and the fact that the flux density is different in different sections of the magnetic path and varies with operating conditions. Furthermore, skewing of the rotor constrains the bar currents to flow in paths which are strictly nonaxial, thus altering the stator-rotor coupling and axially redistributing the airgap flux. Both of these effects are lost with a homogeneous sheet rotor. Obviously, such techniques are unable to cope directly with saturation of the magnetic circuit and skewed slots.

Some authors have examined the problem experimentally avoiding assumptions. O Gol [50] considered two fault cases. The first one involved a large squirrel cage induction motor subject to frequent DOL starting. The second case involved a cage fracture simulated by drilling a hole into a bar of a squirrel cage induction machine. In both cases measurements were made for the healthy and faulty rotor.

However, the consideration of all types of faults would make an experimental method a very laborious, expensive and lengthy exercise. Even then, it is difficult to see how such factors as skew and saturation might be included. Certainly, more modern techniques of numerical analysis seem to overshadow experimental methods.

2.3 CONCLUSION

The overall performance aspect of induction machines operating under abnormal conditions has been dealt with by many authors. Each of them has used either rotating field or symmetrical components theory. From some of these theories, equivalent circuits were developed and generalised and they have proved to be very useful in visualising and analysing both the steady-state and transient performance. Some other authors felt that the equivalent circuit is of limited use and reverted to rotating field theory. Although they got good results, they were unable to model accurately saturation, skew and other phenomena encountered in electrical machines which are the result of tooth effects and electric or mechanical asymmetries. The remaining authors used either experimental methods which is a laborious, expensive and lengthy exercise if all types of faults are considered or numerical field solution using the finite element method.

Many of the earlier methods assume that for time-varying situations, fluxes, currents, etc., changed sinusoidally with time. Relative motion between stator and rotor was ignored and, in some methods, saturation was taken into account using saturation factors. Although this approach has proved to be a valuable tool, it cannot cater for the phenomena arising from mmf, saturation and permeance harmonics which are particularly important in machines with small airgaps; it is essential that movement and time variation of permeability is taken into consideration.

Non of the methods published so far have considered motors with defective rotors operating from variable frequency, inverter supplies. Generally, this is because the conditions which give rise to rotor faults, as discussed in Chapter 1, are associated with direct, on-line, starting on a fixed frequency sinusoidal supply. However, it is not uncommon for inverters to be retrofitted to existing fixed speed drives and as machines with rotor faults, which have gone unnoticed, may be operated from inverters. This makes a study of the likely consequences worthwhile.

To model accurately induced currents, time and space harmonic effects, and saturation effects throughout the time-cycle requires the use of a numerical time-stepping method. This leads to a more accurate representation of the

physical problem to be modelled; the stator windings can be arranged in their natural phase belts and allowance made for rotor movement and skew effect.

By their very nature, finite element time-stepping techniques are inherently expensive to use as they involve a huge number of elements in addition to the need for re-organisation of the airgap meshes with the rotor position and, therefore, they are time-consuming and require large storage. They are not suitable for such studies i.e. squirrel cage induction machines fault simulation not in terms of accuracy but in terms of costs. Therefore, one has to look for an alternative method which takes into account the above mentioned properties and which is less expensive.

The author believes that the method described in this thesis is simple, general and reasonably accurate. It is also readily suitable for broken bar simulation at different speeds.

It must be remembered, however, that nature is far more complicated in reality than any model. The art lies in devising a model simple enough to handle, but complex enough to bring out the effects we seek to evaluate.

CHAPTER THREE

METHOD OF ANALYSIS

3. METHOD OF ANALYSIS

3.1 INTRODUCTION

The analysis of electrical machines, in general, is frequently performed by reference to some form of equivalent circuit. Any equivalent circuit is a pictorial presentation of the mathematical equations. As for three-phase induction motors, the analysis is usually based on either a magnetic equivalent circuit or an electrical equivalent circuit. Both of these approaches have been used for a long time and they represent most succinctly the operation of the machine.

In this thesis the magnetic equivalent circuit is used along with the electric circuit equations. This chapter will describe the method of analysis used in the derivation of the model and the solution of the performance equations. This procedure contains a number of simplifying assumptions necessary to obtain a solution within finite bounds of computational time and program complexity. These assumptions and their implications will be discussed in the following section.

3.2 ASSUMPTIONS

Several simplifying assumptions have to be made in the analysis. The assumption of a pseudo three-dimensional field description probably causes the largest errors, but there are also simplifications related to the modelling of iron properties that cause inaccuracy in the results. The main simplifications are discussed below in the following sections.

3.2.1 PSEUDO THREE-DIMENSIONAL MODEL

For accurate results a complete three-dimensional formulation should be used in the calculation of the magnetic field of an induction machine. Three-dimensional finite element formulations have been developed for the analysis of time-dependent magnetic fields [59], but their practical applications are still restricted to relatively simple geometries. It is also doubtful if the magnetic steel could be fully described accurately in a three dimensional machine model except in a general sense. In this work a very simple pseudo three-dimensional magnetic circuit model is used. The three-dimensional effects, of skew are modelled in a set of two-dimensional problems while the end-region fields are taken into account separately.

1) END WINDINGS

Currents in the end windings of a machine induce components to the flux linkages of the stator and rotor windings that are not included in the fluxes computed from the two-dimensionally modelled regions. These additional flux linkages are taken into account in the voltage equations.

Probably the easiest way to add the effect of the end-region fields into the voltage equations is to model the end windings as resistances and constant inductances, whose values are determined by simplifying analytical methods or by measurements [88, 89].

The results of Chapters 5 and 6 have been computed using the end-winding inductances obtained from the difference between the total leakage inductance

calculated from the short circuit test and the total leakage inductance calculated from the derived inductances (see section 5.4.2 for more details).

In the squirrel cage winding, a given conductor is not specially related to any one of the remaining conductors, and no two of them carry currents of the same phase. Therefore, it is convenient to regard a squirrel cage winding as one composed of N_r separate phases. In order to simplify the analysis, it is convenient to replace the squirrel cage winding by one in which the conductors are extended, bent down to the shaft and all joined together at the axis. The resistance and inductance of the end rings are considered by adding suitable increments to the actual resistance and inductance of the conductors. This derivation for replacing the squirrel cage winding is based on the fundamental effects of the bar and end winding currents. The end winding current is the integration of the bar currents. Therefore the end winding harmonic current effects are very small, and it is assumed they may be ignored.

2) CURRENTS IN THE IRON CORE

The core of an electrical machine is made up of thin electrical steel sheets. An insulation layer on the sheets isolates them from each other. The losses due to eddy-currents in the sheets are minimised by making the sheets as thin as economically practical.

The punching of the core sheets breaks the insulation layer at the edges of the sheets. This may lead to galvanic contacts between adjacent sheets and further to eddy-currents that flow from sheet to sheet. It is difficult to take these eddy-currents into account in the analysis because of their statistical nature. Punching also affects the magnetic properties of the sheet edges.

The rotor bars of an induction machine are usually in galvanic contact with the surrounding electrical steel sheets. A potential difference between two rotor bars induces a current that flows through the sheets from one bar to the other. Currents along the iron sheets are not consistent with the two-dimensional approximation. It would be possible to treat these currents in a simplified manner within the slice method used to model the skew. This would complicate the analysis considerably for a second order effect. Furthermore, in the experimental machine used, the bar shape differs from the slot shape and the contact surface is very small. There are also difficulties in the determination of the contact resistances between rotor bars and lamination sheets. Thus, in this case, all interbar currents in the electrical steel sheets are neglected. The laminated iron core is treated as a non-conducting, magnetically non-linear medium.

3) SKEWED ROTOR SLOTS

The slots of either rotor or stator of an induction motor are usually skewed. Normally, in a skewed rotor, the rotor slots are not parallel to the shaft and the stator slots. In the conventional calculation of an induction machine the

effect of skewing is treated with a skew factor that affects the magnetic coupling between the stator and rotor windings.

A somewhat different method is to consider a skewed machine to be made up of several slices that have been cut from an ideal two-dimensional machine by planes perpendicular to the shaft. The rotors of adjacent slices have been rotated by an angle corresponding to the skew. The winding currents are assumed to be continuous from slice to slice. The magnetic field of each section is solved separately using a two-dimensional formulation.

The average core saturation level of a loaded skewed induction motor varies along the shaft direction [90]. Thus a skewed machine saturates somewhat differently from an unskewed machine. The slice model takes into account the variation of the saturation level in the axial direction. The effect cannot be treated properly with a simple skew factor.

Consideration of skewed slots increases the program time because it is nearly equivalent to dividing the machine into five unskewed machines. The program was carefully designed to use the same arrays used for the unskewed machine so that no extra memory space would be required.

3.2.2 THE NONLINEARITY OF IRON

The non-linear magnetisation of iron complicates the solution of magnetic fields in electrical machines. In numerical solution routines saturation leads to time-consuming iteration to determine the correct operating point. Iron also

has significant hysteresis in its B-H characteristics. The reluctivity is not a single-valued function of e.g. flux density, but depends on the history of the system.

In principle it is possible to take both hysteresis and saturation into account in a step-by-step solution. The difficulty lies in the lack of a phenomenological model for the magnetisation that is easy to implement and fast to use in a computer routine and still gives the material properties accurately. Both the magnitude and the direction of a flux density vector in a machine core vary. The points of flux density vectors trace very complicated curves, especially in teeth at the airgap region. A good hysteresis model should be able to treat an arbitrary magnetic field excitation. Such a model would contain much information which had to be gathered experimentally before the parameters of the model could be determined.

In the time-stepping method used in this thesis, a single-valued monotonic reluctivity curve for the core material is used. Hysteresis and eddy-currents in core sheets are not included in the model. This means that iron losses are totally neglected.

3.2.3 TEETH PERMEANCES

The permeances of rotor and stator teeth were calculated at one-third of the height of the teeth from the narrow end for the moderate saturation condition

and slight taper present in the test machine. This traditional approach proved to be quite satisfactory.

3.2.4 MAGNETIC CIRCUIT ASYMMETRY

Rotor and stator surfaces were assumed concentric in order to simplify the calculation. A model which includes such asymmetry is outside the scope of this thesis.

3.2.5 SHORT CIRCUIT LEAKAGE INDUCTANCE

The total leakage inductance calculated from short circuit tests was divided equally between the stator and rotor winding when referred to the stator.

3.3 METHOD OF ANALYSIS

The method of analysis, used in this thesis, is based on a very simple pseudo three-dimensional model of the magnetic circuit which is solved to find a very close approximation to the distribution of the flux inside the machine accounting for saturation and slotting effects.

The numerical solution is voltage forced with both stator and rotor currents being determined directly from the circuit equations. As the saturation conditions under load are considerably influenced by skew, the three-dimensional nature of the machine needs to be modelled in the majority of cases. This is achieved by dividing the machine axially into a number of un-skewed segments (typically five), each with their rotor teeth displaced radially

from their neighbours by a fraction (one fifth) of the skew angle (as shown in Figure 3.1).

Figure 3.1a shows a skewed machine whereas Figure 3.1b shows an unskewed rotor divided into three sections. These sections are rotated from one another by one third of the skew angle as illustrated in Figure 3.1c.

The inductances (self and mutual) along with the variation of the inductances with the rotor position over the time step are inserted into the circuit equations which are used to time step the winding currents forward using a numerical integration routine Runge-Kutta and Adams numerical integration routines.

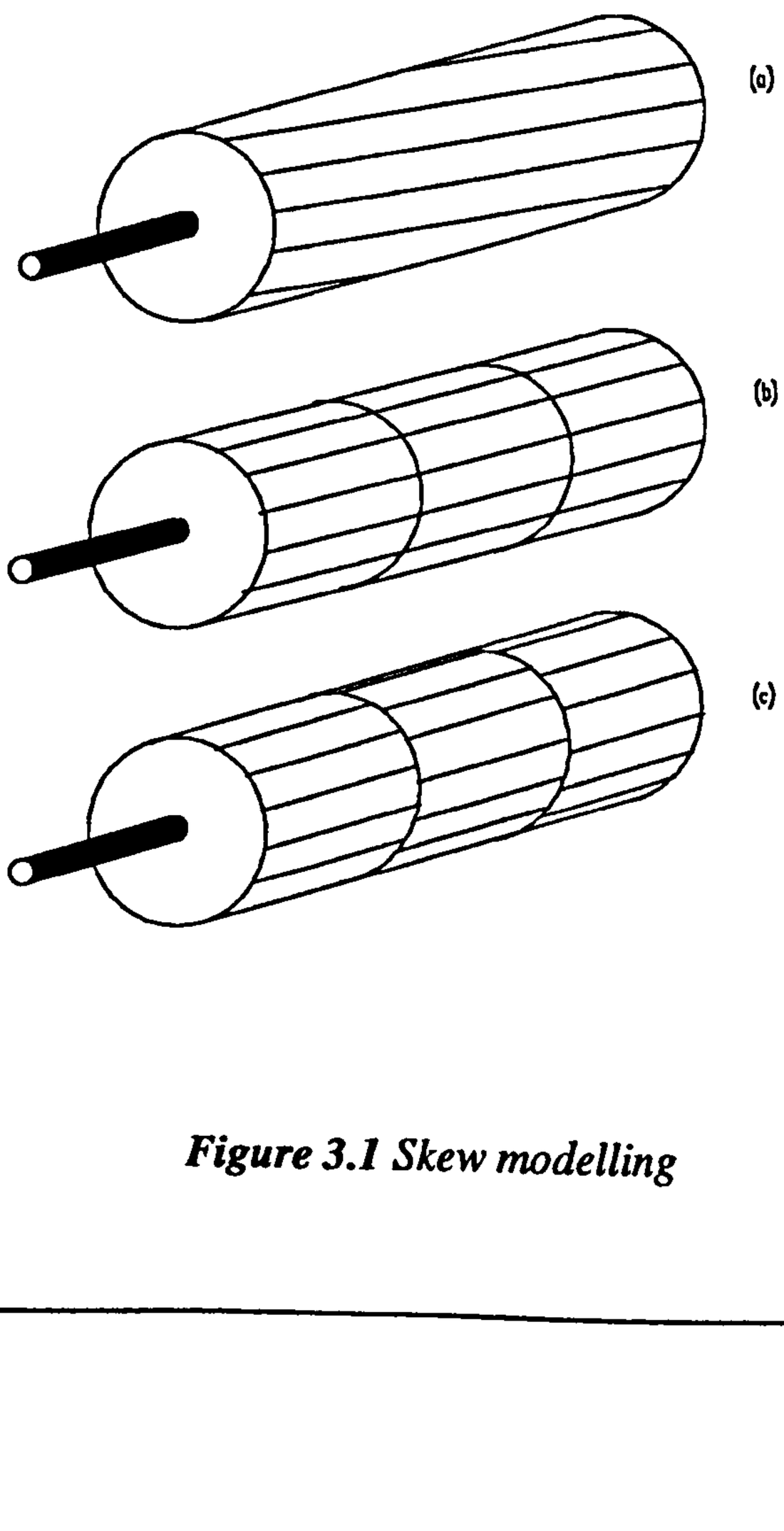

***Figure 3.1** Skew modelling*

The mechanical equation (3.5) is also included so that the rotor can be moved to the appropriate angular position at the end of the time step. All these steps will be described in the following sections.

3.3.1 MACHINE PERFORMANCE EQUATIONS

In normal operation, the voltages applied to the rotor circuits are zero both for the wound rotor and the squirrel cage machines. For the impressed stator voltages V_a, V_b and V_c of a three-phase machine, the performance equation is determined from:

$$[v] = [R] \cdot [i] + \frac{\partial \theta}{\partial t} \cdot \frac{\partial [L]}{\partial \theta} \cdot [i] + [L_{inc}] \cdot \frac{\partial [i]}{\partial t} \tag{3.3}$$

which is rearranged, to calculate the performance, to the following form

$$\frac{\partial [i]}{\partial t} = [L_{inc}]^{-1} \cdot \left([v] - \left([R] + \omega_r \cdot \frac{\partial [L]}{\partial \theta} \right) \right) \cdot [i] \tag{3.4}$$

where [v], [i] and $\frac{\partial [i]}{\partial t}$ are vector column matrices representing the instantaneous phases voltage, current and current time derivative, while [R] is the diagonal matrix containing the stator and rotor phase resistances, and [L], $\frac{\partial [L]}{\partial \theta}$ are square matrices containing self and mutual inductances for each phase and their derivatives and $[L_{inc}]$ is the incremental inductance matrix.

To complete the mathematical electric circuit equations defining the behaviour of the machine at its terminals, the mechanical equation is required to be included.

$$T_e = T_m + D \cdot \frac{d\theta}{dt} + J_m \cdot \frac{d^2\theta}{dt^2} \tag{3.5}$$

From which

$$\frac{d^2\theta}{dt^2} = \frac{T_e - T_m - D \cdot \frac{d\theta}{dt}}{J_m} \tag{3.6}$$

and

$$\frac{d\theta}{dt} = \int \frac{d^2\theta}{dt^2} \tag{3.7}$$

where T_e and T_m are the electromagnetic and load torque respectively, J_m the total moment of inertia and D the damping moment.

These equations were solved numerically using a well known Rung-Kutta and Adams integration formulae. All that is required is for the independent variables, the voltage waveforms which are applied to the electrical terminals of the machine and the torque applied to the mechanical terminal, to be defined as a function of time. Naturally, the initial conditions which apply at the start of the integration process need to be clearly defined for the dependent variables of winding current and speed.

The number of electrical equations for a three-phase machine with a three-phase wound rotor is six. For a squirrel cage machine, the independent windings are not so easily defined as there are no terminals brought out. If one neglects inter-bar current then the separate elements of a single cage rotor circuit comprise of the rotor bars themselves and twice as many end ring circuits as those bars. As the end ring components are mostly relatively small, it is usual to lump their circuit effects into those of the bars themselves. This reduces the number of independent electrical rotor circuits to the number of bars which is a considerable saving.

The solution of the terminal equations for the machine requires that the inductances associated with each of the electrical circuits is evaluated. It also requires the variation of inductance with rotor position to be determined. These inductances are a function not only of the proportions of the magnetic circuit of the machine and the materials from which it is made but also of the current in all of the electrical circuits at the instant that they are to be evaluated.

3.3.1.1 INDUCTANCE COMPUTATION

After the solution of the magnetic circuit and the determination of the saturation conditions at an instant in time (see next section), the principle of superposition can be applied at that instant to the magnetic circuit keeping the saturated permeance and incremental permeance of the magnetic elements unchanged. Each winding in the model is individually excited by a current

(usually one amp) while the other winding currents are set to zero and the fluxes evaluated using the incremental permeance which link that winding then define its incremental self inductance while those linking other windings define their incremental mutual inductances with the excited one. This procedure is repeated for each one of the axial sections. The flux contributions from each one of these sections are summed to find the total flux linkage in each case.

The self and mutual inductances evaluated by this technique reflect all the irregularity caused by saturation, skew and slot openings. Therefore, all these inductances will vary with the rotor position.

The magnetic circuit model used covers all paths for the zigzag leakage, belt leakage, slot leakage and the airgap flux. Therefore, all inductance components except for the end-winding leakage is determined. The end-winding leakage is determined as mentioned in section 3.2.1 and added to the inductance calculated above.

In the case of a squirrel cage rotor, each bar represents one phase, therefore the self and mutual inductances can be calculated for the rotor winding by following the same procedure outlined above.

3.3.1.2 RATE OF CHANGE OF INDUCTANCES

The variation of inductance with the rotor position is determined by subtracting two sets of inductances evaluated using total permeance under the

same saturation conditions but where the rotor displacement differs by a small angle. The result is then divided by this small angle.

3.3.1.3 ELECTROMAGNETIC TORQUE EQUATION

The instantaneous torque is obtained from the change of the stored magnetic energy with a very small change of rotor position. The energy stored in a magnetically coupled circuit is defined by:

$$W_m = \frac{1}{2} \cdot [I]^t \cdot [L] \cdot [I] \tag{3.8}$$

The torque due to change in the energy stored in the magnetic circuit is given by:

$$T_i = \left. \frac{\partial W_m}{\partial \theta} \right|_{I=const} = \frac{1}{2} \cdot [I]^t \cdot \frac{\partial [L]}{\partial \theta} \cdot [I] \tag{3.9}$$

where $[I]^t$ is the transposed version of [I]

$\frac{d[L]}{d\theta}$ is the inductance derivative matrix

The steady-state average torque is computed from adding the instantaneous torques up in a certain steady state region and divided by the number of instantaneous torques as follows:

$$T_{AV} = \frac{\Sigma T_K}{K} \tag{3.10}$$

while the steady-state pulsating torque was evaluated as the difference between the instantaneous maximum and minimum torque values within the steady-state region, giving the torque causing vibration. This pulsating torque was evaluated as follows;

$$T_p = T_{max} - T_{min} \tag{3.11}$$

where T_P is the pulsating torque.

T_{max} and T_{min} are the biggest and smallest instantaneous torque values in steady state region.

3.4 MAGNETIC CIRCUIT EQUATIONS

To solve for the fluxes in the machine, the permeance matrix method is used. This is based on Ampere's magnetic circuit law, which, using the usual notations, states that:

$$\oint \mathbf{H} \cdot d\mathbf{l} = \iint \mathbf{J} \cdot d\mathbf{s} \tag{3.12}$$

which can be discretised into the form:

$$\sum H_i \cdot l_i = \text{current enclosed} \tag{3.13}$$

or

$$\sum \phi_i \cdot S_i = \text{current enclosed} \tag{3.14}$$

where S_i is the reluctance of element i.

The physical model, in this case the machine cross-section, which this equation represents can similarly be discretised into elements which are connected to form the magnetic circuit of the machine cross-section(see next section). Equation (3.14) is the equivalent of a voltage drop around a loop, its nodal equivalent can also be obtained. In this thesis, the nodal form of the equation is used. In this way it resembles closely the finite difference or first order finite element models of the magnetic circuit. However, with so very few nodes in this non-linear network it is possible to obtain a solution for the flux distribution with much less calculation than would be required for these alternative models and hence saves computing time. The potentials at the nodes and the fluxes are the two quantities of interest. They are used to calculate the permeances of the elements of the magnetic circuit. The basic magnetic network equation to be solved is:

$$[\Lambda_n]\cdot[F_n]=[\phi_n] \tag{3.15}$$

This is a non-linear equation since the nodal permeance matrix $[\Lambda_n]$ is a non-linear function of the branch mmfs $[F_b]$. These mmfs are derived directly from the nodal mmfs $[F_n]$. The iterative solution to the non-linear equations can be found using the Newton-Raphson technique which is described in the next section.

3.5 THE SOLUTION OF NON-LINEAR EQUATIONS

3.5.1 INTRODUCTION

Non-linear equations are, equations where at least one variable appears in a form more complicated than simply multiplied by a constant. In general we are interested in solving equations of the form F[X] = 0, where both F and X are vectors. What makes such equations difficult to solve is that there is no general algorithm for solving them directly. Since there is no close form solution, an iterative technique must be used.

Nonlinearity complicates matters, making it harder to find convergent methods, and even harder to find such methods which are reasonably efficient. The most suitable method is Newton-Raphson method.

3.5.2 NEWTON-RAPHSON METHOD

For simplicity the Newton-Raphson formula is derived in terms of two equations in two variables. Let these equations be:

$$\begin{aligned} f_1(x,y) &= 0 \\ f_2(x,y) &= 0 \end{aligned} \tag{3.16}$$

or in vector form F(X) = 0, where x, y are the components of the vector X. If x_0 and y_0 are approximate values of the solution to this system of equations. Then

$$\begin{aligned} x &= x_0 + \Delta x \\ y &= y_0 + \Delta y \end{aligned} \tag{3.17}$$

where Δx and Δy are small.

The system of equations may be expanded in terms of Δx, Δy by Taylor's theorem to give,

$$\begin{aligned} f_1(x_0+\Delta x, y_0+\Delta y) = 0 = f_1(x_0,y_0) + \frac{\partial f_1}{\partial x}\cdot\Delta x(\text{for } x=x_0, y=y_0) + \\ \frac{\partial f_1}{\partial y}\cdot\Delta y(\text{for } x=x_0, y=y_0) + 0(\Delta x^2, \Delta y^2) \\ f_2(x_0+\Delta x, y_0+\Delta y) = 0 = f_2(x_0,y_0) + \frac{\partial f_2}{\partial x}\cdot\Delta x(\text{for } x=x_0, y=y_0) + \\ \frac{\partial f_2}{\partial y}\cdot\Delta y(\text{for } x=x_0, y=y_0) + 0(\Delta x^2, \Delta y^2) \end{aligned} \tag{3.18}$$

in vector form, this can be written as

$$-F = J\cdot\Delta X \tag{3.19}$$

and solving

$$\Delta X = -J^{-1}\cdot F \tag{3.20}$$

where J is known as the Jacobean matrix of the system of equations. Thus if X_0 is an approximate solution to the system of equations then $X_0 - J^{-1}\cdot F$ is a better approximation to the solution, provided that J is a non-singular matrix. In the general form, for a set of equations

$$F(X) = 0 \tag{3.21}$$

and an estimate of a solution, X given by X_n we may say that

$$X_{n+1} = X_n - J^{-1}\cdot F(X_n) \tag{3.22}$$

When using this formula, there must be some way of deciding when a solution to the equations under consideration has been found, or a solution close enough to satisfy the requirements. This was done by formulating a function known as an error function.

If after r iterations $X_r = (x_1, x_2, ..., x_n)$, then the error function e_r is defined by:

$$e_r = (\Sigma[f_i(x_r)]^2)^{0.5} \tag{3.23}$$

e_r is known as the Euclidean norm of the vector F. It is evident that as e_r approaches zero the individual terms $f_i(x_r)$ on the right hand side must become zero since they are all squared and thus positive. This indicates that e_r is a satisfactory measure of error, and that reducing e_r to zero will ensure that the equations are satisfied.

3.6 MAGNETIC CIRCUIT MODEL

In this section the formation of the induction machines magnetic equivalent circuit will be described. From Equation (3.14) it is apparent that the flux is assumed uniform over an element and the element is approximated by an equivalent rectangle. The length of the element is equal to the length of the rectangle and the width is the average width of the cross-sectional area perpendicular to the flux path. The problem now is to discretise the machine cross-section into magnetic elements, each element is represented by its

permeance. This is done such that the flux that would be expected cuts the average width of the elements perpendicularly.

The accuracy of the magnetic circuit model depends on the number of elements used. Instead of having a single mean flux path for each iron part, more flux paths would give a better accuracy. This would, however, increase the number of elements and hence computing time. Only a single mean flux path was used to keep computing time to minimum.

At very high saturation levels, because of the increase of the mmf drops in the magnetic steel elements, the main flux tends to stray more through the air. This can be compensated for in the teeth and core sections to some extent by the use of the constructed curves of the flux across the elements cross-section against the mmf drop across the element as shown in Figures 3.2, 3.3 and 3.4. For high values of flux the graph continues as straight line with a permeability of μ_0.

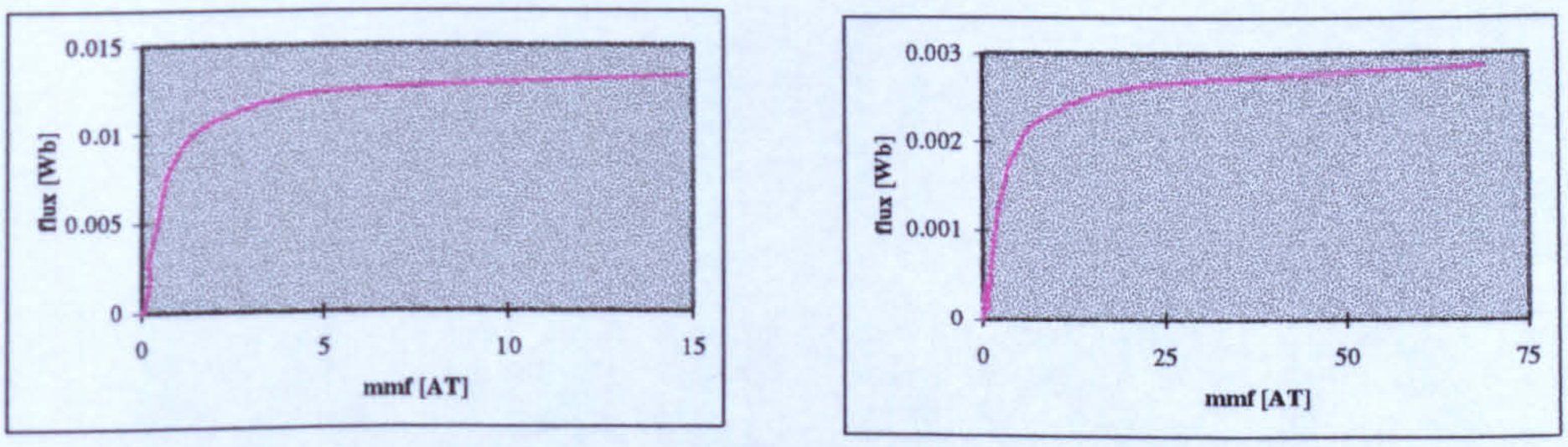

Figure 3.2 *Flux-mmf curves for stator core (left) and stator teeth (right)*

The leakage flux paths through the tooth tips of semi-closed or totally closed, (in the case of some cage rotors), slots require the use of a more complex permeance model along similar lines to that for teeth and core sections.

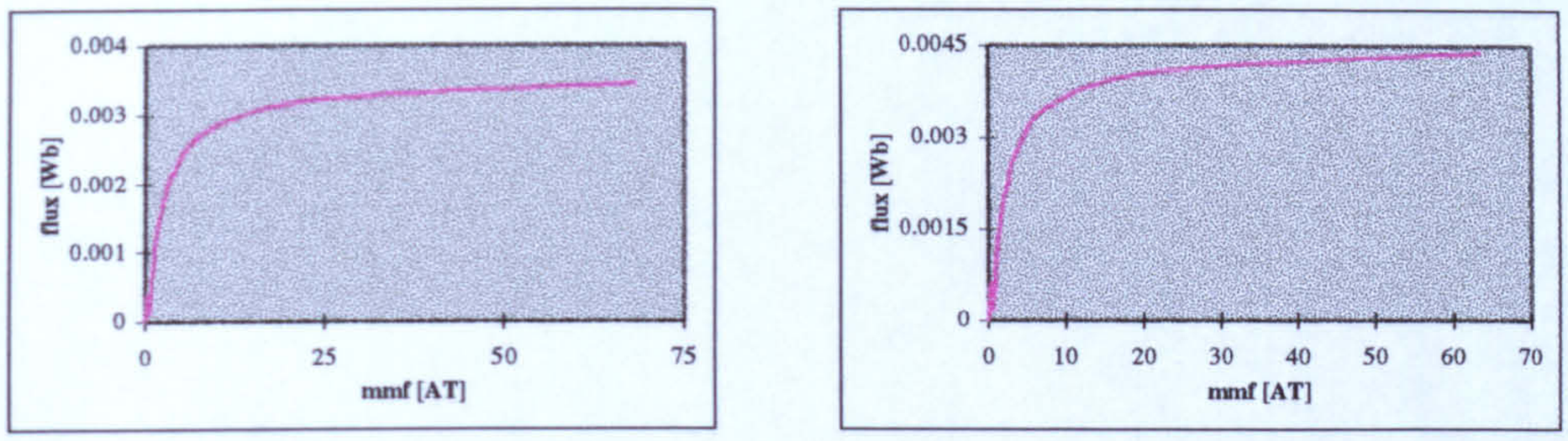

Figure 3.3 *flux-mmf curves for rotor teeth (left) and rotor core (right)*

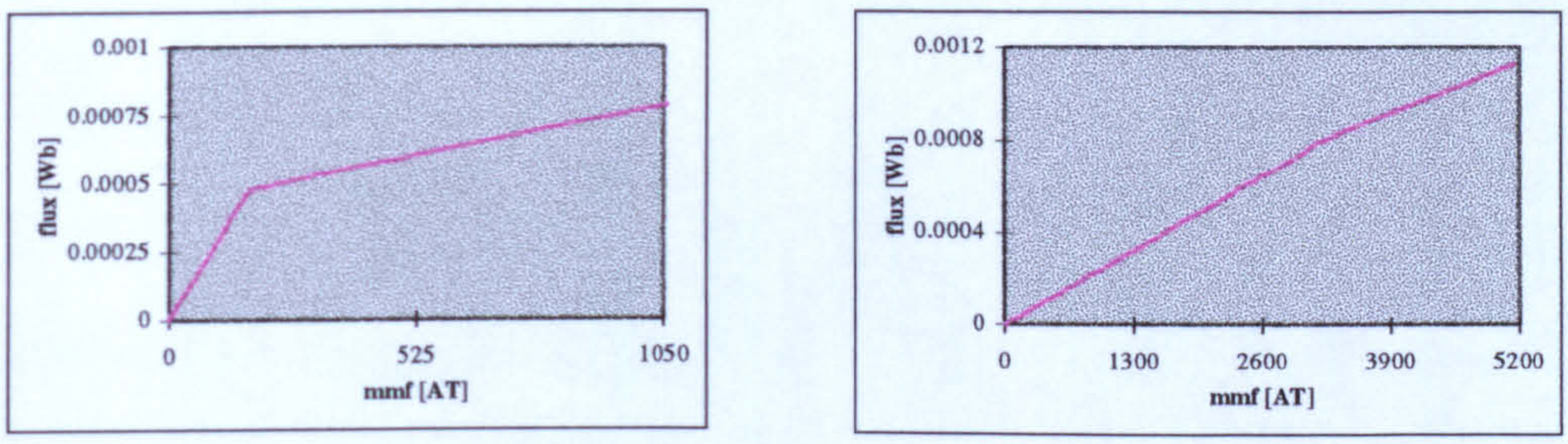

Figure 3.4 *flux-mmf curves for stator (left) and rotor(right) tooth-tips*

Figures 3.5 and 3.6 show a typical slot with its equivalent permeance elements.

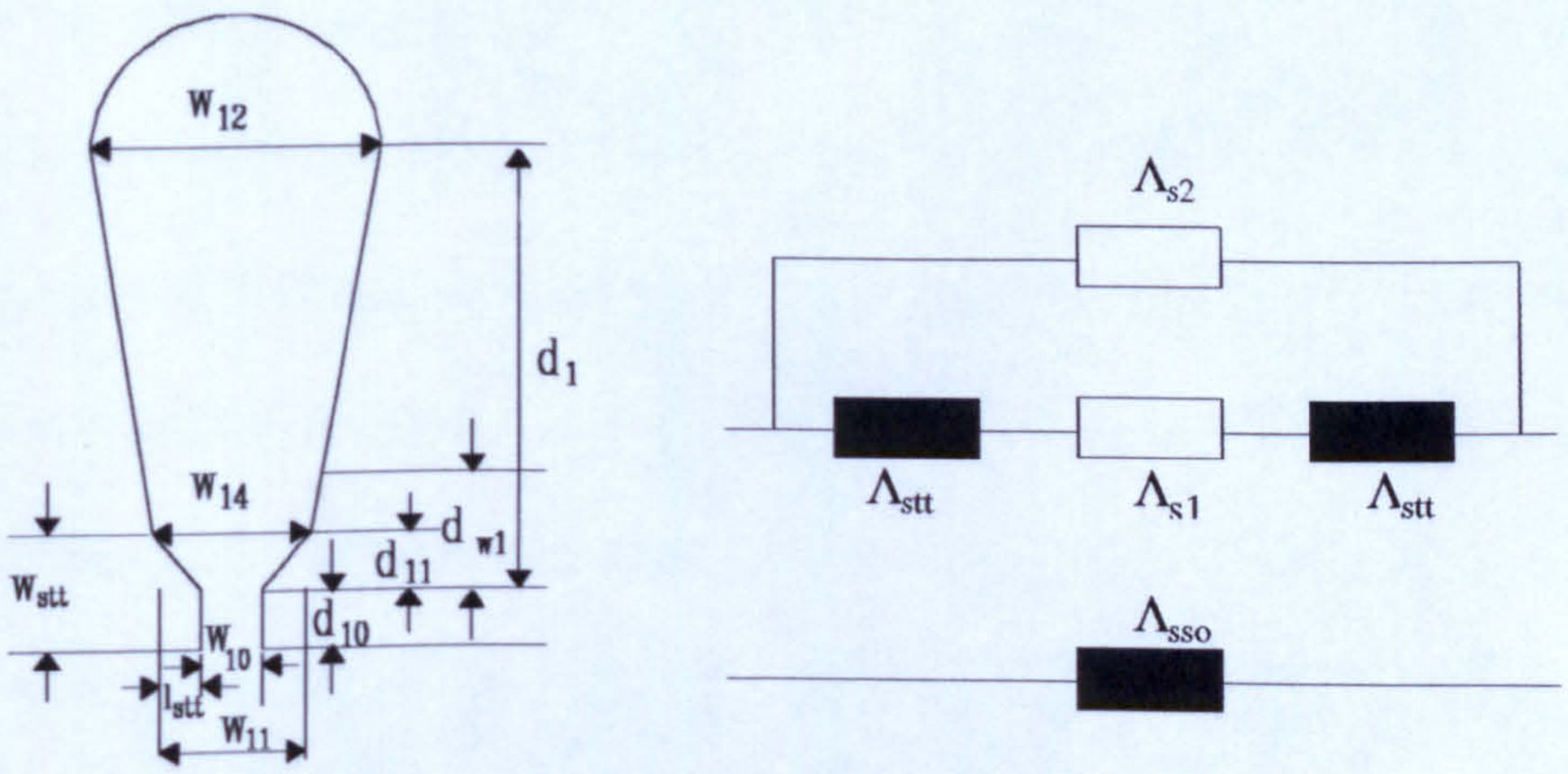

Figure 3.5 *Stator slot and tooth-tips equivalent permeance and physical dimensions.*

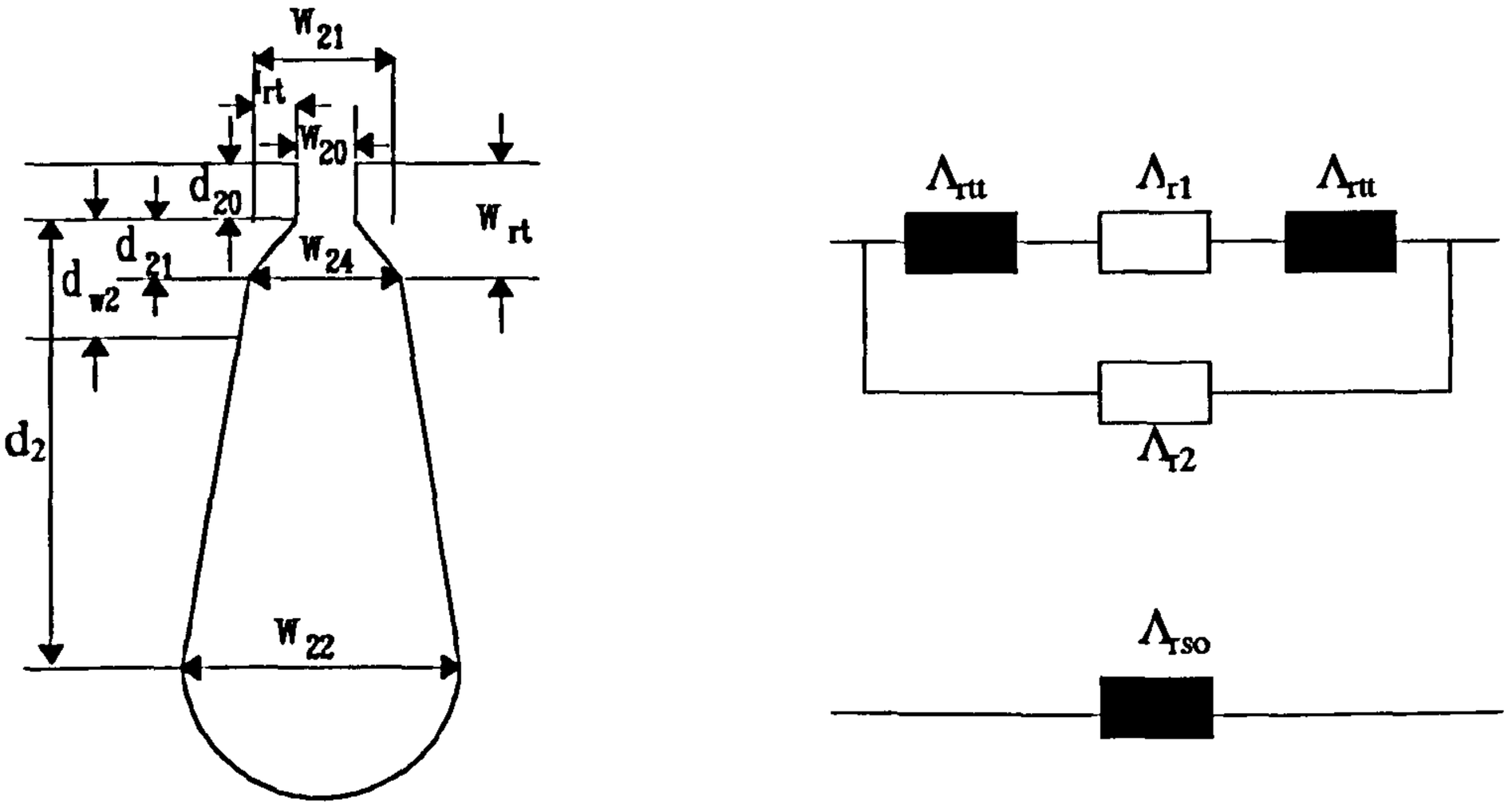

***Figure 3.6** Rotor slot and tooth-tips equivalent permeance and physical dimensions.*

The weighted normal slot leakage flux passing through the body of the slot passes through a permeance Λ_{s2} (Λ_{r2} for the rotor slot) in parallel with a three component permeance section representing the tooth tips Λ_{stt} (Λ_{rtt} for the rotor) which saturate and the slot opening Λ_{s1} (Λ_{r1} for the rotor) which is air. The equivalent permeance of the connection Λ_{sso} (Λ_{rso} for the rotor) is used in the model. To ease calculation this was represented as a curve of flux against the MMF drop across the element. The weighting factor for the slot permeance was chosen to provide the correct slot leakage inductance with the full slot conductors.

The tooth tip permeance model developed above causes errors in the flux paths in so far as the total equivalent flux crossing the body of the slot is assumed to pass down the total length of the teeth while in reality it causes a variation of flux density along those teeth. This is not normally a serious

problem in terms of saturation but could cause a small error in the calculation of the winding inductances due to the over estimation of the slot leakage inductance. Errors in leakage inductance will give rise to errors in the calculation of the winding current.

The airgap permeance is evaluated as a function of what is termed the overlap angle of tooth influence. Figure 3.7 shows one quarter of a cross-section through a wound rotor machine. In this figure the radial lines of intersection between two teeth on opposite sides of the gap are termed 'overlap angles'. The magnetic circuit is analysed over as many poles as are required for magnetic symmetry. For a healthy machine with balanced windings the problem may be simplified to the solution of less than a complete machine cross section. Depending on the symmetry half pole, 1 pole or a pole pair may be all that is required.

The angular positions of the i^{th} stator slot, assuming that the angle of the first stator slot coil side of the first group is zero, are given (in radians) by

$$\Theta_s[i] = (i-1)\cdot\frac{2\cdot\pi}{N_s} \qquad i = 1, 2, ..., N_s \tag{3.24}$$

At any rotor position, the angular position of rotor slots are a function of the rotor speed (ω_r). Assuming that the angle between the first rotor and stator slot coil sides of the first groups is $\omega_r t$, the angle of the i^{th} rotor slot is

$$\Theta_r[i] = \omega_r t + (i-1)\cdot\frac{2\cdot\pi}{N_r} \qquad i = 1, 2, ..., N_r \tag{3.25}$$

Having calculated the angular position of both stator and rotor slots, the 'overlap angles' can be found. These are defined as the angle between the centre of a slot on one member and the centre of the neighbouring slot on the opposite member.

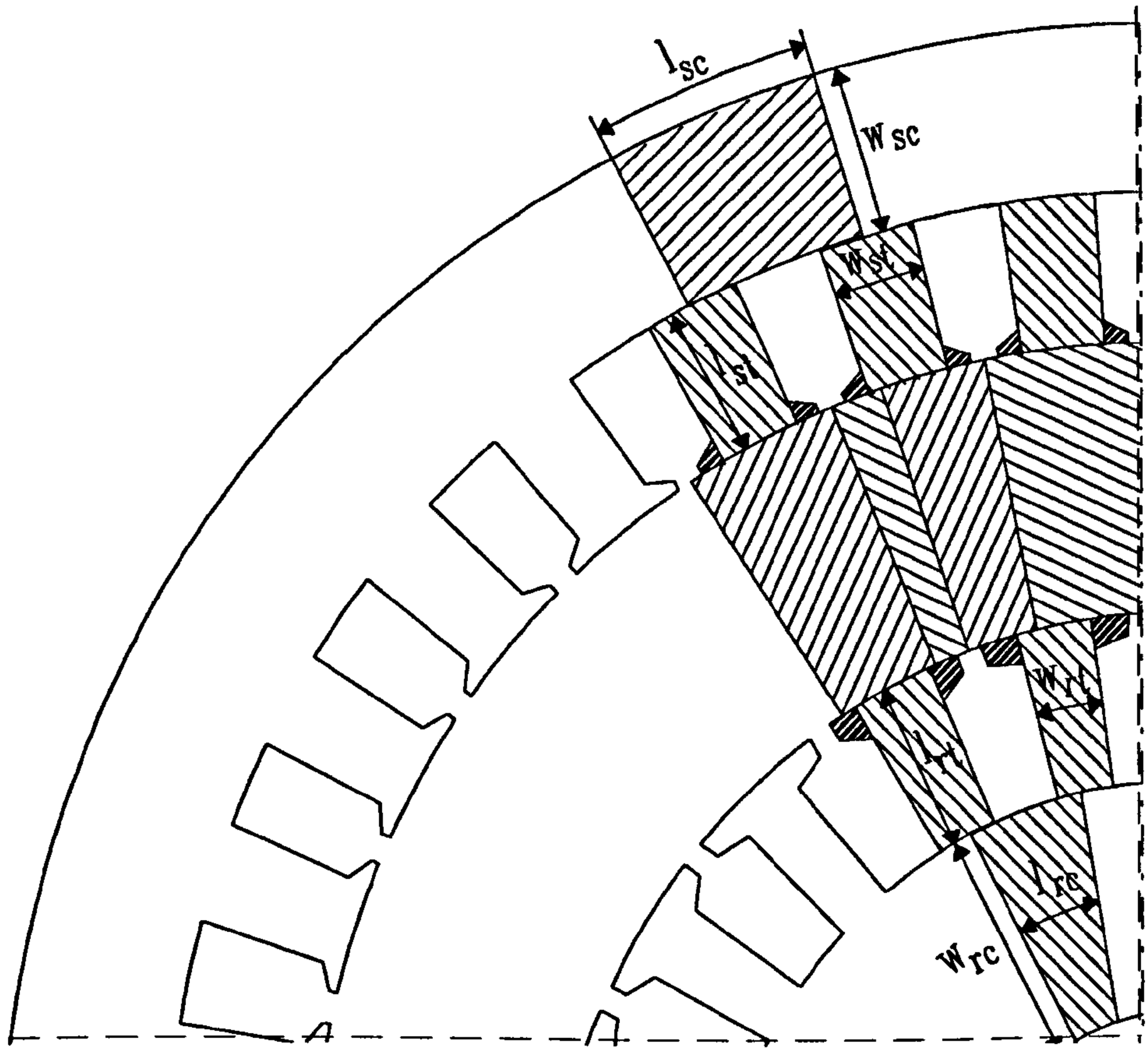

Figure 3.7 One quarter of a cross-section of an induction motor

The maximum number of these 'overlap angles' is equal to the total number of stator and rotor slots, that is N_s+N_r.

Knowing the angular position of the stator and rotor slots, the 'starts' and 'ends' of each slot on either side of the air gap are determined. Depending on

the number of slots on each member, two cases may occur as illustrated in Figure 3.8:

a) the stator slot pitch is greater than the rotor slot pitch.

b) the rotor slot pitch is greater than the stator slot pitch.

According to each case and to the relative position of the teeth on either side of the air gap, the 'overlap angles' are determined. This procedure is repeated for each rotor position. At a certain step it does happen that the 'start' of the last rotor tooth is less than the 'end' of the stator one and its 'end' is greater than the stator's one. In this case, the rotor tooth is split into two effective teeth and the same procedure is repeated as outlined above.

The 'overlap angles' are used to compute the airgap permeances as outlined in section 3.7.3. The magnetic circuit also includes the magnetomotive force (mmf) for both stator and rotor slots (which are outlined in section 3.8), and the permeances of the back iron, teeth and tooth-tips for both stator and rotor(which are explained in section 3.7.1).

To analyse the magnetic circuit shown in Figure 3.9, a set of equations was written to represent it. The derivation of this set of equations is based on Kirchoff's second law which states that the algebraic sum of the fluxes leaving a node is equal to the algebraic sum of those entering that node.

$$\sum \Lambda_{in} \cdot (F_n - F_i) = 0 \tag{3.26}$$

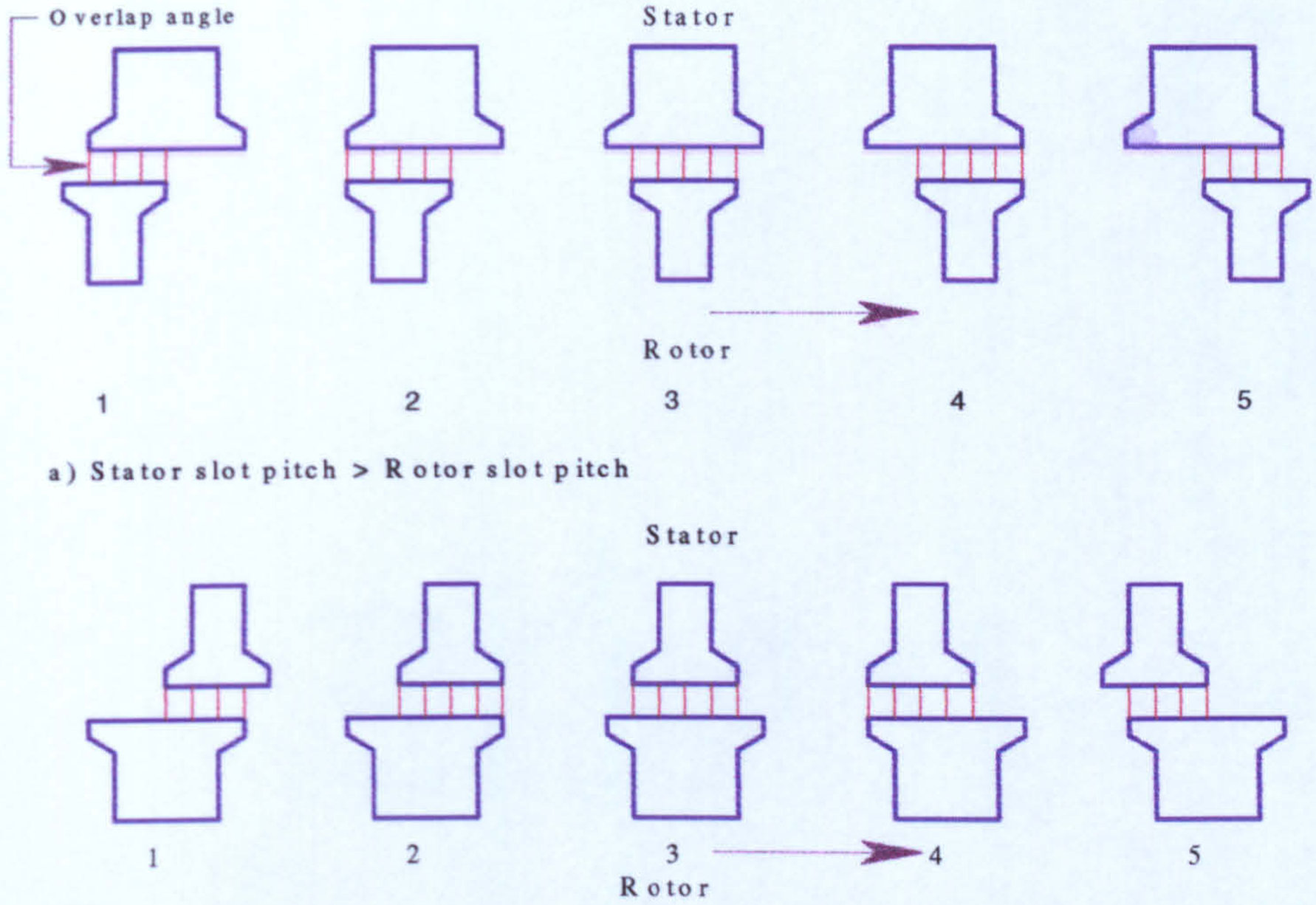

***Figure 3.8** Relative positions between stator and rotor teeth*

The equations are formed systematically using the incidence matrix approach by forming net lists defining the nodal connections of each elemental permeance. The resulting, non-linear equations were formulated in matrix terms. The number of these equations is equal to the number of nodes which is $2 \cdot (N_s + N_r)$. The number of equations does not change with rotor position unlike the equivalent mesh formulation.

In order to explain the method of deriving the non-linear system of equations, a part of the equivalent magnetic circuit which consists of four slots on the stator and three slots on the rotor has been considered, requiring 28 non-linear equations (Figure 3.10).

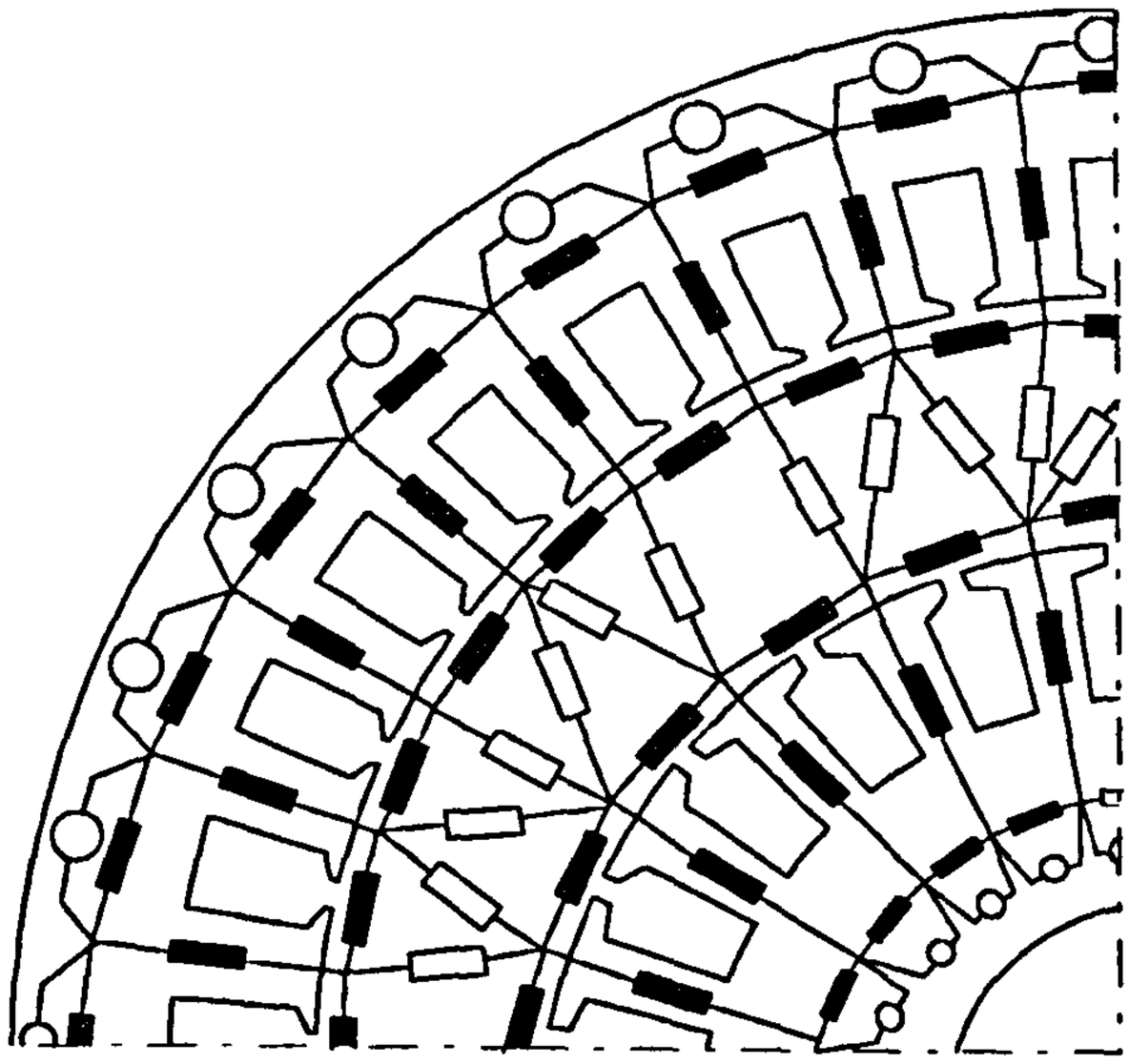

Figure 3.9 Equivalent magnetic circuit of Figure 3.7

The set of equations is as follows:

$$
\begin{aligned}
(\Lambda_{12}+\Lambda_{15}+\Lambda_{14})\cdot F_1 \;-\; \Lambda_{12}\cdot F_2 \;-\; \Lambda_{14}\cdot F_4 \;-\; \Lambda_{15}\cdot F_5 \;&=\; \phi_{s1}-\phi_{s4}\\
-\Lambda_{12}\cdot F_1 \;+\; (\Lambda_{12}+\Lambda_{23}+\Lambda_{26})\cdot F_2 \;-\; \Lambda_{23}\cdot F_3 \;-\; \Lambda_{26}\cdot F_6 \;&=\; \phi_{s2}-\phi_{s1}\\
&\cdots\cdots\\
-\Lambda_{1411}\cdot F_1-\Lambda_{1412}\cdot F_{12}-\Lambda_{1413}\cdot F_{13}+(\Lambda_{1411}+\Lambda_{1412}+\Lambda_{1413})\cdot F_{14} &= \phi_{s3}-\phi_{s4}
\end{aligned}
$$

in matrix form

$$[\Lambda_n]\cdot[F_n]=[\phi_s] \tag{3.28}$$

It is noted that

$[\Lambda_n]$ is a square matrix $2\cdot(N_s+N_r)\times 2\cdot(N_s+N_r)$

$[F_n]$ and $[\phi_s]$ are vectors $2\cdot(N_s+N_r)$

If [A] is the incidence matrix where its elements are defined as

$A_{ij} = 1$ if the j^{th} element is incident to and oriented away from the i^{th} node.

$A_{ij} = -1$ if the j^{th} element is incident to and oriented toward the i^{th} node.

$A_{ij} = 0$ if the j^{th} element is not incident to the i^{th} node.

$$[\Lambda_n] = [A]\,[\Lambda_b][A]^t \tag{3.29}$$

$$[F_b] = [A]^t[F_n] \tag{3.30}$$

therefore,

$$[\Phi_s] = [A]\,[\Lambda_b][F_b] \tag{3.31}$$

where $[A]^t$ is the transpose of [A]

In this equation the elements of $[\Lambda_n]$ depend on the elements of $[F_n]$ and the elements of $[\phi_s]$ depend on those of $[\Lambda_n]$. The solution of this equation is outlined in section 4.2.

3.7 MAGNETIC CIRCUIT PERMEANCES

As it has been mentioned in the previous section, in order to form the permeance matrix, one needs to compute the permeances of each element in the magnetic circuit.

The magnetic circuit portions considered, as shown in Figure 3.7, are:

a) stator core (back iron).

b) stator teeth.

c) stator tooth-tips.

d) stator slot openings.

e) airgap

f) rotor core (back iron).

g) rotor teeth.

h) rotor tooth-tips.

i) rotor slot openings.

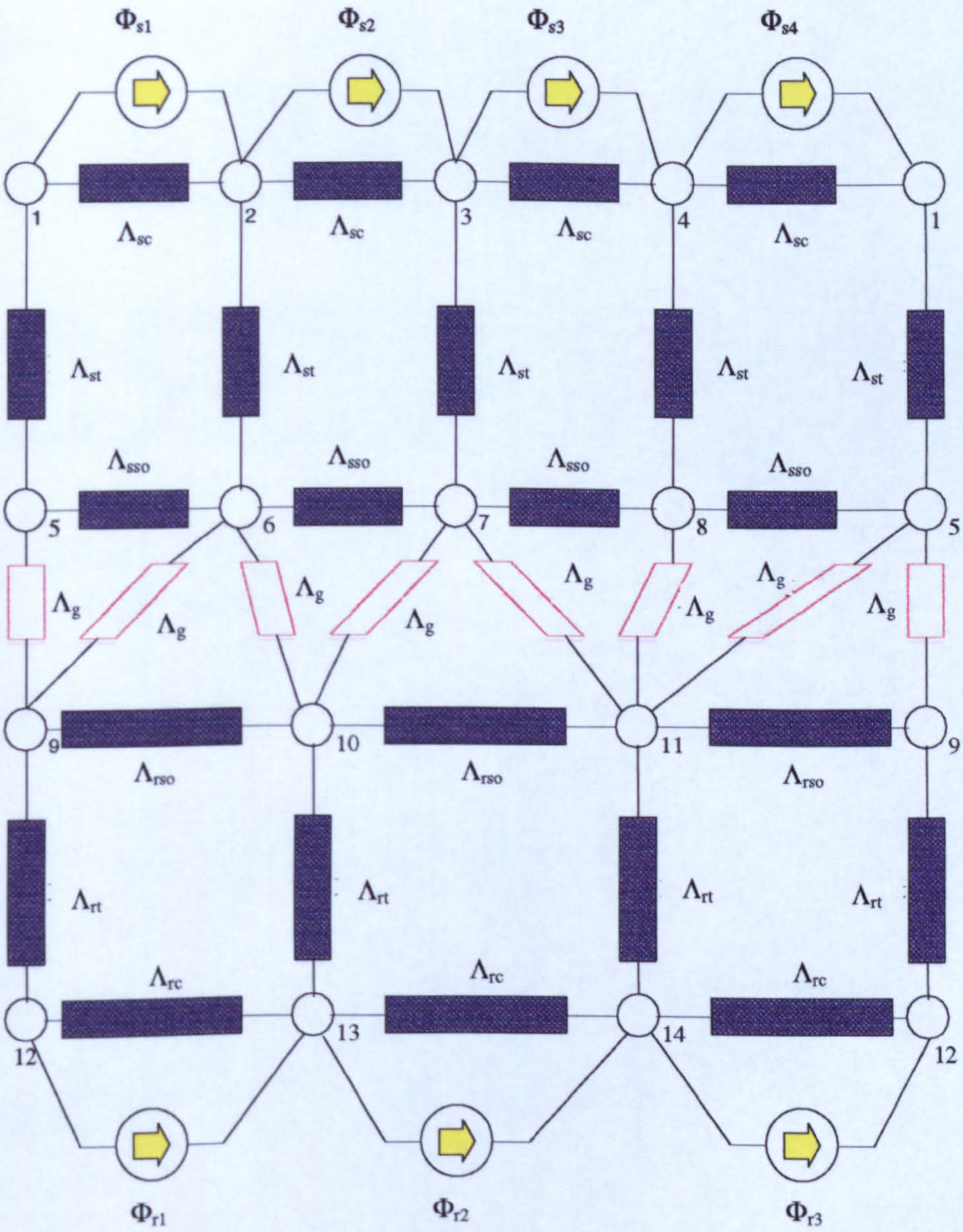

***Figure 3.10** Equivalent magnetic circuit for Ns=4 and Nr=3*

3.7.1 STATOR AND ROTOR CORES AND TEETH PERMEANCES

The permeance of the i^{th} element of the stator core is given, as a function of its permeability, by:

$$\Lambda_{cs}(i) = \mu_{cs}(i) \cdot \frac{W_{cs} \cdot L}{L_{cs}} \tag{3.32}$$

where L_{cs} is the average length of the stator core iron per slot pitch calculated from the average diameter between the bottom of the stator slot and the machine's outside diameter,

L is the core length,

W_{cs} is the width of the element of the stator core.

$$\mu_{cs}(i) = \frac{B(i)}{H(i)} \tag{3.33}$$

Replacing $\mu_{cs}(i)$ into (3.32) we get,

$$\Lambda_{cs}(i) = \frac{B(i)(W_{cs} \cdot L)}{H(i) \cdot L_{cs}} \tag{3.34}$$

thus,

$$\Lambda_{cs}(i) = \frac{\phi_b(i)}{F_b(i)} \tag{3.35}$$

where $\Phi_b(i)$ is the flux flowing in element i

$F_b(i)$ is the mmf drop in element i.

In the same way the stator teeth, rotor teeth and rotor core elemental permeances are written as:

$$\Lambda_{ts}(i) = \frac{B(i)\cdot(W_{ts}\cdot L)}{H(i)\cdot L_{ts}} = \frac{\Phi_b(i)}{F_b(i)} \tag{3.36}$$

$$\Lambda_{tr}(i) = \frac{B(i)\cdot(W_{tr}\cdot L)}{H(i)\cdot L_{tr}} = \frac{\Phi_b(i)}{F_b(i)} \tag{3.37}$$

$$\Lambda_{cr}(i) = \frac{B(i)\cdot(W_{cr}\cdot L)}{H(i)\cdot L_{cr}} = \frac{\Phi_b(i)}{F_b(i)} \tag{3.38}$$

$$\Lambda_{stt}(i) = \frac{B(i)\cdot[0.5\cdot(W_{stt}+d_{10})\cdot L]}{H(i)\cdot L_{stt}} = \frac{\Phi_b(i)}{F_b(i)} \tag{3.39}$$

$$\Lambda_{rtt}(i) = \frac{B(i)\cdot[0.5\cdot(W_{rtt}+d_{20})\cdot L]}{H(i)\cdot L_{rtt}} = \frac{\Phi_b(i)}{F_b(i)} \tag{3.40}$$

where the terms in the equations are defined in Figures 3.5 and 3.6 (slot dimensions).

3.7.2 SLOT LEAKAGE PATHS

The expressions for the semi-closed slot permeances (Λ_s and Λ_r) have been calculated by Angst [20] as shown in Equations (3.41) and (3.42) for the stator and the rotor respectively. Each is split into two parts. The first part is concerned with the slot openings while the second part is concerned with the lower slot portions.

$$\Lambda_s = K_s \cdot \left(\frac{d_{10}}{W_{10}} + \frac{2 \cdot d_{11}}{W_{10} + W_{11}} \cdot \left(1 + \frac{W_{11} - W_{10}}{20 \cdot W_{10}} \right) \cdot F_1 + \frac{d_{w1} - d_{11}}{W_{14}} \right) + \frac{(3 \cdot K_s + 1)}{4} \cdot \left(\frac{2 \cdot (d_1 - d_{w1})}{3 \cdot (W_{14} + W_{12})} \right) \cdot \sqrt{\frac{W_{12}}{W_{14}}} \quad (3.41)$$

$$\Lambda_r = \frac{N_s \cdot K_{ws}^2}{N_r \cdot K_{wr}^2} \left(K_r \cdot \left(\frac{d_{20}}{W_{20}} + \frac{2 \cdot d_{21}}{W_{20} + W_{21}} \cdot \left(1 + \frac{W_{21} - W_{20}}{20 \cdot W_{20}} \right) \cdot F_2 + \frac{d_{w2} - d_{21}}{W_{24}} \right) + \frac{(3 \cdot K_r + 1)}{4} \cdot \left(\frac{2 \cdot (d_2 - d_{w2})}{3 \cdot (W_{24} + W_{22})} \right) \cdot \sqrt{\frac{W_{22}}{W_{24}}} \right) \quad (3.42)$$

The meaning of the symbols are in Figures 3.5 and 3.6. The saturation factors and winding terms are put equal to unity as they are accounted for in other ways in the model. After simplification, the two part slot permeances will be as follows:

$$\Lambda_{s1} = \frac{d_{10}}{W_{10}} + \frac{2 \cdot d_{11}}{W_{10} + W_{11}} + \frac{d_{w1} - d_{11}}{W_{14}} \quad (3.43)$$

$$\Lambda_{s2} = \frac{2 \cdot (d_1 - d_{w1})}{3 \cdot (W_{14} + W_{12})} \cdot \sqrt{\frac{W_{12}}{W_{14}}} \quad (3.44)$$

$$\Lambda_{r1} = \frac{d_{20}}{W_{20}} + \frac{2 \cdot d_{21}}{W_{20} + W_{21}} + \frac{d_{w2} - d_{21}}{W_{24}} \quad (3.45)$$

$$\Lambda_{r2} = \frac{2 \cdot (d_2 - d_{w2})}{3 \cdot (W_{24} + W_{22})} \cdot \sqrt{\frac{W_{22}}{W_{24}}} \quad (3.46)$$

3.7.3 AIRGAP PERMEANCES

a) SLOTTING EFFECTS

Owing to the relatively small airgap in an induction motor, the slot opening has an appreciable effect on the magnetic flux in the airgap. However, the effect of a slot opening in term of disturbing the airgap field does not extend very far under a tooth since the semi closed slot openings considered in this thesis themselves are normally small compared to a tooth pitch. Open slots can be similarly accommodated but only if the slot pitch to airgap length ratio is large. The decrease in permeance can be regarded as an increase in the airgap length. For a single slot, Carter [91] derived his coefficient σ which could be used to calculate the airgap extension factor K_g. There are two approximations suggested by F.W. Carter [91] to calculate the airgap extension factor K_g for a doubly-slotted surface. These are:

$$K_g = K_{g1} \cdot K_{g2} \tag{3.47}$$

$$K_g = K_{g1} + K_{g2} - 1 \tag{3.48}$$

where

$$K_{g1} = \frac{\lambda_1}{\lambda_1 - \sigma_1 \cdot W_{10}} \tag{3.49}$$

$$K_{g2} = \frac{\lambda_2}{\lambda_2 - \sigma_2 \cdot W_{20}} \tag{3.50}$$

$$\sigma_1 = \frac{2}{\pi}\left\{A\tan\left(\frac{W_{10}}{2\cdot L_g}\right) - \frac{L_g}{W_{10}}\cdot\log\left(1+\left(\frac{W_{10}}{2\cdot L_g}\right)^2\right)\right\} \tag{3.51}$$

$$\sigma_2 = \frac{2}{\pi}\left\{A\tan\left(\frac{W_{20}}{2\cdot L_g}\right) - \frac{L_g}{W_{20}}\cdot\log\left(1+\left(\frac{W_{20}}{2\cdot L_g}\right)^2\right)\right\} \tag{3.52}$$

After consideration of the gap coefficients for 200 different sets of values of the variables $\frac{SSO}{L_g}, \frac{RSO}{L_g}$, LMDS (stator slot pitch) and LMDR (rotor slot pitch), Binns [92] has found that the equation

$$K_g = 0.5\cdot\left(K_{g1}\cdot K_{g2} + K_{g1} + K_{g2} - 1\right) \tag{3.53}$$

gave the resultant gap extension factor K_g to a very close approximation. Abdel-kader [72, 77] used the triangular approximation. In this thesis, the triangular wave approximation is used (see appendix B).

b) AIRGAP PERMEANCES

These are given as a function of overlap angles β, stack length L, airgap length L_g and K_g as follows,

$$\Lambda_g(i) = 4\pi\cdot 10^{-7}\cdot\frac{\beta(i)\cdot R_a\cdot L}{L_g\cdot K_g} \tag{3.54}$$

where β(i) overlap angle of element i

R_a airgap mean radius

L core length

L_g airgap length

K_g gap-extension factor

3.8 WINDING ARRANGEMENT AND MAGNETOMOTIVE FORCES

The operation of the machine depends primarily on the current distribution round the core surfaces, and the analysis of the winding is concerned only with this distribution. The detailed arrangement of the end connections is of secondary importance except for evaluation of end winding leakage inductance. Thus the general arrangement is the same for all types of machines.

In this work the mmfs in all slots were considered individually. By doing so the assumption that the airgap mmf wave is sinusoidally distributed in space was avoided. With known stator and rotor currents it is possible to calculate the instantaneous MMF per slot according to the winding arrangement.

3.8a STATOR MAGNETOMOTIVE FORCES

These were computed as in the example of a double layer winding for a two-pole, 24-stator slot, shown in Figures 3.11a and b for full pitch and chorded windings respectively.

If n : number of conductors per coil side.

N_s: number of slots.

i_a: instantaneous current in phase a.

i_b: instantaneous current in phase b.

i_c: instantaneous current in phase c.

q : number of slots per phase and per pole.

d_s: number of slots of chord.

For a full pitch winding,

$$\begin{aligned} F_i &= 2 \cdot n \cdot i_a && i = 1 \text{ to } q \\ F_i &= -2 \cdot n \cdot i_c && i = q+1 \text{ to } 2 \cdot q \\ F_i &= 2 \cdot n \cdot i_b && i = 2 \cdot q+1 \text{ to } 3 \cdot q \\ F_{i+3q} &= -F_i && i = 3 \cdot q+1 \text{ to } n_s \end{aligned} \tag{3.55}$$

For a chorded winding we then have,

$$\begin{aligned} F_i &= 2 \cdot n \cdot i_a && i = 1 \text{ to } q-d \\ F_i &= n \cdot (i_a - i_c) && i = q-d+1 \text{ to } q \\ F_i &= -2 \cdot n \cdot i_c && i = q+1 \text{ to } 2 \cdot q-d \\ F_i &= n \cdot (-i_c + i_b) && i = 2 \cdot q-d+1 \text{ to } 2 \cdot q \\ F_i &= 2 \cdot n \cdot i_b && i = 2 \cdot q+1 \text{ to } 3 \cdot q-d \\ F_i &= n \cdot (i_b - i_a) && i = 3 \cdot q-d+1 \text{ to } 3 \cdot q \\ F_{i+3q} &= -F_i && i = 1 \text{ to } 3 \cdot q \end{aligned} \tag{3.56}$$

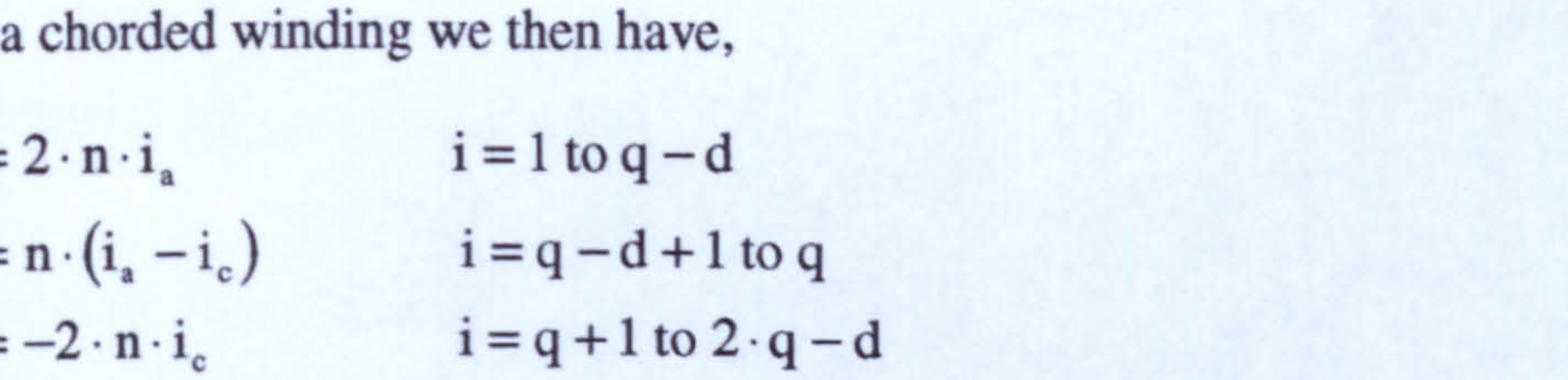

a) Chorded winding

b) Full pitch winding

Figure 3.11 *Double layer winding, two pole and 24 slots*

All that is required therefore to define the winding arrangement and mmf vector is simple winding data and current values. If $[A_w]$ is the winding matrix then,

$$[F_s] = [A_w]^t[I]^t \tag{3.57}$$

3.8b ROTOR MAGNETOMOTIVE FORCES

As it has been mentioned earlier, each rotor bar is considered as one phase. Therefore, the magnetomotive force of a phase is equal to the current flowing in that bar.

3.9 CONCLUSION

A time-stepped Magnetic Circuit technique for modelling transient and steady state performance of induction motors has been described theoretically. A number of simplifying assumptions necessary for a solution with reasonable computational time has been discussed then the method of analysis was presented. Therein we determined the performance equation along with the mechanical equation. Following that we showed how the transformer and rotational inductances necessary for the performance equation were determined from the saturated permeances. The determination of the latter was also presented by solving the non-linear circuit equations. We saw that at each instant t a Newton-Raphson procedure is used to compute the saturated permeances for the specified stator and rotor currents. The saturated solution is then used to compute the winding inductances and rotational inductances

which are then inserted into the circuit equations. These equations are then used to time step the winding currents forward using a numerical integration routine. The mechanical equation was also used so that the rotor can be moved to the appropriate angular position at the end of the time step. The new currents are then inserted into the windings at the new rotor position to provide the next magnetic circuit solution from which new inductance values are determined and inserted again into the circuit equations and this procedure is repeated.

It was also shown how this method is quite general and can be applied to wound and squirrel cage rotor induction machines. The windings can virtually have any configuration and the applied voltage can have any form. This model is capable of handling saturation, slotting, skew and relative position between stator and rotor slots effects. In the next chapter this method is more described as it is implemented on a digital computer.

CHAPTER FOUR

LOGIC OF COMPUTATION

4. LOGIC OF COMPUTATION

4.1 INTRODUCTION

In this chapter a description of the method of computation as it is used in the computer program is given. The steps followed here have already been explained in Chapter 3. The program is written in the form of procedures so that any change at any stage will not affect the whole program but only the part concerned and therefore the program can be improved and/or updated easily when required.

The main factor that limits the use of numerical field solution analysis methods in the routine calculation of electrical machines is the large amount of computation needed in the solution. Most of the simplifications discussed in Chapters 2 and 3 were made in order to decrease the computation time. As the use of a more precise method usually leads to longer solution times, a compromise between the accuracy and the solution time has to be made when choosing the method. In addition to this, the relatively long time constants associated with the windings of induction motors complicate the use of the step by step method in the simulation of steady state operation. If zero currents are used as the initial state, several periods of the line frequency have to be simulated before a steady state is reached. However, the results of the sinusoidal approximation can be used to find an initial state that is nearer to the steady state. The program is written so as to keep computer time and

storage as minimum as possible. The steps of computation can be divided into five main parts:

1. Solution of the magnetic circuit equations.
2. Calculation of the inductances.
3. Calculation of inductance variation with rotor position.
4. Torque equations.
5. Solution of performance equations.

These steps are shown in Figure 4.1 and will be explained in more details in the following sections.

4.2 THE SOLUTION OF THE MAGNETIC CIRCUIT EQUATION

This section represents a very important part of this chapter because of the importance of the nonlinearity of the elements of the magnetic circuit. Our objective is to compute the permeance matrix which will be used later in the calculation of the transformer and rotational matrix inductances which in their turn will be used in the solution of the performance equations of the electrical machine. The main steps involved are:

- Reading of the input data.
- Calculation of the magnetomotive forces.
- Calculation of the flux sources.
- Calculation of the injected flux sources at the nodes.
- Calculation of the permeances.
- Logic of solution of the non-linear equations.

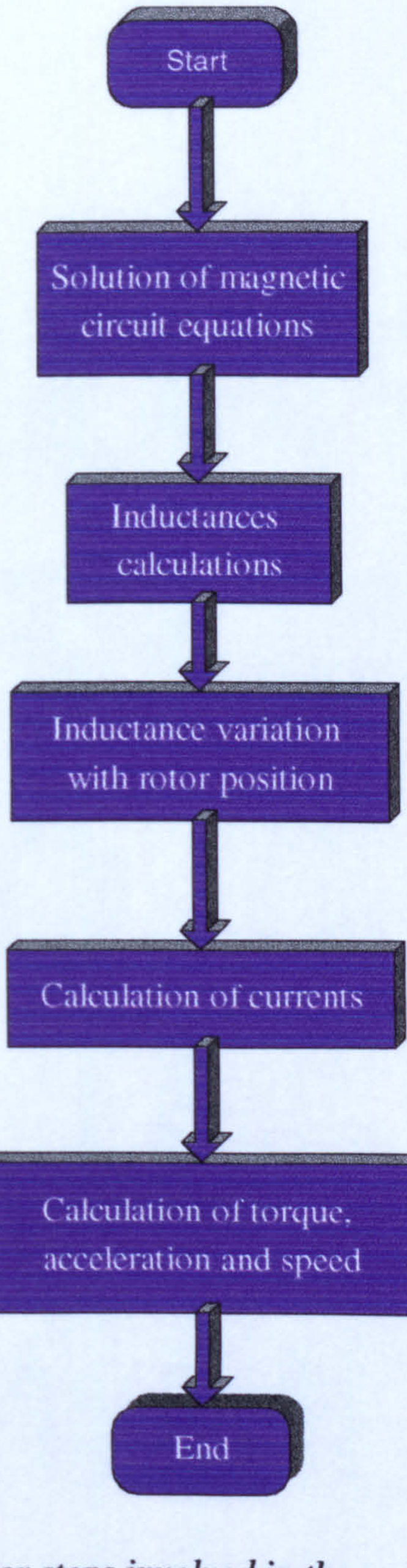

Figure 4.1 *The major steps involved in the method of computation*

4.2.1 INPUT DATA

The input data consists of :

a) Data relating to field and armature windings:

- Number of poles
- Number of stator slots
- Number of rotor slots
- Number of turns per coil
- The chording angle slots
- Applied voltage

b) Stator Laminations and slot dimensions

- Stator core length
- Stator external diameter
- Stator internal diameter
- Stator teeth length
- Stator teeth width
- Stator slot opening

c) Rotor Laminations and slot dimensions

- Rotor core length
- Rotor external diameter
- Rotor shaft diameter
- Rotor teeth length
- Rotor teeth width
- Rotor slot opening

and finally the airgap length.

4.2.2 CALCULATION OF THE MAGNETOMOTIVE FORCES

The magnetomotive force per slot is simply the sum of the ampere conductors per coil side contained in that slot. The ampere conductors of a coil side is equal to the number of conductors per coil side times the current flowing in that coil. These are computed using either the procedure ***SIXTY*** or ***TWENTY*** depending on the distribution of the winding. The procedure ***SIXTY*** is used for a 60 spread winding. Whereas for a 120 spread, the procedure ***TWENTY*** is used.

4.2.3 CALCULATION OF THE FLUX SOURCES

The flux sources follow automatically from the computation of the magnetomotive force per slot which were computed in the previous section. They are simply equal to the product of the latter and the permeance of the back iron element bounding that slot.

4.2.4 CALCULATION OF THE NODE INJECTED FLUXES

The injected node fluxes are straight forward. They are equal to the algebraic sum of the fluxes flowing into that node. These are achieved by the procedure ***FLUX***.

4.2.5 CALCULATION OF THE PERMEANCES

The permeance of each element is calculated as described in section 3.7. The permeances of the iron parts are computed by the procedure ***COREPERM***, whereas the airgap ones are obtained by the procedure ***GAPER***. And finally,

those of the slot opening and slot body are computed using the procedures ***OPENING*** and ***SLOTBODY*** respectively.

As we saw in Chapter 3, the permeance elements of the network have been evaluated as a series of curves from which values corresponding to particular saturation conditions and rotor positions can be determined. The curves are stored in a file as data points. The necessary interpolation between these points is performed by using the cubic spline technique which is briefly described in the following section.

4.2.6 CUBIC SPLINE INTERPOLATION

4.2.6.1 INTRODUCTION

In the case of approximations to iron characteristics, two separate curves were required, one for the permeance, the other for its derivative. Quadratic convergence would not be guaranteed unless the curves were at least once continuously differentiable. For characteristics ordinarily associated with saturable iron, the convergence rate can be quite sensitive to the consistency of the curves given for permeance and its derivative.

Using a divided difference approximation for the derivative is invariably not good enough. Therefore, the iron should preferably be characterised by a single very smooth curve, from which both the permeance and its derivative may be obtained simultaneously. These requirements appear to be well

satisfied, at low computational costs, if cubic splines are used to model the permeance characteristic.

4.2.6.2 METHODOLOGY

To obtain a cubic spline fit, the following requirements are imposed:

- The derivatives must be continuous at all segment end points, i.e. the first derivative at the extreme right of one segment must equal the value obtained at the extreme left of the adjoining segment.

- The curvature must be continuous at all segment end points; i.e. the second derivative evaluated at the extreme right of one segment must yield the same value as when evaluated at the extreme left of the adjoining segment.

- The slope at $\Phi = 0$ (or B=0), (left most point of left most segment), must be zero, i.e. permeance must be constant at very low fluxes (B).

- In the right most segment (which continues to infinite flux density) the slope is constant.

These requirements, expressed in the form of a system of simultaneous algebraic equations, uniquely determine all endpoint slopes if endpoint values, and the slope of the right most segment, are known. This infinite segment is absolutely essential in modelling because, as shown by Chari [93] and Anderson [94], a unique solution cannot be guaranteed unless the material

characteristic is monotonic for all values of B. Although in practical circumstances solutions beyond the curve are likely never to be encountered, trial flux densities during the first iteration or two may reach very high values, and lead to false solutions, unless this point is observed.

$$y_i = y(x_i) \qquad i = 1, 2, ..., N \tag{4.1}$$

Let us consider the interval $[x_j, x_{j+1}]$.

In this interval, linear interpolation gives

$$y = A \cdot y_j + B \cdot y_{j+1} \tag{4.2}$$

where

$$A = \frac{x_{j+1} - x}{x_{j+1} - x_j} \tag{4.3}$$

$$B = 1 - A = \frac{x - x_j}{x_{j+1} - x_j} \tag{4.4}$$

if we suppose we have also tabulated $y^{(2)}$, we next decide to use $y_j^{(2)}$ and $y_{j+1}^{(2)}$ as linear coefficients of two linearly independent cubic polynomial terms which will not spoil the agreement with the tabulated functional values y_j and y_{j+1}, for any choice of $y_j^{(2)}$ and $y_{j+1}^{(2)}$.

$$y = A \cdot y_j + B \cdot y_{j+1} + C \cdot y_j^{(2)} + D \cdot y_{j+1}^{(2)} \tag{4.5}$$

where

$$\begin{aligned} C &= \frac{1}{6} \cdot \left(A^3 - A\right) \cdot \left(x_{j+1} - x_j\right)^2 \\ D &= \frac{1}{6} \cdot \left(B^3 - B\right) \cdot \left(x_{j+1} - x_j\right)^2 \end{aligned} \tag{4.6}$$

$$\frac{d^2y}{dx^2} = A \cdot y_j^{(2)} + B \cdot y_{j+1}^{(2)} \tag{4.7}$$

therefore, $y^{(2)}$ is a tabulated second derivative and it is continuous. The first requirement is achieved by setting:

$$\frac{dy}{dx}\left(\text{for } x = x_j \in [x_{j-1}, x_j]\right) = \frac{dy}{dx}\left(\text{for } x = x_j \in [x_j, x_{j+1}]\right) \tag{4.8}$$

this leads to,

$$\frac{x_j - x_{j-1}}{6} \cdot y_{j-1}^{(2)} + \frac{x_{j+1} - x_{j-1}}{3} \cdot y_j^{(2)} + \frac{x_{j+1} - x_j}{6} \cdot y_{j+1}^{(2)} = \frac{y_{j+1} - y_j}{x_{j+1} - x_j} - \frac{y_j - y_{j-1}}{x_j - x_{j-1}} \tag{4.9}$$

these are N-2 linear equations in the N unknown $y_j^{(2)}$ j = 1,...,N. Therefore, there is a two parameter family of possible solutions. For a unique solution, we need to specify two further conditions, typically taken as boundary conditions at x_1 and x_N. The most common ways of doing this are:

1) the slope at the highest value is constant.

2) the slope at Φ=0 must be zero, i.e. permeance must be constant at very low fluxes.

The reason that cubic spline are especially practical is that the set of equations obtained, along with the two additional boundary conditions, are not only linear, but also tridiagonal. Each $y_i^{(2)}$ is coupled only to its nearest neighbours at i±1. Therefore, the equations can be solved in N operations by the tridiagonal algorithm.

As the permeance of the iron part is a function of the flux density in the element which is highly non-linear, iterations are, therefore, necessary to obtain the correct results. Care must be taken to ensure the iterations converge, especially, at the first step in the time solution.

4.2.7 LOGIC OF SOLVING NON-LINEAR EQUATIONS

The basic equation given in Chapter 3 (equation 3.15) describes a magnetic circuit defining a magnetic field problem. $[\Phi_s]$ is a source vector containing fixed flux sources. $[\Lambda]$ is the permeance matrix which is a function of the network fluxes. [F] are the magnetic potentials of the network nodes. For the network, these will only be one value of $[\Lambda]$ and [F] for each $[\Phi_s]$ and since $[\Lambda]$ is a function of $[\Phi]$ then an iterative procedure is required to find $[\Lambda]$.

The procedure adopted is the Newton-Raphson method because of its quadratic convergence. An initial guess is made at [F] termed $[F]_0$. From this value of [F], the mmf drop across each branch $[F_b]$ is determined by subtracting the mmf at the source node from that at the sink node. The branch permeance and incremental permeances are then derived from curves of branch flux against branch mmf (stored in the computer using cubic splines interpolation). From this, $[\Lambda]_0$ and $[\Lambda]_0^{inc}$ are formed. It is unlikely that with this first guess that

$$[\Phi_s]-[\Lambda]_0\cdot[F]_0=0 \qquad (4.10)$$

The nonzero result of this flux equation can be viewed as an excess of flux.

Thus,

$$[\Phi]_{excess} = [\Phi_s] - [\Lambda]_0 \cdot [F]_0 \tag{4.11}$$

The incremental permeance matrix may then be used to locate an improved value of [F]. The excess mmf required is found from,

$$[F]_{excess} = \left([\Lambda]_0^{inc}\right)^{-1} \cdot [\Phi]_{excess} \tag{4.12}$$

Finally, the new improved guess $[F]_1$ is found from,

$$[F]_1 = [F]_0 - [F]_{excess} \tag{4.13}$$

or

$$[F]_1 = [F]_0 - \left([\Lambda]_0^{inc}\right)^{-1}\left([\Phi_s] - [\Lambda]_0 \cdot [F]_0\right) \tag{4.14}$$

or in general,

$$[F]_{n+1} = [F]_n - \left([\Lambda]_n^{inc}\right)^{-1}\left([\Phi_s] - [\Lambda]_n \cdot [F]_n\right) \tag{4.15}$$

The criteria for convergence is based on the Euclidean Norm of the excess nodal fluxes $[\Phi]_{excess}$. Care must be taken to ensure the iterations converge, especially, for the first time step. In the computer program this is achieved by the procedure ***NEWTON*** within which the procedure ***EUCLID*** is called along with ***COREPERM*** (for core permeances computation),and ***GAPER*** (for airgap permeances computation) as mentioned in the previous section. This is shown in Figures 4.2 a and b :

4.3 CALCULATION OF THE INDUCTANCES

The self and mutual inductances vary with saturation, rotor position and airgap geometry. They are calculated from the flux linkages of each winding due to the other windings excited alone in turn. Once the saturated conditions have been determined, to ensure that the principle of superposition can be applied to the magnetic circuit, the saturated permeance of the magnetic elements are kept unchanged. They are calculated as follows:

1) Determine the magnetic fluxes at a particular rotor position at the appropriate saturation levels and currents. This produces a unique matrix [Λ].

2) The winding under consideration is fed with 1A, while the other windings are left open circuit and [Λ] is unchanged.

3) Determine the magnetic fluxes for the particular rotor position corresponding to the 1A excitation.

4) Multiply the magnetic fluxes by the number of turns they link to evaluate the flux linkage for each slot.

5) Sum up the flux linkage for those slots that belong to the excited phase winding to form its self inductance. The mutual inductances between that phase and other phases, on the stator and rotor are formed by summing the flux linkages for the remaining phases.

To ease the explanation of the process it is convenient to assume that both rotor and stator are fitted with Gamme Ring windings. Thus the stator slots

have their return conductors located outside of the stator core. Similarly, the rotor return conductors which have no finite size, can be considered to pass down an infinitely small hole through the rotor shaft.

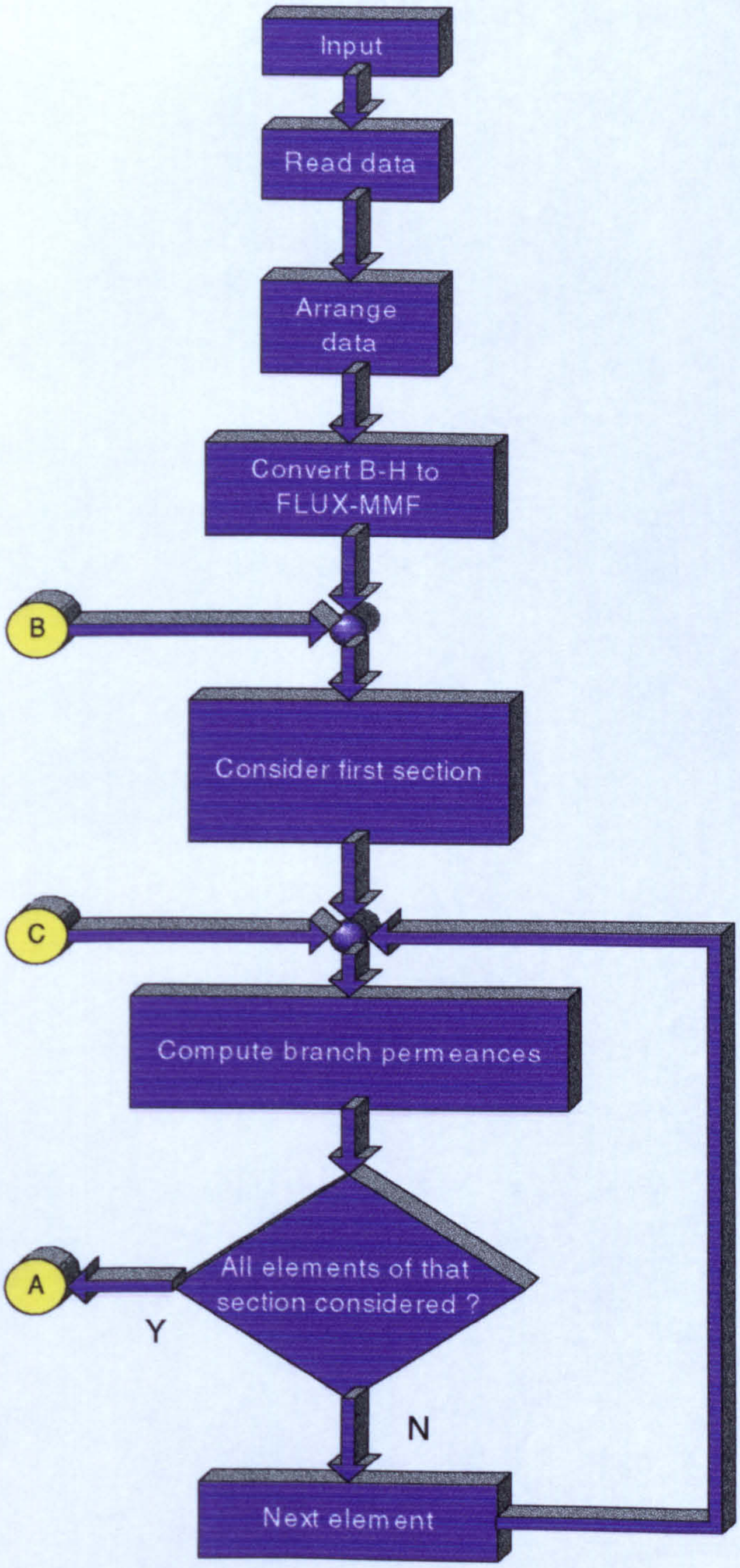

***Figure 4.2 a** Solution of non-linear equations*

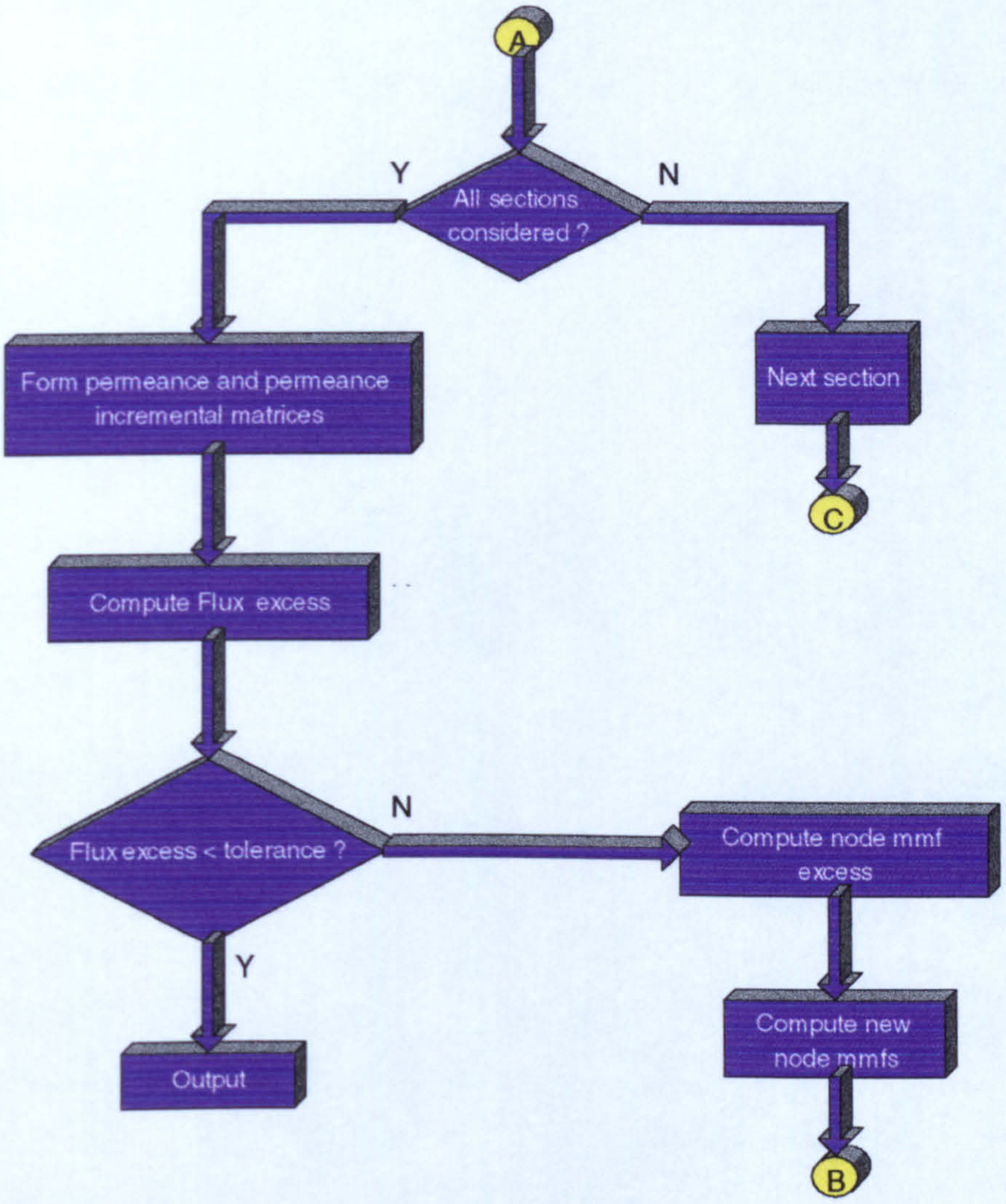

***Figure 4.2 b** Solution of non-linear equations continued...*

With Gamme Ring windings these return conductors form no real purpose and are excess to requirements.

This is clearly seen from the fact that the sum of the currents passing down this infinitely small hole in the rotor shaft is zero.

However, the concept of the Gamme Ring winding makes it easy to see that the flux linking the conductors in a stator slot is just that flux passing through

the core section behind the slot under consideration. Similarly, the flux linking a rotor slot is the flux passing through the rotor core section behind that slot.

The infinitely small hole in the rotor shaft which forms the return path for the Gamme Ring conductors should pass down the effective magnetic neutral of the machine. In this case the hole is down the centre of the reference node of the equivalent magnetic network.

This model is capable of calculating all of the normal leakage fluxes associated with induction machines. That is, slot leakage, phase-belt leakage, skew leakage and differential harmonic leakage. However, the end-winding leakage is not evaluated at all and therefore has to be determined for each winding and then added to the self inductance for that winding.

For more details see Figures 4.3 a and b.

4.4 INDUCTANCE VARIATION WITH ROTOR POSITION

The variation of inductance with rotor position is determined by subtracting two sets of inductances evaluated under the same saturation conditions but where the rotor displacement differs by a small angle $d\Theta_r$. The result is then divided by this small angle.

The inductance matrices are evaluated in the same way as for the incremental inductances. However, it is not necessary for the end winding

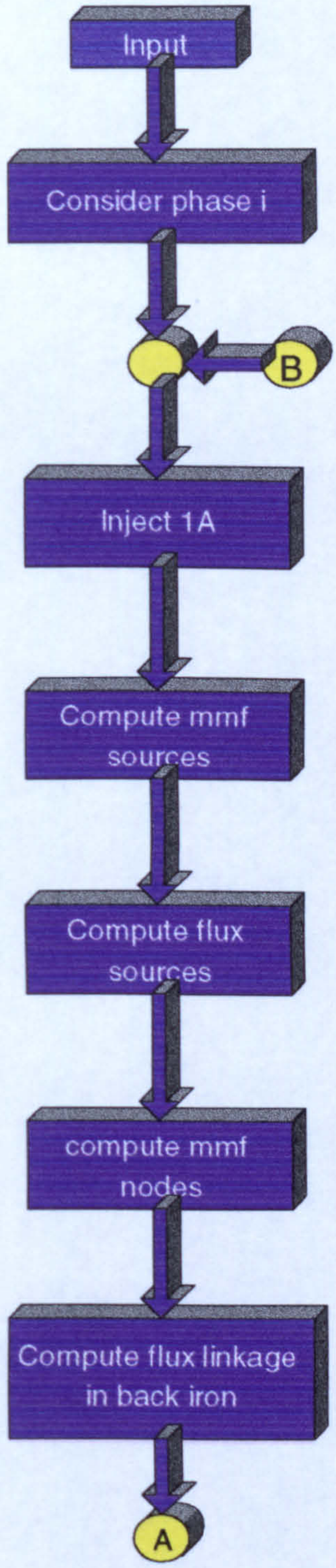

***Figure 4.3 a** Logic of computation of inductances*

leakage to be included in the calculation process since this is assumed to be independent of the rotor's angular position relative to the stator to a first approximation. The flow chart in Figure 4.4 illustrates this computation.

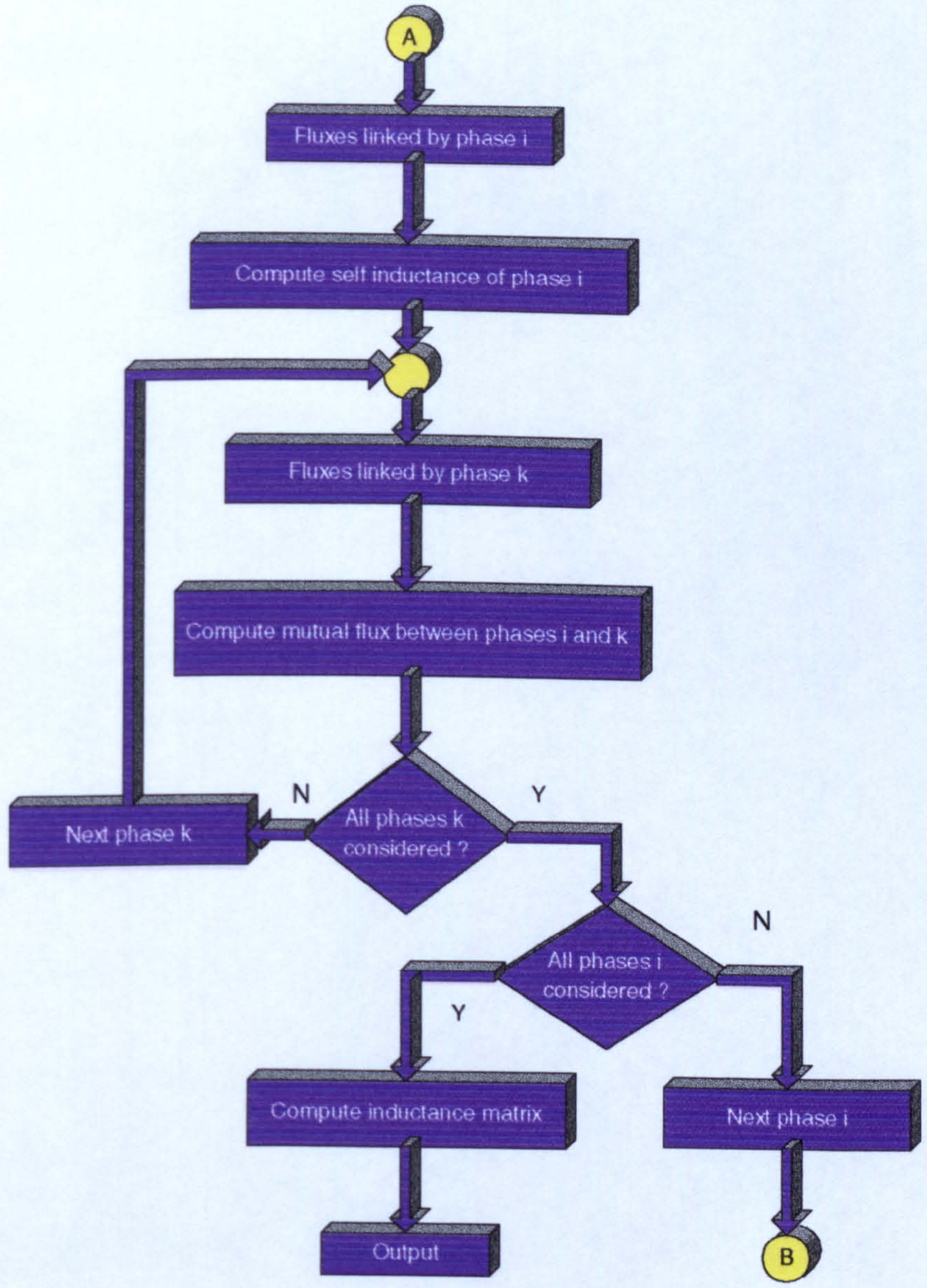

***Figure 4.3 b** Logic of computation of inductances continued...*

4.5 SOLUTION OF PERFORMANCE EQUATION

The performance equations of the electrical machine are given in chapter 3.

There are several numerical methods which can be used to solve these differential equations. Both the simple Euler, Adams and The 4^{th} order Runge Kutta methods were employed. Satisfactory results were obtained with either technique though accuracy would be expected from the Runge Kutta method but as this requires four derivatives, a much greater time is required to get a solution.

4.5.1 SOLUTION OF DIFFERENTIAL EQUATIONS

4.5.1.1 INTRODUCTION

Differential equations are often not solvable analytically. In such cases, a numerical solution is required and consequently, it is prone to errors.

A method is said to be stable if small errors die out after many steps, and unstable if they grow after many steps. Thus, methods for solving differential equations must be evaluated with respect to three properties:

- The truncation error generated per step of the method, that is, the error due to the fact that we are using a finite step rather than an infinitesimal step dt or, equivalently, to the fact that we are truncating an infinite series.
- The propagated error properties or stabilities of the method.
- The amount of computational error generated when executing a step of the method.

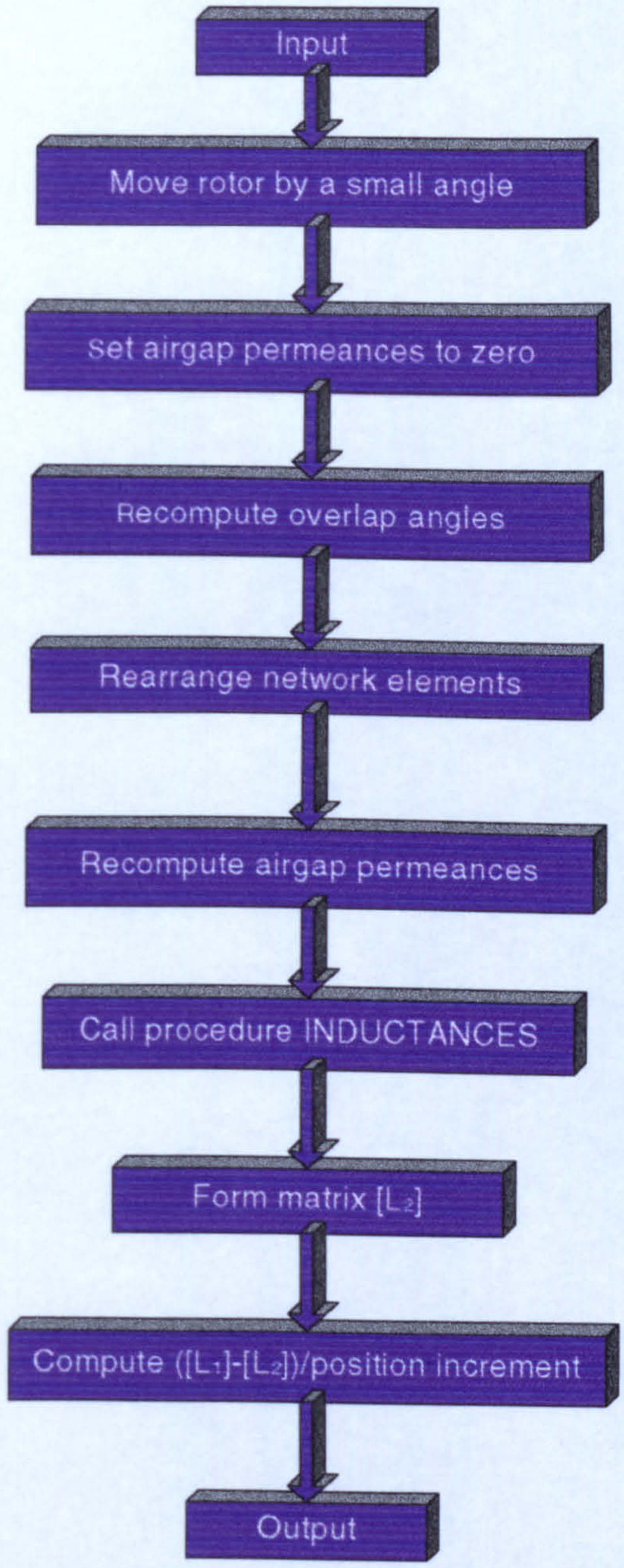

***Figure 4.4** Logic of computation of inductance variation with rotor position*

4.5.1.2 EULER'S METHOD

It is the method which moves from step to step to give the computed value of

Y_{i+1} given Y_i using the equation:

$$Y_{i+1} = Y_i + dt \cdot F(X_i, Y_i) \tag{4.16}$$

Graphically, it can be interpreted as moving a step-length dt from Y_i in the direction of the tangent to Y(X) at X_i.

4.5.1.3 MULTISTEP PREDICTOR CORRECTOR METHODS

Studies have shown that methods with error of order 5 or 6 in dt provide the best compromise between method complexity and truncation-error size. To produce predictor-corrector methods of this order without using derivatives higher than the first, we must use points previous to X_{i-1} in the extrapolation formula. Amongst these methods we have Adams-Bashforth predictor,

$$Y_{i+1(p)} = Y_i + \left(\frac{dt}{24}\right)\cdot\left(55\cdot Y_i^{(1)} - 59\cdot Y_{i-1}^{(1)} + 37\cdot Y_{i-2}^{(1)} - 9\cdot Y_{i-3}^{(1)}\right) \tag{4.17}$$

and Adams-Moulton corrector,

$$Y_{i+1(c)} = Y_i + \left(\frac{dt}{24}\right)\cdot\left(9\cdot Y_{i+1}^{(1)} + 19\cdot Y_i^{(1)} - 5\cdot Y_{i-1}^{(1)} + Y_{i-2}^{(1)}\right) \tag{4.18}$$

with an automatic error estimate,

$$e_{i+1(c)} = \left(\frac{19}{270}\right)\cdot\left(Y_{i+1(c)} - Y_{i+1(p)}\right) \tag{4.19}$$

Furthermore, we can mop up the truncation error $O(dt^6)$ by the formula,

$$Y_{i+1(m)} = \frac{\left(251\cdot Y_{i+1(c)} + 19\cdot Y_{i+1(p)}\right)}{270} \tag{4.20}$$

The Adams method, made up of the above predictor, corrector, and mop-up, is relatively stable. Lapidus and Seinfeld [95] compare this method to other predictor-corrector methods with fifth-order error initially and sixth-order

error after mop-up, and conclude that the Adams method is the best general-purpose method.

The Adams method requires X_0, X_1, X_2, and X_3 to get started. To compute X_1, X_2 and X_3, we need a method which has fifth-order or sixth-order error and which does not use any points preceding the current point X_i. In the following section, we describe a method such as we require.

4.5.1.4 RUNGE KUTTA METHODS

A self-starting method that has error of order 5 in dt and does not use derivatives higher than the first is required. To achieve these goals, more points than just X_i must be used but preceding points are not allowed. An approximate to the integral $Y(X)^{(1)} \cdot dt = dt \cdot Y_{avi}^{(1)}$ is sought. To compute $Y_{avi}^{(1)}$, there must be values of $Y^{(1)}$ at values of X symmetrically distributed across $[x_i, x_{i+1}]$. At the start there will be only Y(X). To obtain a better estimate of the average slope, the first step should to predict the slope at the midpoint of the interval.

$$Y_{i+\frac{1}{2}(1)} = Y_i + \frac{dt}{2} \cdot f(X_i, Y_i) \tag{4.21}$$

given this estimate of $Y_{1+\frac{1}{2}}$, $f\left(X_{i+\frac{1}{2}}, Y_{i+\frac{1}{2}(1)}\right)$ is a better estimate than $Y_i^{(1)}$ of the average slope in the interval. This average slope estimate can be used to obtain an even better estimate of the slope at $X_{i+\frac{1}{2}}$,

$$Y_{i+\frac{1}{2}(2)} = Y_i + \frac{dt}{2} \cdot f\left(X_{i+\frac{1}{2}}, Y_{i+\frac{1}{2}(1)_i}\right) \tag{4.22}$$

Using this value, an improved estimate of the average slope can be computed, with which over a whole interval it is possible to compute an estimate for Y_{i+1}:

$$Y_{i+1(1)} = Y_i + dt \cdot f\left(X_{i+\frac{1}{2}}, Y_{i+\frac{1}{2}(2)_i}\right) \tag{4.23}$$

This estimate of Y_{i+1} has truncation error of order 3 in dt. Mopping up with the 4 estimated values $\left(Y_i^{(1)}\right)$, $Y_{1+\frac{1}{2}(1)}$, $Y_{i+\frac{1}{2}(2)}$ and $Y_{i+1(1)}$, thereby computing a final estimate for the average slope,

$$Y_{avi}^{(1)} = K_1 \cdot f(X_i, Y_i) + K_2 \cdot f\left(X_{i+\frac{1}{2}}, Y_{i+\frac{1}{2}(1)}\right) + K_3 \cdot f\left(X_{i+\frac{1}{2}}, Y_{i+\frac{1}{2}(2)}\right) + K_4 \cdot f\left(X_{i+1}, Y_{i+1(1)}\right) \tag{4.24}$$

and thus, a final estimate for Y_{i+1},

$$Y_{i+1} = Y_i + dt \cdot Y_{avi}^{(1)} \tag{4.25}$$

The weights K_1, K_2 and K_3 are chosen to maximise the order of dt in the truncation error of the method. The result is $K_1 = 1/6$, and $K_2 = K_3 = 1/3$. The resulting, truncation error is $O\left(dt^5\right)$. Generally, these Runge-Kutta methods have the following properties:

- They are quite stable.
- They are quite time consuming.
- They are self starting.
- They do not provide automatic error estimation.

The Runge-Kutta methods are not uncommonly used, especially for computing starting values and required mid-interval values for predictor-corrector methods and in cases where stability or storage requirements are the dominant issues. However, because of the inefficiency of the Runge-Kutta methods, the high quality of the Adams predictor-corrector method (even though it is quite as stable as the Runge-Kutta methods), and the automatic error estimation capability of the Adams method, the latter is more popular. In fact, the Adams method, augmented by a Runge-Kutta method to compute starting values and required mid-interval values, is the most commonly used method for solving first-order ordinary differential equations in one unknown.

The flow chart for the performance equation calculations is shown in Figures 4.5 a and b. All that is required is for the independent variables, that is the voltage waveforms applied to the electrical terminals of the machine and the torque applied to the mechanical terminal, to be defined as a function of time.

One of the advantages of this method is that there is no restriction on the waveform of the supply voltage and therefore it can be used with any configuration of terminal voltages. Since variable speed drives are more and more often constructed using cage induction motors supplied by static frequency converters which increase the noise level of the motor, and introduce pulsations in the torque which this method is capable of modelling.

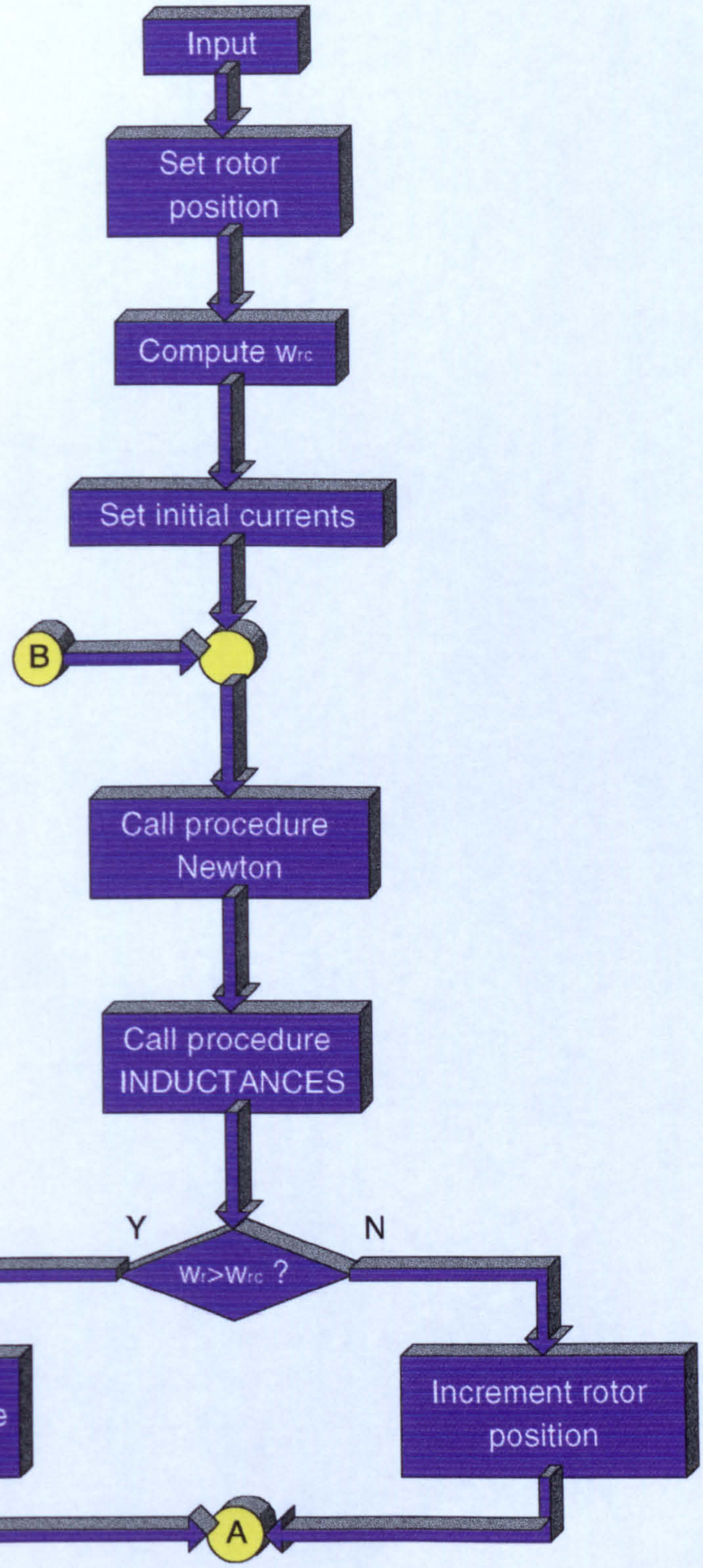

Figure 4.5 a *Performance equations calculation*

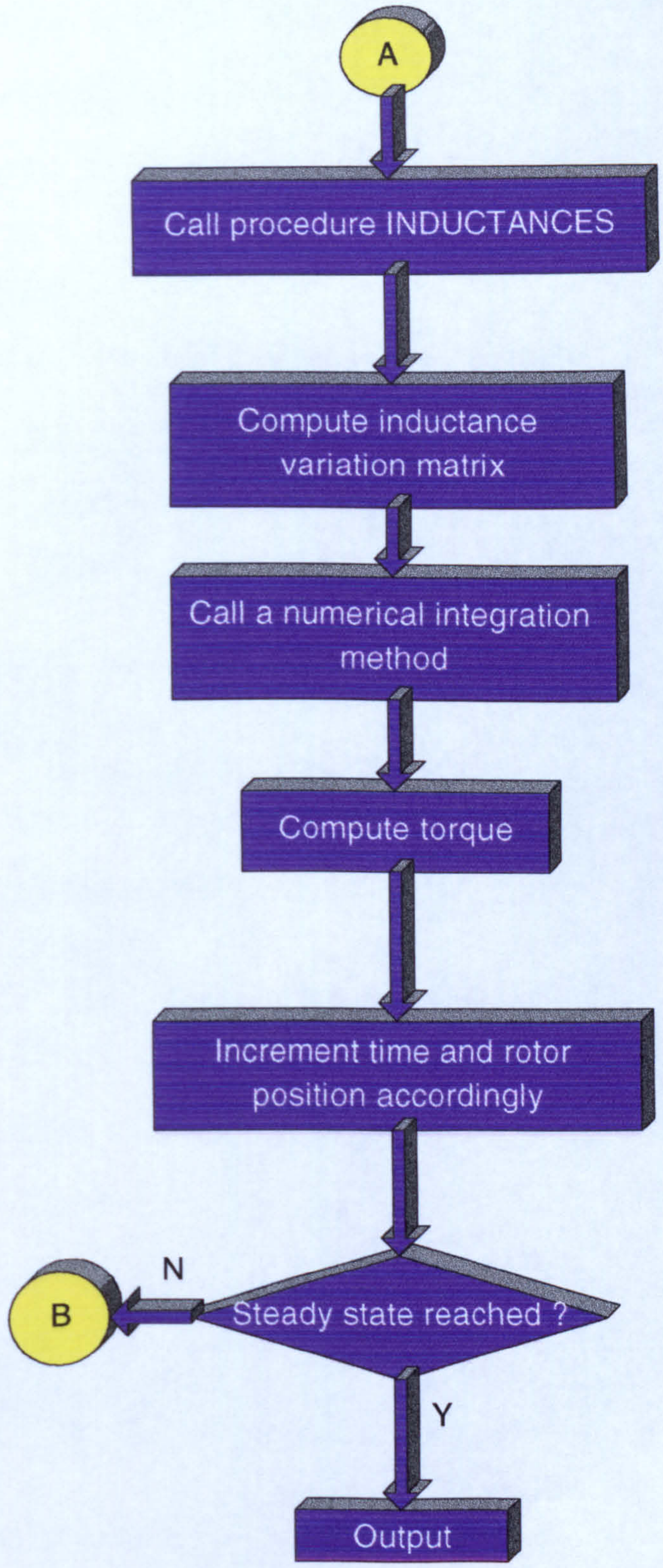

***Figure 4.5 b** Performance equations calculation continued....*

Therefore a supply from a PWM inverter can be used in the simulation. For this purpose, a procedure for PWM waveform generation has been developed.

4.6 INVERTER SIMULATION

In the simulation of the PWM inverter output a Natural Sampling Switching strategy was used. Natural Sampling is an analogue and outdated method of PWM generation. The mere reason for its use in this work is its simplicity and ease of implementation in the computer program. In order to generate the switching signals, a control signal V_c at the desired frequency, amplitude and phase is compared with a repetitive switching frequency triangular waveform as shown in Figure 4.7. The frequency of the triangular waveform establishes the inverter switching frequency and is generally kept constant along with its amplitude V_t. Let f_s be the switching of the triangular waveform (called carrier frequency) and V_c the control signal used to modulate the switch duty ratio and has a frequency f_1 (called the modulating frequency) which is the desired fundamental frequency of the inverter voltage output. The amplitude modulation ratio is defined as

$$m_a = \frac{\hat{V}_c}{\hat{V}_t} \tag{4.26}$$

The frequency modulation ratio is defined as

$$m_f = \frac{f_s}{f_1} \tag{4.27}$$

The inverter switches in Figure 4.6 are controlled based on the comparison of V_t and V_c. At any instant in time the PWM wave is high if the carrier wave is lower than the modulating wave and the output voltage is

$$\begin{aligned} &v_c > v_t, \qquad T_{A+} \text{ is on}, \qquad v_{Ao} = \frac{V_d}{2} \\ &v_c < v_t, \qquad T_{A-} \text{ is on}, \qquad v_{Ao} = -\frac{V_d}{2} \end{aligned} \tag{4.28}$$

The PWM waveform produced is shown in Figure 4.8.

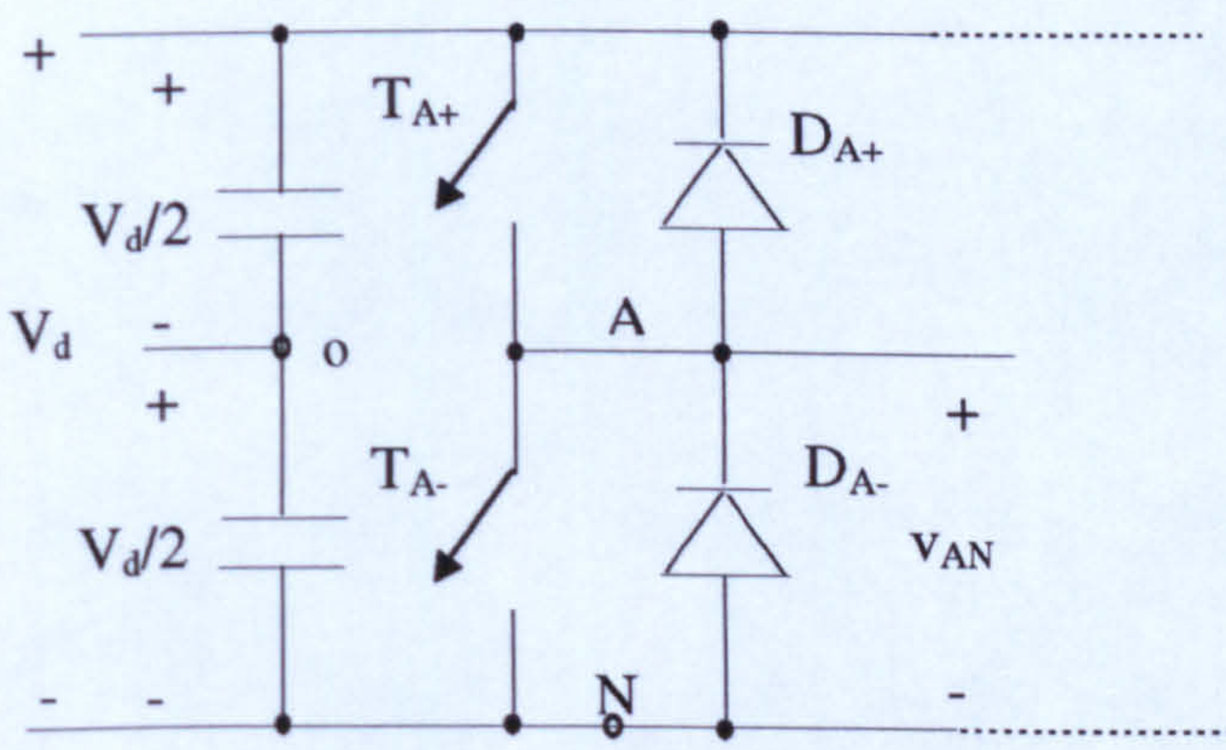

***Figure 4.6** One-leg switch-mode inverter*

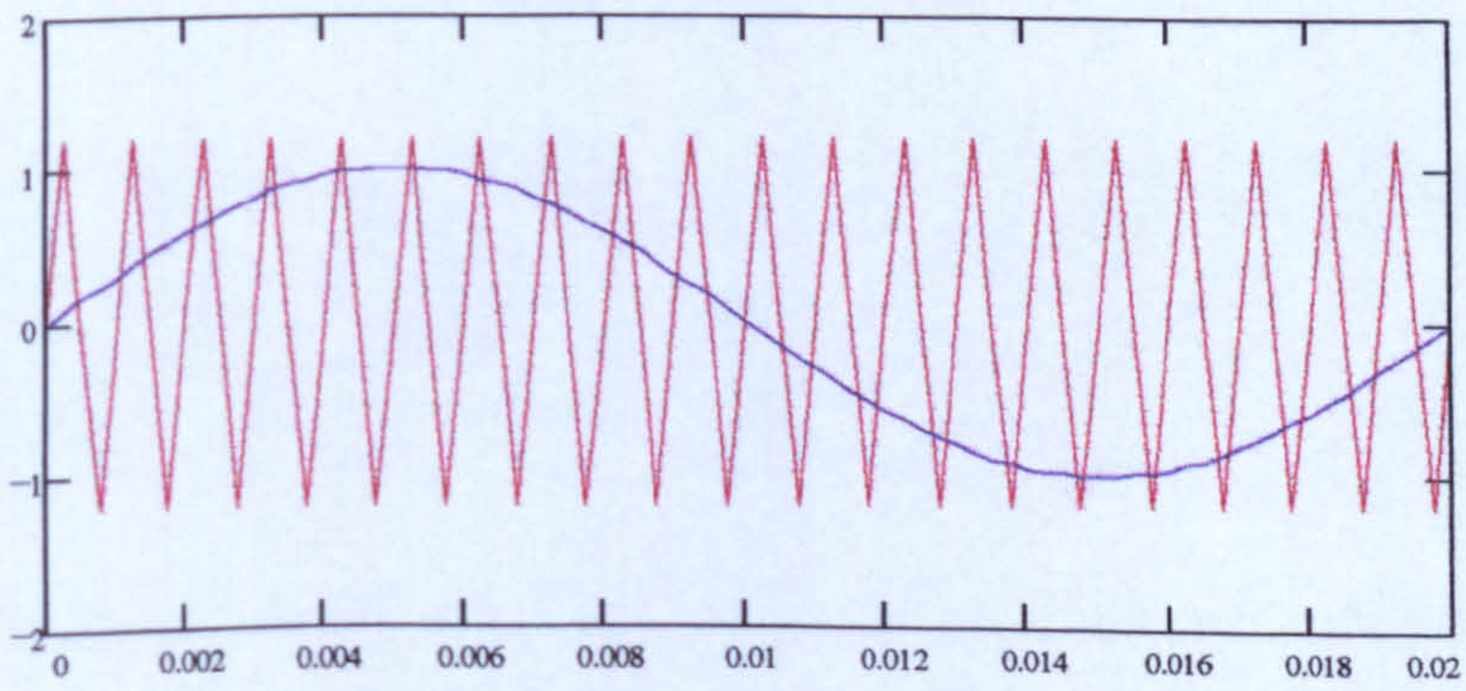

***Figure 4.7** Modulating & Carrier Signals*

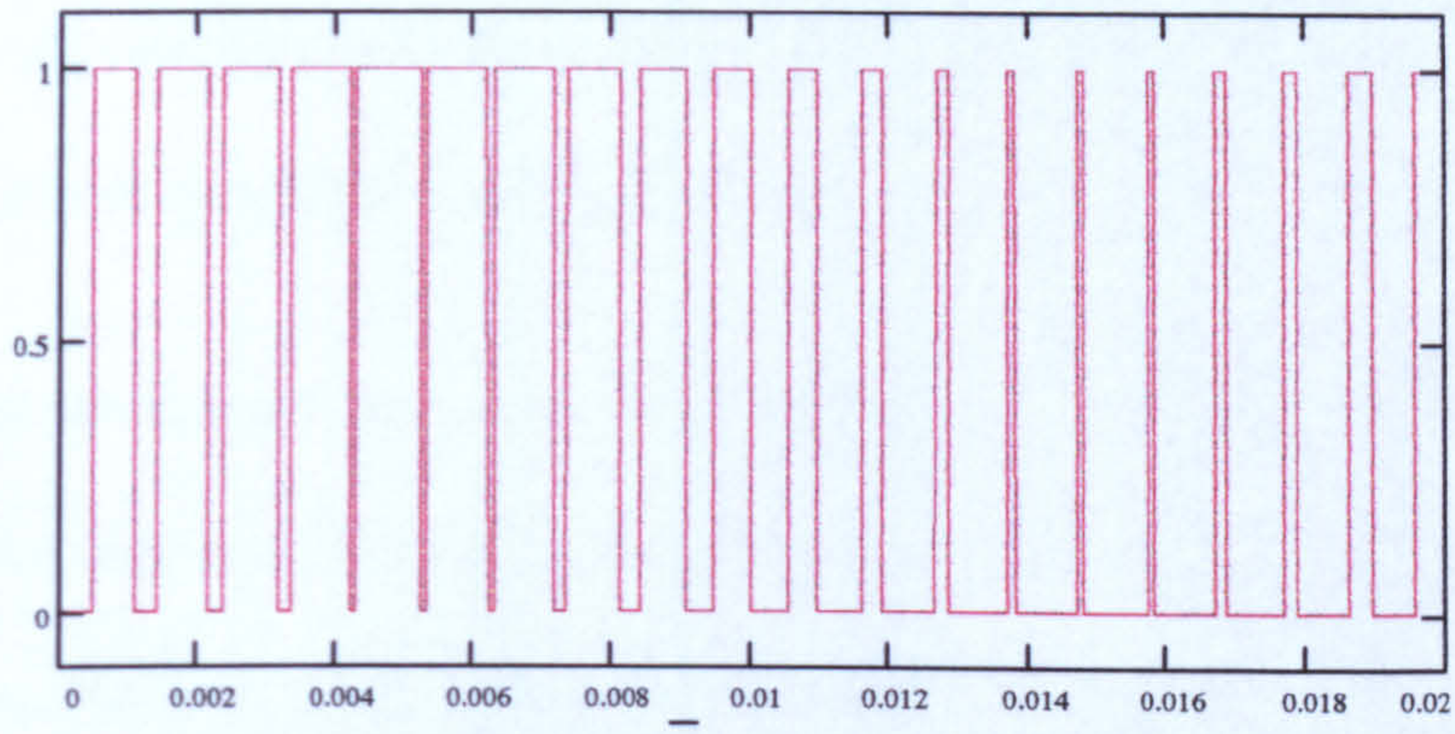

***Figure 4.8** Natural Sampling PWM Waveform*

4.7 COMPUTATIONAL DIFFICULTIES

Amongst the problems that arise is the one encountered in modelling steady-state performance of induction motors in that at the initiation of the time-stepping procedure, information concerning initial currents (field distribution in the machine) at steady-state is not available.

This mismatch of supply and internal conditions produces direct as well as alternating currents in the stator windings and rotor circuits of the motor and so simulations have to be performed until the direct current components have decayed to zero if steady state results are desired.

The number of time cycles required to reach steady-state solution for the induction motor can vary according to the load under consideration. Computational effort can be considerable, since for each cycle, 1000 time steps may be necessary with each time step requiring several iterations to handle magnetic linearity and skew subdivisions. But compared to the finite

element time-stepping techniques which are inherently expensive to use, this method is very suitable for such simulations.

When the work first began, this could take up to 5 minutes for each step on the VAX mainframe. However, with a more efficient matrix solver, solution times have been reduced to very few seconds per step. Long solution times should not discourage the use of this technique since it can be reduced by improved matrix solution methods and by use of faster computers as they become available.

4.8 CONCLUSION

The analogy between the electric and magnetic circuits has been well known for a long time but it has been left undeveloped. This may have been due to the lack of the necessary numerical tools and computing facilities. It is also due in part to the development of finite difference and finite element methods for more detailed magnetic field evaluation.

So why is not advantage taken of the modern computers available and numerical mathematics methods developed to try and solve electrical machines problems by means of the magnetic equivalent circuit. Today's fastest computers will be tomorrow's slowest ones with the fast technological evolutions.

In this chapter a description of a program which took advantage of numerical tools and computing resources to apply the magnetic circuit to electrical

machines problems solutions is outlined. The program is able to predict the performance of the machine. Although it can be applied to investigate various problems, in this thesis it will be used to study the effect of broken bars on the performance characteristics and other aspects of the machine. The results are compared with those obtained experimentally.

CHAPTER FIVE

VALIDITY OF THE MODEL

5. VALIDITY OF THE MODEL

5.1 INTRODUCTION

This chapter forms an important part of the work described in this thesis. The experimental results obtained here are very important for two reasons. First, they serve to justify the theoretical model developed in the previous chapters and secondly, they give us more confidence in carrying out the simulation of the asymmetrical rotor effects on the performance of the machine which is the main purpose of the work presented in this thesis.

The experiments carried out follow closely the development of the model so that the model is justified at every stage. Any discrepancy which did exist at each stage required improvement to the model, before it was developed further.

From the computational work described in the earlier chapters, it is apparent that the final differential equations describing the performance of the machine were developed in three main stages:

- The solution of the magnetic circuit equation.
- The calculation of inductances and other parameters.
- The formulation of the performance equation.

The experimental work which follows approximately the stages described above is:

1. Measurement of magnetising characteristic.

2. Measurement of machine's parameters:

   a) Measurement of winding self and mutual inductances.

   b) Measurement of winding leakage inductances.

   c) Measurement of winding resistances.

3. Measurement of performance: Current-speed and torque-speed curves.

4. Measurement of current waveforms and spectra.

Having described the steps followed in deriving the computational technique in chapters 3 and 4, and the steps which are to be followed in the experimental part, the next logical stage is to setup the test rig. The availability of modern facilities in the Machines and Drives Laboratory at Nottingham University has facilitated the task.

5.2 EQUIPMENT

The type of equipment and its calibration has a great influence on the accuracy of the experimental results. In this section a description of the equipment used and its accuracy where appropriate will be given

5.2.1 TEST RIG ARRANGEMENT

Figure 5.1 shows the test rig schematic diagram. This diagram shows a test motor coupled mechanically to a dc load machine whose speed is controlled by the input armature voltage obtained from the generator of a Motor-Generator set. This voltage is regulated by the field current of the generator. For tests involving the simulation of broken bars a flywheel of inertia 2 kgm^2

was added to the test rig to limit speed variation with severe unbalance of the cage winding. The remaining inertia of the test rig was 0.4 kgm^2. In the following sections these components are described very briefly.

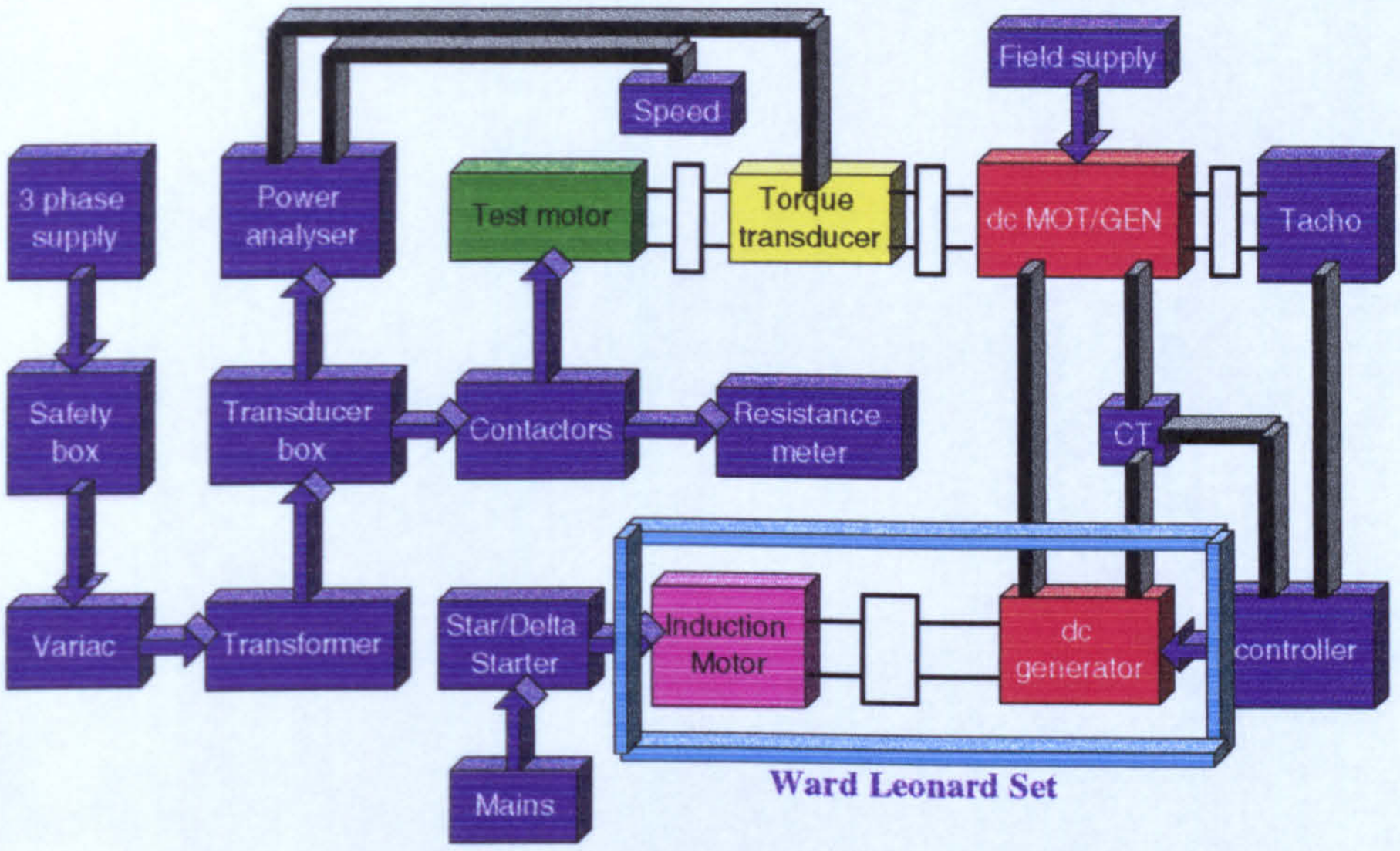

Figure 5.1 *Experimental test rig*

5.2.1.1 SPECIAL SQUIRREL CAGE MOTOR

In the analysis of the squirrel cage rotor asymmetries or defects, the bars (resistances and currents) must be easily accessible so that cage defects, such as bar breaks, are introduced with relative ease and without introducing rotating imbalances. In this experimental investigation, in order to be able to achieve these requirements, a three-phase, 50Hz, 10hp, 6-pole, Brush, wound-rotor machine was used as a base. This machine was modified to produce a stationary external cage keeping the rotating three-phase winding.

First of all, the machine was dismantled carefully in order not to damage the electromagnetic circuit. Then the machine dimensions required for the

computer simulation were obtained by careful measurement. Finally, the stator winding was replaced by copper bars. These bars were extended at one end and fixed with a removable link to the endring leaving enough space where current transducers could be fitted (see Figure 5.2). The rated voltage for the rotor winding was 200 volts.

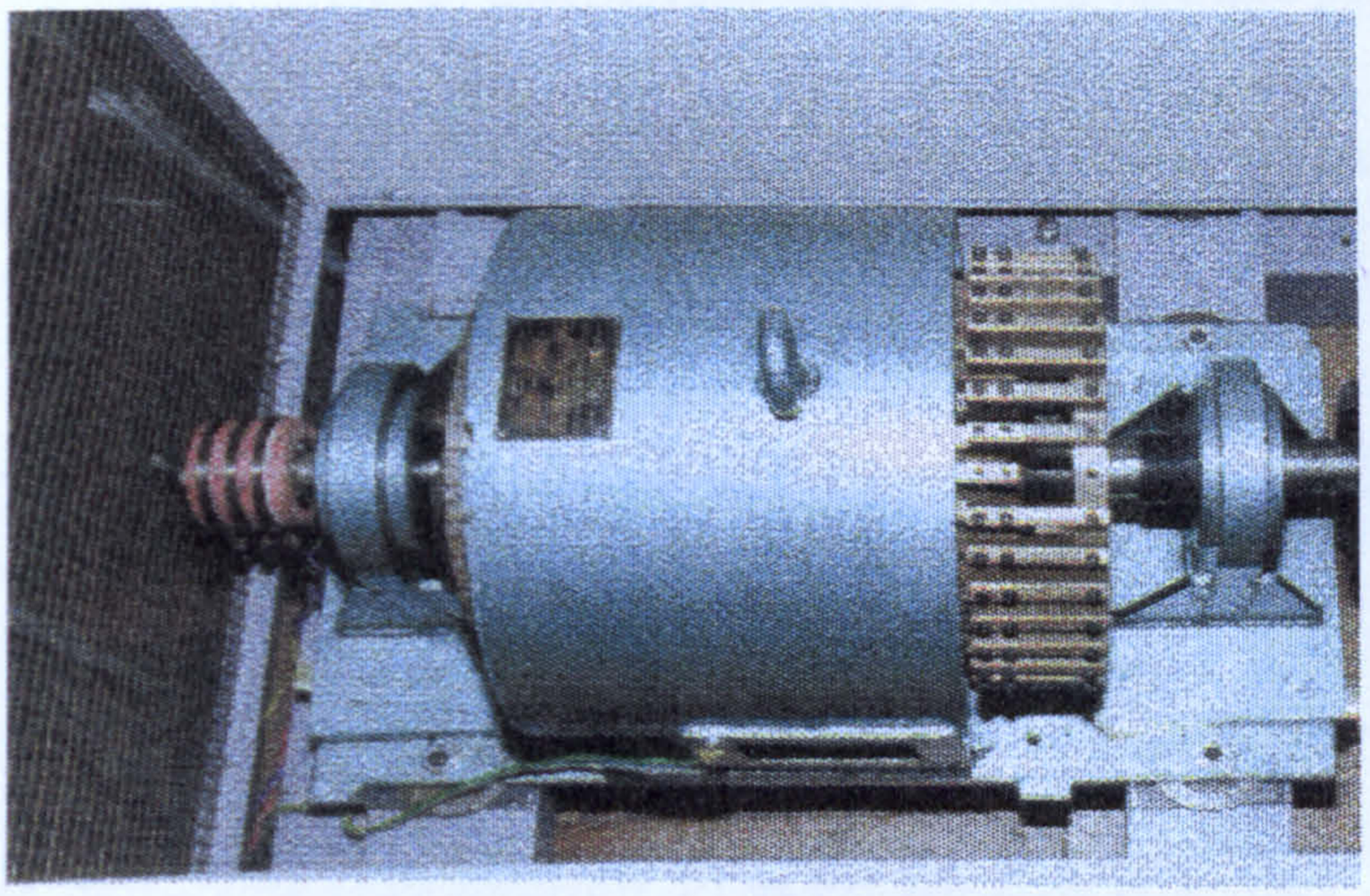

***Figure 5.2** Inverted test machine*

5.2.1.2 THE WARD-LEONARD SYSTEM

In order to control the rotor speed, the dc load machine requires a variable armature voltage. This voltage can be obtained from a dc generator running at constant speed. This, however, requires another ac motor to drive the dc generator which forms the Ward-Leonard set. The armature voltage of the generator is controlled by controlling its field current by means of a control circuit, using a single-phase controlled rectifier. The torque demand is converted into a voltage by a potentiometer and is the input to the control loop. The feedback signal for closed loop control is supplied from a current transducer measuring the armature current as an equivalent to the torque.

5.2.1.3 DATA ACQUISITION SYSTEM

The data acquisition system consisted of: transducers, signal conditioning, data acquisition hardware, analysis hardware and software, and a personal computer. In the following sections a description of the elements of the data acquisition system used in this project for test and measurement will be given.

1- CURRENT TRANSDUCERS

In order to measure the three phase currents, a three-phase sensor box was used. Currents up to 60 A were required to be measured using the test rig. In order to step down these currents and provide complete isolation of the main circuit, 3 LEM Hall effect current transducers of 2000:1 ratio, were employed. The box caters for the measurement of three-phase line currents and three-phase voltages.

The sensor box was calibrated using a high precision current source. The calibrator was a Ballantim Transductance Amplifier, model 1620A of 100A capacity from dc to 1KHz and a bandwidth of upto 10KHz at lower currents. To find the scaling factor of each phase, a current of a precisely known amplitude and frequency was injected, from the calibrator, into the input of the box each phase in turn. No major deviations were noticed in all three phases. A good linearity was obtained in the range up to 2KHz.

2- TORQUE MEASUREMENT

In order to measure the torque, a torque transducer which operates on the principal of Weatson bridge/strain gauge was mounted between the shafts of the induction motor and the dc load machine. The output signal from this transducer was fed to a transducer amplifier connected to the torque input of the NORMA power analyser and calibrated to read torque in Nm.

To calibrate the torque meter, one end of the shaft was securely locked and known weights were suspended one by one from the calibration arm at a known distance and readings from the NORMA power analyser were taken. The scaling factor of the torque was then adjusted [92]. The torque was measured with an accuracy of 0.2% and 0.5% repeatability due zero offset error.

3- SPEED MEASUREMENT

An optical probe was connected to a frequency counter, of 0.1Hz to 120MHz frequency range to measure speed. This unit senses the light reflected from a reflective tape, stuck to the rotating shaft. The counter measures the period between pulses and then computes the speed [93]. It has an accuracy of 0.01%.

4- WAVEFORM RECORDER / SPECTRUM ANALYSER

To capture and store the current waveform and its spectrum, an Advantest digital spectrum analyser series R9211C was used. This spectrum analyser uses FFT techniques that are software based rather than hardware based

giving more flexibility of analysis. The R9211C combines an analog-to-digital converter and a powerful computer in one compact package. It has many features [94] among which:

- an internal floppy disk for saving data
- waveform averaging to improve signal-to-noise ratio
- horizontal, vertical, and band markers for marking accurate waveform measurements, including automatic peak and harmonic tracking functions
- a running zoom feature to expand frequency resolution.

There are four measurement modes two of which were used for this work. These two modes are: waveform measurement mode to analyse a signal in the time domain and a spectrum measurement mode to analyse a signal in the frequency domain.

The waveforms captured and stored in floppy disk using the Advantest Servo Analyser could not be converted to ASCII data, due to the lack of conversion software, a Lecroy 9304A digital oscilloscope was used to provide the waveforms illustrated in this thesis. The data was stored on disk, converted to ASCII data and then plotted on an IBM compatible PC.

Some of its features include [95]:

- 50K of acquisition memory per channel
- Floppy Disk Storage

5.2.2 TEST PROCEDURE

The test procedure was as follows:

1) The Motor of the Ward-Leonard set was switched on.
2) The dc motor was brought up to speed under torque control.
3) The test motor voltage supply was increased gradually using a variac.
4) The speed was adjusted by controlling the load torque using the reference potentiometer.
5) The current waveforms and spectra were then stored on a floppy disk.
6) The data analysed off-line on an IBM compatible PC.

5.3 MAGNETISATION CURVE

The magnetisation curve is obtained with the motor driven at synchronous speed. The input current is measured with different excitation voltages applied to the test motor. In order to compare the measured and computed results, the computer program is run for the same conditions as those recorded for the experimental tests. A, relatively, long computation time is needed for each point to allow the transient dc components to die out. The results for the measured and computed curves are shown in Figure 5.3.

The overall agreement between the computed and measured magnetisation curves, as shown in Figure 5.3, gives confidence in the use of the technique for analysing the induction machines magnetic circuit, including the effect of slot openings, and saturation. The average error over the range of voltages used is 3.11%.

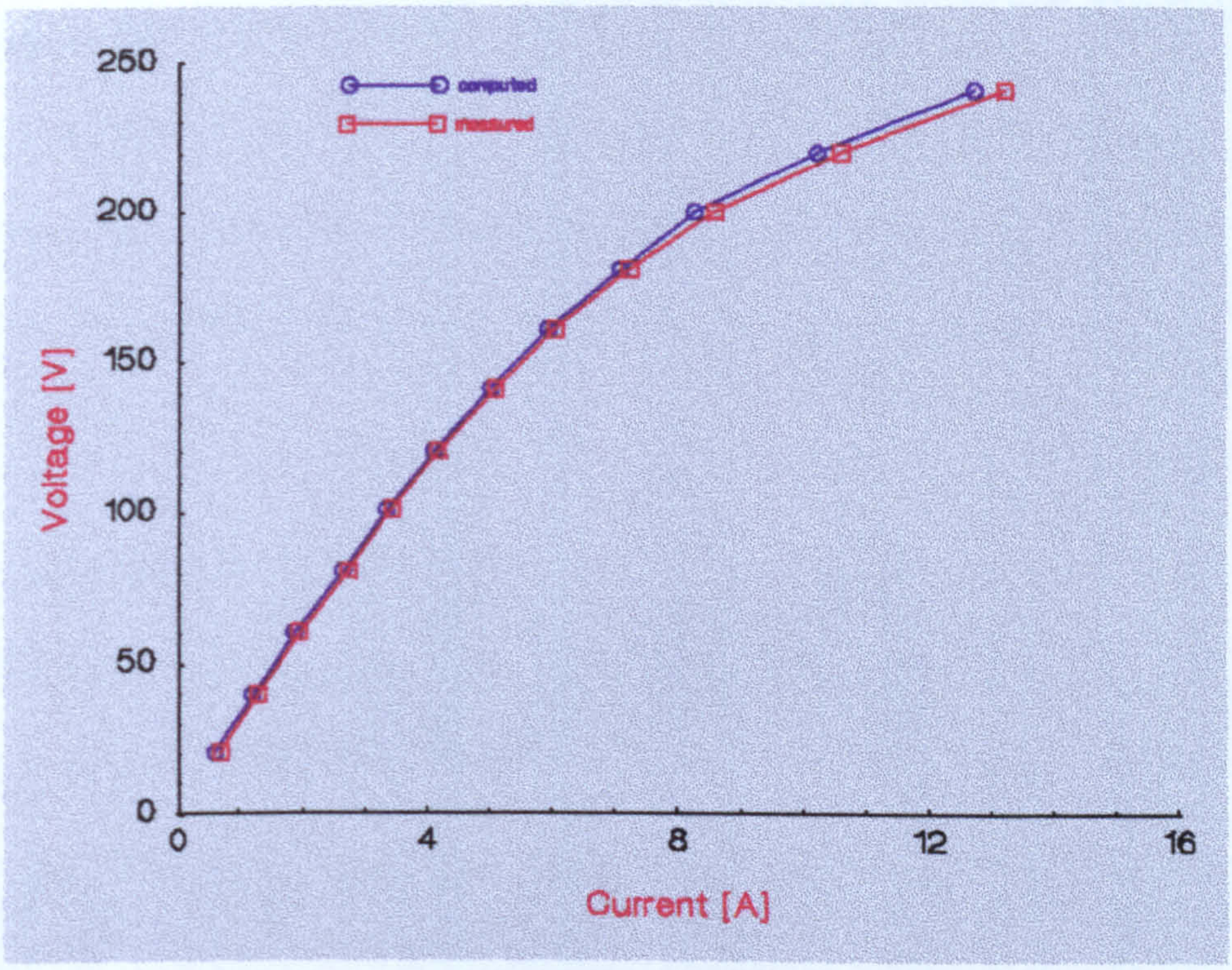

Figure 5.3 *No-load magnetisation curve*

The error is very small at low voltages (0.8%) but it starts increasing beyond the rated voltage. This is probably due to difference between the modelled B-H curve and the actual magnetic material.

5.4 MEASUREMENT OF MACHINE'S PARAMETERS

5.4.1 RESISTANCE MEASUREMENT

The measurement of the winding resistances was performed using a dc voltage applied to the winding concerned and the current through and the voltage across the winding were recorded. This procedure was repeated for each winding in turn.

5.4.1.1 THREE PHASE WINDING RESISTANCE

As the three phase winding for the test machine was on the rotor one, to avoid non-linearity due to the brushes, the measurements were carried out from the terminals of the winding. This was done using a 4 wire micro-ohmmeter.

5.4.1.2 BAR RESISTANCE

The difficulty here was that there was no direct access to the ends of each bar. The only way of doing it was to disconnect each bar at one end by removing its link and isolate it from the endring. The micro-ohmmeter was then used on each bar but contact resistance would still influence the effective bar resistance when the link was replaced.

5.4.2 END WINDING LEAKAGE INDUCTANCE

The end winding leakage inductance is not calculated directly from the machine data though it could be, by using one of the formulae available in literature [96]. In this case it is found by equating results from an experimental short circuit test at 70.7 V and an equivalent computed short circuit test at the same voltage. The value of end winding leakage added for the stator was 0.38mH and for the rotor 0.023 mH.

In practice, end winding leakage will indirectly accommodate small constant errors which may be present in the computation of the remaining leakage reactances. However, the end winding leakage reactance is normally a small

part of the total leakage reactance, particularly for machines of high pole number, and this can be seen to be true in this case by reference to Figure 5.5.

5.4.3 SELF AND MUTUAL INDUCTANCES MEASUREMENT

Tests were made at standstill on 50Hz and 120V supply. The self inductance of any phase is obtained by applying a known voltage at rated frequency and measuring the current, while the mutual inductance between any two phases can be obtained by measuring the voltage induced in one phase due to the current flowing in the other phase.

The measurements are taken for different current values at fixed rotor position in order to examine the saturation effect. The results are shown in Figure 5.4. As for the rotor self and mutual inductances and the stator-rotor mutual inductances, the difficulty is again with the access to the ends of the rotor bars. Consequently, in this experiment, we did not measure the rotor self and mutual inductances and the rotor-stator mutual inductances. However, the very good agreement for the stator would be expected to be repeated for the simpler rotor winding.

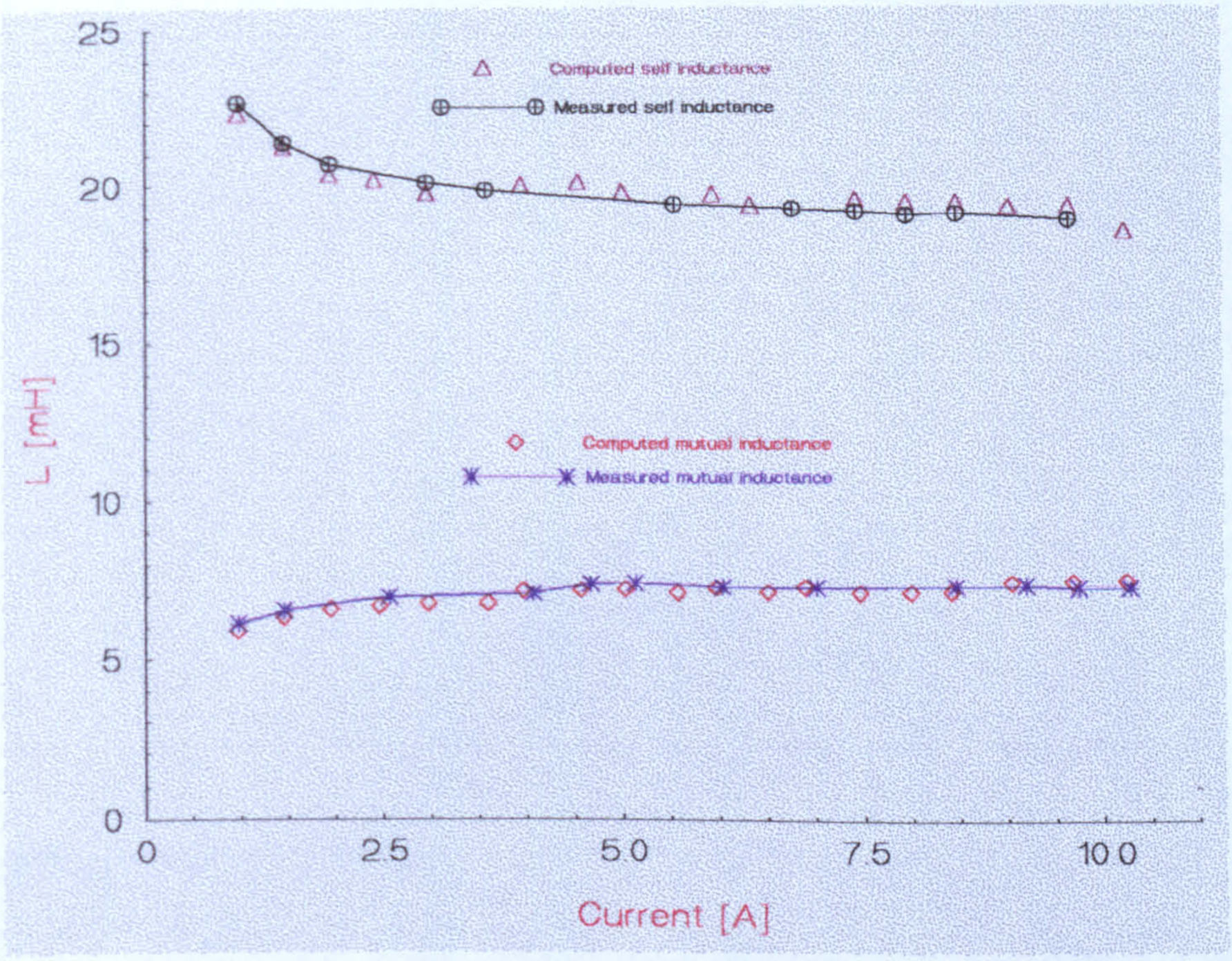

Figure 5.4 *Stator self and mutual inductances*

5.4.4 LEAKAGE INDUCTANCE MEASUREMENT

The leakage inductances of the machine are determined by a locked rotor test. The total leakage inductance is referred to the stator side and arbitrarily divided equally between stator and rotor. This procedure was repeated for different current values in order to determine the saturation effect. Figure 5.5 shows the results. It can be seen that the leakage inductance decreases with increasing winding current as expected.

Clearly, the agreement between the computed results and measured values give the method of calculation great support, and reasonable performance prediction would be expected from the proposed model. The maximum percentage error for the self inductance is less than 2% and an average error of 1%.

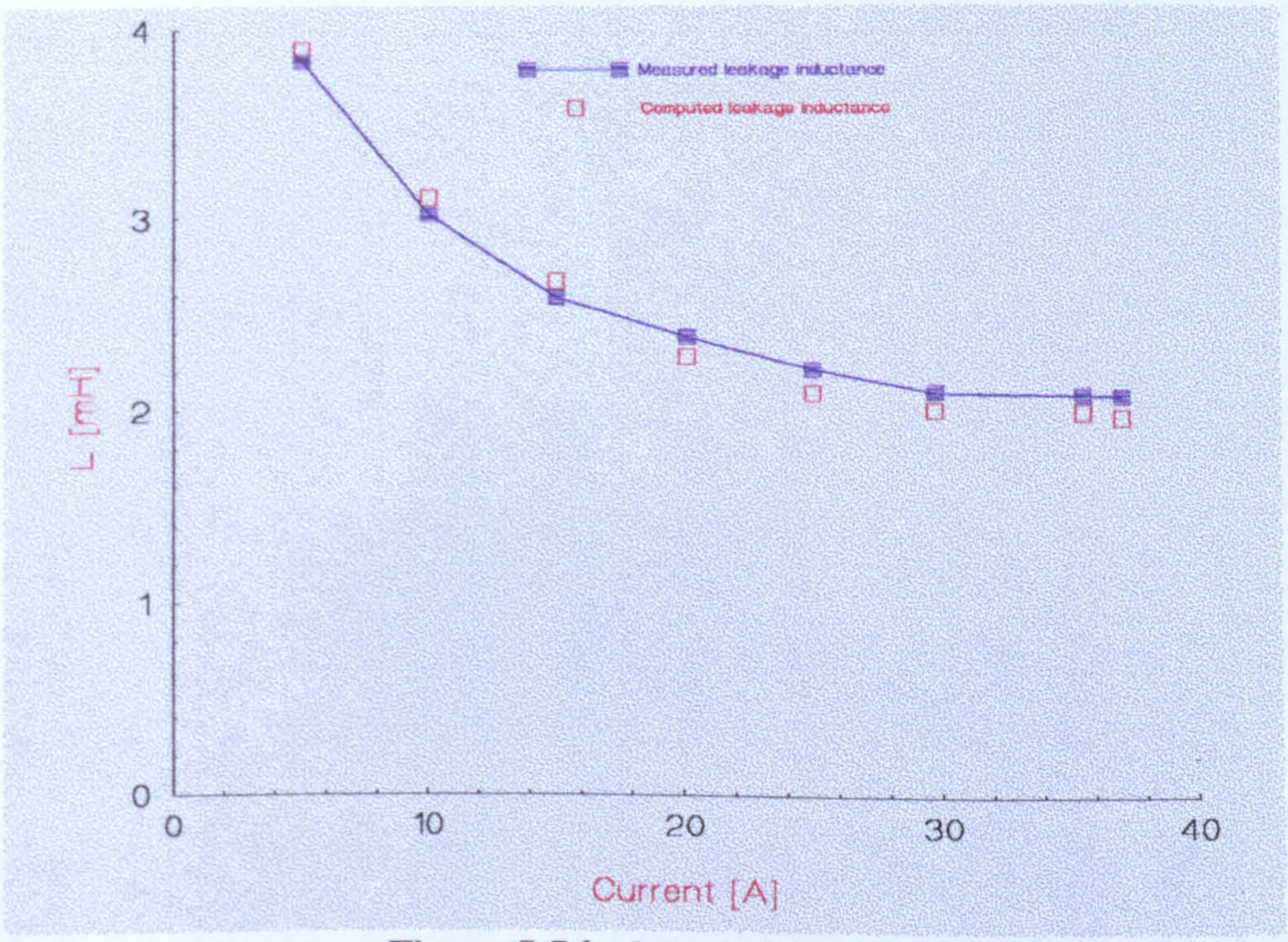

Figure 5.5 *leakage inductance*

As for the mutual inductance the maximum error is less than 3.8% and an average error of 1.4%. The largest error for the measurement of the machine parameters is with the leakage inductance which is 6.1% at large saturation and an average error over the range of current used is 3.4%. This is quite reasonable because the values obtained from the test measurements are supposed to be equally divided between stator and rotor. Nevertheless, these results are reasonable and very encouraging.

5.5 TORQUE-SPEED AND CURRENT-SPEED CURVES

These curves are obtained at reduced voltage to avoid excessive current at low speed. The saturation effects would, therefore, be less than would occur when starting on full load voltage. It was shown in the previous section that the computed and measured magnetisation curves show good agreement.

That is very important because the torque of the induction machine is obtained from the change of the energy stored in the magnetic field. The method of computation of the instantaneous and average torque has been described in chapters 3 and 4. Using the Ward Leonard set, at several different speeds, the current and torque are measured. The performance curves are shown in Figure 5.6.

The comparison between the two curves show good agreement. The percentage error in the operating range is less than 2% while it starts to increase at very low speeds . This is due to skin effect which is not catered for in the model. This is due to the fact that at low speeds the rotor frequency is approaching that of the supply and therefore the rotor resistance appears higher.

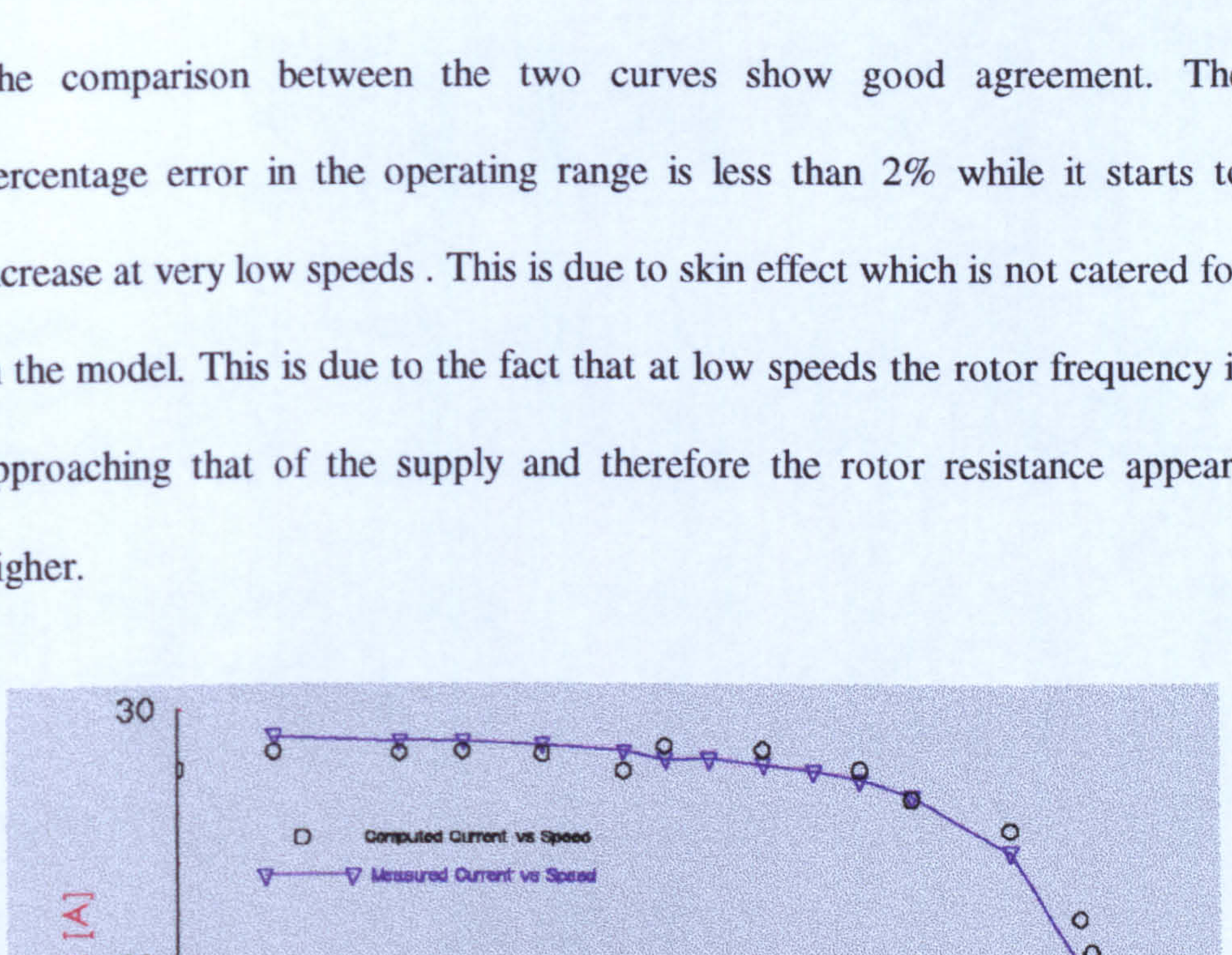

Figure 5.6 *Performance Characteristic*

5.6 STATOR CURRENT WAVEFORM AND SPECTRUM

The comparison between the measured and computed values of the machine parameters and performance characteristics showed good agreement. In this section the stator current waveforms and spectra are checked.

Figures 5.7, 5.8 and 5.9 show the experimental and computed stator current waveforms at noload, 1% and a 2% slip respectively. They are included to show uniformity of amplitude of current. At a first glance, one can see that these waveforms are not pure sinusoid but have some ripples. This distortion may be caused by a number of harmonics from different sources.

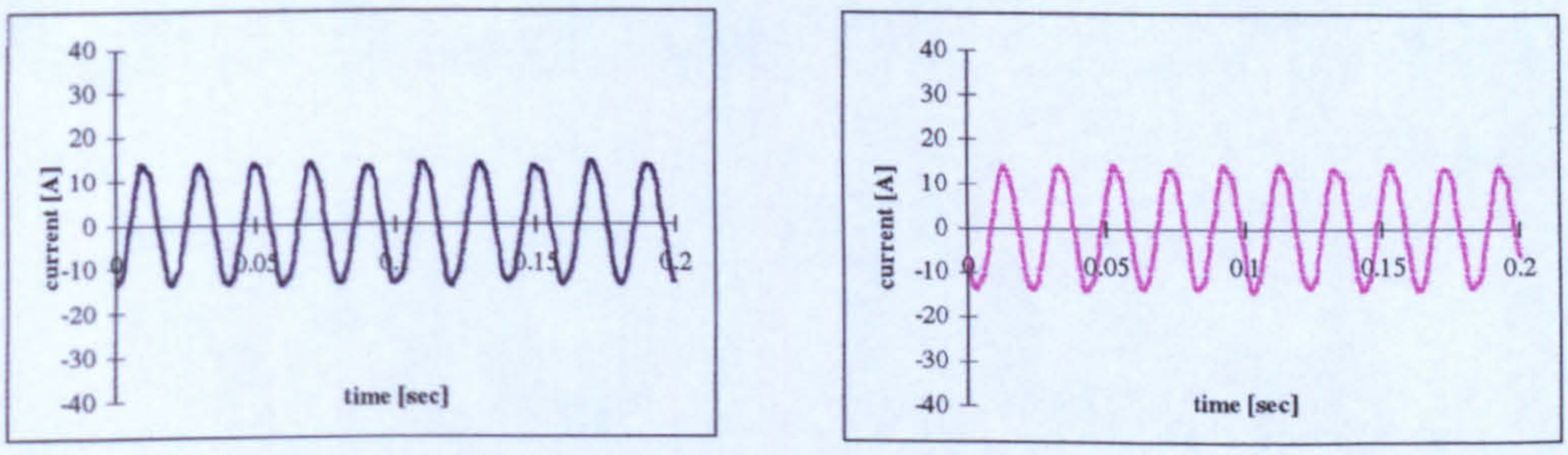

Figure 5.7 *Measured (left) and computed (right) stator current waveforms for slip = 0%.*

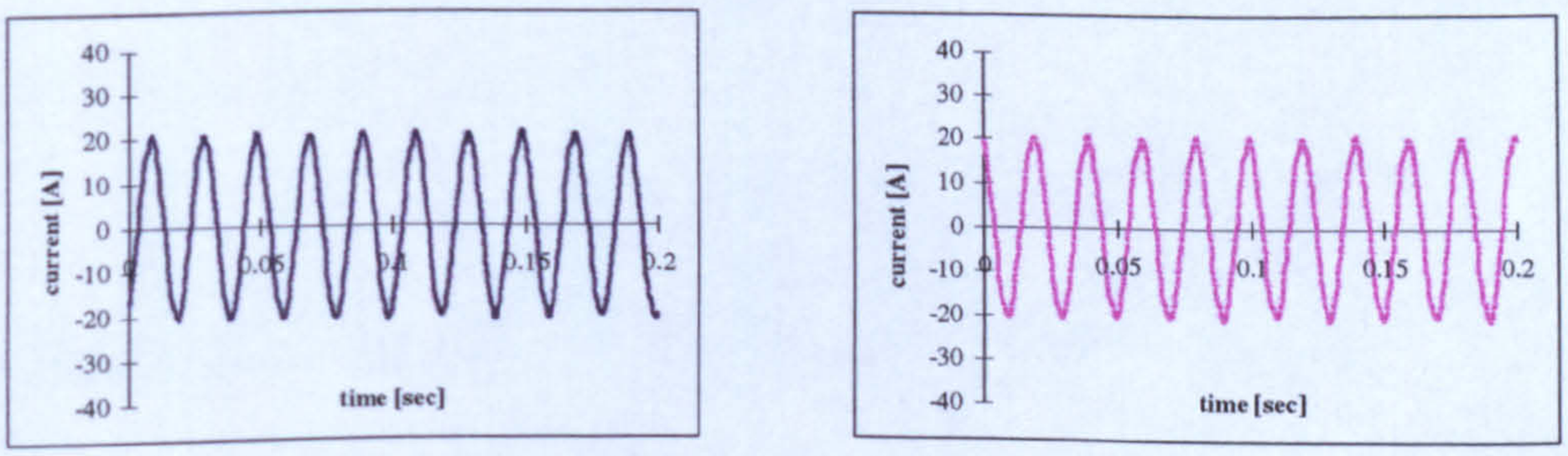

Figure 5.8 *Measured (left) and computed (right) stator current waveforms for slip = 1%.*

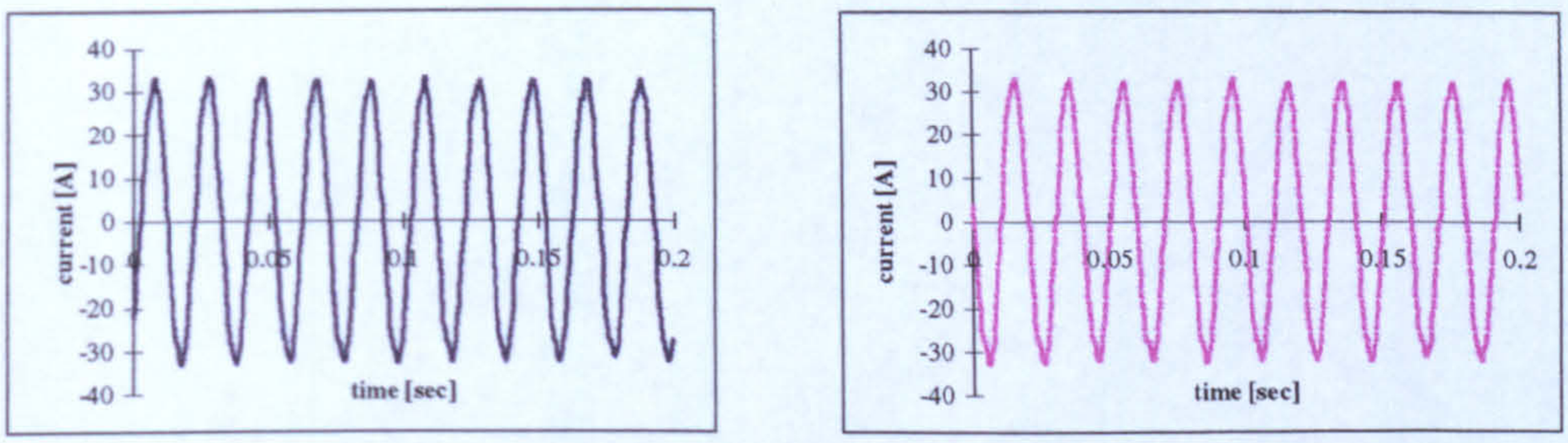

Figure 5.9 *Measured (left) and computed (right) stator current waveforms for slip = 2%.*

These sources include mmf harmonics caused by the placement of stator coils in discrete slots, permeance variation due to varying saturation in the iron. The presence of stator and rotor slots also causes the permeance of the magnetic circuit to vary with position.

In the time domain these waveforms seem to differ only in amplitude. However, the load application will distort the harmonic content of the stator current as it is shown in Figures 5.10.

From the current spectra of Figure 5.10 it is very clear that, although the motor was supplied from the mains 50 Hz supply, there are other components than the fundamental. It can also be seen that the dominant harmonic components are the 5th, 7th, 11th, ..., etc.

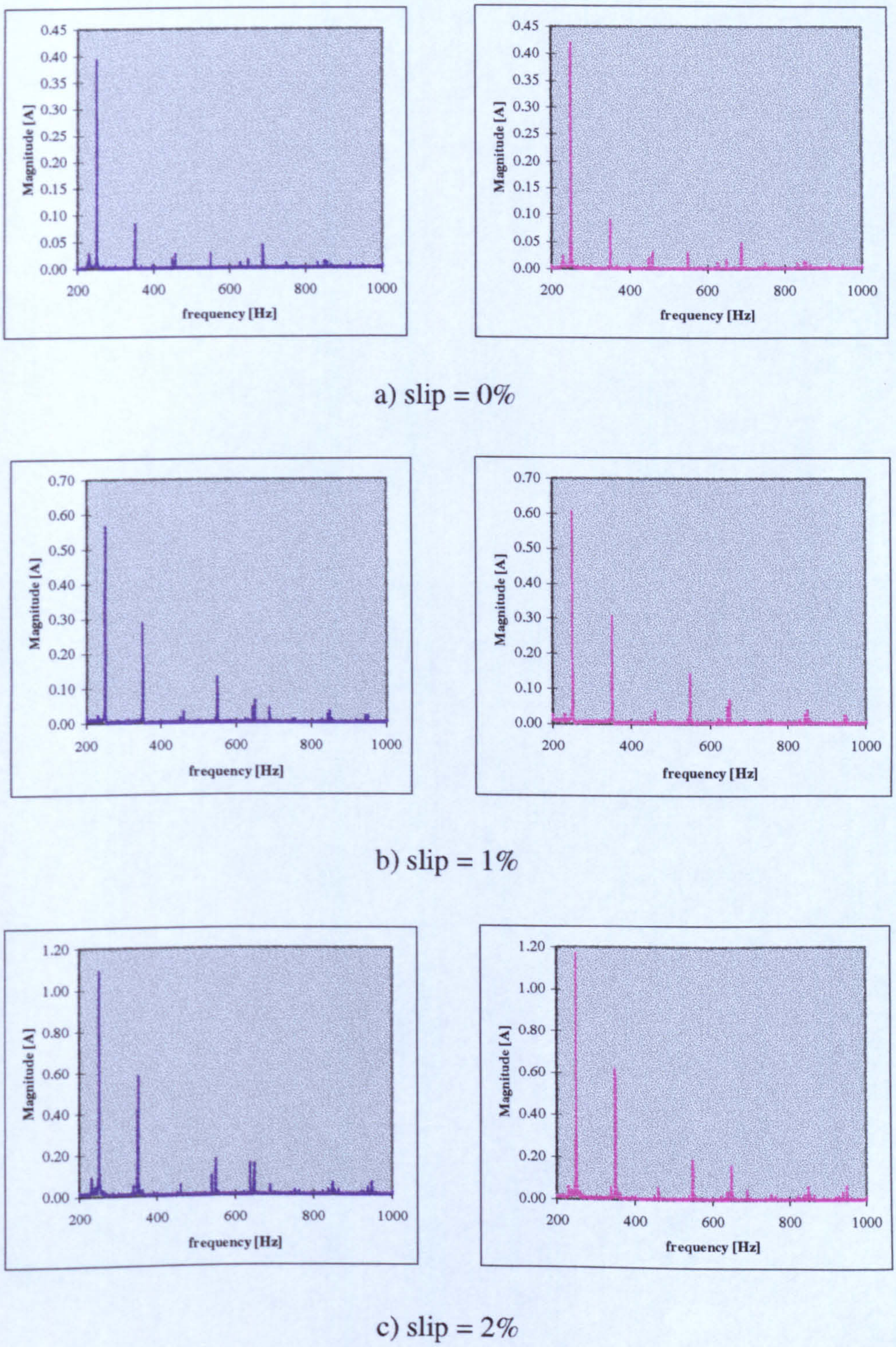

a) slip = 0%

b) slip = 1%

c) slip = 2%

Figure 5.10 *Effect of load on measured (left) and computed (right) stator current spectra.*

The following table summarises the most significant frequency components of the 10 hp motor fed from the 50 Hz mains.

	Magnitude [A]					
	slip = 0%		slip = 1%		slip = 2 %	
Frequency [Hz]	measured	computed	measured	computed	measured	computed
50	13.08	13.43	19.27	19.83	26.11	26.86
250	0.50	0.53	0.73	0.77	1.34	1.41
350	0.12	0.13	0.40	0.42	0.49	0.51
450	0.02	0.02	0.02	0.01	0.02	0.02
550	0.04	0.04	0.17	0.18	0.22	0.23
650	0.02	0.02	0.10	0.10	0.15	0.15
750	0.01	0.01	0.01	0.01	0.03	0.02
850	0.01	0.01	0.04	0.05	0.06	0.06
950	0.01	0.01	0.04	0.05	0.06	0.07

Table 5.1 *Magnitude and frequency of main components of stator current spectra.*

5.7 CONCLUSION

The validity of the analytical technique described in the previous chapters has therefore been well demonstrated. The agreement between the computed results and measured values of the machines parameters gives the method of calculation great support and, consequently, a reasonable performance

prediction was obtained. The prediction of the output torque using the change of stored energy in the airgap would therefore appear to be equally well supported.

These encouraging results give confidence in carrying out the analysis of broken bars effects in squirrel cage induction motors which is presented in the next remaining chapters.

CHAPTER SIX

BROKEN BARS SIMULATION

6. BROKEN BARS SIMULATION

6.1 INTRODUCTION

The existence of a fault in a machine represents a change from the originally specified condition of that machine. However, such a change cannot occur in isolation without causing associate changes in externally measurable quantities. Thus, in the case of an induction machine with cage fractures one can expect changes to occur in input power, input current, shaft torque and speed, frame vibration as well as acoustic noise. And it is towards the development of such an understanding that the present chapter is directed. The objective is to describe a method for evaluating the effects of the presence of rotor defects on the performance of an induction machine.

In this chapter it is intended to examine the effect of broken bars on the electromagnetic torque, magnetic flux density, rotor bar currents and the stator currents and current spectra. And finally, the last section is reserved to an inverter-fed induction motor.

To model one or more broken bars, the bar resistance is set to a relatively high resistance (10000 times). The analysis described in this chapter is quite general, since there is no restriction on the distribution of the broken bars. The only exception is that the end ring impedances are lumped with the bar impedance and, therefore, end ring faults cannot be studied. These can be catered for but this would increase the computation time.

6.2 ROTOR ASYMMETRIES EFFECTS

When the machine is operating under normal balanced conditions, rotor currents will produce positive sequence mmfs only as shown in Figure 6-1. If ω_1 is the supply angular frequency and s is the slip and when only the fundamental space harmonic is considered then the rotor currents angular frequency is $s\omega_1$. The angular speed of the positive sequence rotor mmf w.r.t the stator will be:

$$\omega_r + s\omega_1 = \omega_1(1-s) + s\omega_1 = \omega_1 \tag{6.1}$$

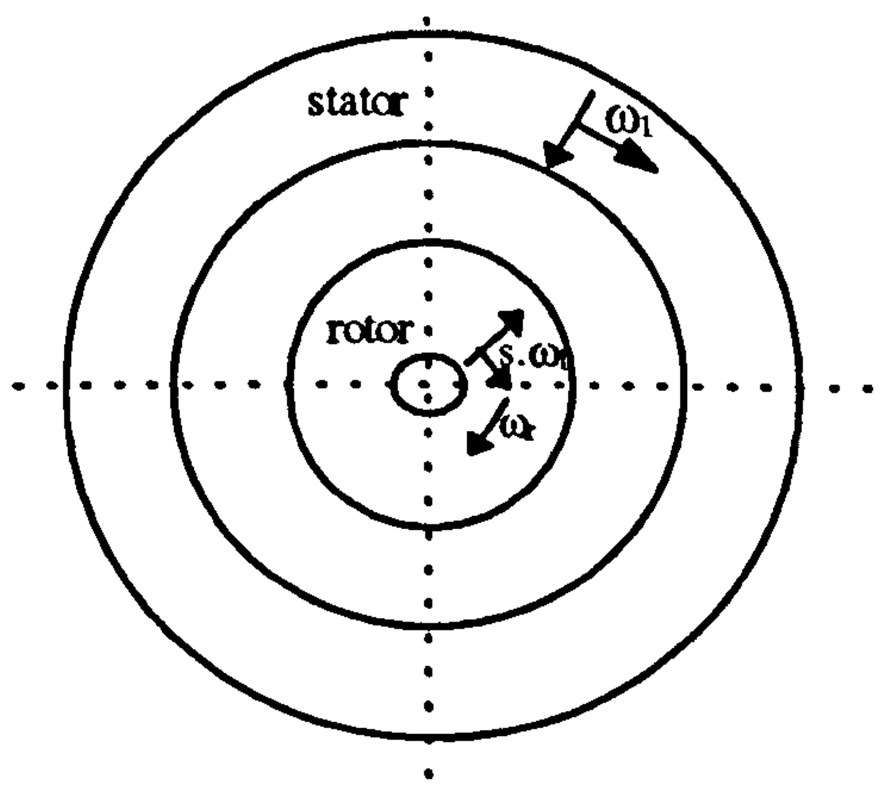

***Figure 6.1** Stator and rotor fields under normal operation*

When an asymmetry is present in the rotor circuit, the rotor currents will produce a negative sequence rotor mmfs in addition to the positive sequence mmf as depicted in Figure 6-2.

The angular speed of the negative sequence rotor mmf w.r.t the stator is:

$$\omega_r - s\omega_1 = \omega_1(1-s) - s\omega_1 = (1-2s)\omega_1 \tag{6.2}$$

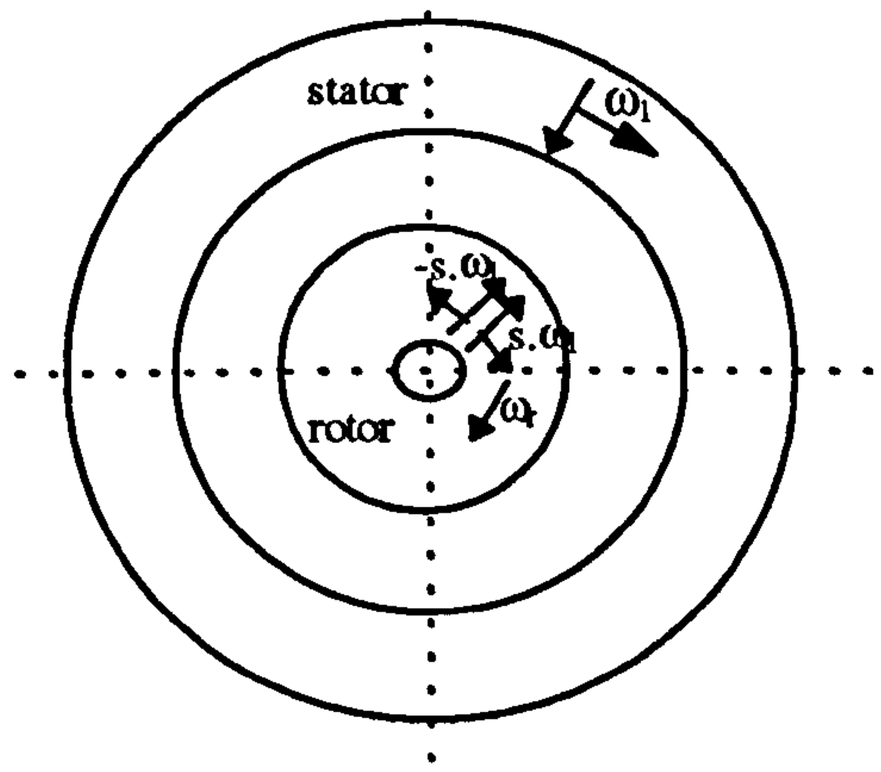

***Figure 6.2** Stator and rotor fields under faulty operation*

Therefore, the positive sequence rotor currents result in positive sequence e.m.fs and currents in the stator windings of angular frequency ω_1 and the negative sequence rotor currents result in negative sequence e.m.fs and currents in the stator windings of angular frequency $(1-2s)\omega_1$.

Moving from bar to bar, away from the broken bar, the fields produced by the additional currents change in a stepwise manner. The stepped nature of this field distribution will result in a series of additional space harmonics being produced in the airgap. The fundamental will always have 2 poles, but due to the structure of three phase windings, only harmonics of order h=P, 5P, 7P,...etc., where P is the number of pole pairs, will influence the stator current spectrum.

The stator windings are housed in slots, so the resultant fields produced by the stator are also stepped in nature. This will result in space harmonics being induced into the airgap, each one of which will induce a rotor bar current of different frequency and hence its own injected fault current. The angular frequency of the additional fields due to the rotor injected fault currents w.r.t the stator is given by:

$$h \cdot \omega_r \pm s \cdot \omega_1 = h \cdot (1-s) \cdot \omega_1 \pm s \cdot \omega_1 \qquad (6.3)$$

where the $\pm$ sign is included because the fault produces both positive and negative rotating fields and h gives the harmonics order h=1, 5, 7, ...etc.

Since the angular frequencies of the positive and negative sequence stator currents differ by $2s\omega_1$, oscillations, which can be undesirable for the supplying network, are present in the stator currents.

Most of the published work in international conferences and journals concentrated on current spectrum analysis. This is because the stator current signal is available and easily accessible for induction motors and it contains well defined components, as shown above, which can be detected. In this chapter the emphasis will also be on the stator current waveform spectrum.

6.2.1 MAGNETIC FLUX DENSITY

The flux density in the stator back iron, stator tooth and stator tooth-tip for a healthy rotor are illustrated in Figures 6-3, 6-4 and 6-5 respectively. It is very

clear from these curves that the dominant and fundamental frequency will be at the motor excitation frequency of 50 Hz. Higher frequency components will also appear due to the stepped nature of the rotor field and the nonsinusoidal distribution of the stator mmf. These components will be reduced in relative magnitude by virtue of the back iron flux being the integral of the air gap flux.

An asymmetrical rotor reacts to the stator field at frequency f through two counter rotating fields at frequencies ±sf. This behaviour is shown in figures 6-6, 6-7 and 6-8. In the stator back iron and tooth regions facing the broken bars the flux density is higher.

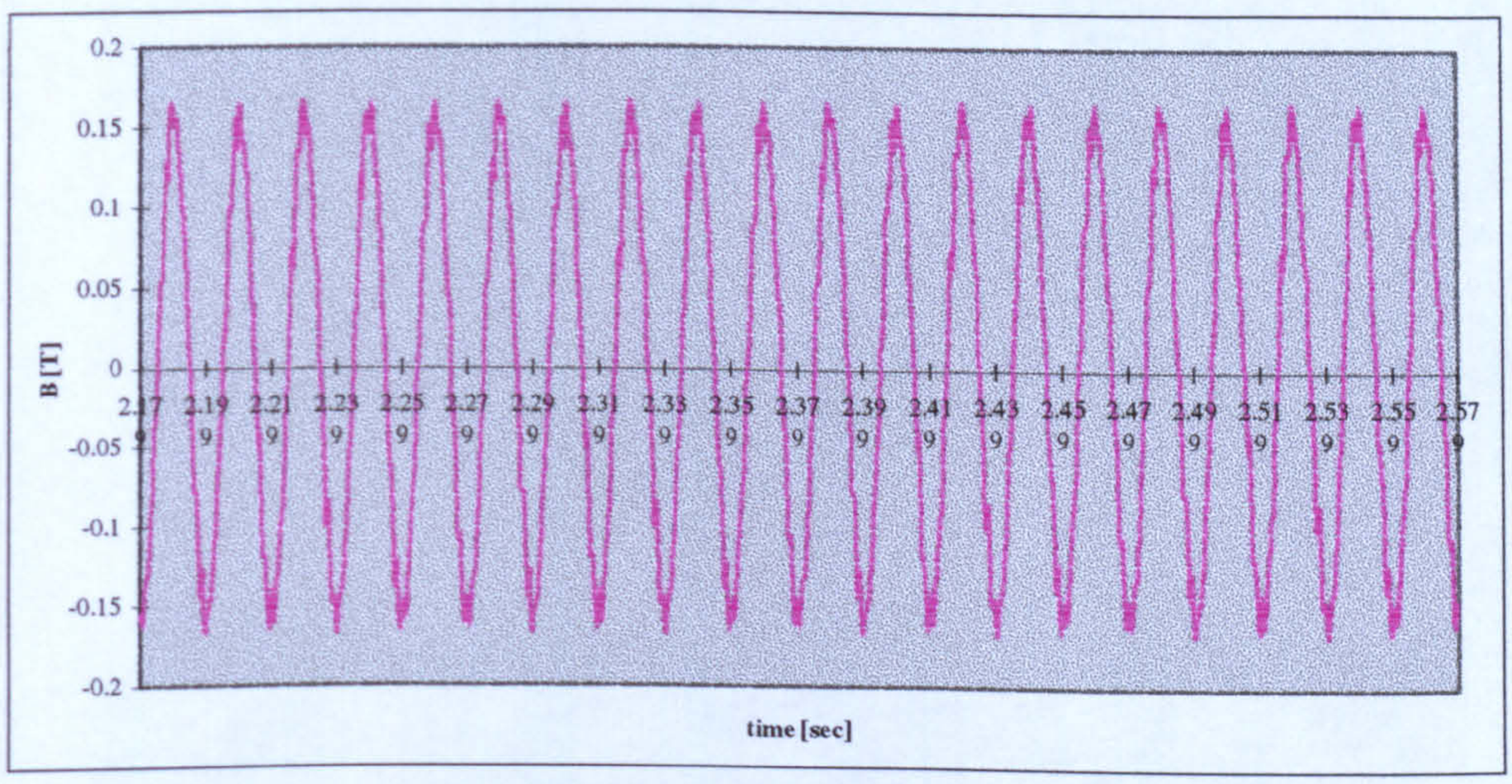

Figure 6.3 *Stator back iron flux density with a healthy rotor*

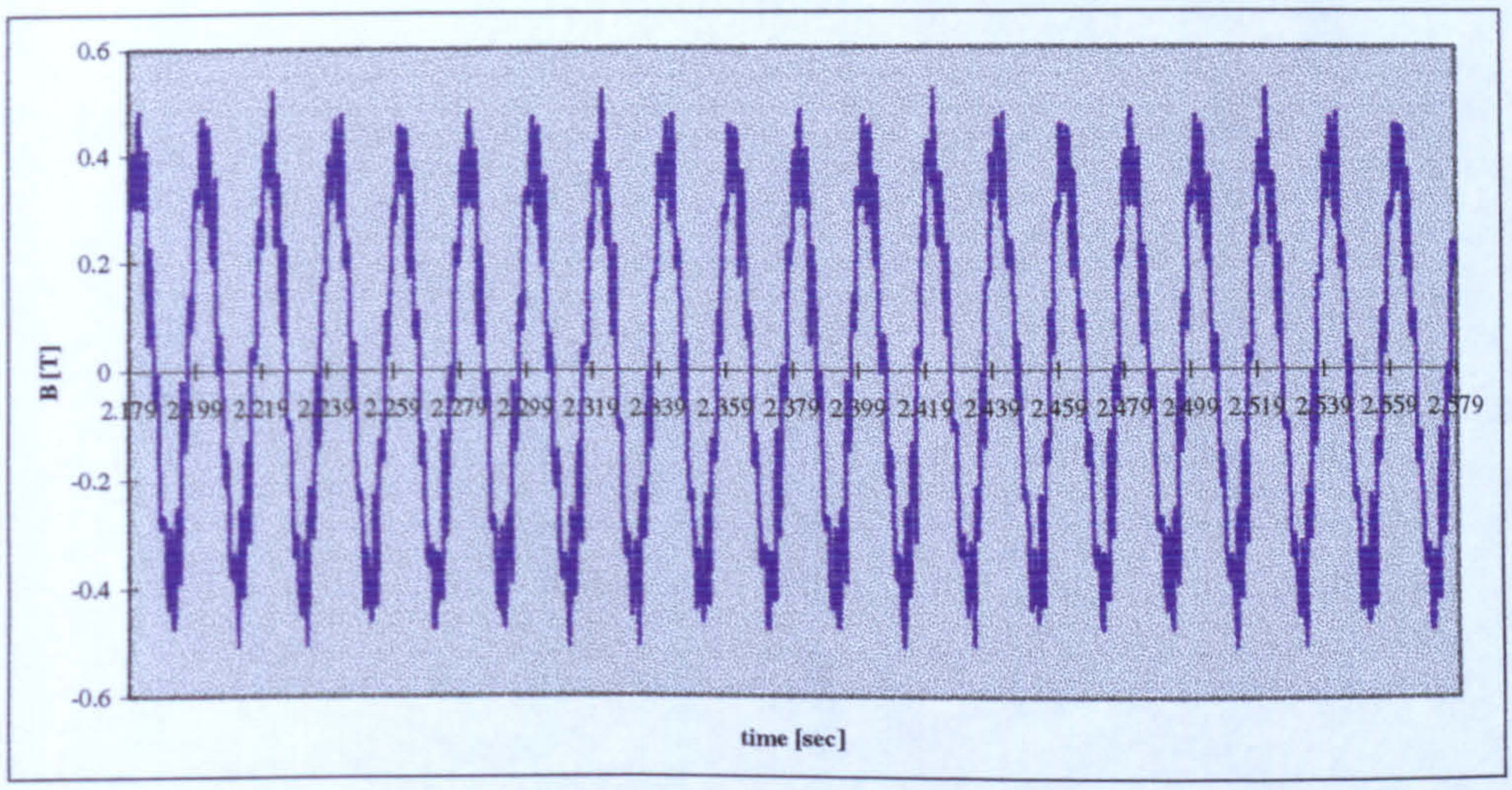

Figure 6.4 *Stator tooth flux density with a healthy rotor*

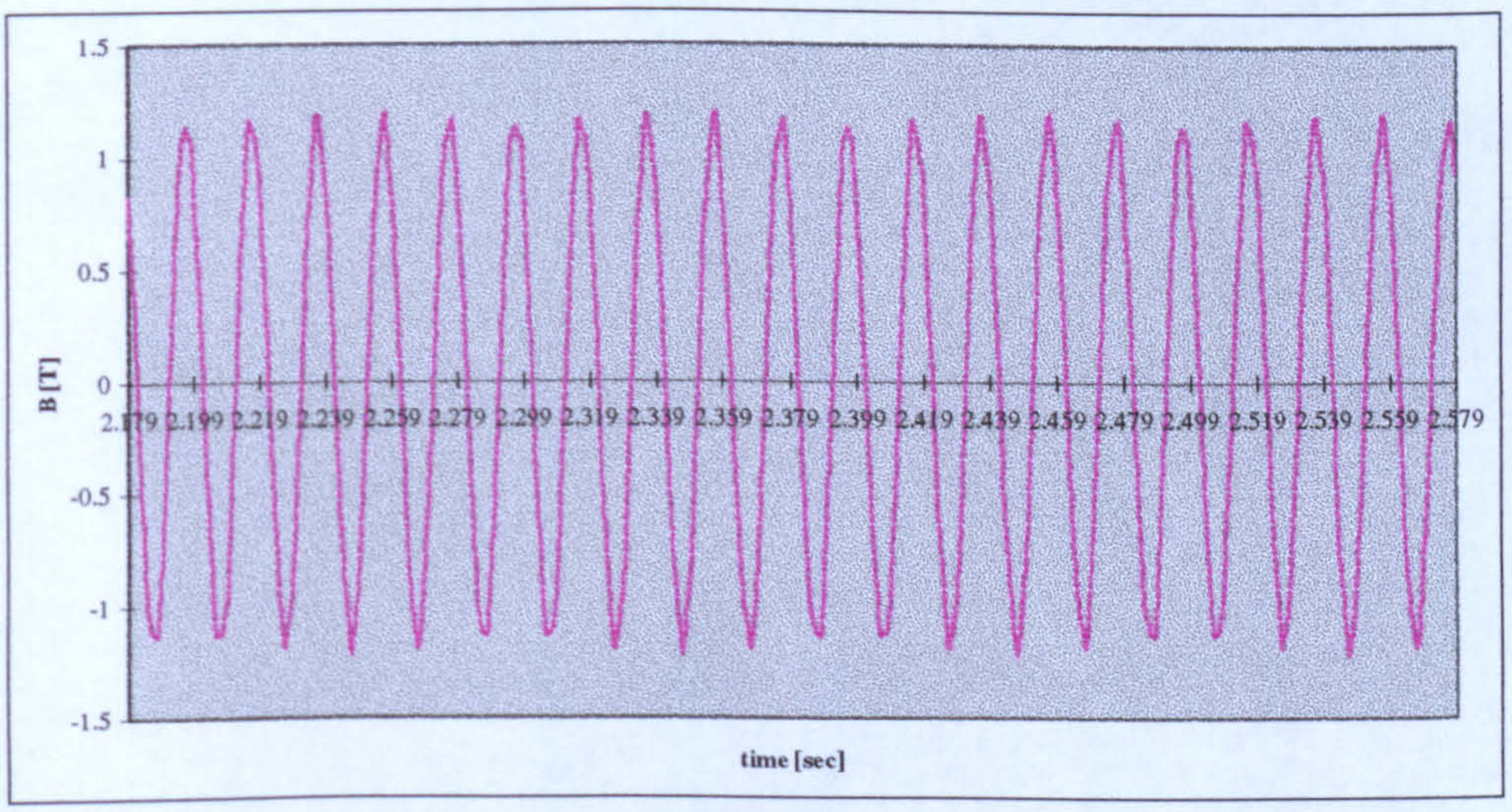

Figure 6.5 *Stator tooth-tip flux density with a healthy rotor*

The increase in magnetic flux densities near the broken bars becomes greater when the number of bars increases. These locally high values are due to the fact that the demagnetising effect of the induced rotor currents is absent in these locations.

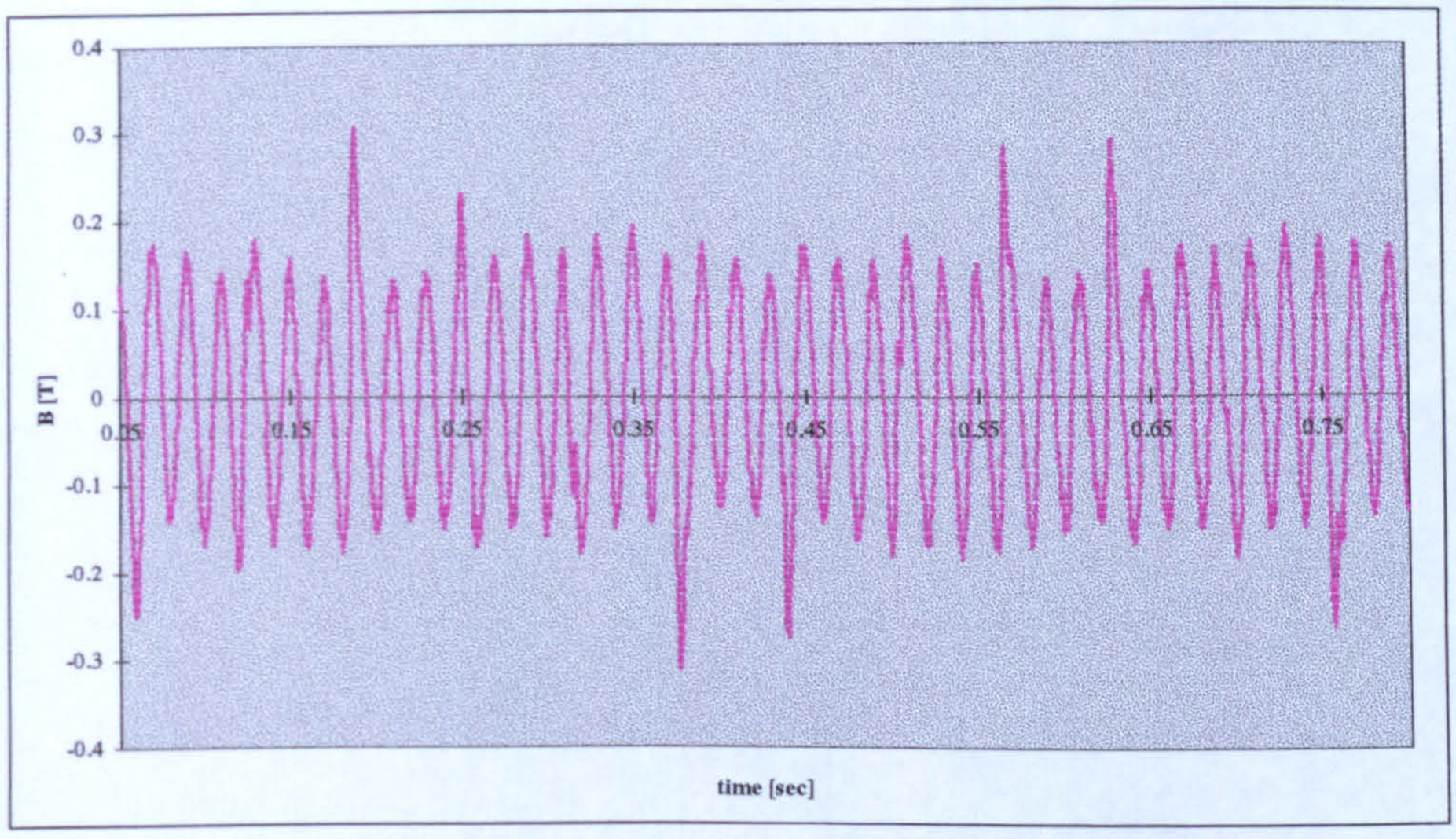

a) Two adjacent broken bars

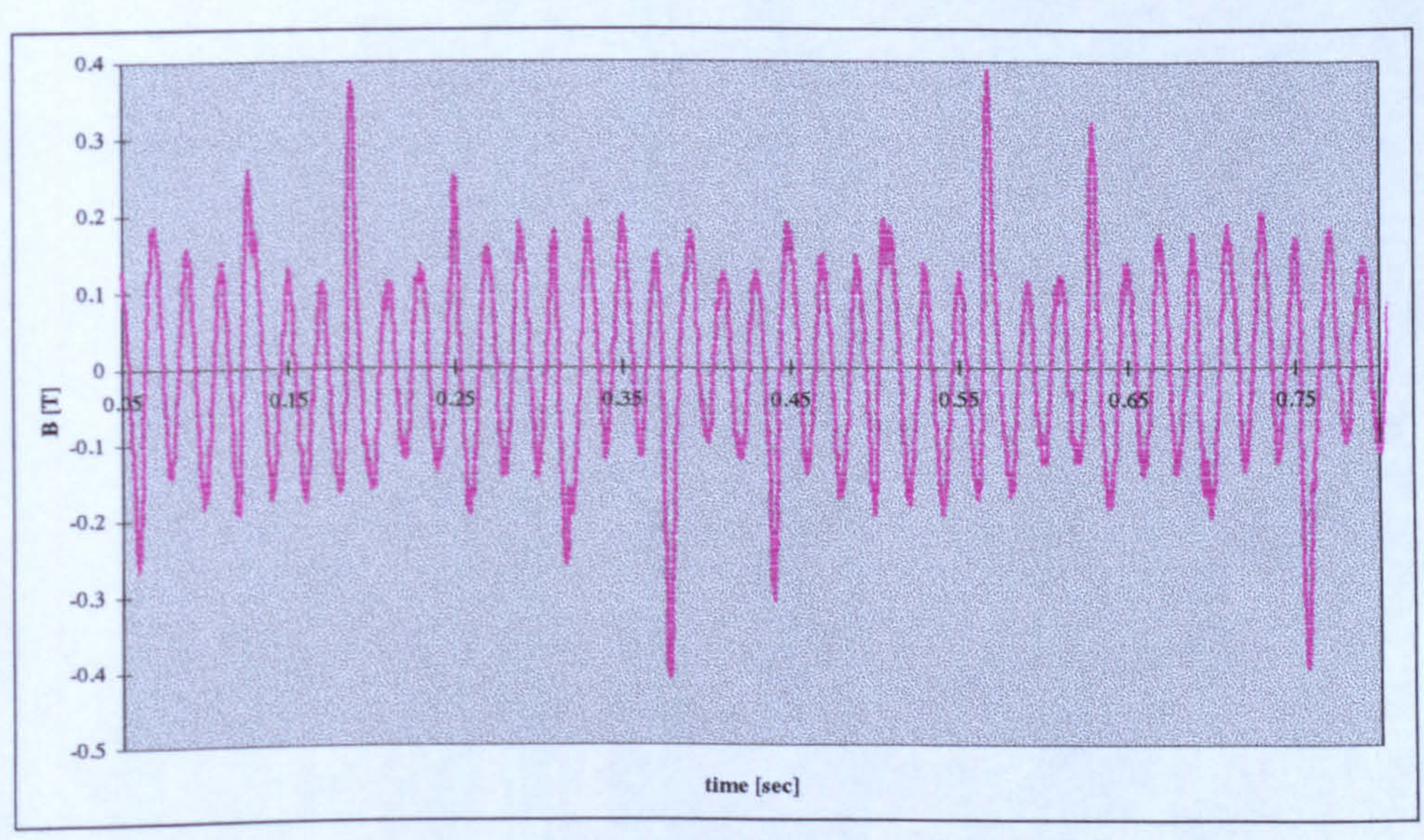

b) Three adjacent broken bars

Figure 6.6 *Stator back iron flux density.*

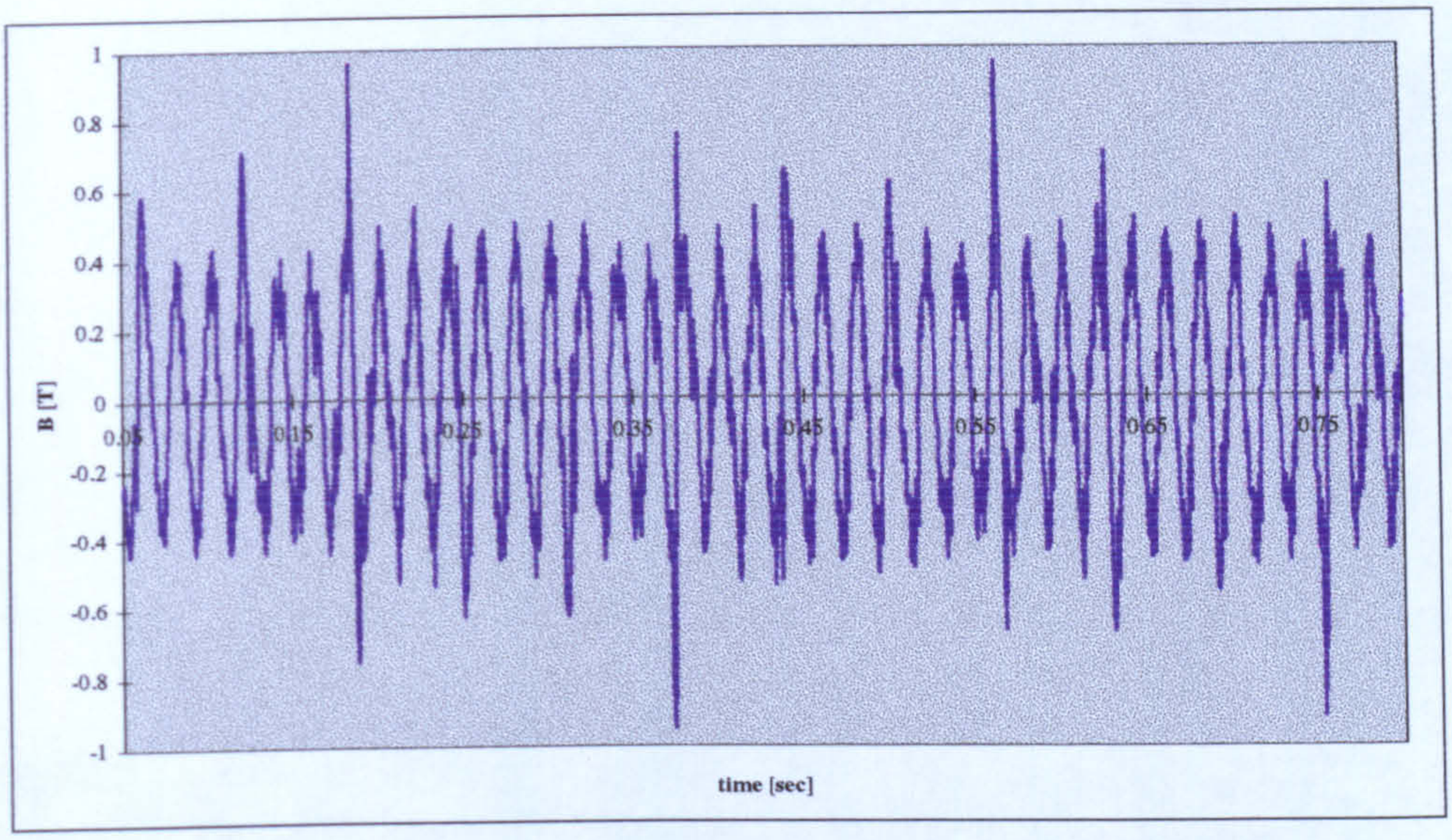

a) Two adjacent broken bars

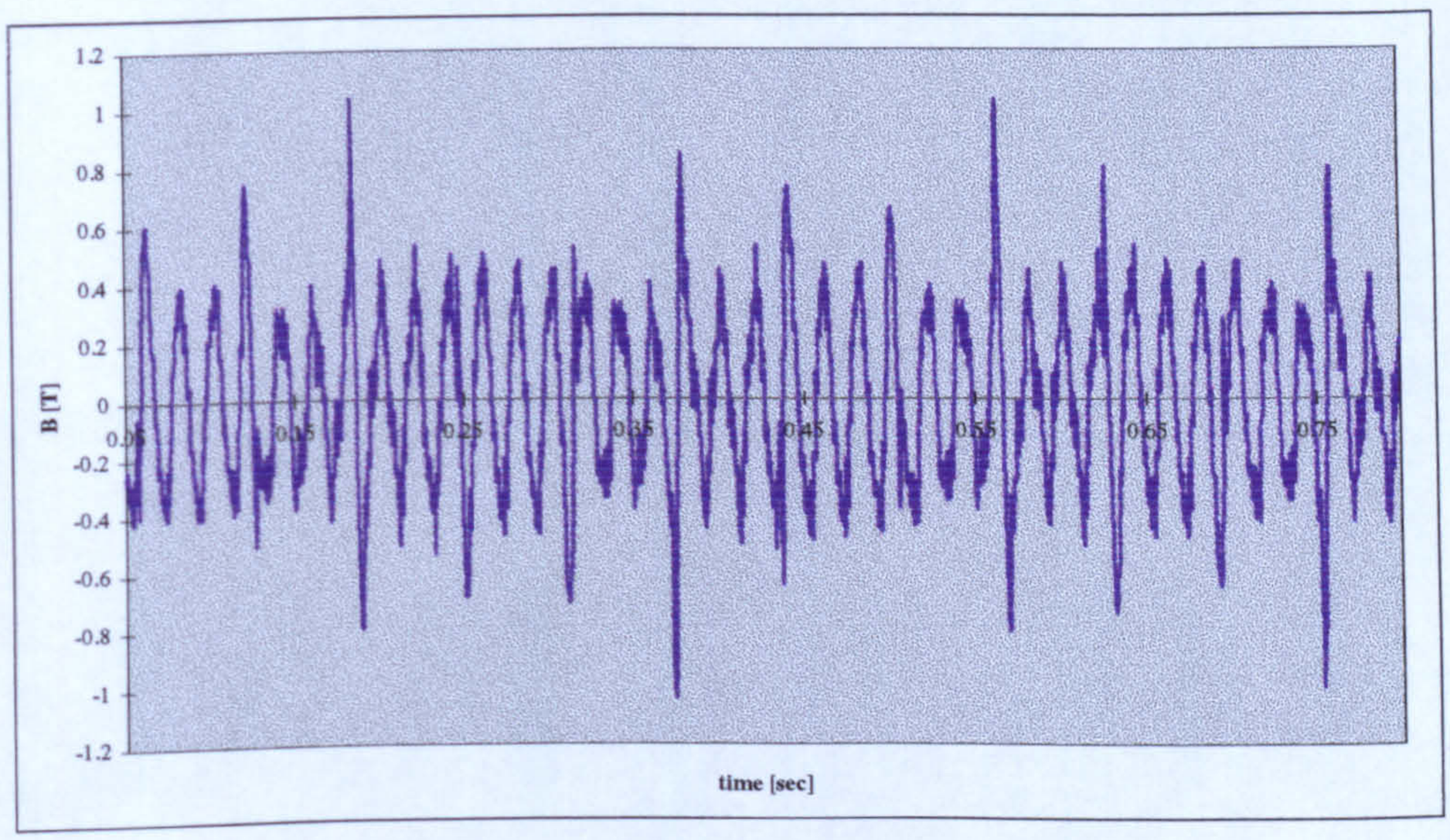

b) Three adjacent broken bars

***Figure 6.7** Stator tooth flux density.*

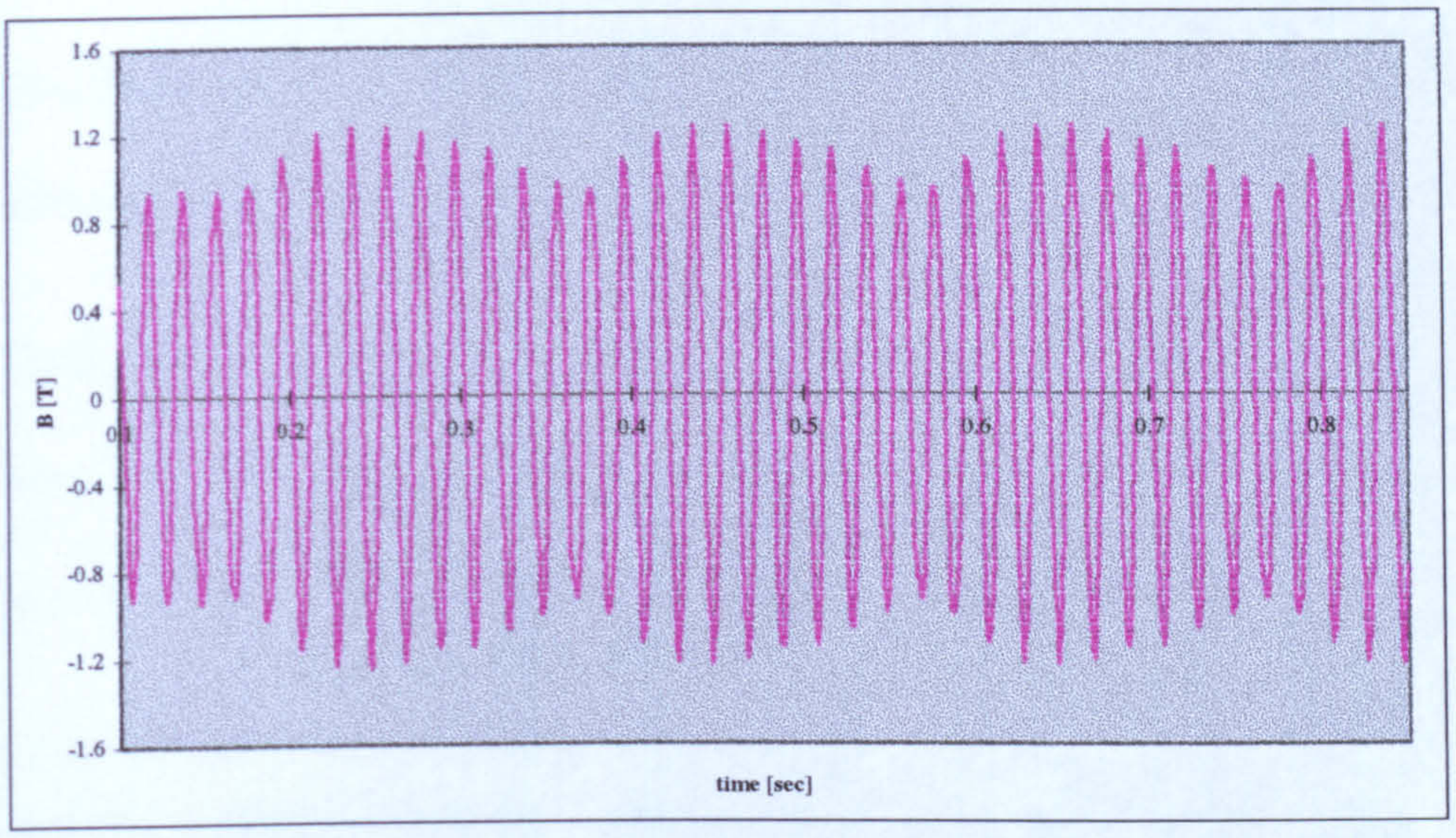

a) Two adjacent broken bars

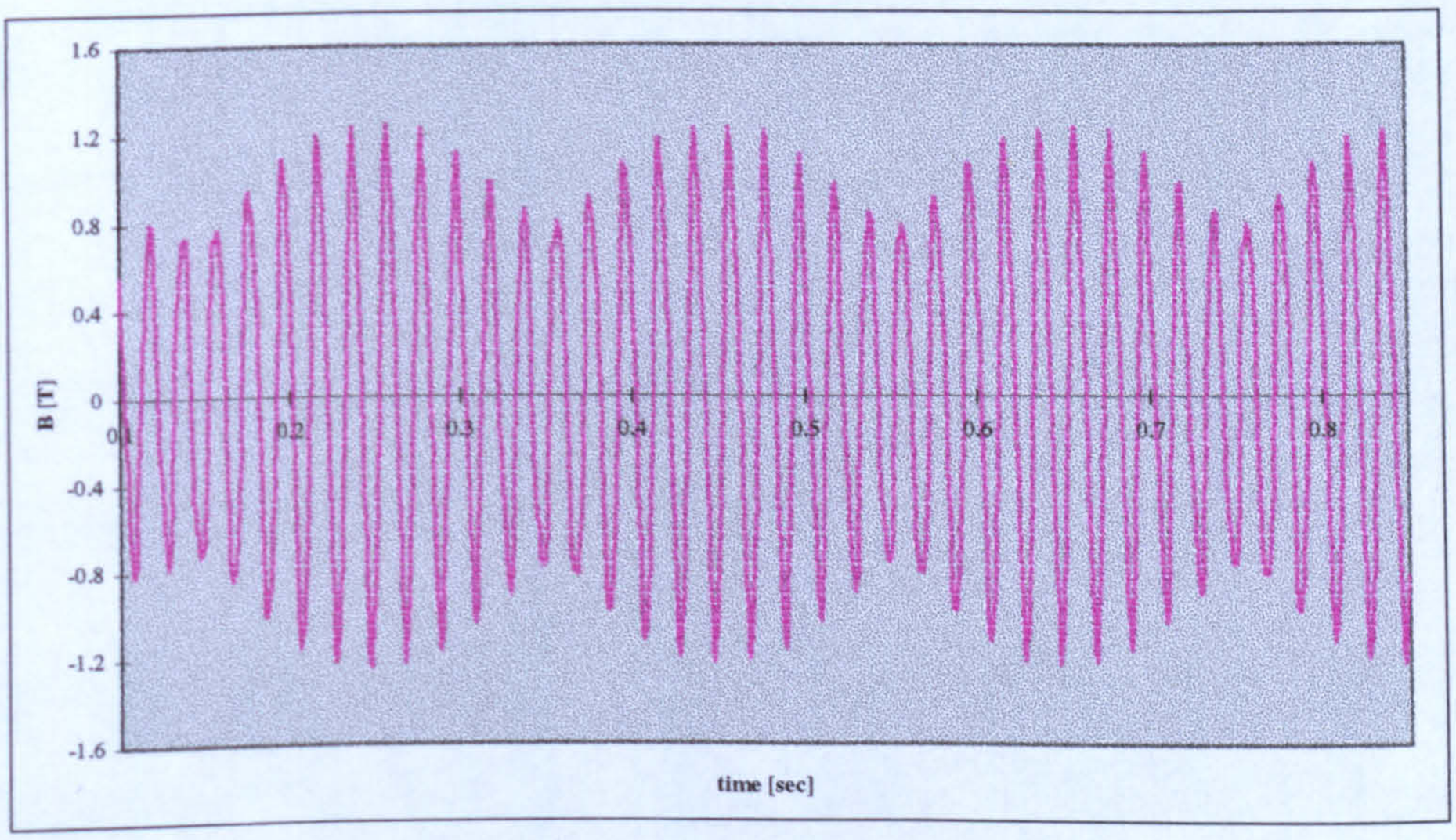

b) Three adjacent broken bars

Figure 6.8 *Stator tooth-tip flux density.*

It is very clear from these curves that when the machine is operating in the linear part of the magnetising characteristic the flux density waveform is no longer sinusoidal. Therefore, in the models where saturation is neglected, the effect of broken bars cannot be modelled correctly.

These flux density curves are also noticeably modulated by the field associated with the broken bars at a characteristic frequency, f_{fault}, given by $f_{fault} = (1-2s)f$.

6.2.2 ROTOR BAR CURRENTS

Bar currents near broken bars become very large as shown in Figures 6-9 and 6-10. This is due to the fact that the bars lying near the broken bars tend to carry a large current to compensate the effect of broken bars. A substantial increase in current can also be seen in the second pair of bars (brown) on either side of faulty bars. This results in an unbalanced distribution of rotor currents. This increased flow of current causes more thermal stresses on these bars and the associated regions of the end rings. The degree of overload depends on the position of the bars to each other.

Furthermore, the temperature distribution across the rotor lamination would be altered by the local heating effect produced by the increased current flow in certain bars and the absence or reduction of current flow in the faulty bars. All of these phenomena contribute to further deterioration of the rotor as well as to secondary failures on the stator. Stator insulation can fail under thermal

stresses imposed by the excessive and often unbalanced stator currents. Thus, timely detection of the onset of rotor imperfections is vital for condition monitoring on large induction machines.

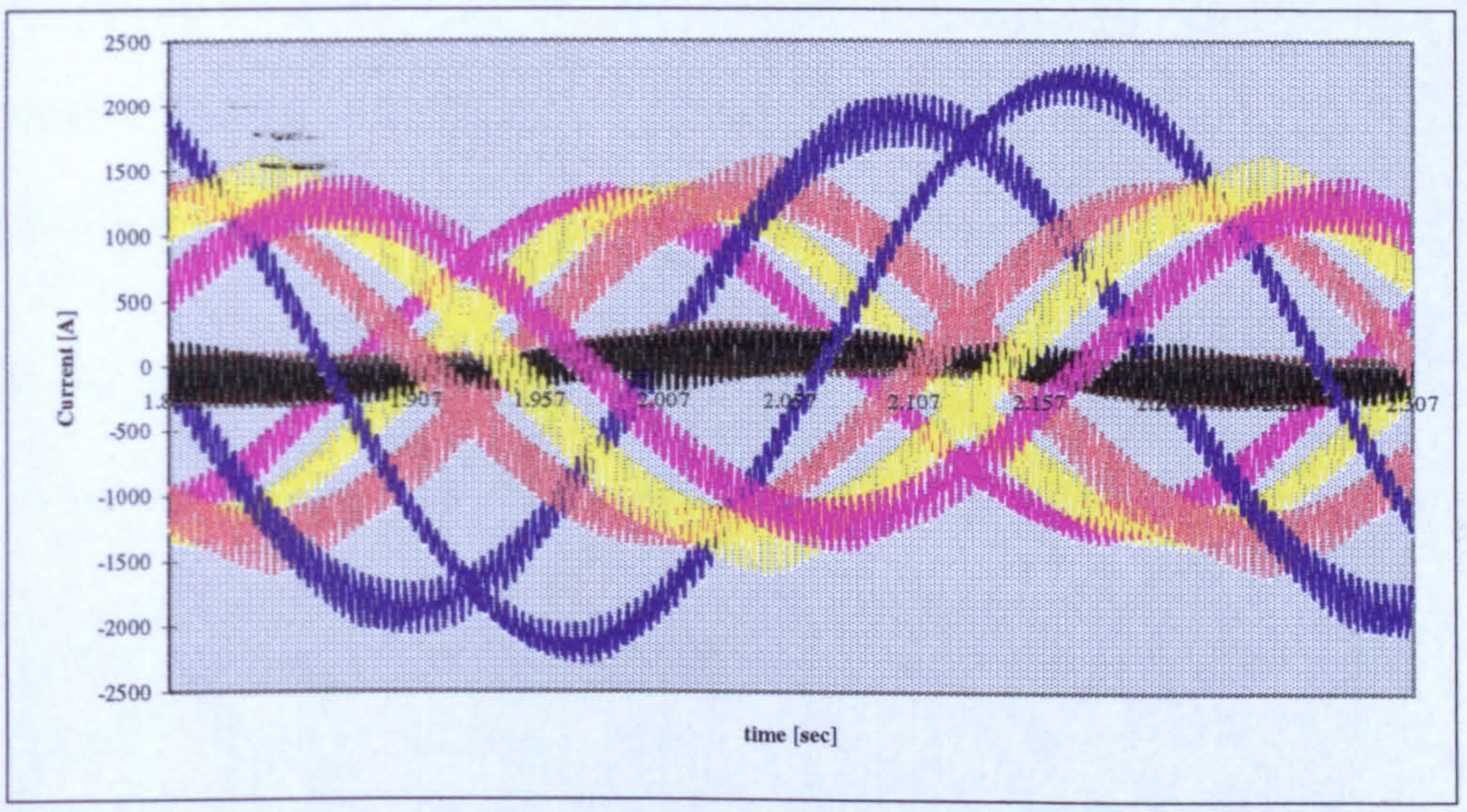

Figure 6.9 *Rotor bar currents with 2 adjacent broken bars*

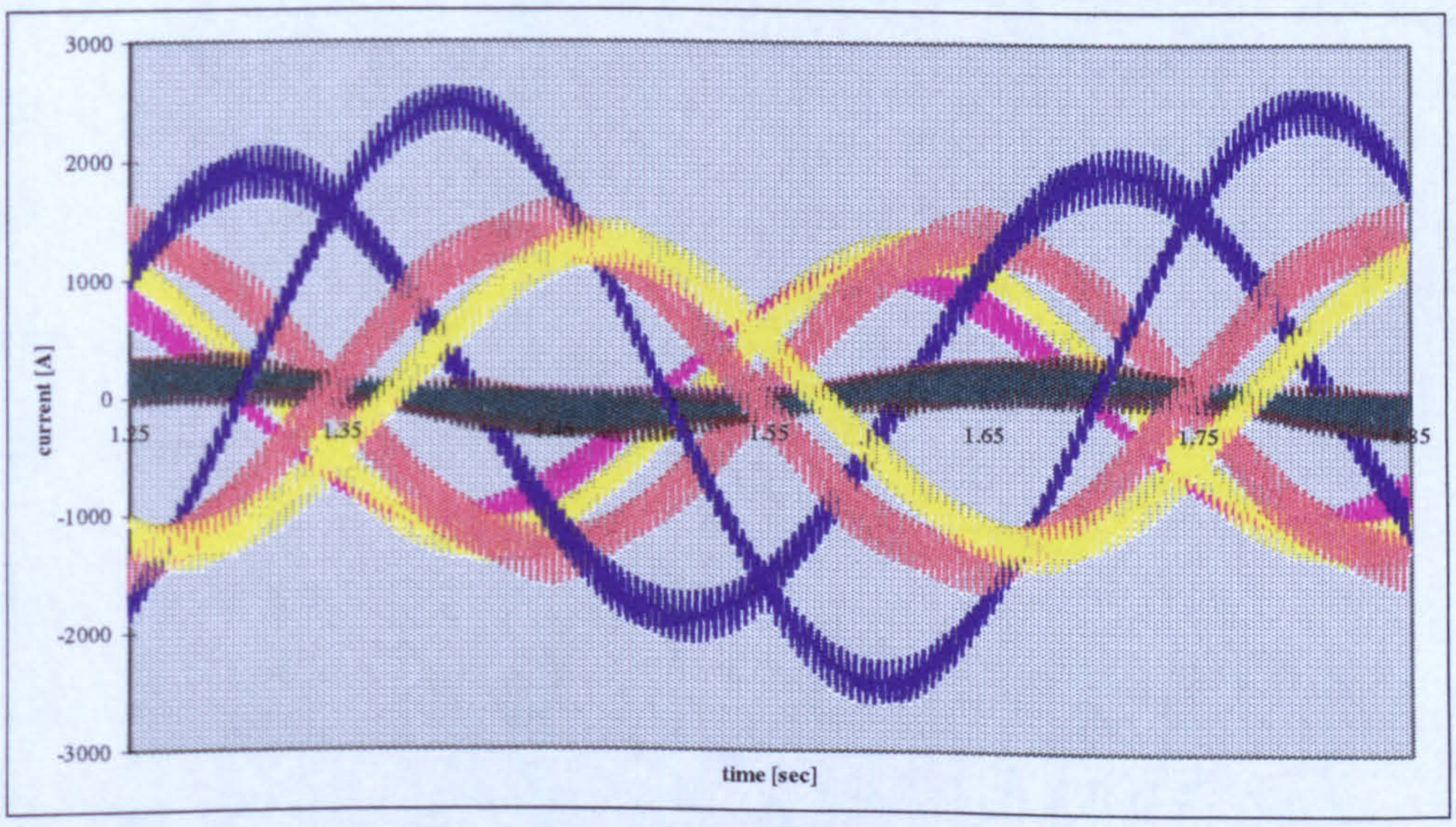

Figure 6.10 *Rotor bar currents with 3 adjacent broken bars*

NB: Blue: first pair on either side of broken bars, Brown: 2nd pair, Yellow: next pair and Pink: the following pair

6.2.3 STATOR CURRENT

The main purpose of this section is to investigate the effect of broken bars, their number and their relative position on the (1-2s)f component of the line current spectrum under different loads. In order to fulfil this task, a large number of tests had to be carried out. The tests were conducted for different loading conditions for each rotor fault.

It has been shown analytically that it should be possible to detect rotor defects, in a squirrel cage induction motor, by analysing the frequency content of a stator line current. The following sections are devoted to the verification of the above statement both from the model developed and experimentally. This is a two fold purpose. By doing so the validity of the model for such study is proved while at the same time confirming what has been achieved so far. The captured current waveforms were stored and analysed off-line along with those obtained from the computer simulation. By examining the resulting spectra, it is clear that the fault signature changes with the load and number of broken bars.

6.2.3.1 WAVEFORM ACQUISITION

Since the fastest fluctuations in the waveform correspond to the highest frequencies, it is clear that these frequencies will be lost if sampling is too low. This deduction is confirmed by Shannon's *Sampling Theorem*, which may be stated as follows:

An analogue signal containing components up to some maximum frequency f_N Hz may be completely represented by regularly-spaced samples, provided the sampling rate is at least $2f_N$ samples per second. In other words $f_s \geq 2f_N$.

The above relationship is necessary to avoid aliasing.

$$\text{Therefore, } \Delta t \leq \frac{1}{2f_N}, \quad T = \frac{1}{\Delta f} \quad \text{and} \quad f_N = \Delta f \cdot \frac{N}{2} \tag{6.6}$$

where f_s is the sampling frequency and f_N is the highest frequency in the spectrum (Nyquist frequency), Δt is the sampling period, Δf is the frequency resolution and T the duration of the input waveform record.

From the previous equations it is very clear that if we want to increase the frequency bandwidth, we have to decrease the sample period. Since $\Delta t = \frac{1}{N \cdot \Delta f}$, for a specified number of samples N, this means decreasing the frequency resolution and shorten the record length. In order to increase the frequency resolution it is necessary to increase the record length.

From Shannon's Theorem and Equation (6.6), if f_N and Δf are specified, the record length must satisfy the following equation:

$$N \geq \frac{2f_N}{\Delta f} \tag{6.7}$$

In order to get meaningful results this condition had to be observed in the data acquisition for spectrum analysis.

In the analysis, the fundamental frequency of the signal is 50Hz and the components of interest swing between 0Hz and 3f Hz. If the highest frequency is specified as 3f (i.e. 150Hz) and the desired frequency resolution is less than 0.1Hz then the number of samples required must be greater than 2*150/0.1=3000 samples.

In the computer program, in order to get reasonable results, the time step was set to 20μs (equivalent to a sampling rate of 50KHz). With this sampling frequency, to have a frequency resolution of only 1.0Hz, which is less than that required for this application, 50000/1.0 = 50000 samples are needed. This is a large number that needs a large memory storage capacity if many waveforms are to be saved. Accordingly, it was decided to store 1 sample every 0.5ms. With this sampling rate (2KHz), a record of 8192 samples yields a frequency resolution of 2000/8192=0.244Hz. At this frequency resolution the fault signature can be detected down to a slip of 0.244%. To increase the frequency resolution, we need either to increase the number of samples or decrease the sampling rate. For this work it is was decided to keep the sampling rate to 2KHz and the record length to 8192 samples. In order to have a direct comparison between the computed and measured results, we chose the same parameters for the test measurements as those for the analytical method.

6.2.3.2 EXPERIMENTAL AND COMPUTED WAVEFORMS

The acquired and computed stator line current waveforms for the case of zero (no broken bars), one and two broken bars are shown in Figures 6-11, 6-12 and 6-13 respectively. From the 8192 samples acquired only 400 samples are drawn. These Figures show how the shape of the line current changes with load and broken bars number.

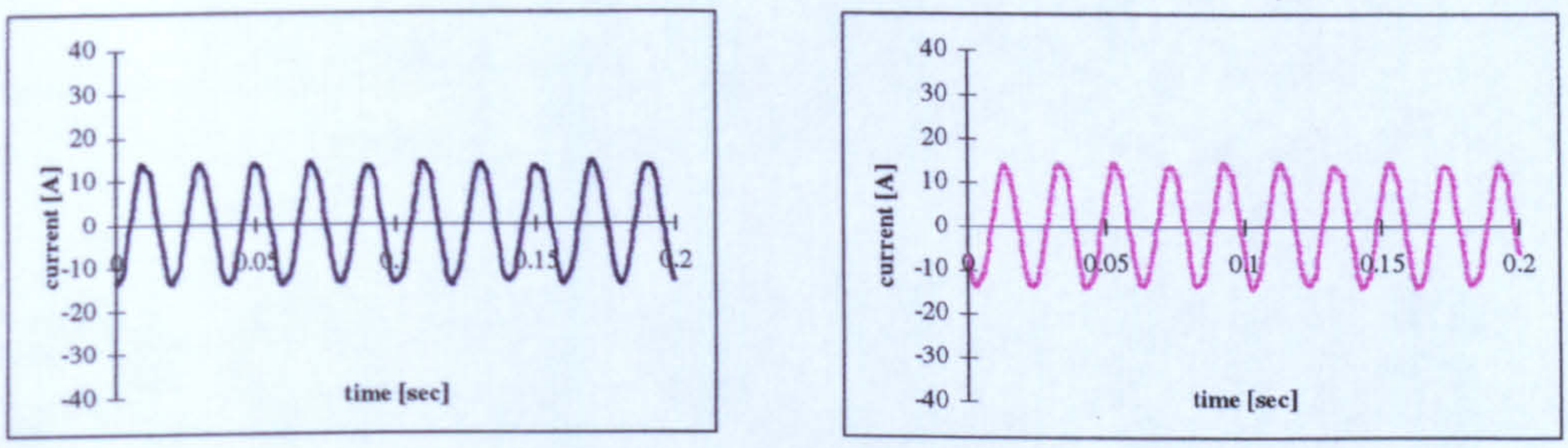

a) slip = 0%

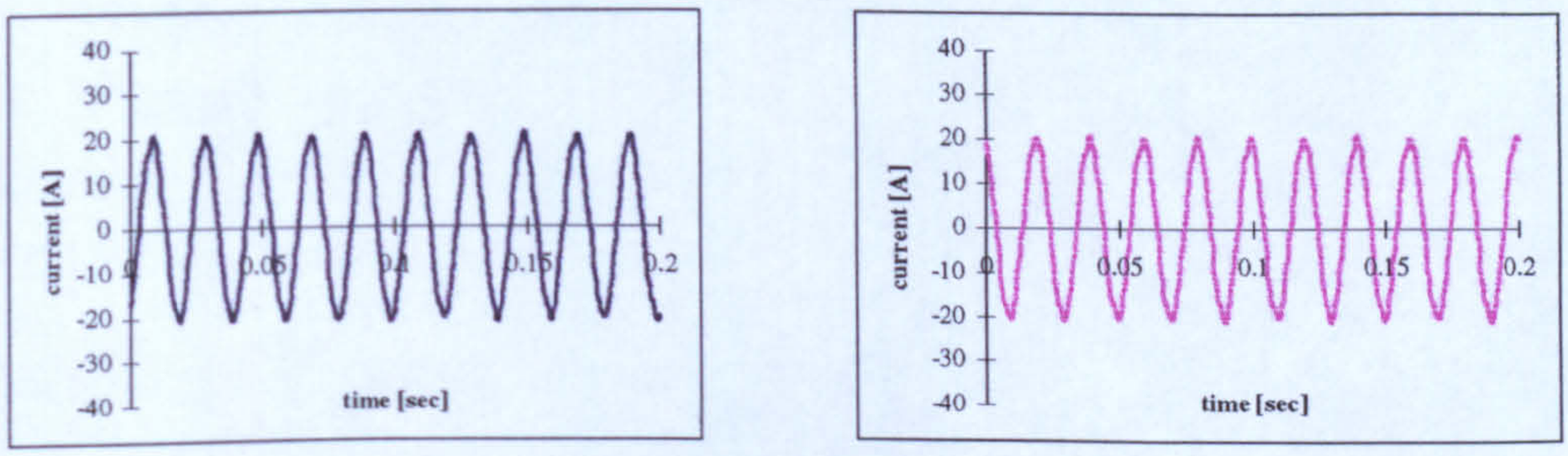

b) slip = 1%

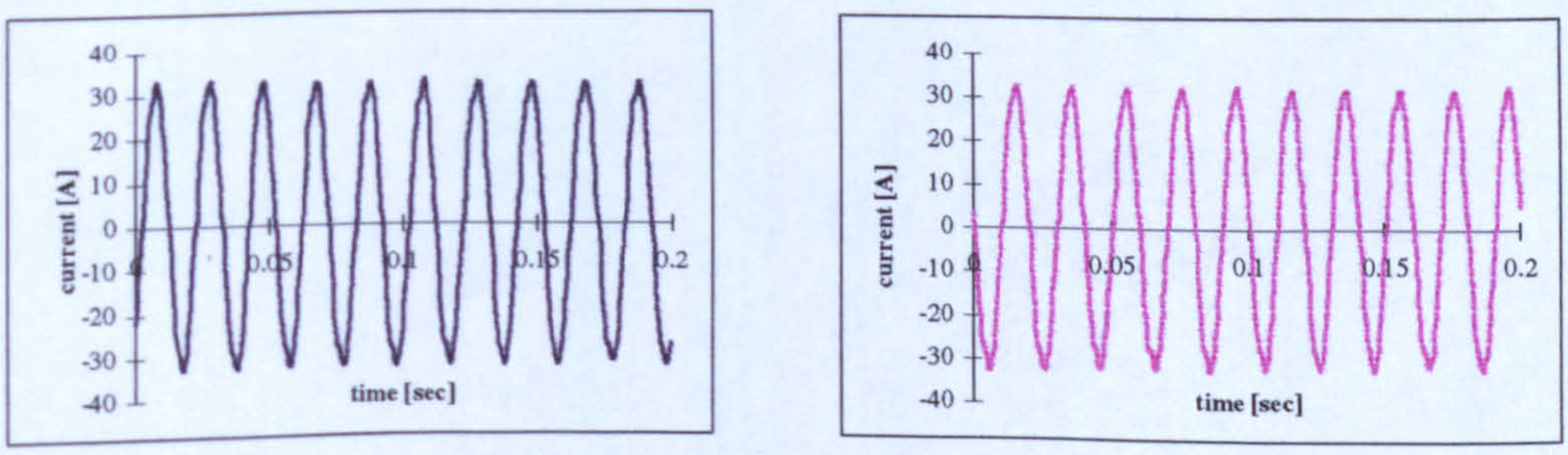

c) slip = 2%

Figure 6.11 *Measured (left) and computed (right) stator current waveforms with healthy rotor for different loads*

One broken bars						
	Measured			Computed		
Slip	Max_{peak}	Min_{peak}	Max-Min	Max_{peak}	Min_{peak}	Max-Min
0%	14.4	13.6	0.8	13.7	13.0	0.7
1%	22.5	21.3	1.2	22.3	21.0	1.3
2%	34.7	32.8	1.9	35.0	33.1	1.9
5%	71.9	65.6	6.3	74.0	67.6	6.4
Two broken bars						
	Measured			Computed		
Slip	Max_{peak}	Min_{peak}	Max-Min	Max_{peak}	Min_{peak}	Max-Min
0%	14.1	12.7	1.4	13.9	12.5	1.4
1%	23.1	21.6	1.5	23.3	21.7	1.6
2%	35.0	32.5	2.5	35.5	33.0	2.5
5%	72.7	64.1	8.6	71.9	63.4	8.5
Three broken bars						
	Measured			Computed		
Slip	Max_{peak}	Min_{peak}	Max-Min	Max_{peak}	Min_{peak}	Max-Min
0%	15.2	13.3	1.9	14.5	12.7	1.8
1%	23.4	20.9	2.5	24.7	21.2	3.5
2%	37.5	32.2	5.3	38.0	32.6	5.4
5%	74.2	61.7	12.5	72.7	61.1	11.6
Four broken bars						
	Measured			Computed		
Slip	Max_{peak}	Min_{peak}	Max-Min	Max_{peak}	Min_{peak}	Max-Min
0%	14.8	12.7	2.1	14.7	12.5	2.2
1%	23.1	20.9	2.2	23.3	21.1	2.2
2%	35.6	30.3	5.3	36.0	30.6	5.4
5%	69.5	55.5	14.0	68.7	54.8	13.9
Five broken bars						
	Measured			Computed		
Slip	Max_{peak}	Min_{peak}	Max-Min	Max_{peak}	Min_{peak}	Max-Min
0%	15.3	12.8	2.5	15.1	12.6	2.5
1%	23.8	20.3	3.5	23.4	20.0	3.4
2%	35.3	29.4	5.9	34.9	29.0	5.9
5%	68.8	53.1	15.7	67.8	52.4	15.4

Table 6-1 *Effect of load and number of broken bars on stator current waveform.*

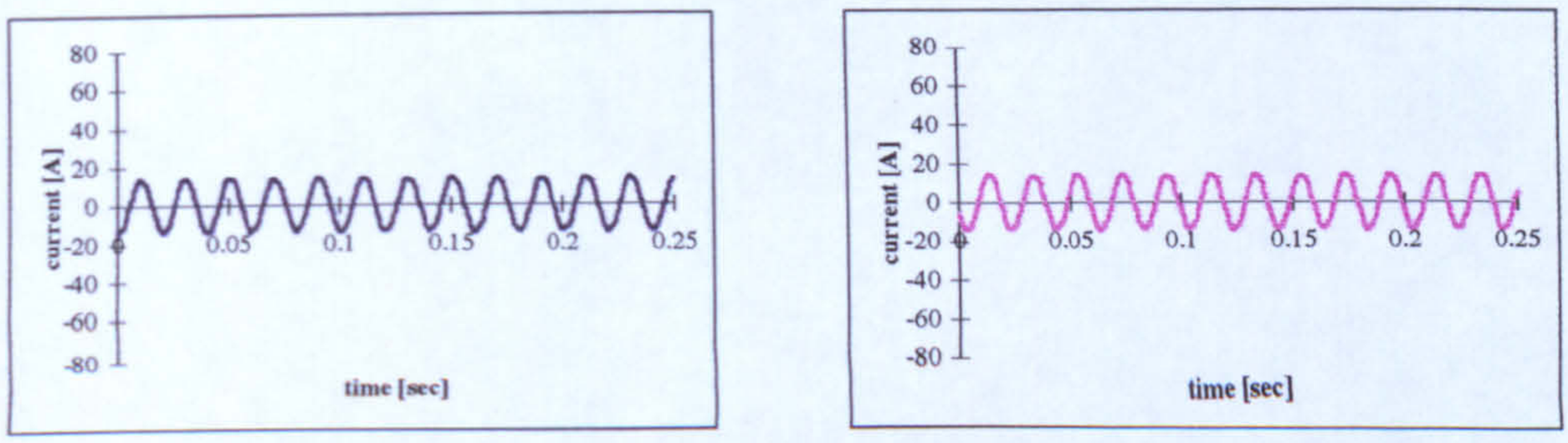

a) slip = 0%

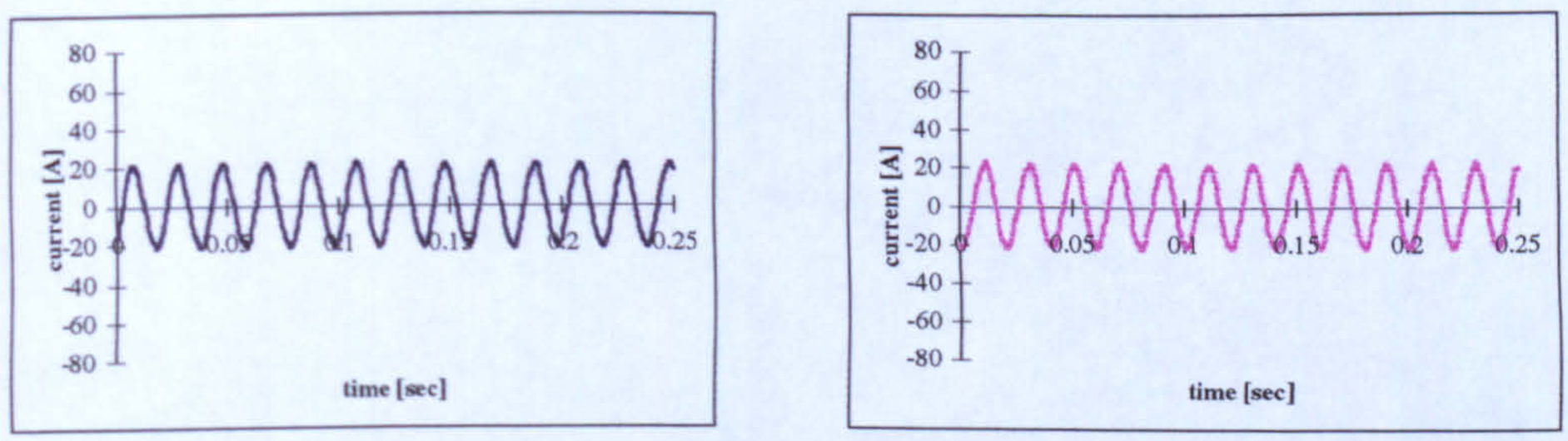

b) slip = 1%

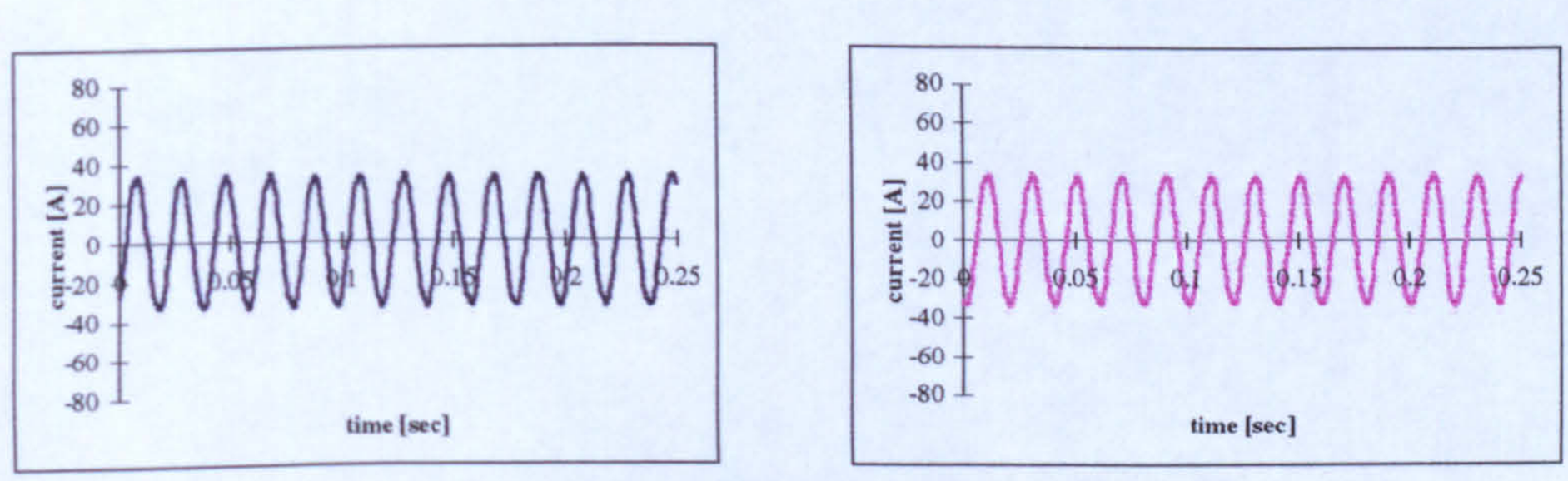

c) slip = 2%

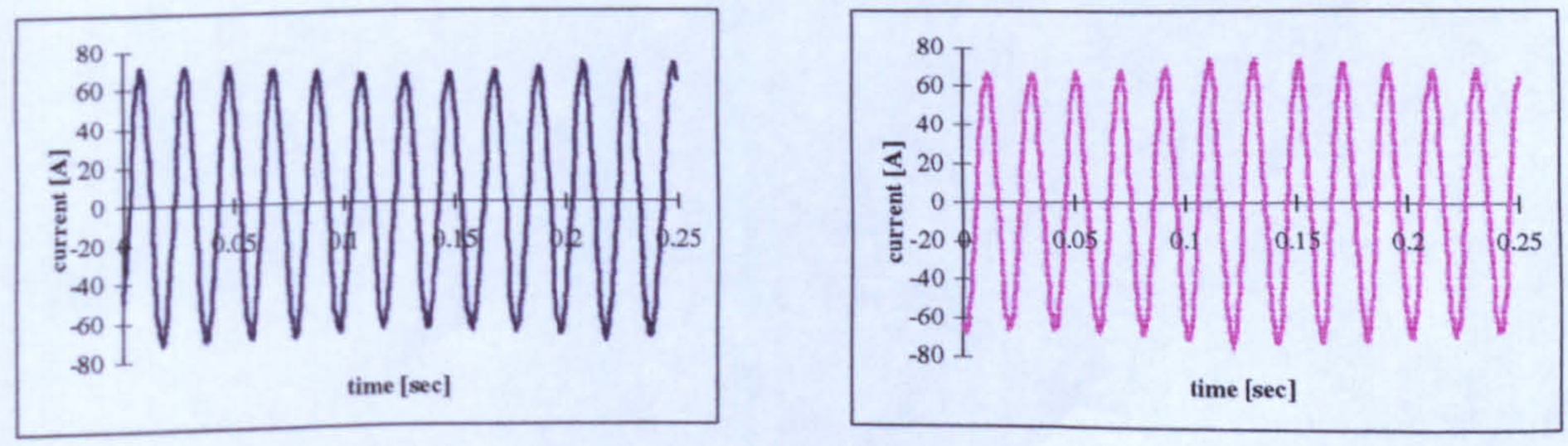

d) slip = 5%

Figure 6.12 *Measured (left) and computed (right) stator current waveforms with one rotor broken bar for different loads .*

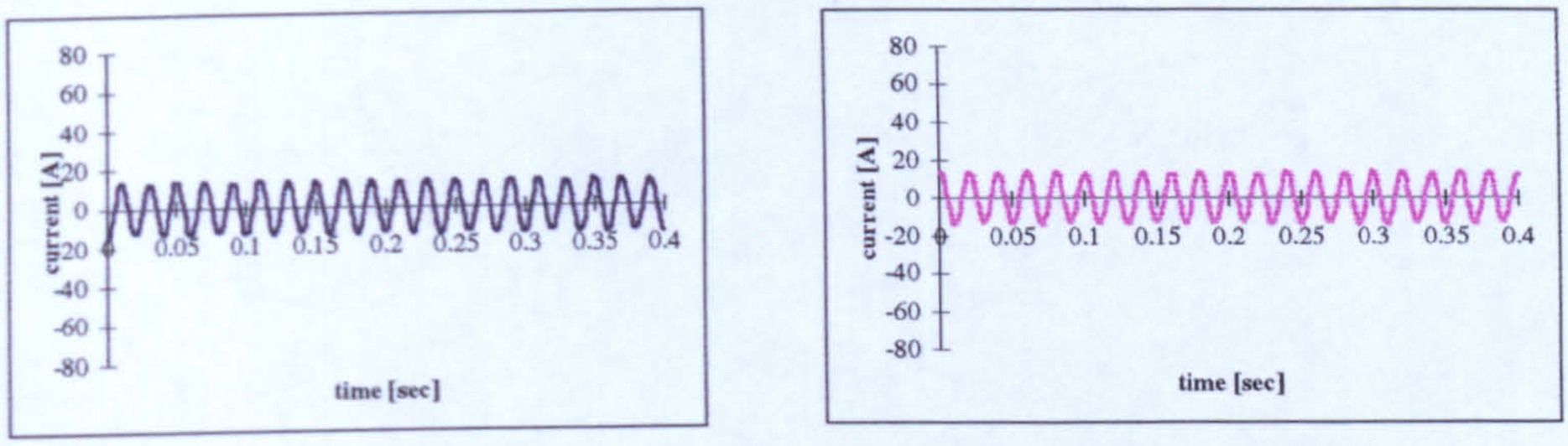

a) slip = 0%

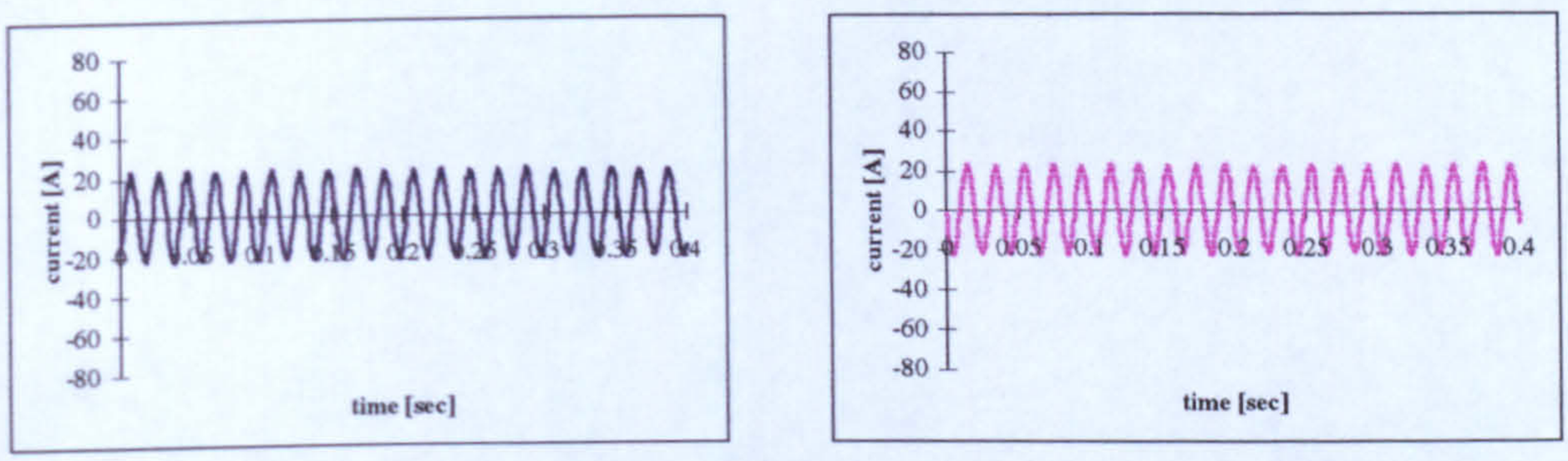

b) slip = 1%

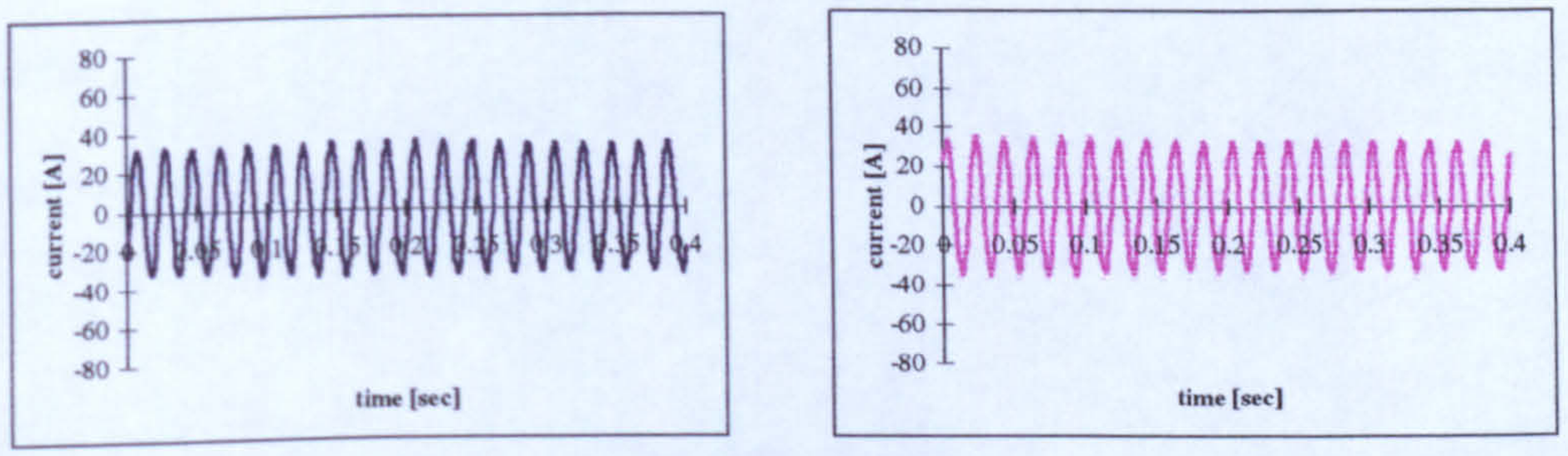

c) slip = 2%

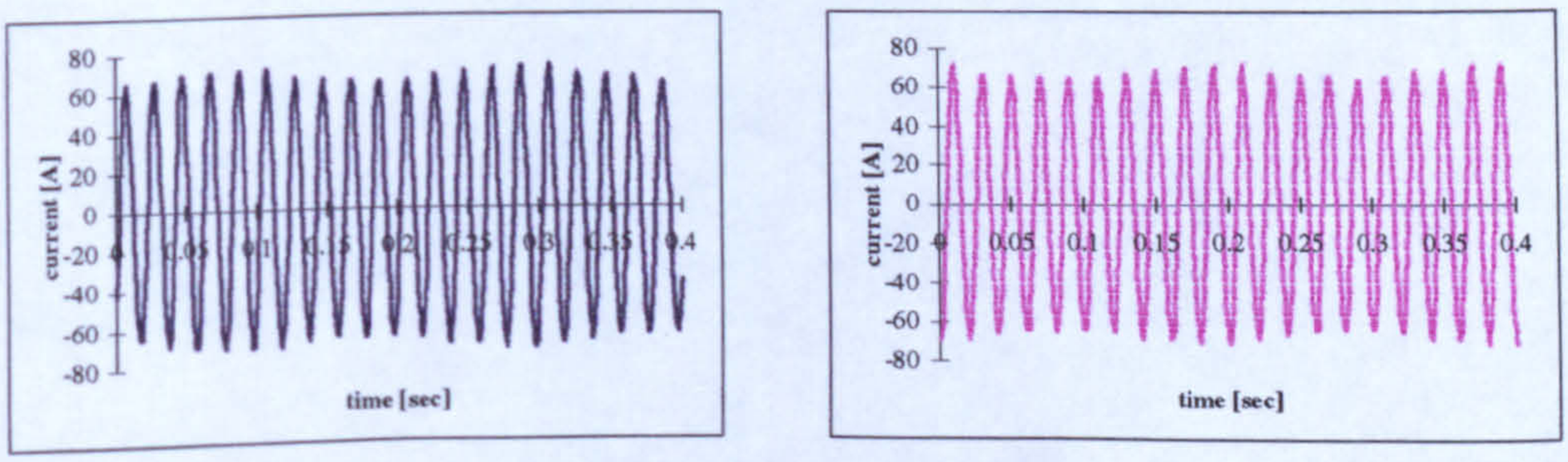

d) slip = 5%

Figure 6.13 *Measured (left) and computed (right) stator current waveforms with two adjacent broken bars for different loads.*

In the time domain these waveforms seem to differ only in amplitude. However, the load application will distort the harmonic content of the stator current as will be shown later in the spectral analysis. It can be seen from these curves that as the load increases the shape of the stator current starts changing. In Figure 6-11 where there are no broken bars, all that can be seen is that the amplitude of the current increases with the load. Whereas in the presence of broken bars, the current waveform is modulated by the fault frequency component. This can be noticed even with one single broken bar. Table 6-1 shows these effects in a clearer and simpler way. It can be seen that the difference between the maximum positive peak and the minimum positive peak increases as the load increases. It also increases with the number of broken bars. The no load speed varied from test to test due to differences in the slope of the torque speed curve resulting from the change of rotor impedance with increasing number of broken bars. Although the tests were nominally no load, in each case the friction and windage losses of the full test rig were supplied by the test motor. This was achieved by reducing the armature current of the dc load machine to zero.

It is very clear from the above results that the model predicts very well the effect of broken bars with very reasonable precision. The error changes between 4.35% and 8% at most.

The effect of the position of the broken bars in relation to each other is depicted in the Figures of appendix D. There is not much information that can

be extracted from these curves neither the shape nor the magnitude can be differentiated. They all look the same. But the good news is that the model is capable of predicting all these asymmetries. There is no restriction on the position or the number of broken bars. On top of that the computed results agree well the experimental ones.

6.2.3.3 SPECTRAL ANALYSIS

The acquired data files, using Lecroy described in the previous section, are processed and graphically viewed using specially developed data analysis programs, which have been developed using Pascal Language.

1- FFT-BASED SPECTRUM COMPUTATION

A computer software, called *SIGNAL* for computing the spectrum of the acquired and computed waveforms was developed using Pascal Language. The program asks for the data filename to be analysed, the sample period, the desired sampling frequency and the appropriate scaling factor for the acquired data.

SIGNAL starts by opening the specified file and reading data, then it finds the file's size (number of data samples). If the number of samples is not a multiple of two it searches for the largest record which is a multiple of 2. The main task of *SIGNAL* is to compute the FFT of the waveform. However, it can compute the mean value and variance. A choice of five windows is available. These are: rectangular windowing, tapered rectangular, triangular, Hanning, Hamming and Blackman windows.

2- EXPERIMENTAL AND COMPUTED SPECTRA

Figures 6.14, 6.15 and 6.16 represent the spectra of the stator current waveform for different load conditions with a healthy rotor, one broken bar and two adjacent broken bars respectively.

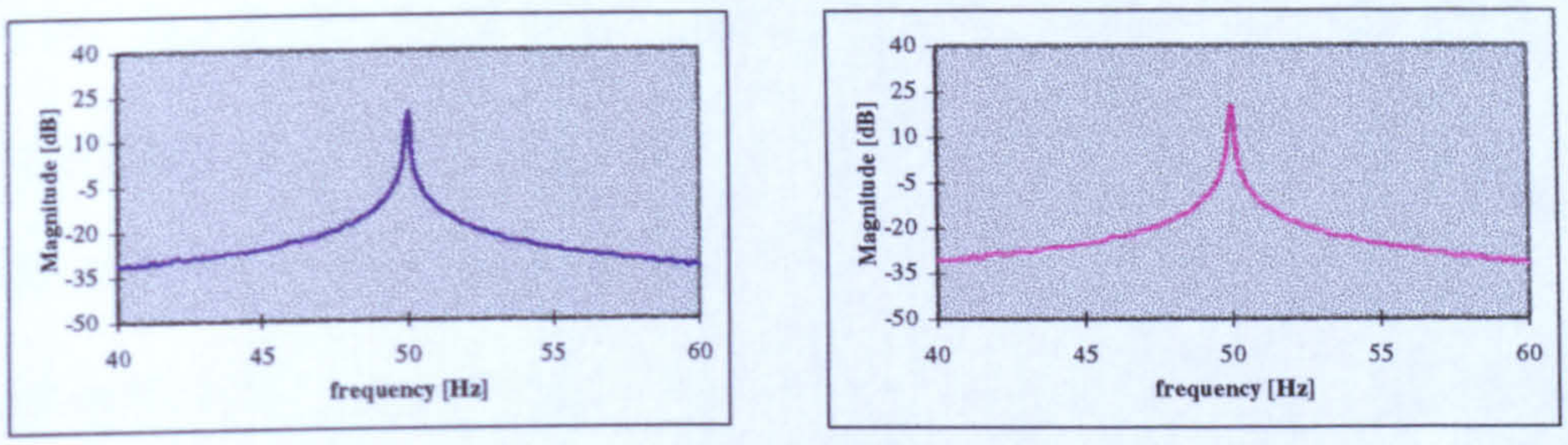

a) slip = 0%

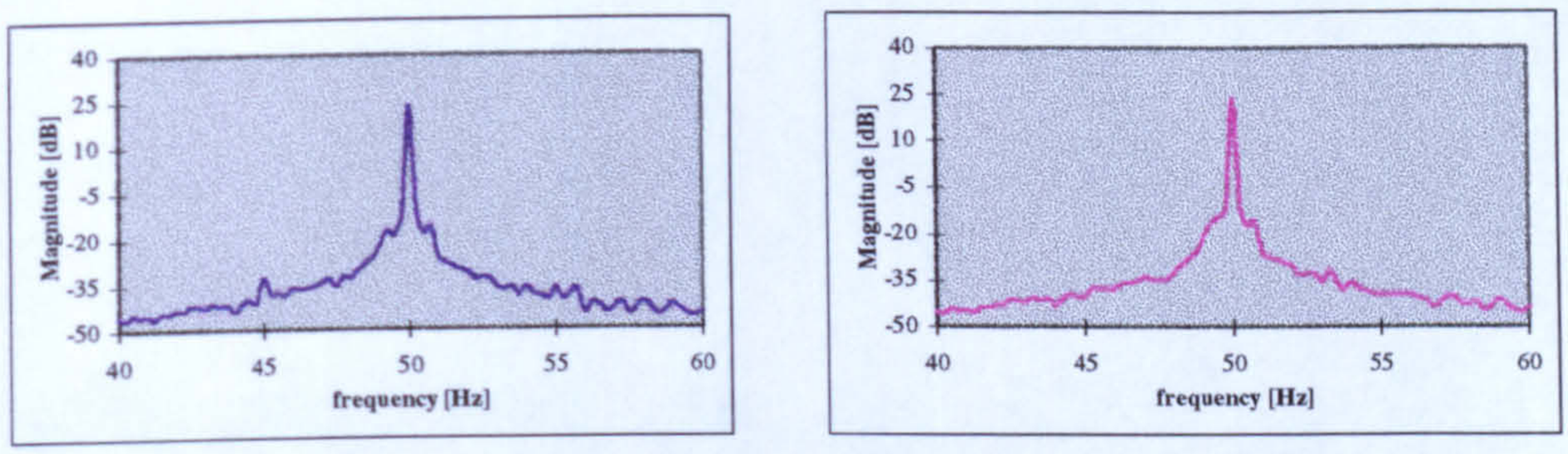

b) slip = 1%

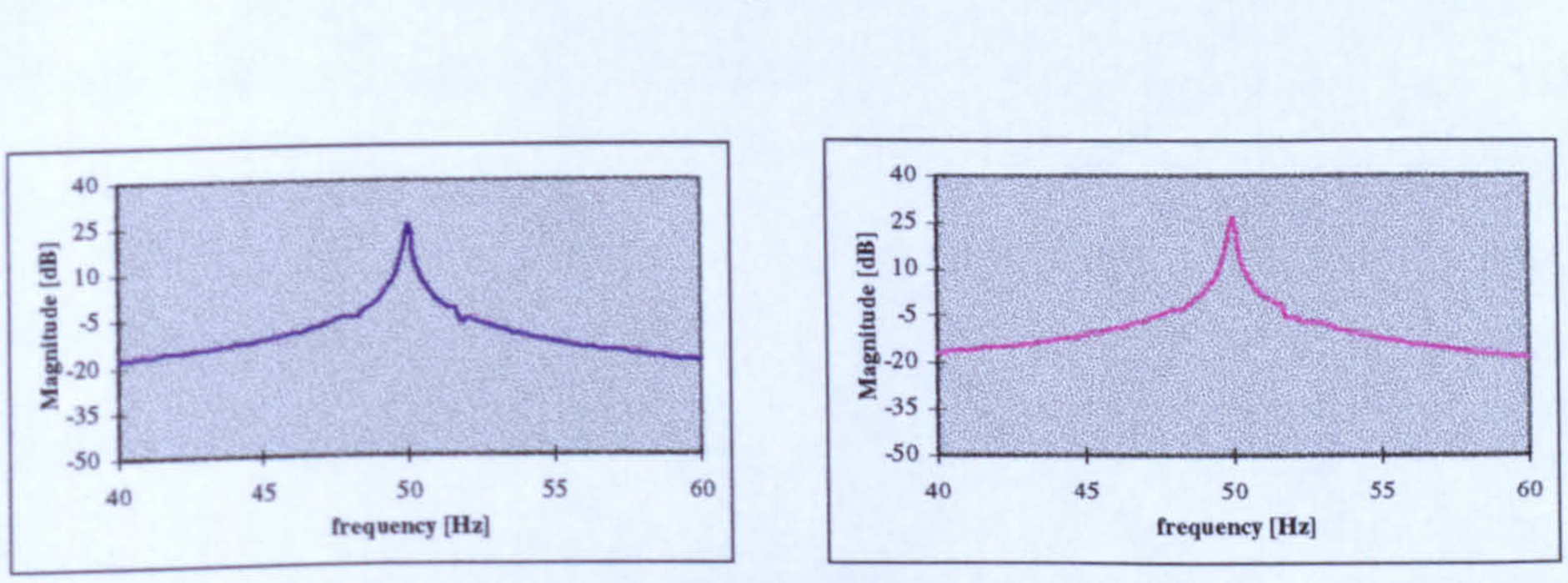

c) slip = 2%

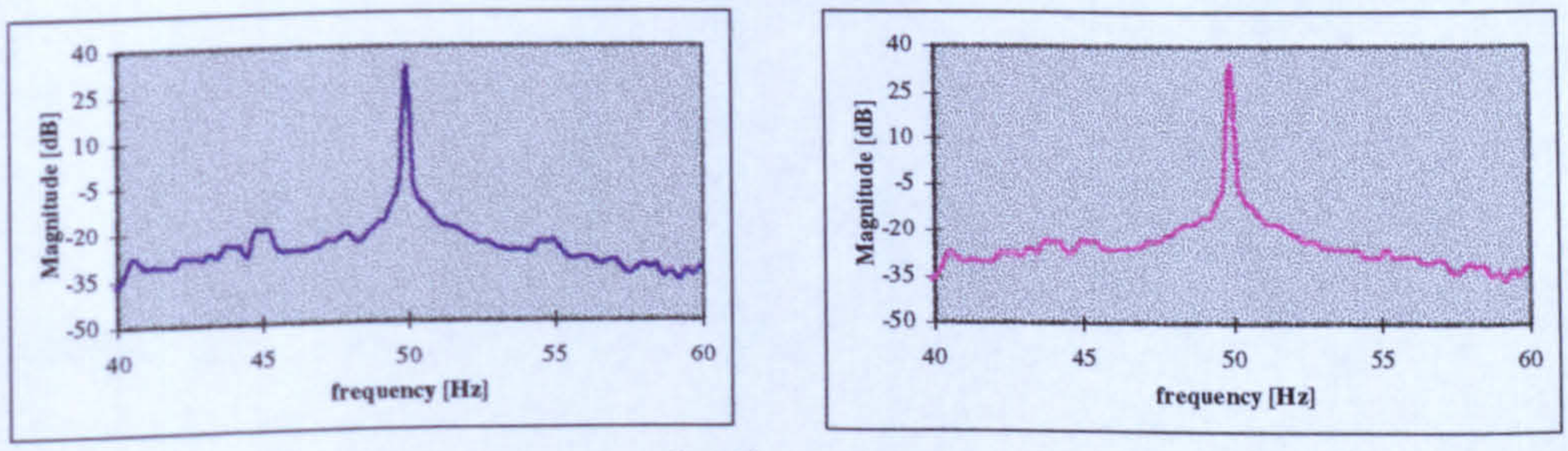

d) slip = 5%

Figure 6.14 *Effect of load on the spectra of the measured (left) and computed (right) stator current waveforms with a healthy rotor. (0dB ≡ 1A)*

It can be seen from Figure 6.14 that as the load increases, the fundamental component of the current spectra for a healthy rotor increases in magnitude. Whereas for a faulty rotor, as shown in Figures 6.15 and 6.16, the fault component increases in magnitude and moves away from the fundamental. Again, the model proves itself valid in the frequency domain analysis as well.

In contrast to the time domain analysis, in the frequency domain, the harmonics components do change with the load, the number of broken bars and their position in relation to each other. For more results see table 6.2.

The effect of load on the fault component is illustrated in Figure 6.17. From these curves it can be seen that, as the slip increases the magnitude of the (1-2s)f component increases. Therefore, the fault can be easily detected under load. For no load conditions this component is very close to the fundamental and of a very low magnitude and thus becomes very difficult to detect.

Figure 6.18 shows the effect of the number of broken bars on the magnitude of the fault signature (1-2s)f. It is very clear that as the number of broken bars increases the magnitude of this component increases.

One broken bar						
	Measured [dB]			Computed [dB]		
Slip (%)	(1-2s)f	f	(1+2s)f	(1-2s)f	f	(1+2s)f
0%	##	19.7	##	##	20.1	##
1%	-12.1	23.5	-14.2	-11.6	24.0	-13.6
2%	-2.0	26.7	-3.8	-1.5	27.2	-3.2
5%	2.2	33.6	-18.7	2.8	34.1	-18.1
Two adjacent broken bars						
	Measured [dB]			Computed [dB]		
Slip (%)	(1-2s)f	f	(1+2s)f	(1-2s)f	f	(1+2s)f
0%	##	16.2	##	##	16.8	##
1%	-9.6	23.8	-13.4	-9.1	24.5	-12.8
2%	-2.0	26.4	-4.3	-1.4	27.0	-3.7
5%	5.0	33.6	-10.7	5.5	34.2	-10.1
Three adjacent broken bars						
	Measured [dB]			Computed [dB]		
Load (%)	(1-2s)f	f	(1+2s)f	(1-2s)f	f	(1+2s)f
0%	##	19.1	##	##	19.6	##
1%	-4.6	23.8	-7.0	-4.1	24.3	-6.5
2%	1.4	24.4	2.5	2.0	25.0	2.4
5%	9.1	33.4	-7.1	9.6	34.0	-6.6
Four adjacent broken bars						
	Measured [dB]			Computed [dB]		
Slip (%)	(1-2s)f	f	(1+2s)f	(1-2s)f	f	(1+2s)f
0%	##	16.2	##	##	16.8	##
1%	-4.8	23.7	-6.1	-4.2	24.3	-5.5
2%	4.0	26.3	0.8	4.6	26.9	1.4
5%	13.9	32.8	-2.7	14.5	33.3	-2.1
Five adjacent broken bars						
	Measured [dB]			Computed [dB]		
Slip (%)	(1-2s)f	f	(1+2s)f	(1-2s)f	f	(1+2s)f
0%	##	19.3	##	##	20.0	##
1%	-5.2	23.6	-4.6	-4.6	24.2	-4.0
2%	5.1	26.0	0.6	5.7	26.6	1.2
5%	14.8	32.6	1.4	14.4	33.2	2.1

***Table 6.2** Effect of load on the fundamental and fault frequency components with different number of broken bars. (the symbol "##" means undetected component)*

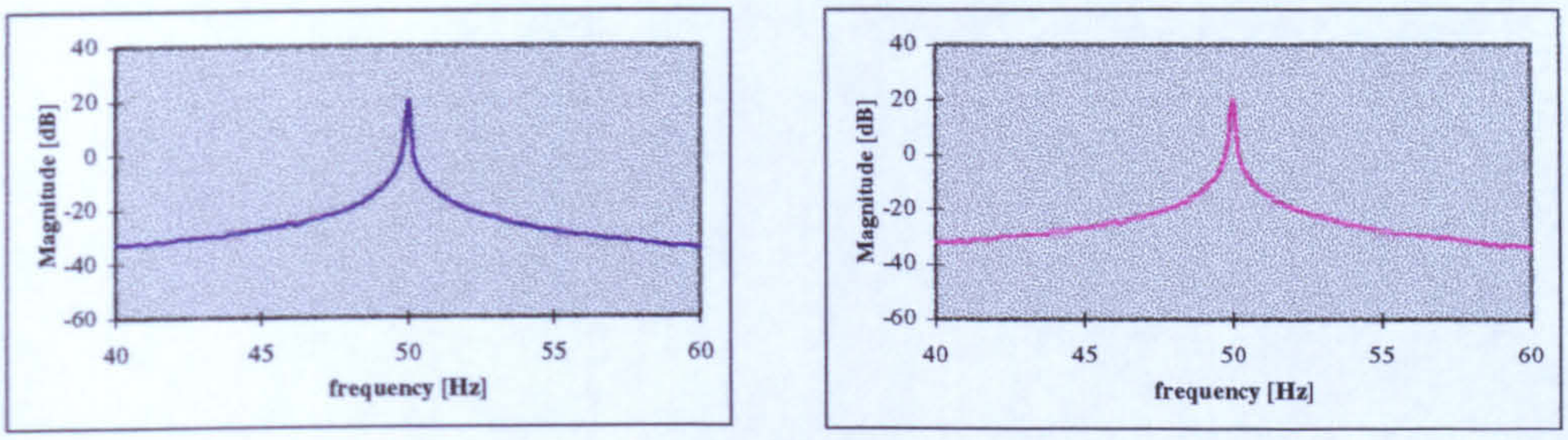

a) slip = 0%

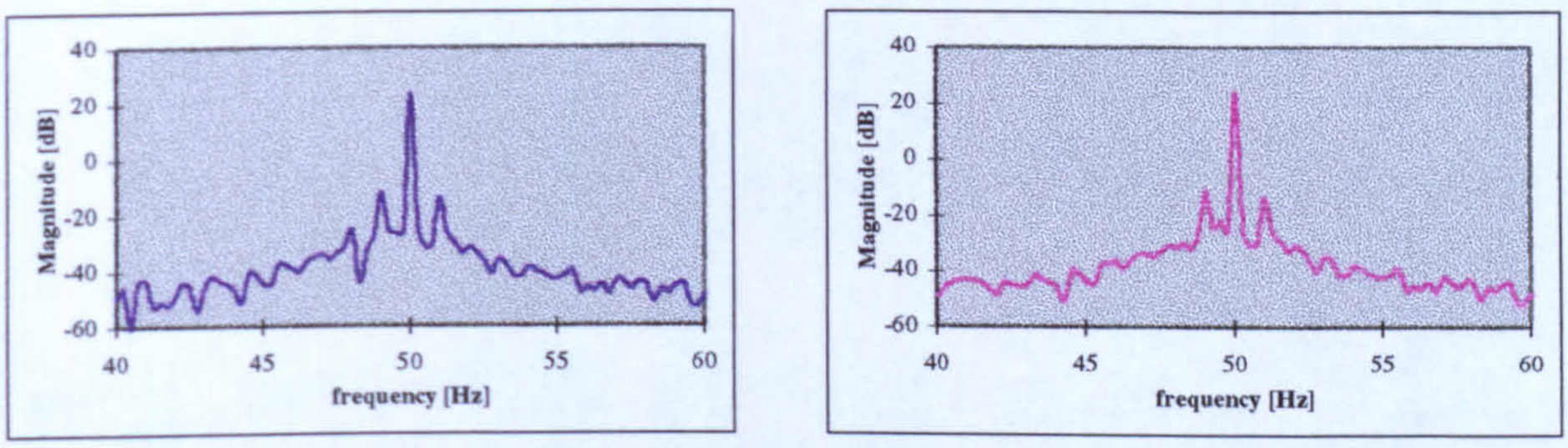

b) slip = 1%

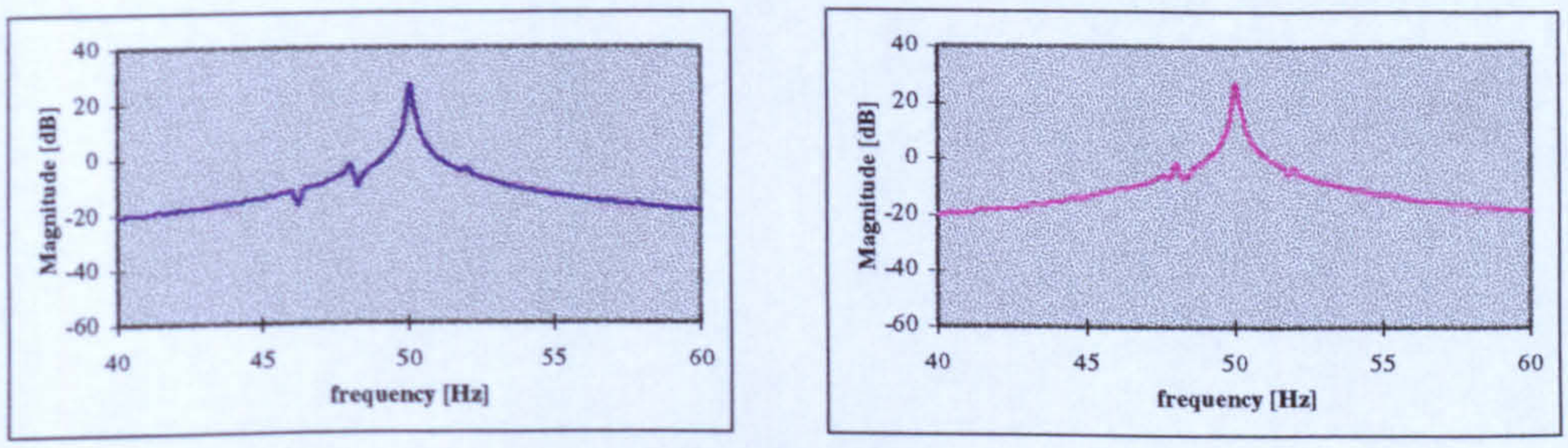

c) slip = 2%

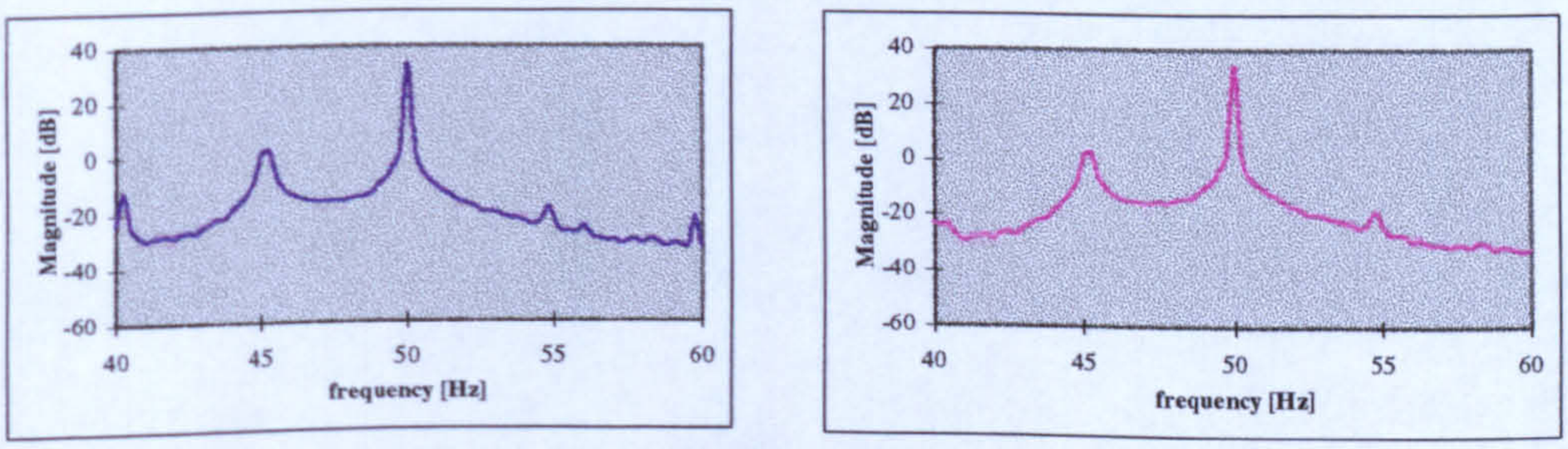

d) slip = 5%

Figure 6.15 *Effect of load on the spectra of the measured (left) and computed (right) stator current waveforms with one broken bar. (0dB ≡ 1A).*

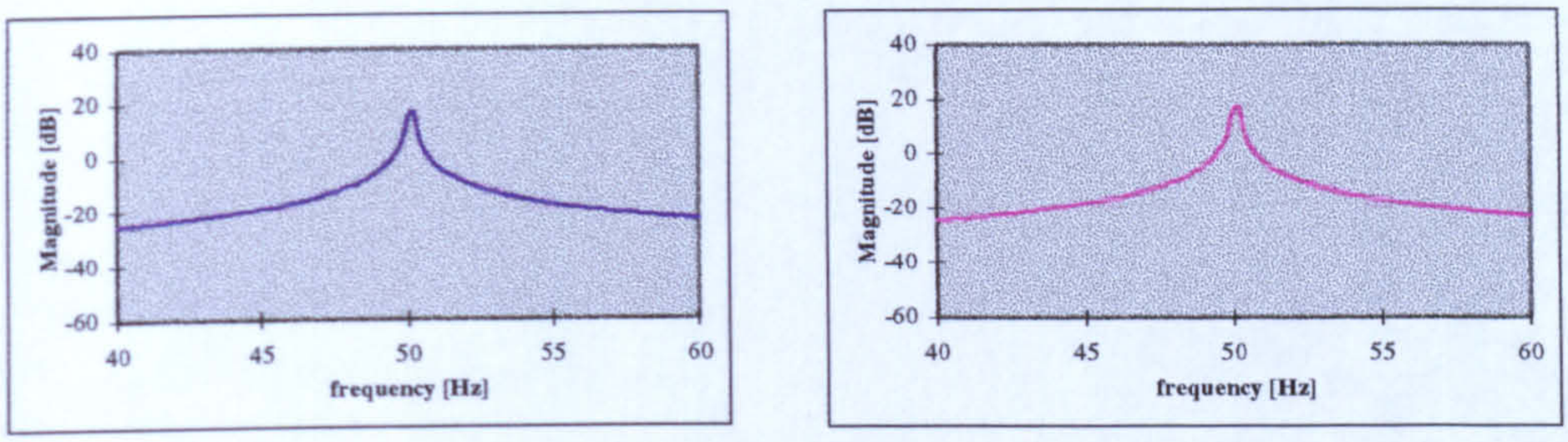

a) slip = 0%

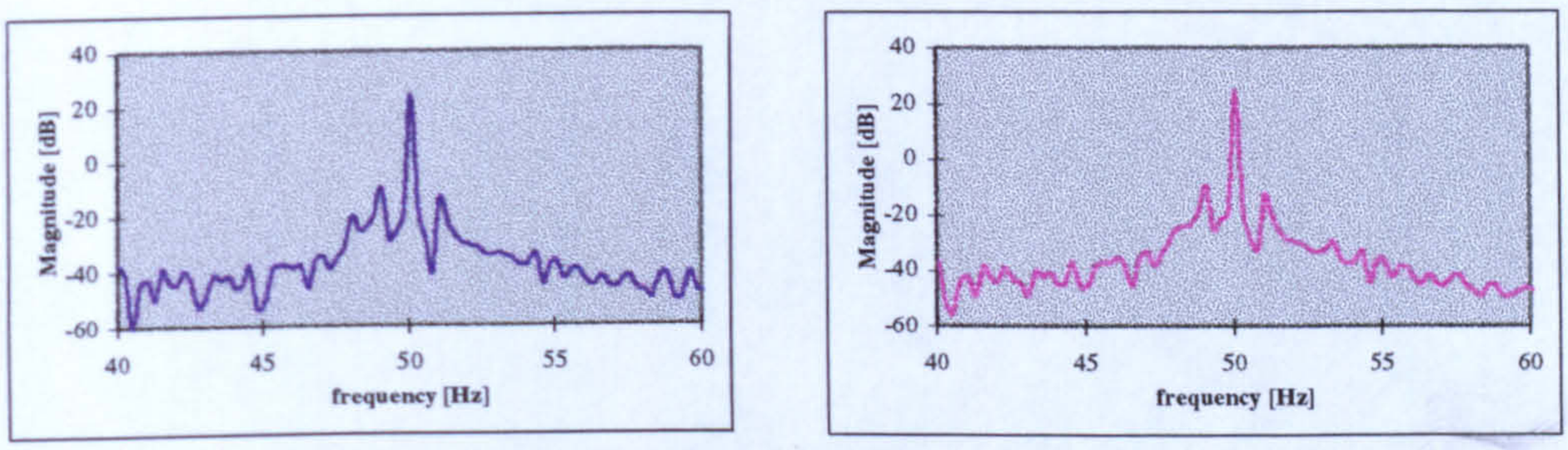

b) slip = 1%

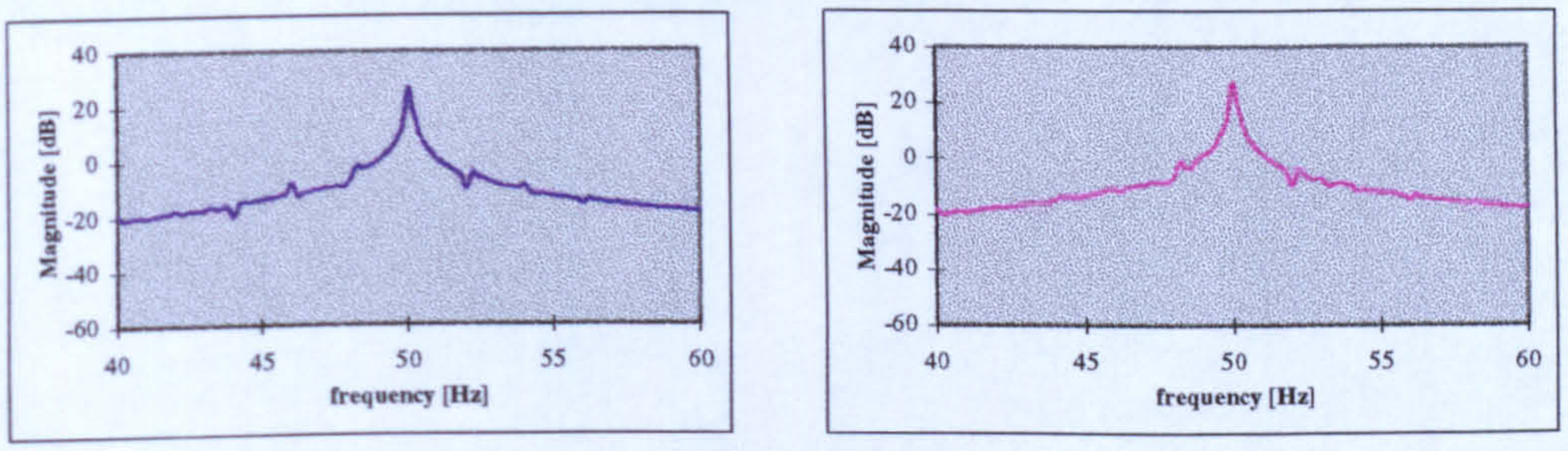

c) slip = 2%

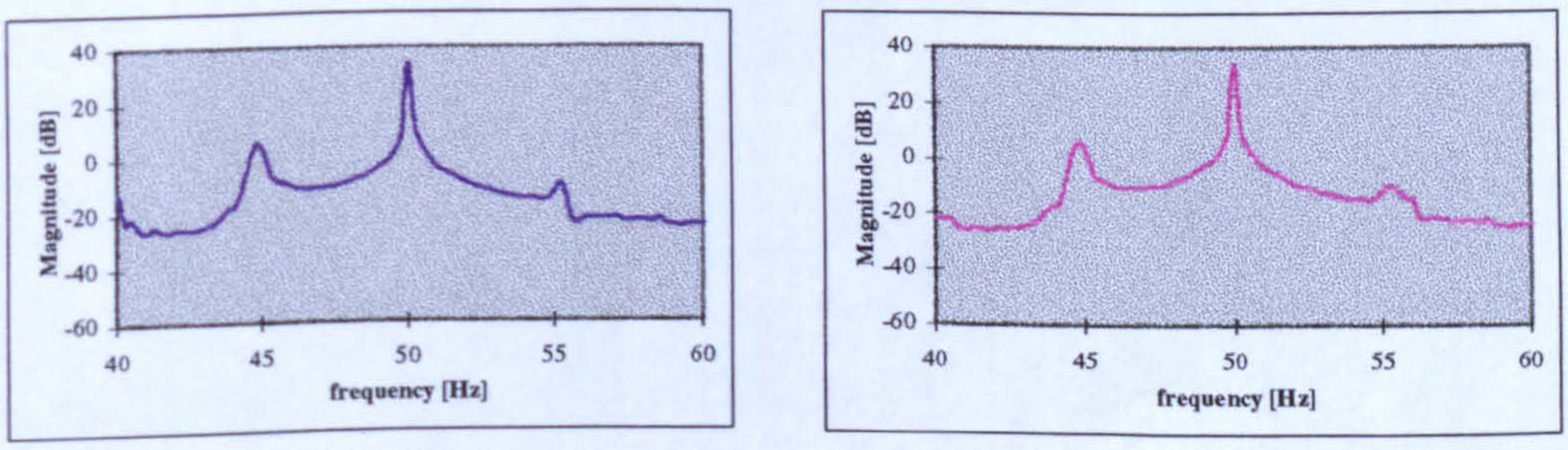

d) slip = 5%

Figure 6.16 *Effect of load on the spectra of the measured (left) and computed (right) stator current waveforms with two broken bars (0dB ≡ 1A).*

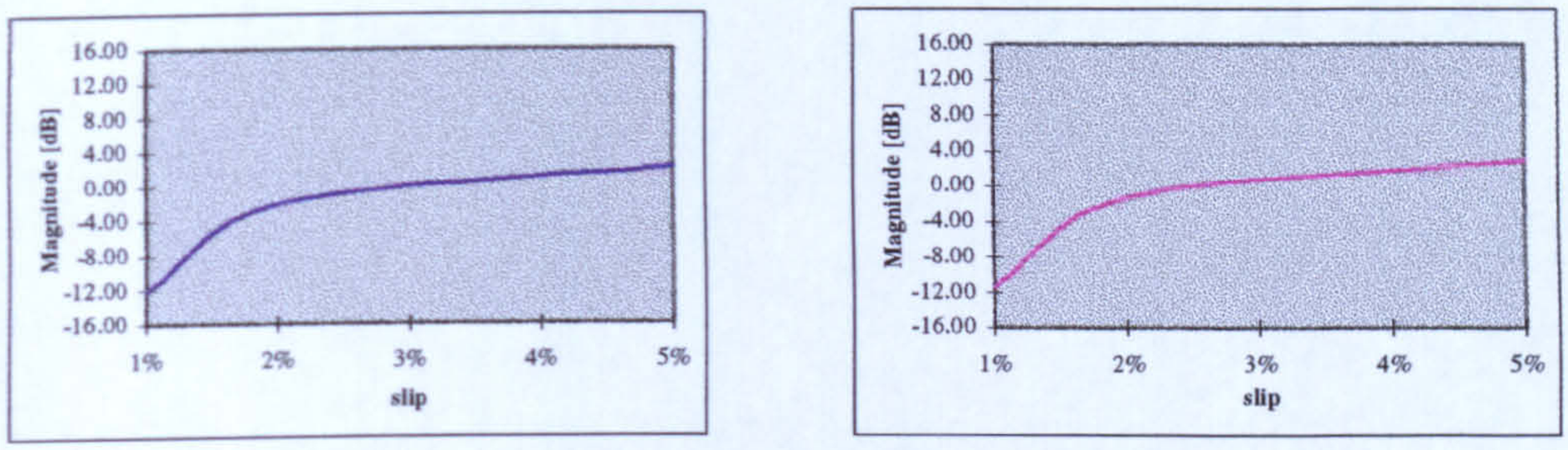

a) one broken bar

b) two broken bars

c) four broken bars

d) five broken bars

Figure 6.17 *Effect of load on the magnitude of the fault component (0dB ≡ 1A).*

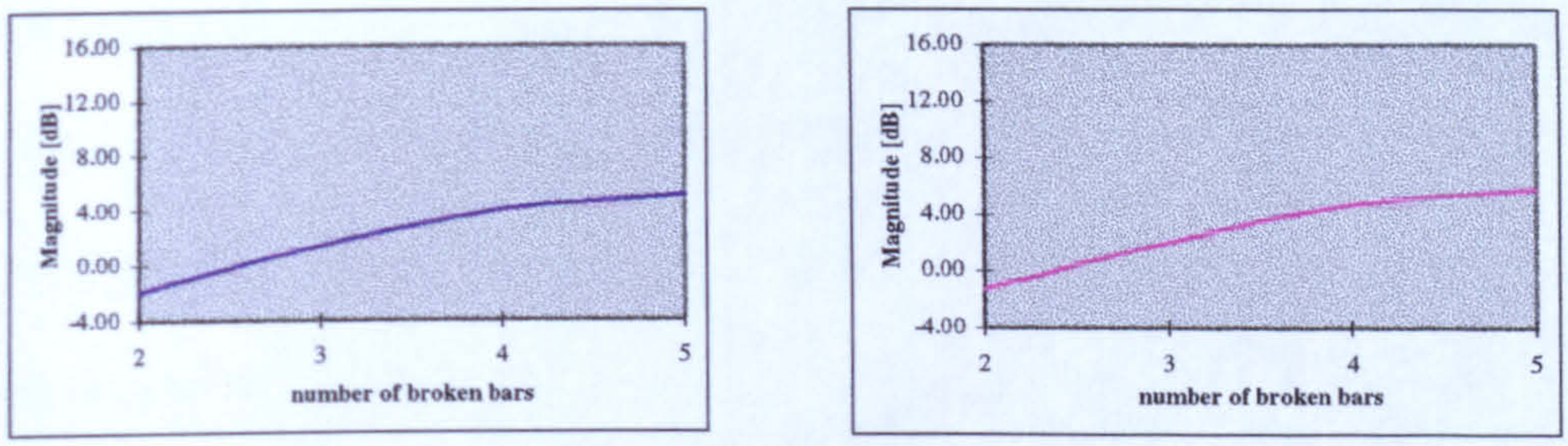

a) slip = 2%

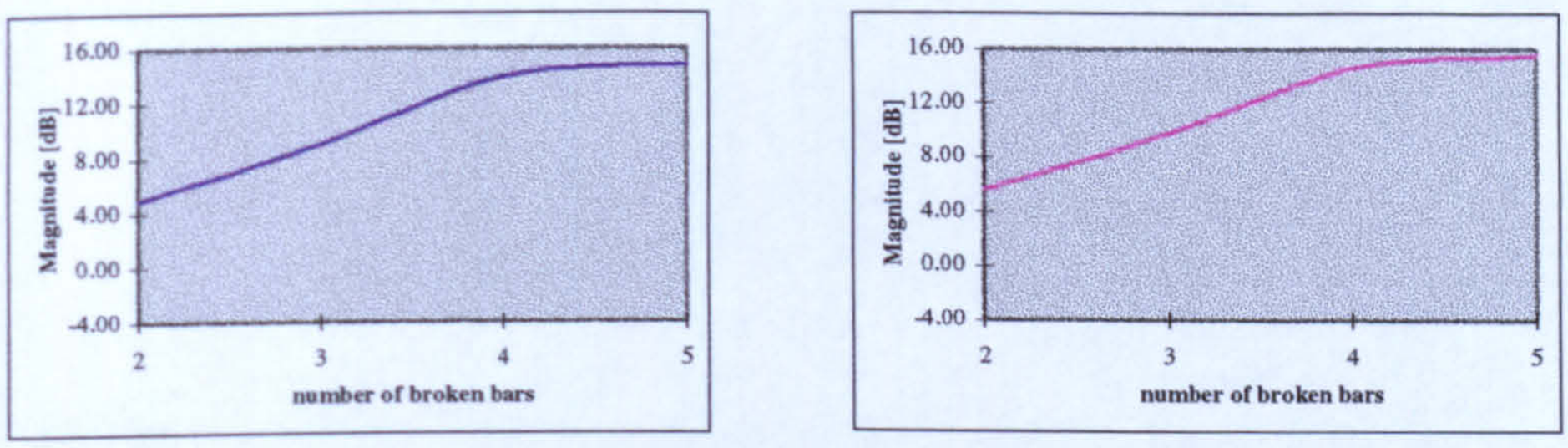

b) slip = 5%

***Figure 6.18** Effect of number of broken bars on the magnitude of the fault component (0dB ≡ 1A).*

6.3 INVERTER-FED INDUCTION MOTOR

As it was shown in the previous chapters, the great advantage of the model developed in this thesis is that it is capable of describing a machine in such detail that the descrete distribution of windings, stator and rotor slotting, skewing, and iron saturation can be included. What gives it more generality is that the machine can be fed from either the mains or nonsinusoidal voltages. In this section, for the sake of completeness, a few results showing the effect of broken bars on some of the parameters of a machine fed from a Pulse Width Modulated voltage source inverter. Figures 6.19, 6.20 and 6.21 show the stator and rotor currents, and the electromagnetic torque of a healthy rotor of an inverter-fed induction motor respectively. The torque pulsations

calculated are of significant magnitude. Such pulsations would be significantly filtered by the rotor inertia and are unlikely to appear at the shaft. The assumption made in the analysis that the airgap face of a tooth is an equipotential is likely to lead to an exageration of the large pulsation magnitude.

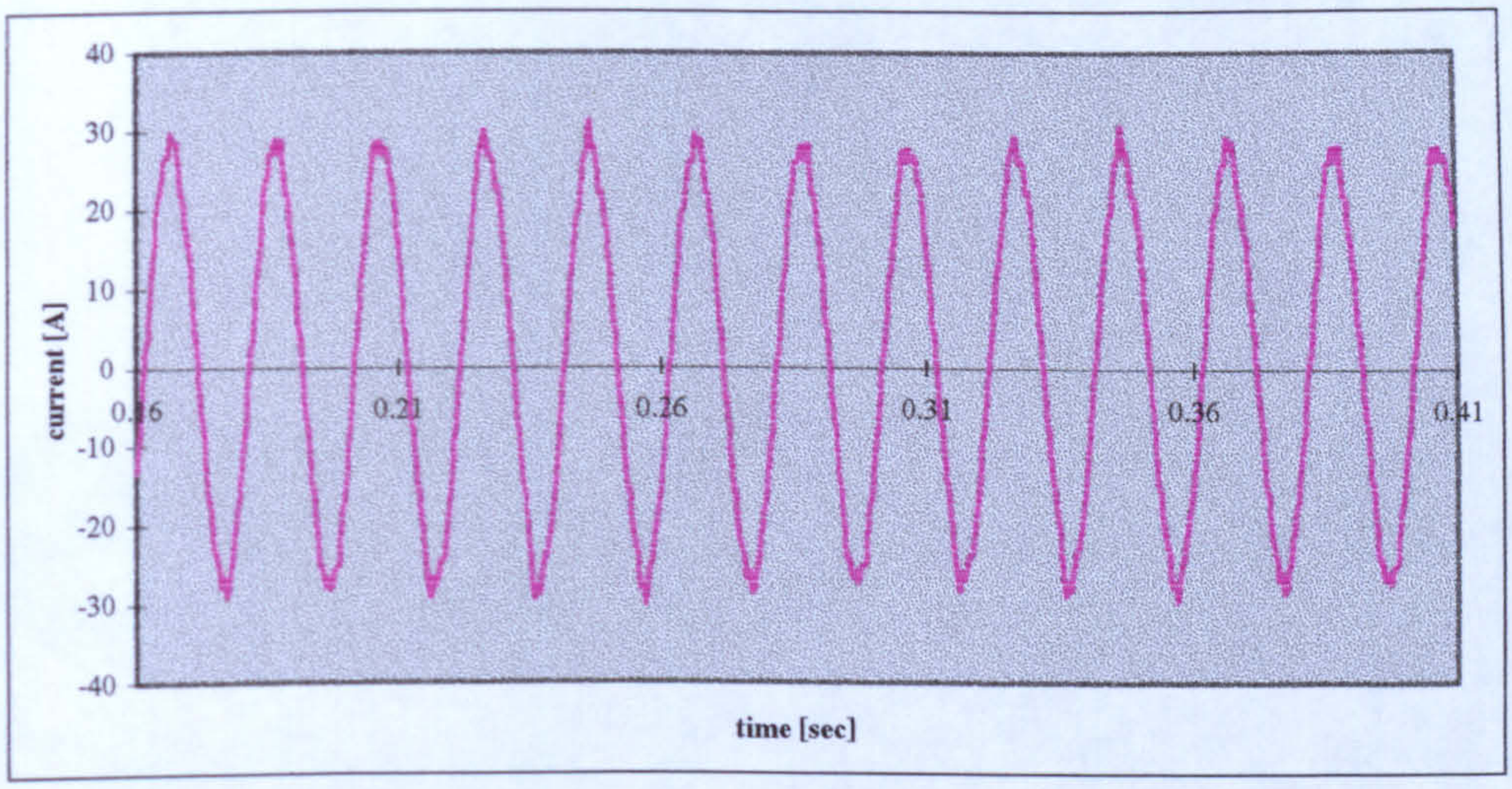

Figure 6.19 *stator current of an inverter-fed induction machine with a healthy rotor*

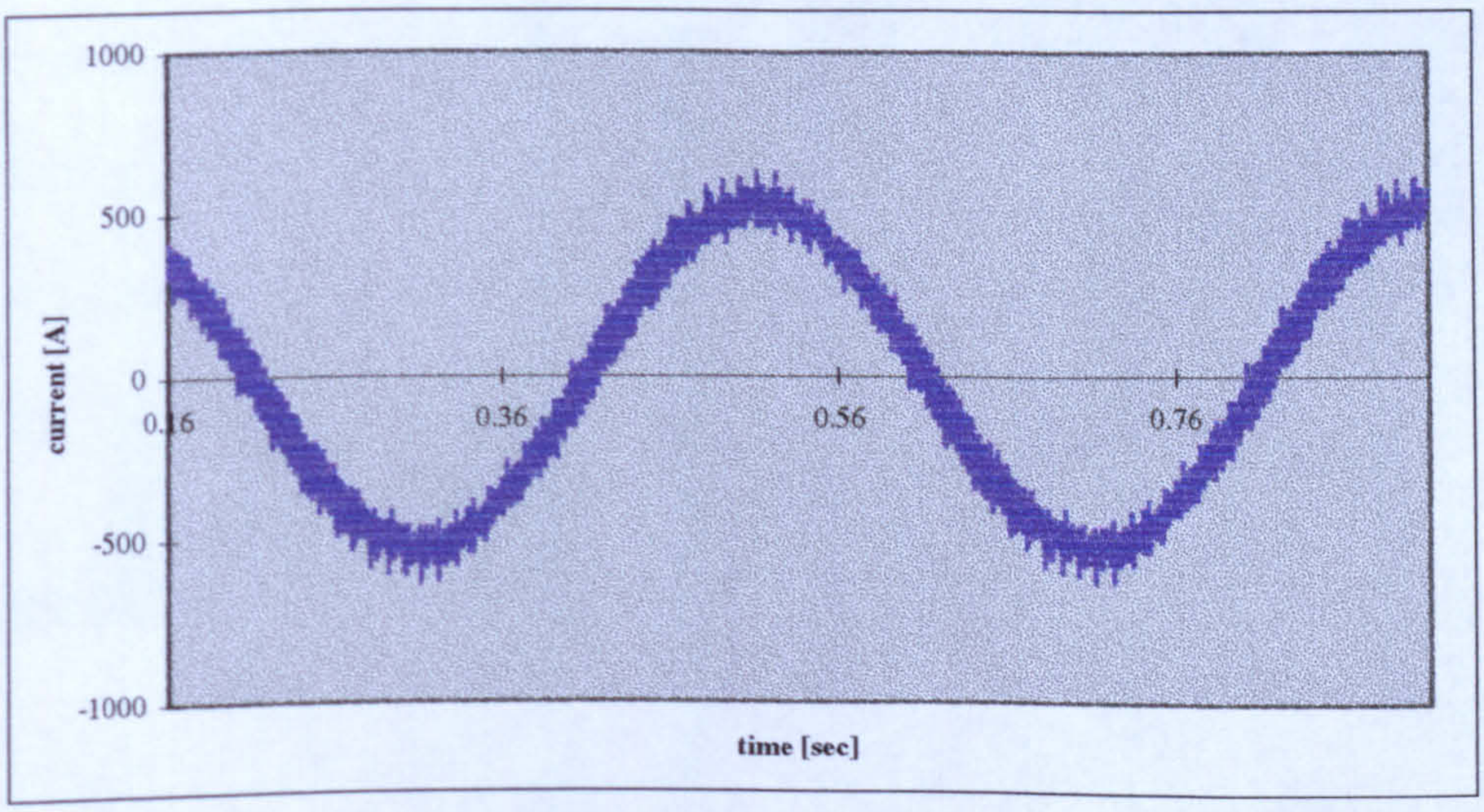

Figure 6.20 *rotor current of an inverter-fed induction machine with a healthy rotor*

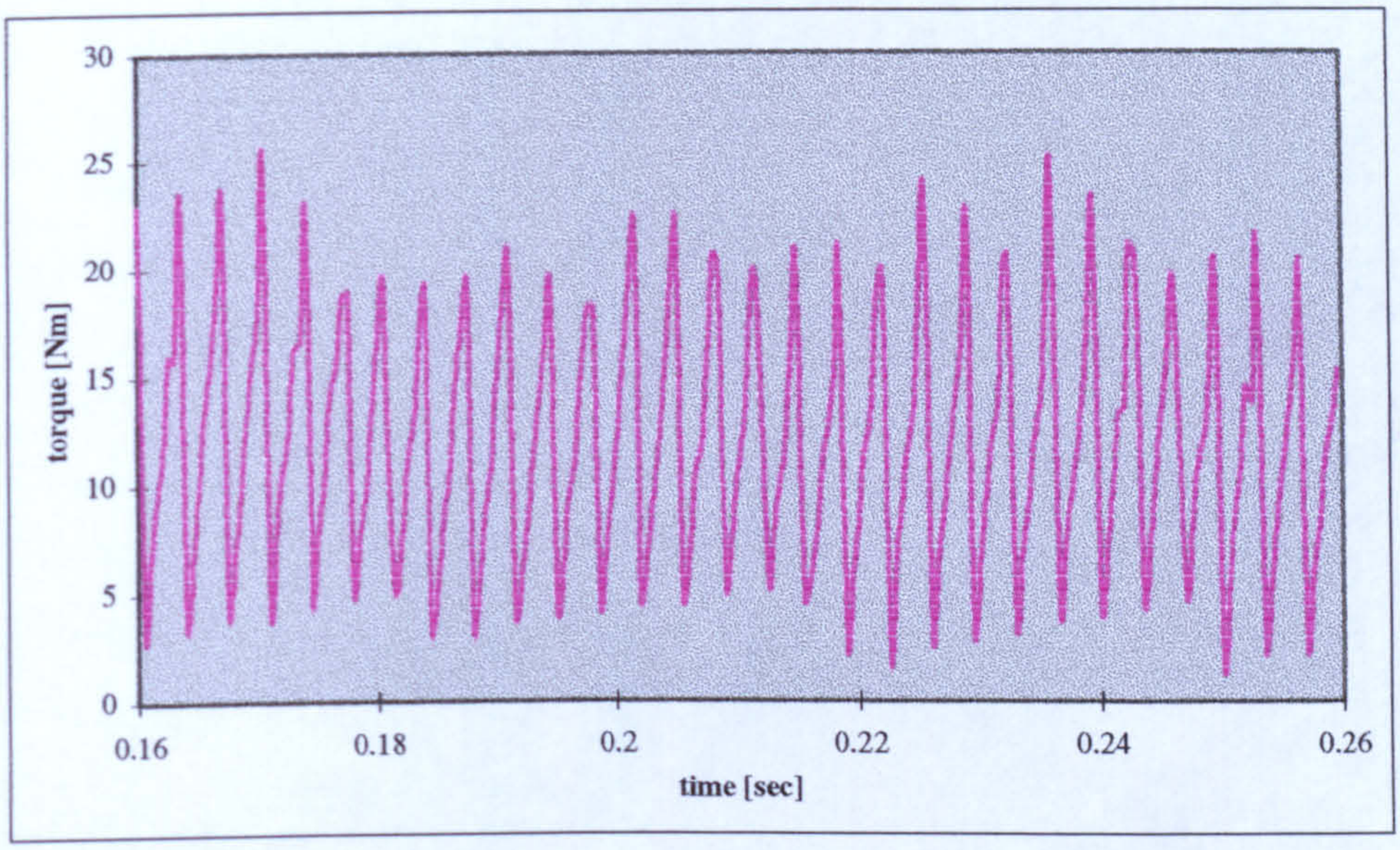

Figure 6.21 *Electromagnetic torque of an inverter-fed induction machine with a healthy rotor*

The same results are shown in Figures 6.22, 6.23 and 6.24 but this time with two bars of the rotor are disconnected. The stator current waveform is now seen to have been modulated at twice slip frequency. whereas the magnitude of the current in the bar next to the broken ones has clearly increased. The electromagnetic torque waveform is no longer steady but is itself modulated by the fault frequency component too. The average torque is also seen to have been reduced.

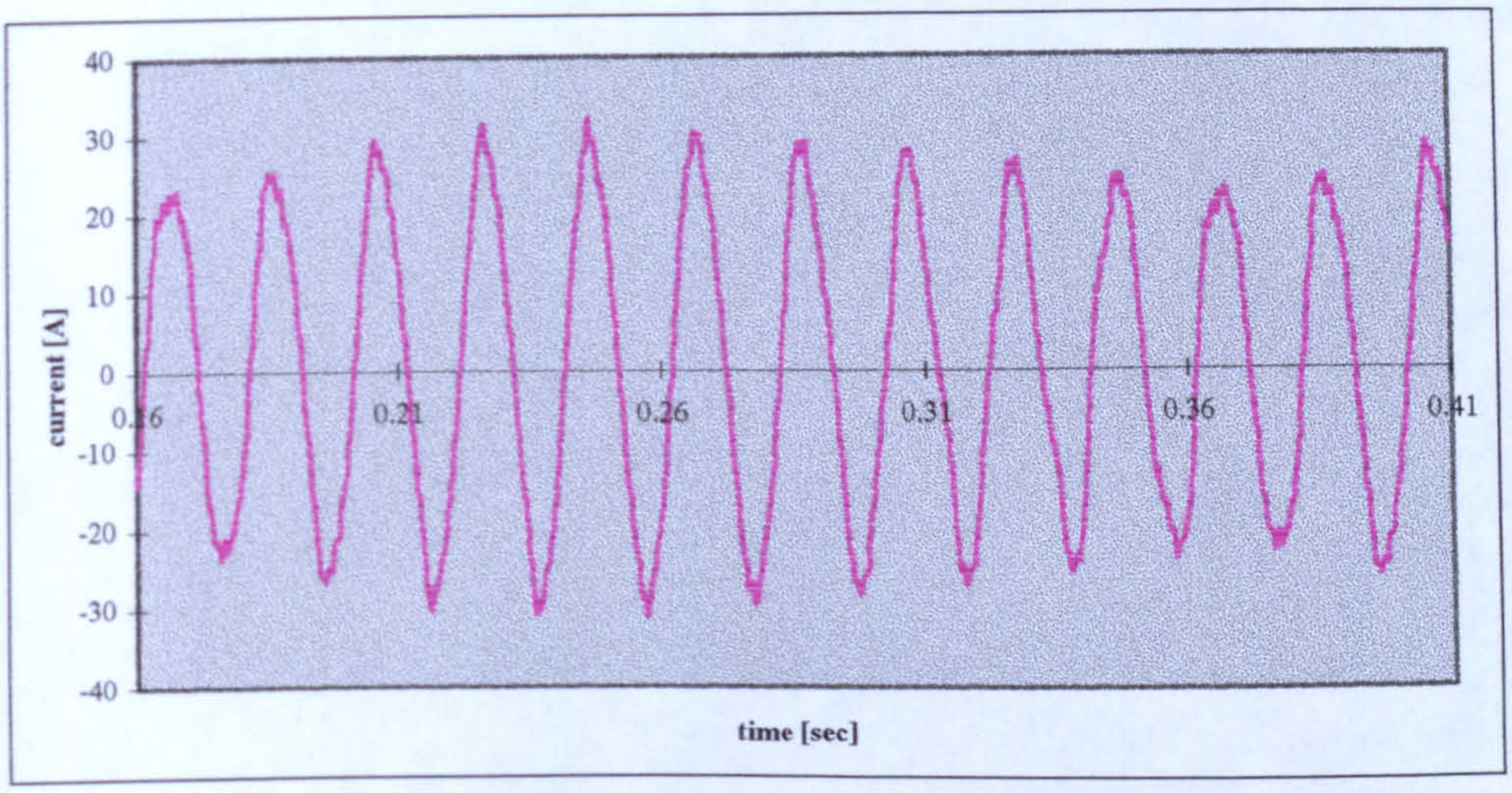

Figure 6.22 *stator current of an inverter-fed induction machine with two adjacent broken bars*

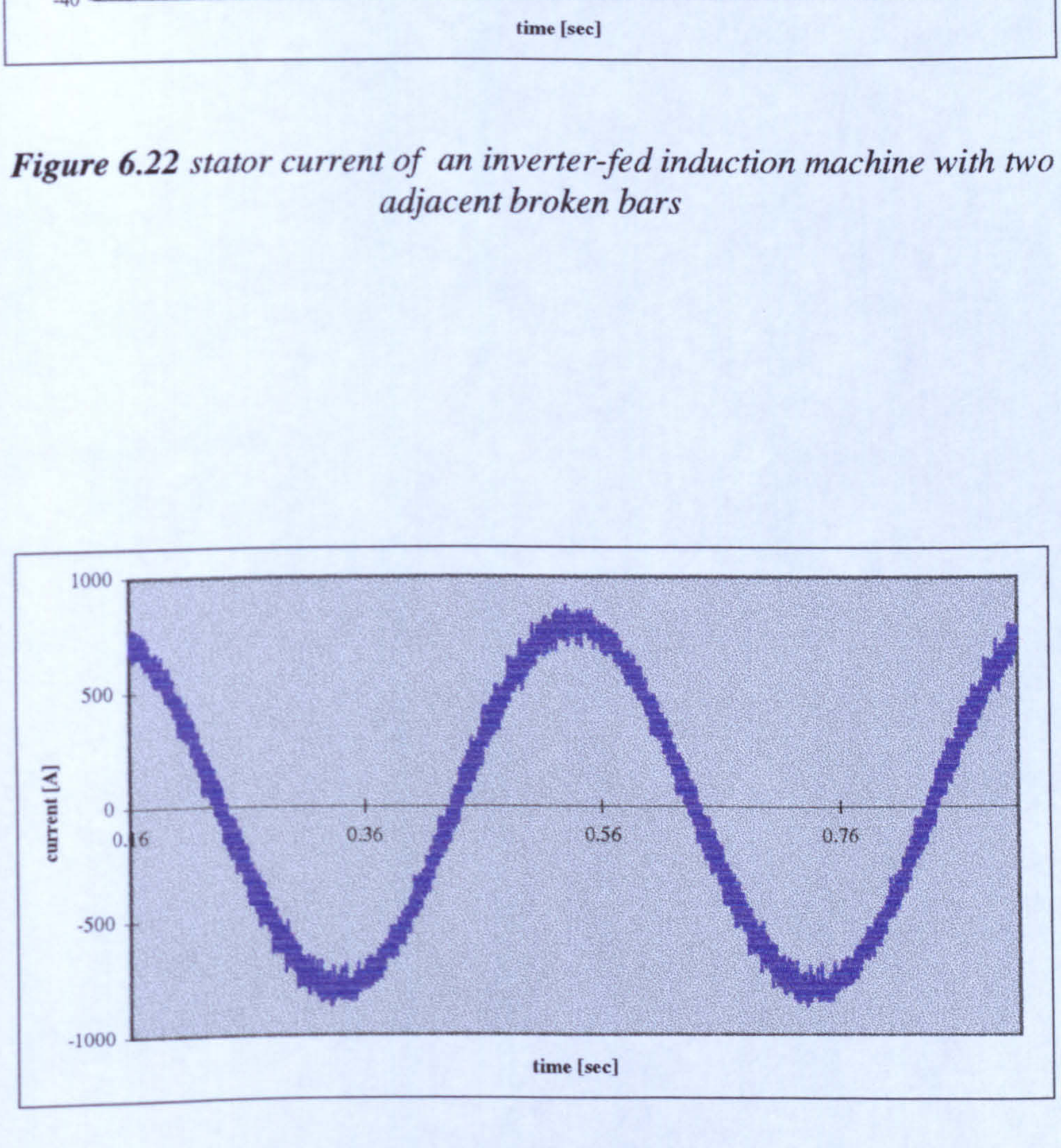

Figure 6.23 *rotor current of an inverter-fed induction machine with two adjacent broken bars*

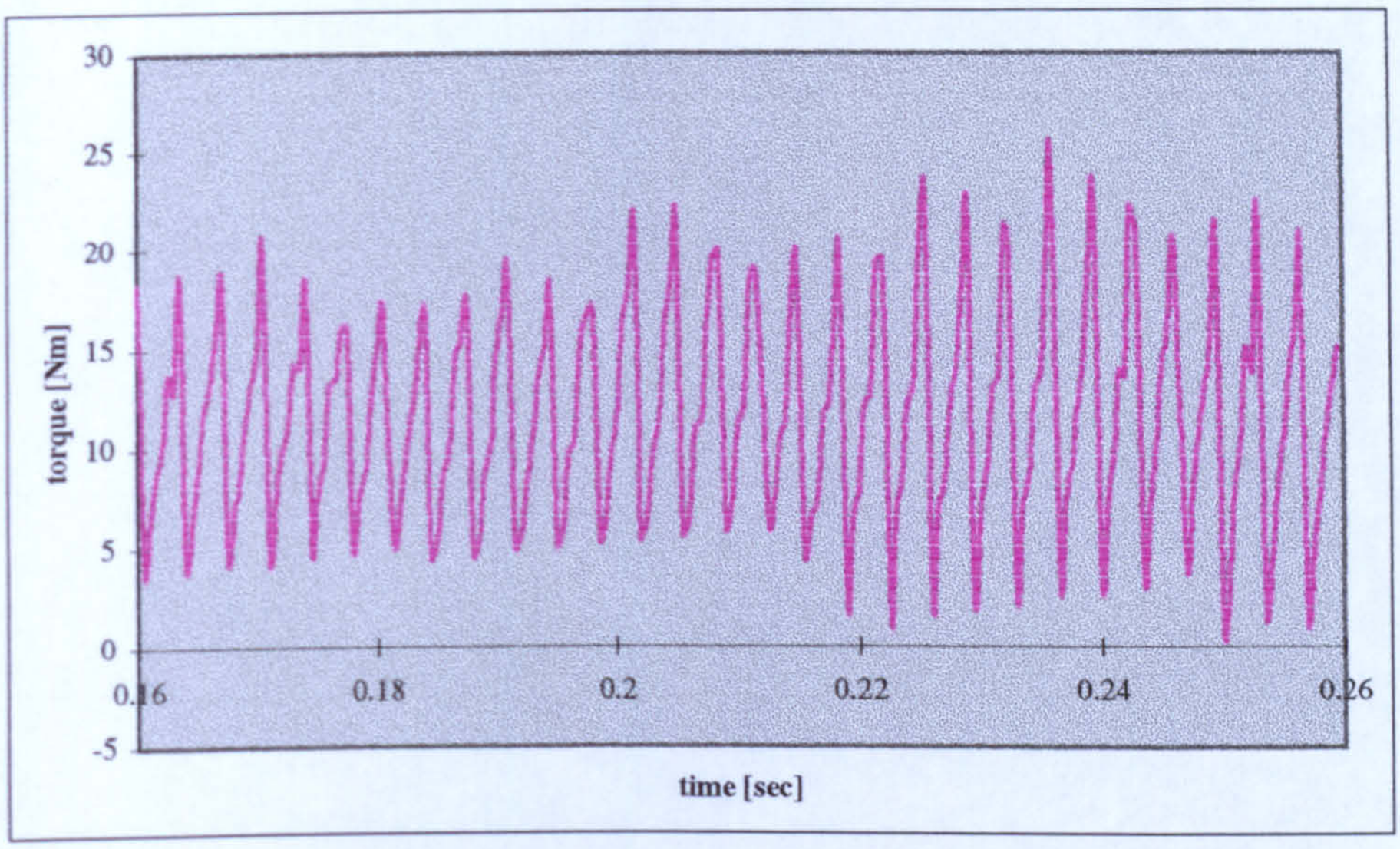

Figure 6.24 *electromagnetic torque of an inverter-fed induction machine with two adjacent broken bars*

By increasing the number of broken bars from two broken bars to six broken bars, the effects mentioned above have accentuated as depicted in Figures 6.25 and 6.26. The modulation is more noticeable and the average torque is more reduced. Figure 6.27 shows the variation of the average electromagnetic torque with the number of broken bars.

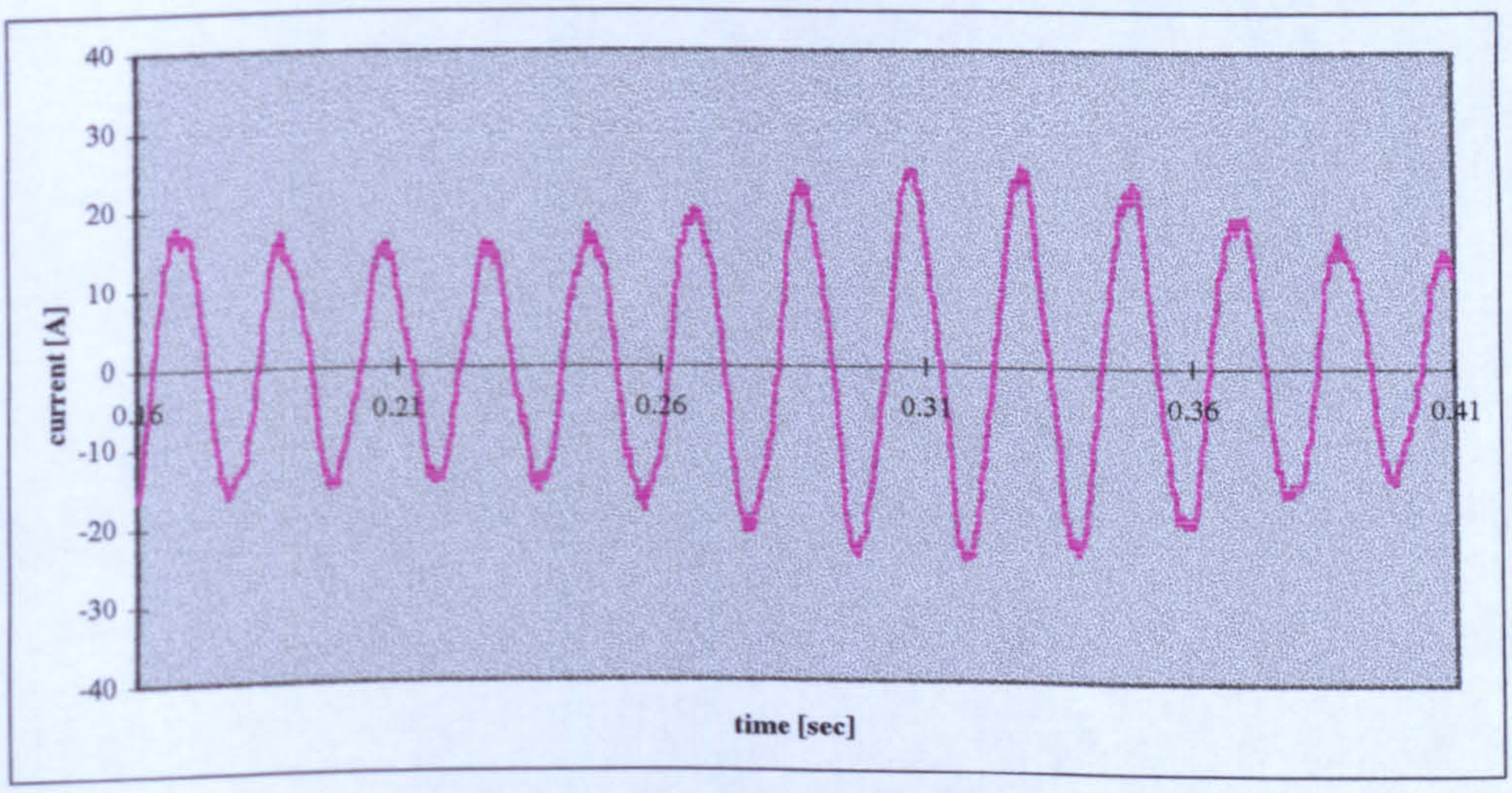

Figure 6.25 *stator current of an inverter-fed induction machine with six adjacent broken bars*

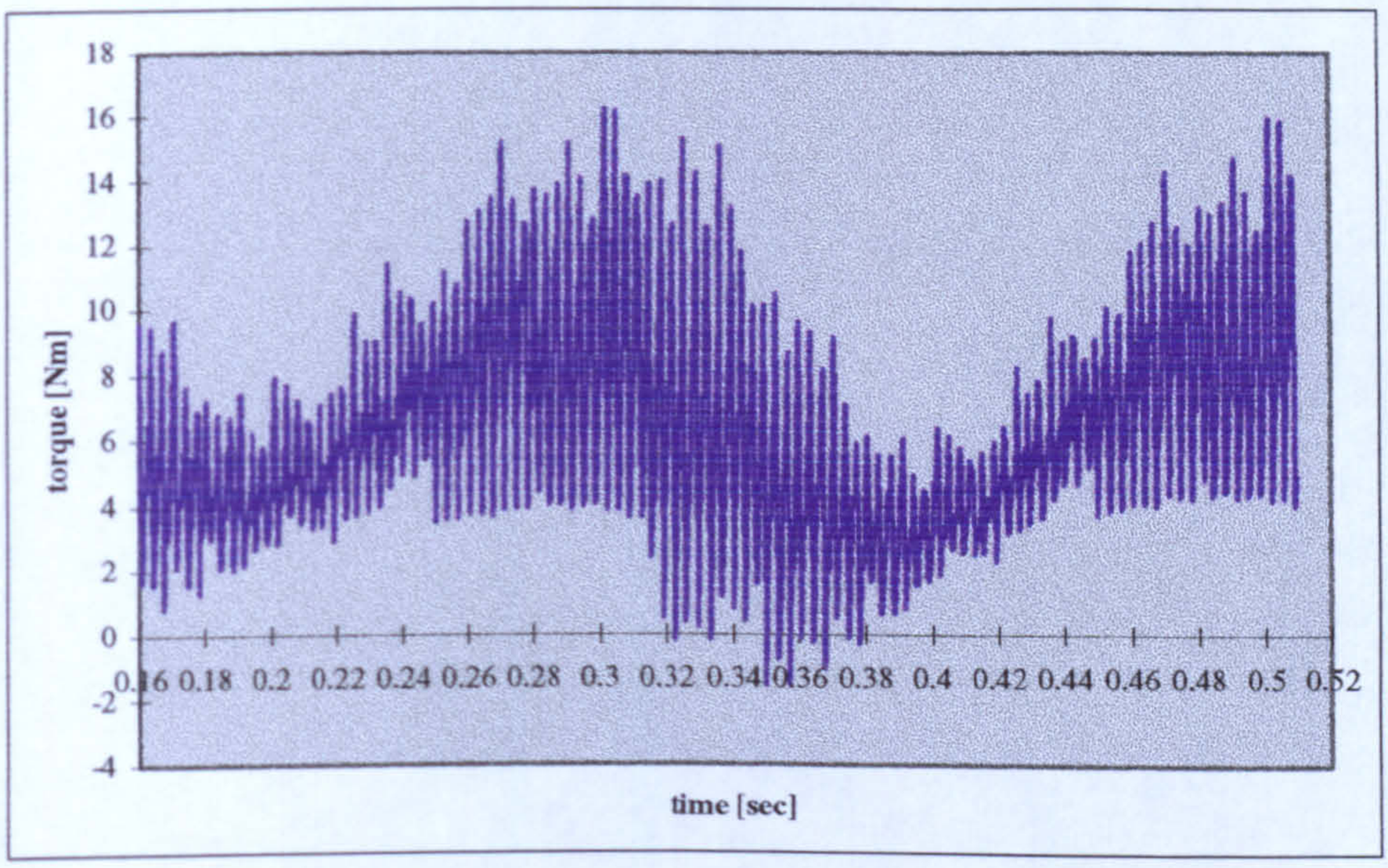

Figure 6.26 *electromagnetic torque of an inverter-fed induction machine with six adjacent broken bars*

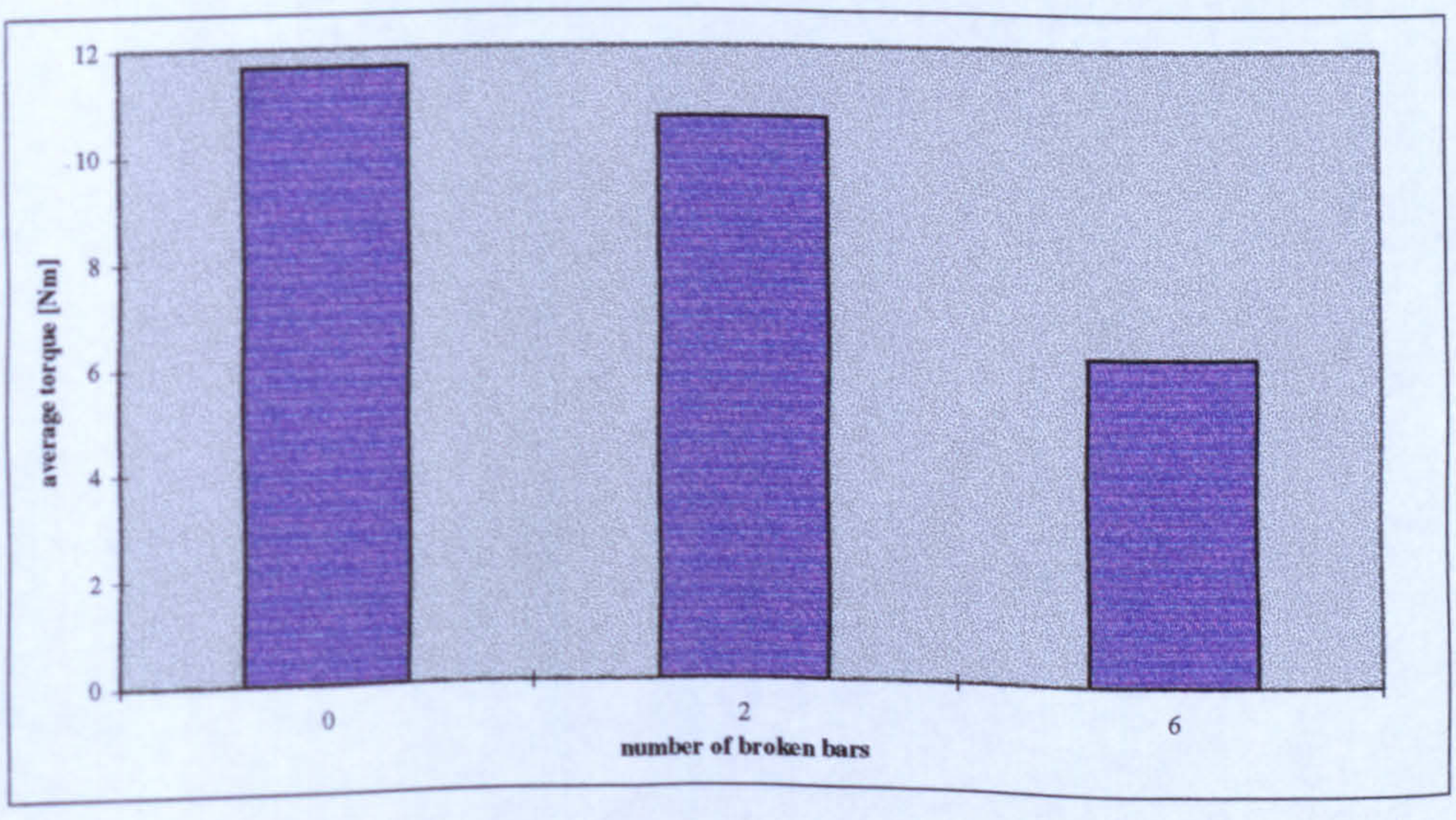

Figure 6.27 *Variation of average electromagnetic torque with the number of broken bars*

6.4 CONCLUSION

It has been shown that, for an unsaturated machine, the magnetic flux density in the stator back iron is no longer sinusoidal near the broken bars but it increases due to the local absence of the demagnetising effect of the bar current. The increase in flux density will lead to additional saturation when the machine is operated at full voltage and full flux. Many of the models [41] [45] developed by previous authors assume there is no change in saturation when analysing the effects of broken bars. The method presented in this thesis caters for the change to saturation conditions automatically. It has also been shown that the rotor current increases in the bars adjacent to the broken ones. This agrees very well with what has been shown by other investigators [41], [46] and [47].

The effect of load and number of broken bars on the waveform and spectrum of the stator current has also been demonstrated. As expected from theory and other researchers, the fault component moves away from the fundamental and increases in magnitude as the load increases.

From the results presented in this chapter it can be concluded that the method of analysis presented in this thesis allows the determination of localised effect (bar currents distribution and magnetic flux distribution) as well as the resultant effects (currents and pulsating torque, etc.) following a broken bar initiation in a squirrel cage induction motor.

CHAPTER SEVEN

CONCLUSION

7. CONCLUSION AND FUTURE WORK

7.1 CONCLUSION

The objective of the work presented in this thesis was to develop an improved, general model for the prediction of induction machine performance with a view to simulating the effect of broken bars in squirrel cage rotors. Experimental verification of the model has been presented in this thesis proving that satisfactory success has been achieved.

The technique is able to cope with all operating conditions, including transients, unbalanced and fault conditions. With this technique, the influence of saturation, skew, slot combinations, winding arrangement, stator and rotor slot openings and tooth-tips on the machine performance can be examined. The method is applicable to squirrel cage machine of single-phase or polyphase windings supplied from either a sinusoidal or nonsinusoidal supply waveform. Wound rotor machines can also be examined if required.

In this simple Magnetic Network Technique, the machine's magnetic circuit is divided into large reluctance elements, forming loops around each slot. Each loop is driven by the ampere-conductors possessed by that particular slot. The permeance of each element (core, teeth, tooth-tips and the equivalent slot permeance) is computed. Those flux lines that cross the airgap are assumed to do so radially, consequently the airgap permeances are determined by the mutual overlap of the stator and rotor teeth. To include the effect of

saturation an iterative technique was employed to determine the values of the non-linear permeances representing the magnetic steel. The Newton-Raphson method was used because of its quadratic convergence. This was done until an error of 0.2% or less was achieved between successive calculations. Comparison between calculated and measured magnetisation curve showed good agreement. Errors were less than 3.1% in the saturated region and less than 0.8% at low voltages. To account for skew, the analytical technique employed considers the machine divided axially into five parallel sections, each displaced from its neighbour by one fifth of the skew angle. The actual winding distribution is employed in the program producing the true values of mmf in the airgap of the model. Broken bars were then simulated by an increase in bar resistance. This model gives insight into all harmonic phenomena in a real, saturated machine under these conditions.

This model covers all possible flux paths between stator and rotor across the airgap. Therefore, the various components of stator and rotor leakage inductance and the self and mutual inductances are precisely determined. The maximum percentage error for the self inductance is less than 2% and an average error of 1%. As for the mutual inductance, the maximum error is less than 3.8% and the average error is 1.4%. The maximum percentage error for the leakage inductance is 6.1%. However, the inductance matrix consists of stator and rotor self and mutual inductances used here as mathematical expressions of the physical machine dimensions, which include all harmonic

effects. Each component of this matrix must be a function not only of all the machine currents, but also of the rotor position. The resulting first order differential equations are solved to determine the machine currents associated with specified operating conditions.

The instantaneous torque of the induction machine is expressed in terms of the dependence of its inductance matrix upon angular position. The pulsating torque has been calculated as the difference between the maximum and minimum instantaneous electromagnetic torques within a steady state region. The percentage error in the steady state performance characteristic is less than 2% over the operating range.

What makes this model more attractive is that, even in the frequency domain analysis, good correlation is obtained for the currents. An error of 2.7% for the fundamental and a maximum error of 11.4% for significant high frequency components are obtained. This error is reasonable because the voltage source assumed in the model is a pure sinusoid whereas the voltage fed from the mains is not.

The simple Magnetic Network Technique successfully predicted the flux distribution in the machine and consequently its performance taking into account the effect of saturation, skew, slotting and relative position of stator and rotor slots. When implemented on a high-speed computer, it becomes a

very powerful tool which can be used both in design and analysis of electromechanical energy converters.

The computer implementation is simple and the computing time is relatively short compared to the other numerical methods. In reference [77], where A.C. Smith, et al used time-stepping finite element method for a wound rotor with one axial machine segment and covering only one pole, the time required to compute the stator current waveform presented took 12400 CPUs on a Cyber 855 mainframe computer. Whereas the same curve, using MNT, would require 563 CPUs only, for a squirrel cage rotor with five axial machine segments, on the ALPHA mainframe computer (that is 22 times faster, or 22*30 faster for a 6 pole 5 segments machine).

This Technique (MNT) has many advantages which make it attractive amongst which are:

1. It involves far fewer elements than finite element analysis.
2. Its ability to transform a complex magnetic circuit into a simple, resistive electrical network.
3. Augmented with the triangular technique for airgap modelling, it is of particular interest because of its simple way of handling infinite reluctances which appear in the airgap representation.
4. The utilisation of Φ-mmf curves for the computation of the permeances to allow for saturation in all parts of the machine.

It was shown in chapter 6, by comparison with experimental results that this technique can be successfully applied to the simulation of broken rotor bars. The results obtained showed that this model can reasonably predict both the frequency and the magnitude of a wide range of the harmonics induced in the stator winding including those normally associated with broken rotor bars at (1-2s)f and (1+2s)f. If the case of one broken, for instance, is considered then errors of 6.0%, 5.8% and 6.5% for (1-2s)f, the fundamental and (1+2s)f components respectively are obtained at full load.

Obviously, the model can be used to determine the patterns of the fault signature of the stator current associated with presence of rotor defects. The simulation program may be applied to different fault situations to help formulate the decision algorithm and incorporating this rule in the detector software.

The main point of interest with respect to this model is that it can be readily applied to the study and prediction of many phenomena and problems with limited alteration. By extensive use of circuit methods, the role of the finite elements has been restricted so that they only account for phenomena which cannot otherwise be accurately modelled. The resultant subordination of numerical field solutions to a simple magnetic circuit model yields significant advantages in terms of simplicity and simulation time without sacrificing accuracy. However, some detail of the magnetic field distribution will of

course be lost in the simplification process. Use of the incidence matrix approach provides ready alteration to rotor and stator slot numbers and very little change is required to simulate different machines.

It is hoped that the information presented in this thesis will fill in some of the gaps of the calculation of the airgap field distribution in time and space, and the consequent problems of pulsating torque, rotor asymmetries and magnetic noise and vibration. The program allows also the relative influence of design changes upon machine performance to be examined.

7.2 FURTHER RECOMMENDATIONS

The main achievement of this project has been the validation of a model for cage induction machines which is capable of modelling the effects of broken bars on the machines performance. Combining a simple magnetic circuit for field solutions with electric circuit equations has been shown to be both relatively fast and accurate. However, although the basic model has been satisfactorily tested, there remains scope for considerable supplementary work.

There are three main areas which can be improved or investigated further. The first one is the improvement to the magnetic circuit model. Secondly, investigation into other methods of solving the equations of performance and thirdly, further investigation into various aspects of operation conditions.

1) It is felt that the next step should be the improvement of the airgap modelling using the finite element method to model slot openings and airgap reluctance change with overlap angle. This will increase the data which needs to be changed when modelling different machines.

2) Establishment of the generality of the model. Chapter 2 presented several simplificative techniques to account for certain phenomena and some other neglections such as skin and hysteresis effects. These could be implemented preferably in order to model motors with the necessary characteristics. For example, if the slot leakage has to be modelled in more detail, as in the case of a motor with deep bars, it would be instructive to separate the bars and slots into n layers isolated from one another. By this action a real bar is replaced with n bars electrically insulated from one another. Hence, instead of one squirrel cage on the rotor side there will be n squirrel cages. This, however, would increase the computing time.

3) Although some results for broken bar effects have been presented in this thesis, it is felt that that more results are necessary with the inclusion of other types of asymmetries such as eccentricity which can be easily incorporated. Some criteria to differentiate between different types of faults could then be deduced.

4) A second major area for confirmation is the simulation characteristic of other operating conditions. The use of a voltage-forced circuit model lends itself to considerable flexibility, and obvious candidates for inclusion here are the simulation of a supply line fault causing a short circuit or the loss of a phase.

5) The differing number of turns in the phase windings and their nonuniform spatial displacement could be investigated in the case of an asymmetrical winding on either the stator or the rotor. This can be easily done using the winding matrix. This is more appropriate to single phase machines however.

6) The final consideration which remains is the question of execution times. Whilst it is believed that this model is fast relative to existing time-stepped finite element models, it is still very CPU intensive.

REFERENCES

REFERENCES

1) Austin H.Bonnett and George C.Soukup:" Analysis of Rotor Failures in Squirrel Cage Induction Motors", *IEEE 1987, pp. 1124-30.*

2) Austin H. Bonnett and George C. Soukup:" Rotor Failures in Squirrel Induction Motors", *IEEE Trans. on Industry Appl., Vol.IA-22, No.6, 1986, pp. 1165-1173.*

3) Austin H.Bonnett and George C.Soukup:" Rotor Failures in Squirrel Cage Induction Motors", *IEEE 1985, pp. 181- 190.*

4) P.E.Clark, I.F.McShane and K.Wakeley:" The diagnosis and solution of electrical machine problems (Pt.1: Design influences)", *IEEE 1985, pp. 171-179.*

5) A.M.Armour and J.W.Walley:"A Magneto-Electric Method for Detecting Defects in Cast Aluminium Rotor Windings for Squirrel Cage Motors", *The M-V Gazette, 1956, pp. 314-317.*

6) R.L.Burns:" Rotor Bar Failures in Large A.C. Squirrel Cage Motors", *Electrical Engineer, 1977, pp. 11-14.*

7) A.Patyk:" Application of Forward/Backward Components to the Analysis of Failure States of the Squirrel-Cage Motor. Part 1: The Theory", *Archiv Fur Elektrotechnik 69 (1986), pp. 429-437.*

8) A.Patyk:" Application of Forward/Backward Component to the Analysis of Failure States of the Squirrel-Cage Motor. Part 2: Calculation of Current Flow Distribution in the Squirrel-Cage and the Stator and of the Components of the Electromagnetic Moment", *Archiv Fur Elektrotechnik 69 (1986), pp. 439-443.*

9) C.Hargis, B.G.Gaydon and K.Kamash:" The Detection of Rotor Defects in Induction Motors", *IEE Conf. Publ.213, 1982, pp. 216-220.*

10) P.J.Tavner:" Condition monitoring - the way ahead for large electrical machines", *IEE conf. Publ. 1989, pp. 159-162.*

11) S.Fruchtenicht, E.Pittius and H.O.Seinsch:" A diagnostic system for three-phase asynchronous machines", *IEE conf. Publ. 1989, pp. 163-171.*

12) C.F. Landy and R Moore:" Further Success in the Detection of Broken and/or Cracked Rotor Bars in Large Squirrel Cage Induction Motors", pp. *145-149, 1987.*

13) P.J. Tavner; K.K. Armin and C. Hargis:" An Electrical Technique for Monitoring Induction Motor Cages", *3rd International Conference on Electrical Machines and Drives, 1987, pp. 43-6.*

14) D.J. Tilak Siyambalapitiya, Peter G. McLaren and Paul P. Acarnley: " A Rotor Condition Monitor for Squirrel-Cage Induction Machines", *IEEE Trans. on Industry Applications, Vol. IA-23, No.2, 1987, pp. 334-40.*

15) J. Penman, M.N.Dey, A.J. Trait and W.E. Bryan: "Condition Monitoring of Electrical Drives", *IEE PROC., Vol.133, Pt.B, No.3, 1986, pp. 142-148.*

16) A.C.Smith: "Harmonic field analysis for slip-ring motors including general rotor asymmetry", *IEEE 1989, Vol.1, pp. 31-37.*

17) K.J.Binns and M.Dye:" Effects of Slot Skew and Iron Saturation on Cogging Torques in Induction Machines", *IEE Proc., Vol.117, No.7, 1970, pp. 1249-1252.*

18) Charles V.Jones:"The Unified Theory of Electrical Machines", *Butterworths, London, 1967.*

19) Oberretl,K.:" New Facts about Parasitic Torques in Induction Motors", *Bull. Oerlikon, 1962, (348), pp. 131-155.*

20) G.Angst:" Saturation Factors for Leakage Reactance of Induction Motors with Skewed Rotors", *1963, pp. 716-725.*

21) Bedrich Heller and Vaclav Hamata:" Harmonic Field Effects in Induction Machines", *Elsevier Scientific Publishing Company, Amsterdam, Oxford, New York 1977.*

22) Gorges H.:"Uber Drehstrommotoren mit verminderter Tourenzhl", *Elektrotechnische Zeitschrift, Vol. 17, 1896.*

23) H. Jordan and W. Schmitt:" Uber den Einflus fehlender Stabe auf das Verhalten von Kurzschlusmotoren", *AEG- Mitt, Vol. 32, 1942, pp. 57.*

24) E.Mishkin:" Disturbances in the Induction Machines due to Broken Squirrel-Cage Rings", *J.F.I., 1955, pp. 133-143.*

25) U. Heller:" Einflus fehlender Lauferstabe auf die elektrischen Eiganschaften von Kurzschluslaufer- Motoren", *ETZ-A, vol. 83, 1964, pp. 94-97.*

26) M.Deleroi:" Squirrel-Cage Motor with Broken Bar in the Rotor - Phisical Phenomena and their Experimental Assessment", *Intern. Conf. on Elect. Mach., Hungary, Vol. 3, pp. 767-70.*

27) D'ALESSANDRO, U. and Pagono E.:" Uber asynchronmotoren mit elektrisch unsymmetrischem Kafiglaufer", *1961, 90, pp. 582-586.*

28) Gabriano, H.L., and Gross, E.T.B.:" The Georges Phenomenon - Induction Motors with Unbalanced Rotor Impedance", *Trans. Amer. Inst. Electr. Engrs., 1950, 69, pp. 1569-1575.*

29) T.H.Barton and B.C.Doxey:" The Operation of Three-Phase Induction Motors with Unsymmetrical Impedance in the Secondary Circuit.", *Paper No. 1784 U, 1955, pp. 71-79.*

30) P. Vas:"Asymmetrical three-phase and single-phase Induction Machines", Period. Polytech. Electr. Eng., Vol. 22, 1978, (4), PP. 185-97.

31) P. De Vera:" Uber Asynchronmotoren mit elektrisch Unsymmetrischen Kafiglaufer", *ETZ-A, Vol. 90, 1969, pp. 582.*

32) P.Vas:" Performance of Three-Phase Squirrel-Cage Induction Motors with Rotor Asymmetries", *Periodica Polytechnica (Electrical Engineering), Vol. 19, 1975, pp. 309-315.*

33) G. Toke and P. Vas:" Application of the Symmetrical Components to the Analysis of Small Rotor Asymmetries of Squirrel Cage Induction Motors", (In Hungarian), *Elektrotechnika, Vol. 69, no. 9, 1976.*

34) J. Vas and P. Vas:" The Operational Characteristics of Induction Motors with Asymmetrical Rotor.", *Journal of the Institution of Engineers (India), Vol 57, pt El 6, 1977, pp. 265-267.*

35) J. Vas and P. Vas:" Transient and Steady state Operation of Induction Motors with Asymmetrical Rotor", *Archive fur Elektrotechnik, Vol. 59, 1977, pp. 55.*

36) J. Vas and P. Vas:" Transient and Steady State Operation of Induction Motors with Stator Asymmetries", *Ibid, Vol. 59, 1977, pp. 121.*

37) P. Vas:" Transient and Steady State Operation of Induction Motors with General Two-side Asymmetries", *Ibid, Vol. 59, 1977, pp. 163.*

38) M.Jufer and M.Abdelaziz:" Influence d'une Rupture de Barre ou d'un Anneau sur les Characteristiques Externes d'un Moteur Asynchrone a Cage", *Bull. SEV/VSE 69, 1978, 17, pp. 921-925.*

39) P.Vas and J.Vas:" Steady State Operation of Squirrel Cage Induction Motors with General Asymmetry", *IE(I) Journal-EL, Vol. 59, 1979, pp. 303-308.*

40) P.Vas:" Steady State and Transient Performance of Induction Motors with Rotor Asymmetry", *IEEE Trans. on PAS, Vol. PAS-101, No. 9, 1982, pp. 3247-51.*

41) S.Williamson and A.C.Smith:" Steady-State Analysis of 3-Phase Cage Motors with Rotor-Bar and End-Ring Faults", *IEE Proc., Vol. 129, Pt. B, No. 3, 1982, pp. 93-101.*

42) M.Poloujadoff:" General Rotating MMF Theory of quirrel Cage Induction Machines with Non-Uniform Airgap and Several Non-Sinusoidal Distributed Windings", *IEEE, 1980, pp. 1292-1304.*

43) S.Williamson and M.A.S.Abdel-Magied: "Unbalanced Magnetic Pull in Induction Motors with Asymmetrical Rotor Cages", *IEE Conf. Publ. 254, 1985, pp. 218-222.*

44) S. Williamson and M.A.S. Abdel-Magied:" Steady-State Analysis of Double-Cage Induction Motors with Rotor-Cage Faults", *IEE PROC. Vol. 134, Pt. B, No.4, July 1987, pp. 199-206.*

45) Motya Ito, Noboru Fujimoto, Etal.:" Effect of Broken Bars on Unbalanced Magnetic Pull and Torque of Induction Motors", *Elect. Eng. in Japan, Vol. 100, No.1, 1980, pp. 42-49.*

46) N. EL Kasabgy, A.R.Eastham and G.E.Dawson:" The Detection and Effects of Broken Bars in Cage Rotor Induction Machines" ,*pp. G22-G28.*

47) Elkasabgy, N.M., Eastham, A.R. and Dawson, G.E.:" The Detection of Broken Bars in the Cage Rotor of an Induction Machine", *IEEE 1988, pp. 181-187.*

48) I.A.M. Amin:" The Characteristic Performance of Induction Motor with Broken Bars by Finite-element Method", *Modelling, Simulation and Control, A, AMSE Press, Vol. 24, No.4, 1989, pp. 39-55.*

49) S. Elder, J.F. Watson and W.T. Thomson:" Fault Detection in Induction Motors as a Result of Transient Analysis", *IEE Conference publ., 1989, pp. 182-186.*

50) O.Gol:" Effect of Cage Fractures on the Performance of Asynchronous Machines", *pp. 1141-1144.*

51) Chari, M.V.K. and Silvester, P.:" Analysis of Turbo-alternator Magnetic Fields by Finite Elements", *IEEE Transactions on Power Apparatus and Systems, PAS-90, 2, 1971, pp. 454-464.*

52) Chari, M.V.K., and Silvester, P.:" Finite-element Analysis of Magnetically Saturated dc Machines", *IEEE Transactions on Power Apparatus and Systems PAS- 90, 5, 1971, pp. 2362-72.*

53) Tandon, S.C., Armor, A.F. and Chari, M.V.K.:" Nonlinear Transient Finite Element Field Computation for Electrical Machines and Devices.", *IEEE Transactions on Power Apparatus and Systems PAS-102, 5, 1983, pp. 1089-96.*

54) Chari, M.V.K. et al.:" Three-dimensional Vector Potential Analysis for Machine Field Problems", *IEEE Transactions on Magnetics MAG-18, 2, 1982, pp. 436-446.*

55) Ito, M. et al.:" Analytical Model for Magnetic Field Analysis of Induction Motor Performance", *IEEE Transaction on Power Apparatus and Systems PAS-100, 11, 1981, pp. 4582-90.*

56) Andresen, E. and Muller, W.:" Berechnung der Anlaufdaten von Asynchron-Kafiglaufermotoren verschiedener Stabformen mit der Methode der finiten Differenzen.", *Archiv fur Elektrotechnik 66, 3, 1983, pp. 179-185.*

57) Williamson, S. and Ralph, J.W.:" Finite Element Analysis for Nonlinear Magnetic Field Problems with Complex Current Sources", *IEE Proceedings A 129, 6, 1982, pp. 391-395.*

58) Williamson, S. and Ralph, J.W.:" Finite Element Analysis of an Induction Motor Fed from a Constant- voltage Source", *IEE Proceedings B 130, 1, 1983, pp. 18-24.*

59) Bouillault, F. and Razek, A.:" Dynamic Model for Eddy Current Calculation in Saturated Electric Machines", *IEEE Transactions on Magnetics MAG-19, 6, 1983, pp. 26-39-42.*

60) Brunelli, B. et al.:" Transient and Steady state Behaviour of Solid Rotor Induction Machines", *IEEE Transactions on Magnetics MAG-19, 6, 1983, pp. 2650- 54.*

61) Brandl, P., Reichert, K. and Vogt, W.:" Simulation des Turbogenerators im stationaren Lastfall", *Brown Boveri Mitteilungen 62, 9, 1975, pp. 444-449.*

62) Nakata, T. and Takahashi, N.:" Direct Finite Element Analysis of Flux and current Distributions under Specified Conditions", *IEEE Transactions on Magnetics MAG-18, 2, 1982, pp. 325-330.*

63) Strangas, E.G. and Theis, K.R.:" Shaded Pole Motor Design and Evaluation using Coupled Field and Circuit Equations", *IEEE Transactions on Magnetics MAG-21, 5, 1985, pp. 1880-1882.*

64) Strangas, E.G.:" Coupling the Circuit Equations to the nonlinear Time-dependent Field Solution in Inverter Driven Induction Motors", *IEEE Transactions on Magnetics MAG-21, 6, 1985, pp. 2408-2411.*

65) Shen, D. et al.:" Solution of Magnetic Fields and Electrical Circuits Combined Problems", *IEEE Transactions on Magnetics MAG-21, 6, 1985, pp. 2288-2291.*

66) Shen, D. and Meunier, G.:" Modelling of Squirrel Cage Induction Machines by the Finite Elements Method Combined with the Circuits Equations", *Proceedings of the International Conference on Evolution and Modern Aspects of Induction Machines. Torino, 8-11 July 1986. Associazione Elettrotecnica ed Elettronica Italiana, pp. 384-388.*

67) Abdelkader F.M., Bradley K.J. and Wright A.:"An Electromagnetic Model for Determining the Flux Density Distribution in Wound Rotor Induction Motors", *Proc. of the International Conference on Electrical Machines, Athens, Greece, September 1980.*

68) Erdelyi, E.A. and Fuchs, E.F.:" Nonlinear Magnetic Field Analysis of D.C. Machines, Part I: Theoretical Fundamentals", *Trans. IEEE, PAS-89, No. 7, 1970, pp. 1546-1554.*

69) Fuchs, E.F. and Erdelyi, E.A.:" Nonlinear Magnetic Field Analysis of D.C. Machines, Part II: Application of the Improved Treatment", *Trans. IEEE, PAS-89, 1970, pp. 1555-1564.*

70) A.Y., Hanalla and D.C., MacDonald:" Anodal Method for the Numerical Solution of Transient Field Problems in Electrical Machines", *IEEE Transactions on Magnetics, Vol. MAG-11, No.5, 1975, pp. 1544-1546.*

71) Zienkiewicz, O.C. and Cheung, Y.K.:" Finite elements in the Solution of Field Problems", The Engineer, Sept. 24, 1965, pp. 507-510.

72) Abdelkader F.M.:"The influence of Winding Slots upon the Air-gap Flux Density Distribution of Induction Machines", *PhD thesis, Nottingham University, 1979.*

73) Amin A.R.A.:"A Model for the Prediction of Induction Motor Performance with Detailed Consideration of the Air-gap Magnetic Field", *PhD thesis, Nottingham University, 1982.*

74) Preston, T.W., Reece, A.B.J. and Sangha, P.S.:" Induction Motor Analysis by Time-stepping Techniques", *COMPUMAG, 1987, pp. 471-472.*

75) Arkkio, A.:" Time-stepping Finite Element Analysis of Induction Motors", *ICEM, 1988, pp. 275-280.*

76) Arkkio, A.:" Finite Element Analysis of Cage Induction Motors Fed by Static Frequency Converters", *IEEE Transactions on Magnetics, Vol. 26, No. 2, March 1990, pp. 551-554.*

77) Smith, A.C., Williamson, S. and Smith, J.R.:" Transient Currents and Torques in Wound-rotor Induction Motors using the Finite Element Method", *IEE Proceedings, Vol. 137, Pt. B, No. 3, May 1990, pp. 160-173.*

78) Williamson, S., Lim, L.H. and Smith, A.C.:" Transient Analysis of Cage Induction Motors Using Finite Elements", *IEEE Transactions on Magnetics, Vol. 26, No. 2, March 1990, pp. 941-944.*

79) Bill, K. and Perzanowski, W.:" Modelling of an Induction Motor Resorting to Double Iterative Finite Boundary Element Technique", *ICEM 1988, pp. 255-259.*

80) Lindfors, H. and Luomi, J.:" A General Method for the Numerical Solution of Coupled Magnetic Field and Circuit Equations", *ICEM 1988, pp. 141-146.*

81) H.C.J. de Jong:" A.C. Motor Design with Conventional and Converter Supplies", *Oxford University Press, 976.*

82) S.J.Yang:" Low-noise Electrical Motors", *Clarendon Press, Oxford, 1981.*

83) E.C. Barns:" An experimrntal study of Induction Machine End-turn Leakage Reactance", *AIEE Transactions 70, 1951, pp. 671-679.*

84) K. Vogt:" Elektrische Maschinen, Berechnung Rotierender Elektrischer Maschienen", *3rd Edition, Berlin, VEB Verlag Technik, 1983, p. 500.*

85) Binns K.J., Hindmarsh R. and Short B.P:" Effect of Skewing Slots on Flux Distribution in Induction Machines", *Proceedings IEE 118, 3/4, 1971, pp. 543-549.*

86) Carter, F.W.:" The Magnetic Field of the Dynamic-electric Machine", *Trans. AIEE, 64, 1926, pp. 1115-1138.*

87) Binns, K.J.:" Calculation of some Basic Flux Quantities in Induction an other Doubly-slotted Electric Machines", *Proc. IEE, 111, 1964, pp. 1847-1858.*

88) Chari, M.V.K.:" Finite Element Analysis of Nonlinear Magnetic Fields in Electrical Machines", *PhD thesis, McGill University, Montreal, March 1970.*

89) Anderson, L.R.:" Numerical Methods for Variable Permeability Magnetostatic Field Problems", *PhD thesis, Oregon State Universiry, 1970.*

90) L.Lapidus and J.H.Seinfeld:" Numerical solution of Ordinary Differential Equations", *section 4.16.*

91) Binns, K.J.:" Cogging Torque in Induction Machines", *Proc. IEE, 115, 1968, pp. 1783-1790.*

92) AC-Power Analyzer D 5255 M (Motorversion), *Operating Instructions, pp.27.*

93) "Timer-counters, PM 6670-72", *Operator's manual, 3rd edition, Industrial and Electro-acoustic systems, Philips, the Netherland, 1984, pp.14-15.*

94) "R9211 Series Digital Spectrum Analyzer", *Guidebook Operations, Advantest Corporation, February 1991.*

95) "LeCroy Digital Oscilloscopes 9304A, 9310A & 9314A Series", Operator's manual, July 1994, pp.1-1.

96) Alger, P. L.:" The Nature of Polyphase Induction Machines ", Wiley, 1951.

APPENDIX A
TEST MACHINE
DETAILS

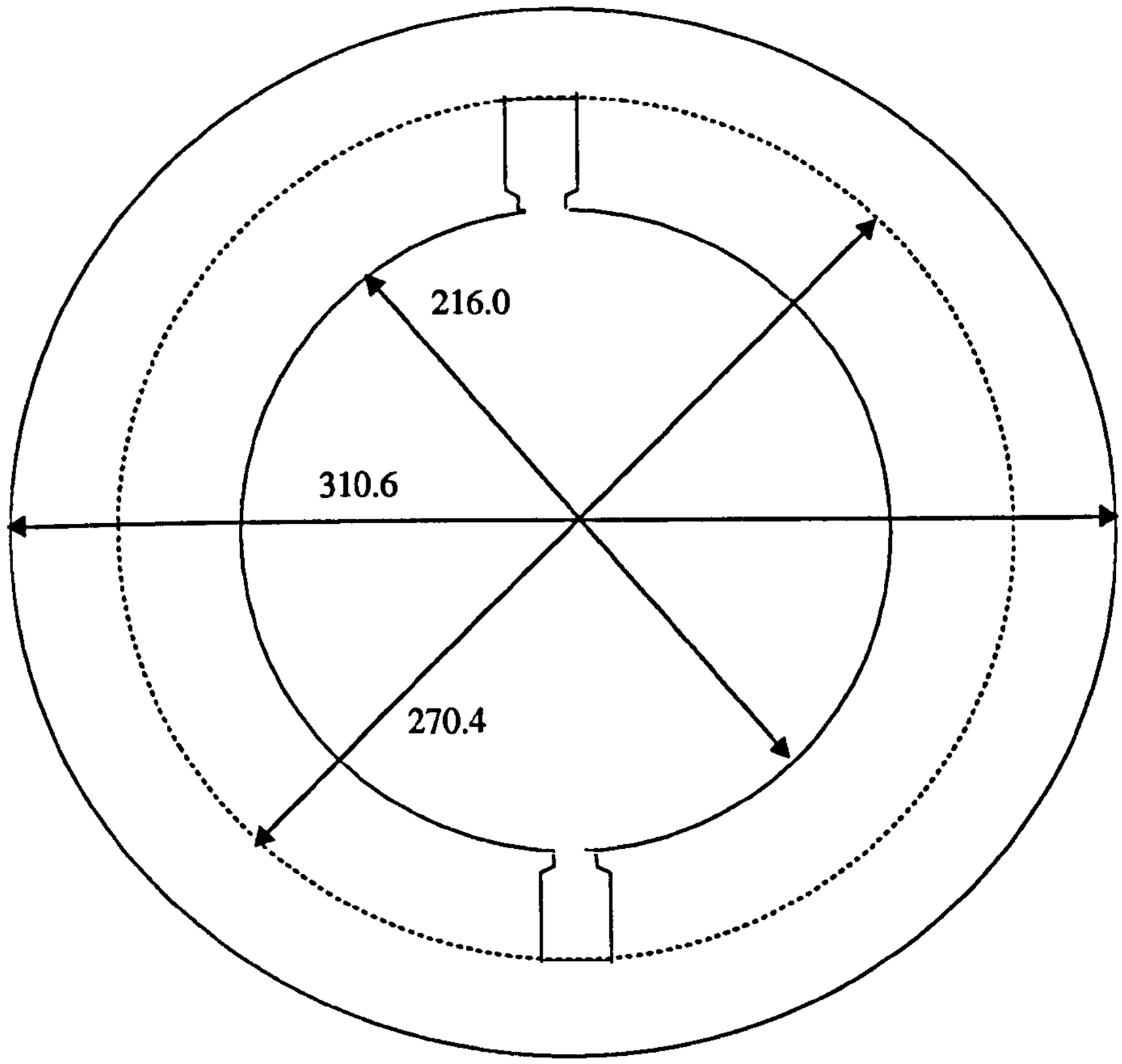

Figure A.1 rotor lamination dimensions (mm).

Fundamental parameter of the rotor (originally stator):

No. of slots:	36
No. of poles:	6
No. of phases:	36
No. of coils:	36
No. of conductors/slot	1
Core length:	147.8 mm

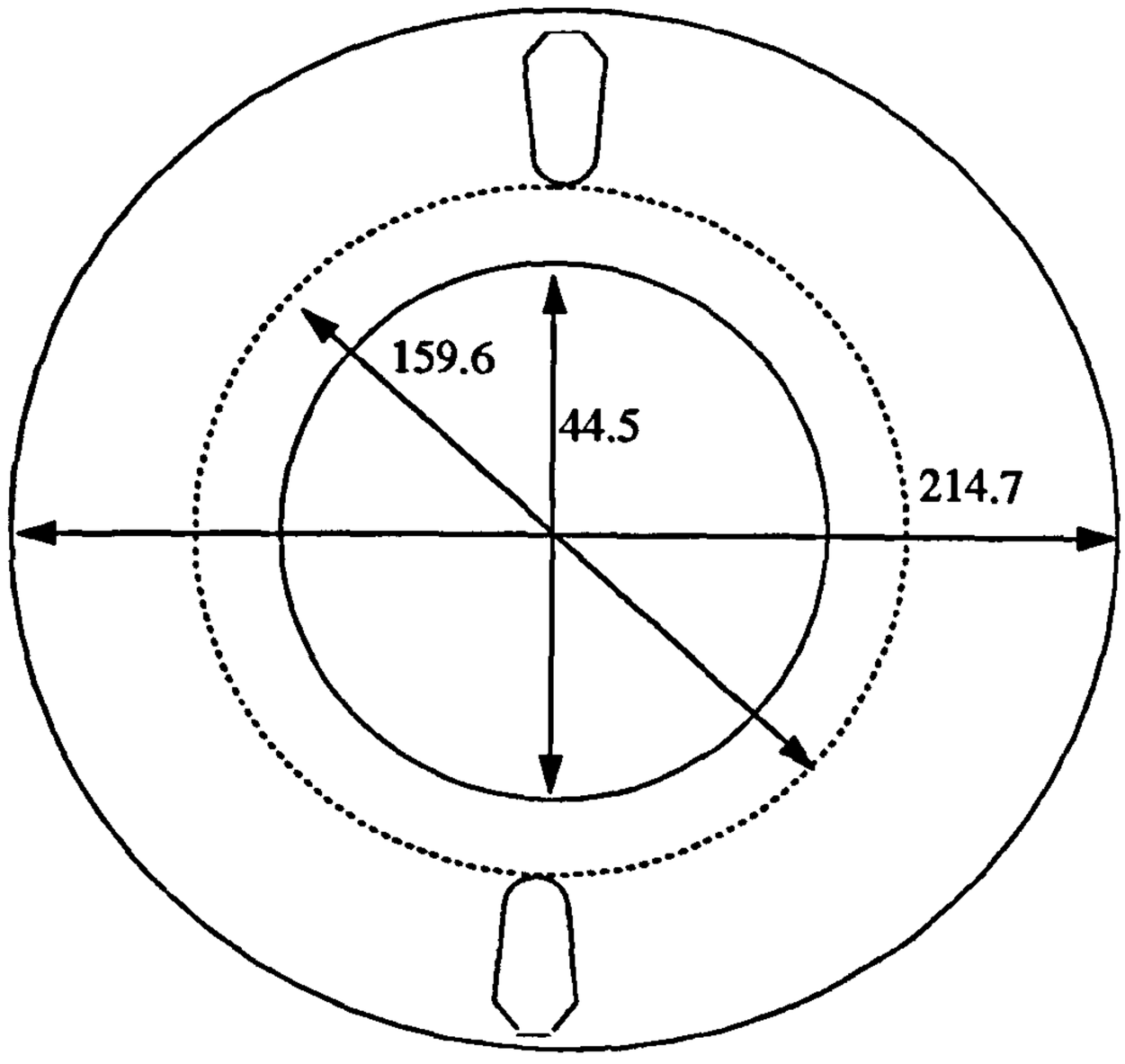

***Figure A.2** stator lamination dimensions (mm).*

Fundamental parameter of the stator (originally rotor):

No. of slots:	54
No. of poles:	6
No. of phases:	3
No. of coils:	54
No. of conductors/slot:	8
Core length:	156 mm
Skew:	1 rotor slot
Airgap length:	0.664 mm

APPENDIX B
TRIANGULAR SLOT OPENING TECHNIQUE

B.1 AIRGAP PERMEANCE CALCULATION

When both sides of the airgap are smooth, the permeance is proportional to the area divided by the radial length. But when it is slotted on both sides, this permeance decreases due to the slot openings. This can be regarded as an increase in the airgap length.

In the triangular technique, the airgap length is assumed to vary linearly with the angular displacement. In other words, the airgap length changes from l_g at the tooth-tip to l_g+H at the centre of the slot opening, where H is the height of the triangle which represents the opening of the slot as shown in Figure B.1.

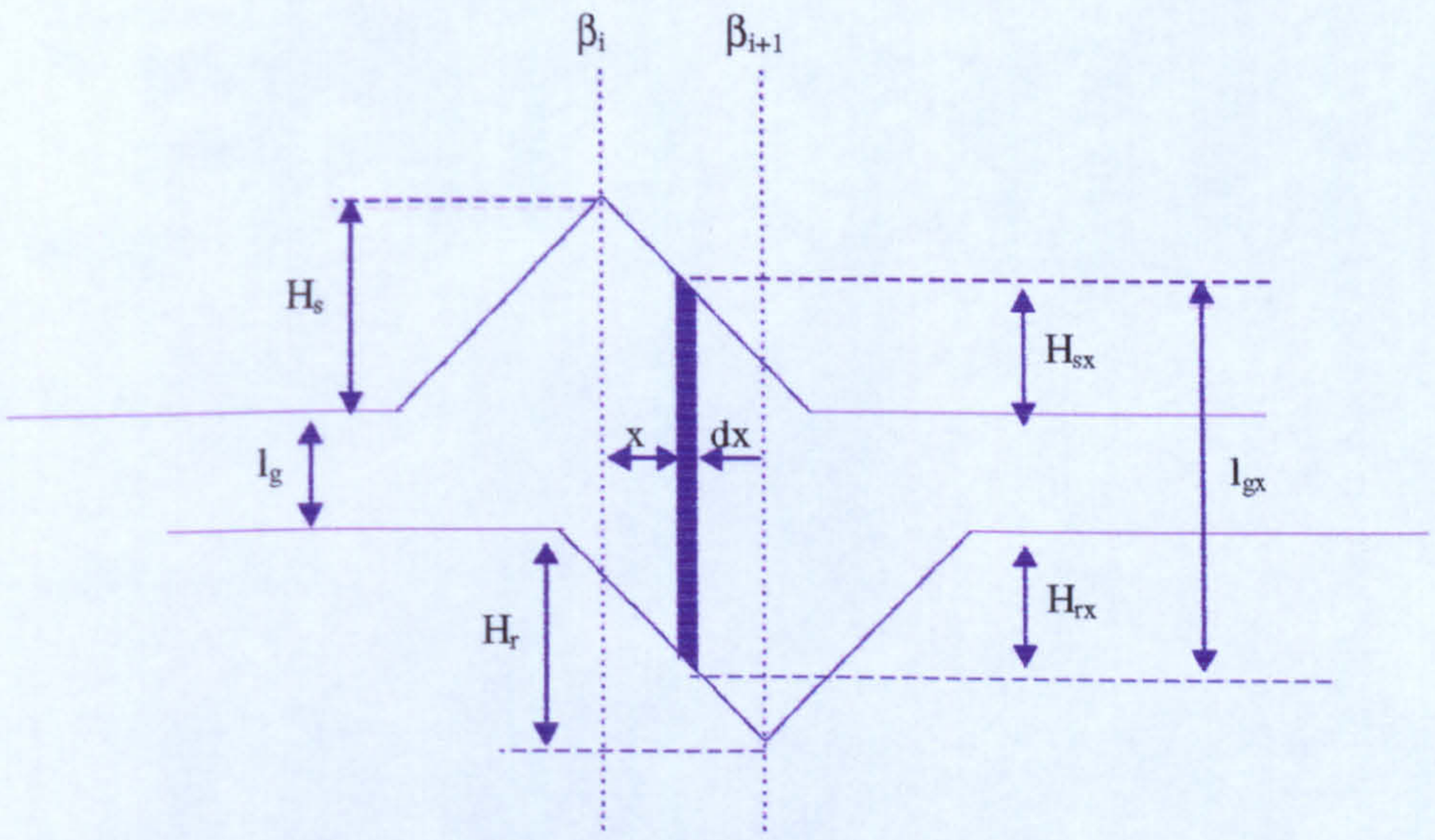

Figure B.1 *Airgap permeance calculation*

The airgap permeance is calculated as follows:

$$l_{gx} = l_g + H_{sx} + H_{rx} \tag{B.1}$$

From Figure B-1 H_{sx} and H_{rx} may be related as

$$\frac{H_{sx}}{H_s} = \frac{\frac{SSO}{2R_a} - x}{\frac{SSO}{2R_a}}$$

and hence

$$H_{sx} = \frac{2R_a H_s}{SSO}\left(\frac{SSO}{2R_a} - x\right) \tag{B.2}$$

and

$$\frac{H_{rx}}{H_r} = \frac{\left(\beta_i - \left(\beta_{i+1} - \frac{RSO}{2R_a}\right) + x\right)}{\frac{RSO}{2R_a}}$$

therefore

$$H_{rx} = \frac{2R_a H_r}{RSO}\left(\beta_i - \beta_{i+1} + \frac{RSO}{2R_a} + x\right) \tag{B.3}$$

replacing (B.2) and (B.3) in (B.1) we get

$$l_{gx} = l_g + H_s + H_r - \frac{2R_a H_r}{RSO}(\beta_{i+1} - \beta_i) + 2R_a\left(\frac{H_r}{RSO} - \frac{H_s}{SSO}\right)x \tag{B.4}$$

$$l_{gx} = C_1 + C_2 x$$

The permeance of the small area l.dx at a distance x is

$$d\Lambda = \frac{\mu_0 l dx}{l_{gx}}$$

Therefore

$$\Lambda_i = \mu_{0l}\int_0^{\beta_{i+1}-\beta_i}\frac{dx}{C_1 + C_2 x}$$

After integration we obtain

$$\Lambda_i = \frac{\mu_0 l R_a}{C_2}\log_e\left(1+\frac{C_2}{C_1}(\beta_{i+1}-\beta_i)\right) \qquad (B.5)$$

When the overlap angle is divided into more than one section, then the permeance of each section is calculated separately. The total permeance of the overlap angle is equal to the sum of the individual permeances of each section.

APPENDIX C

PROCEDURES

USED IN THE

MAIN PROGRAM

C.1 PROCEDURES USED IN THE MAIN PROGRAM

For the sake of clarity and simplicity, the program was built up in the form of procedures or subroutines so that any modifications could be added to specific procedures with the main program remaining intact. In the table below are listed all the procedures used in the main program along with a very brief description of each one of them.

Number	*Name*	*Description*
1	SBE	Generating Stator Back Iron elements
2	STE	Generating Stator teeth elements
3	RTE	Generating Rotor Teeth elements
4	RBE	Generating Rotor Back Iron elements
5	SBEORDER	Reordering Stator Back Iron elements
6	RBEORDR	Reordering Rotor Back Iron elements
7	SSOE	Generating Stator Slot Opening elements
8	RSOE	Generating Rotor Slot Opening elements
9	OVERLAP	Computing Overlap Angles
10	AGE	Generating Airgap elements
11	CARTER	Computing Carter's Factor
12	TOOTHDIM	Computing Tooth dimensions
13	SLOTBODY	Computing Slot permeance
14	OPENING	Computing Slot Opening permeance
15	PROD21	Product of a Matrix by a Vector
16	PROD22	Product of two Matrices
17	DIFF11	Difference of two Vectors
18	DIFF22	Difference of two Matrices
19	EUCLID	Computes the Euclidian Norm
20	FNDANG	Computes Stator and Rotor Slot Angles
21	FNDLEFP	Finds the Largest element for pivot
22	ADAMS	Adam's Integration Technique
23	Newton	Solving Magnetic Circuit
24	COREPERM	Computing Iron Parts permeance
25	GAPER	Computing Airgap permeances
26	FORMAT1	Forms Permeance Matrix
27	BTOTHI	Converts B-H curve to Flux-MMF curves
28	SPLINE	Cubic Spline Interpolation

***Table C.1** Procedures used in the main Program.*

Number	*Name*	*Description*
29	MMFSRC	Computes MMF Sources
30	VOLTAGE	Computes Phase Voltages
31	SIXTY	Computes Slot MMFs for 60 spread
32	TWENTY	Computes Slot MMFs for 120 spread
33	RNGKT	Runge-Kutta Integration Technique
34	TORQUE	Computes Electromagnetic Torque
35	STEP	Increments time and rotor position
36	LINKAGE	Computes Windings Linkage fluxes
37	INDUCTANCE	Computes Winding Inductances
38	DERIVE	Computes Current Derivatives
39	DCOMP	LU- Matrix Decomposition
40	SOLVE	Solves system of linear equations
41	SHAFT	Computes Shaft Permeances

***Table C.1** Procedures used in the main Program Continued...*

APPENDIX D

RESULTS

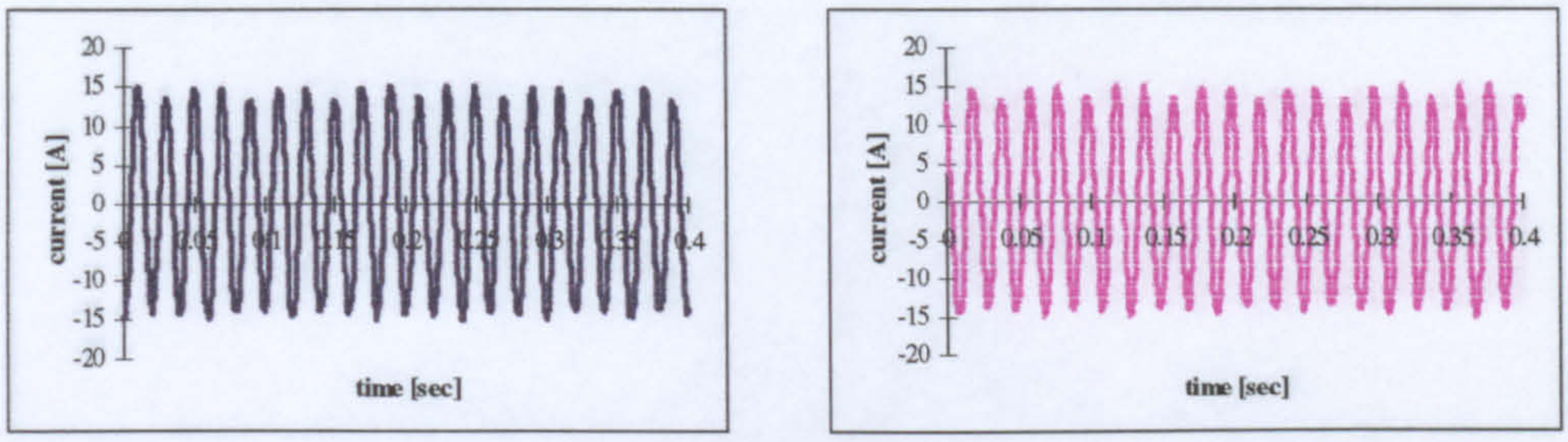

a) slip = 0%

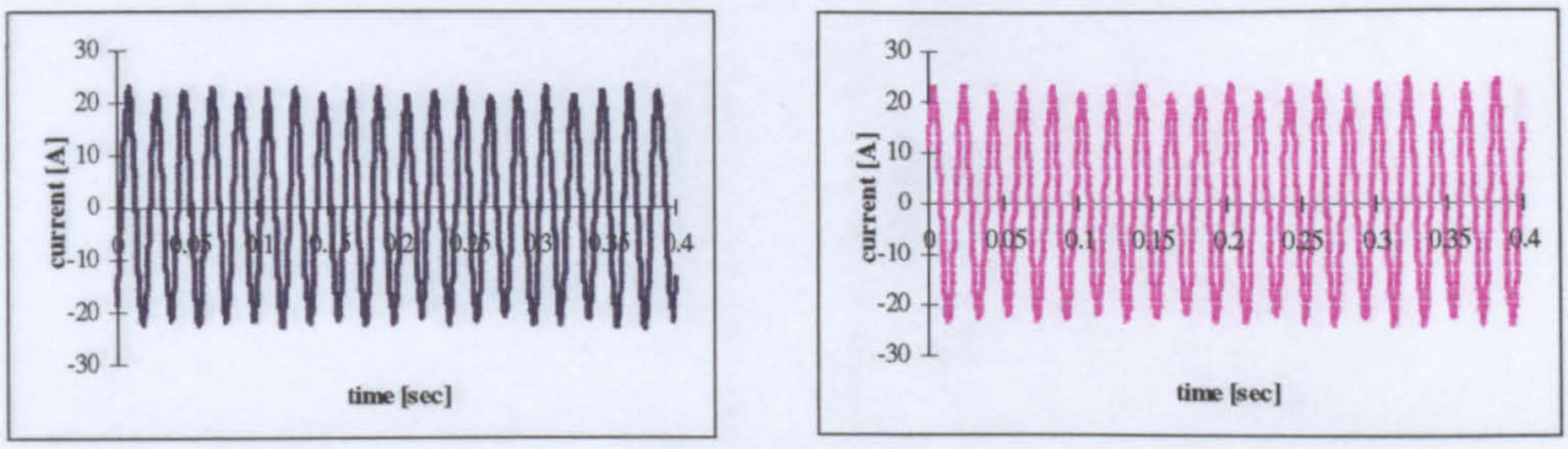

b) slip = 1%

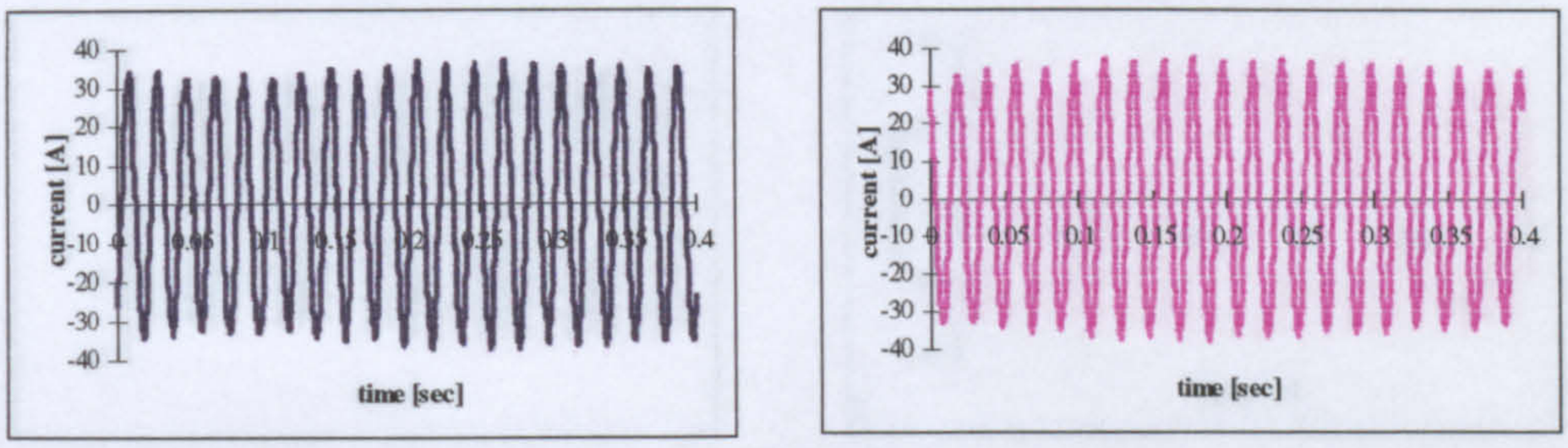

c) slip = 2%

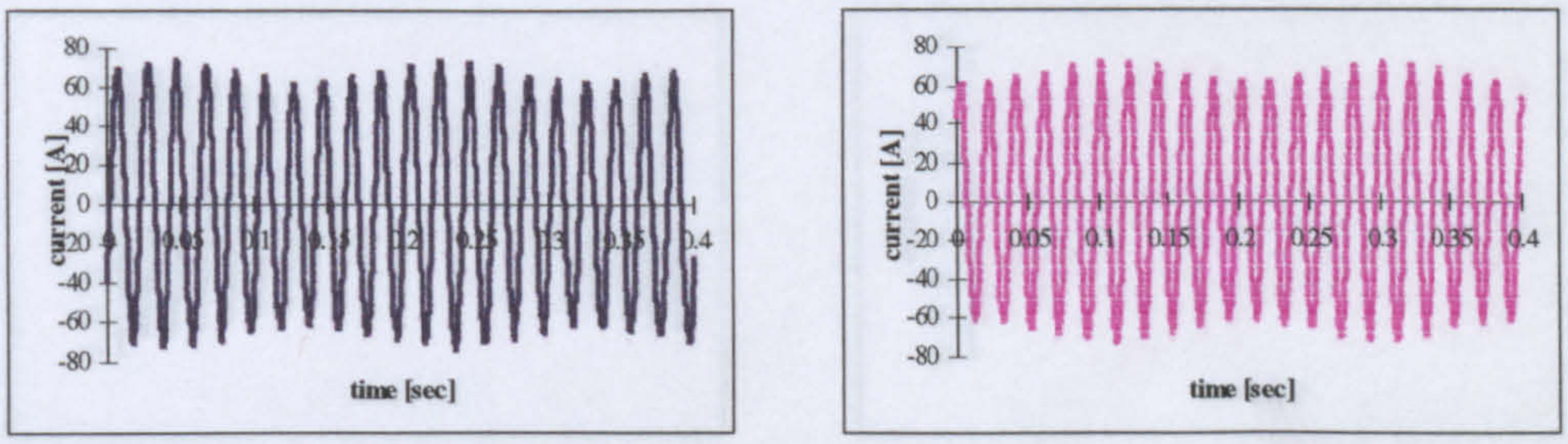

d) slip = 5%

Figure D.1 *Measured (left) and computed (right) stator current waveforms with three adjacent broken bars for different loads.*

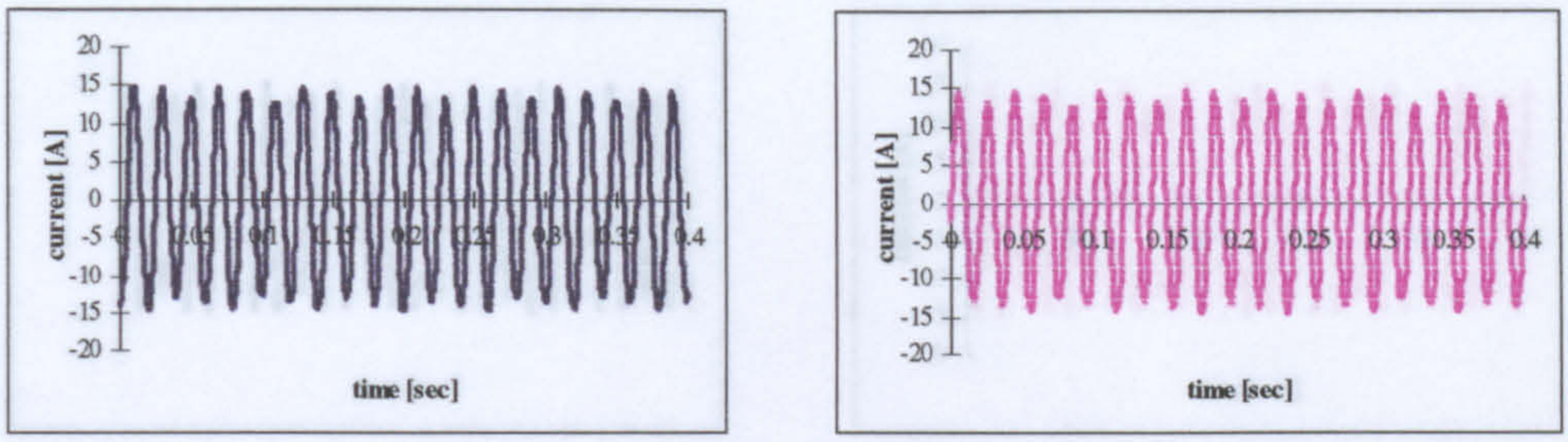

a) slip = 0%

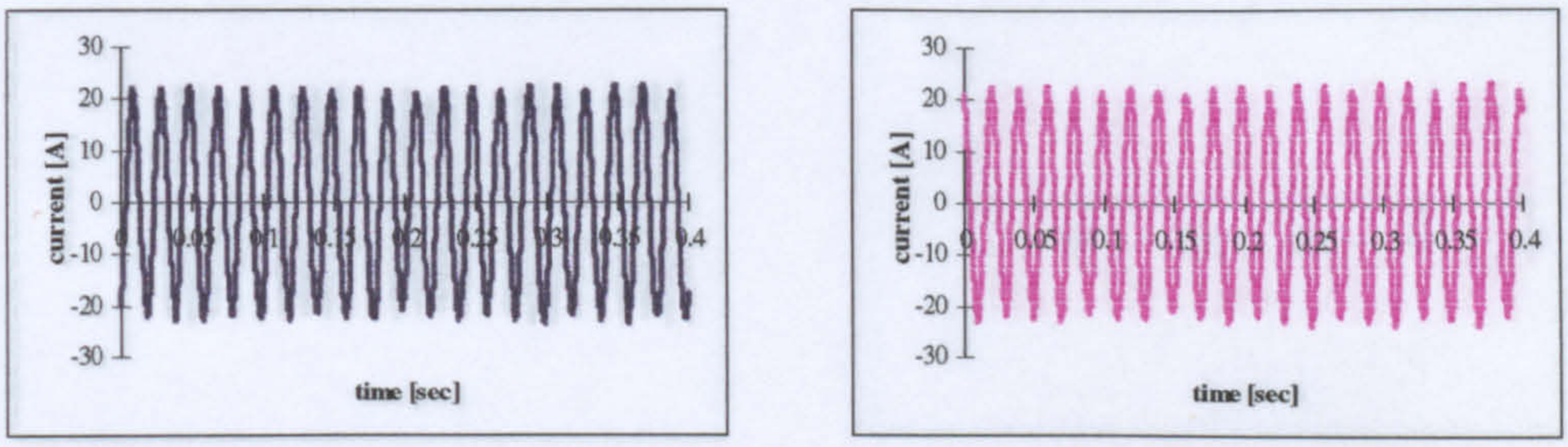

b) slip = 1%

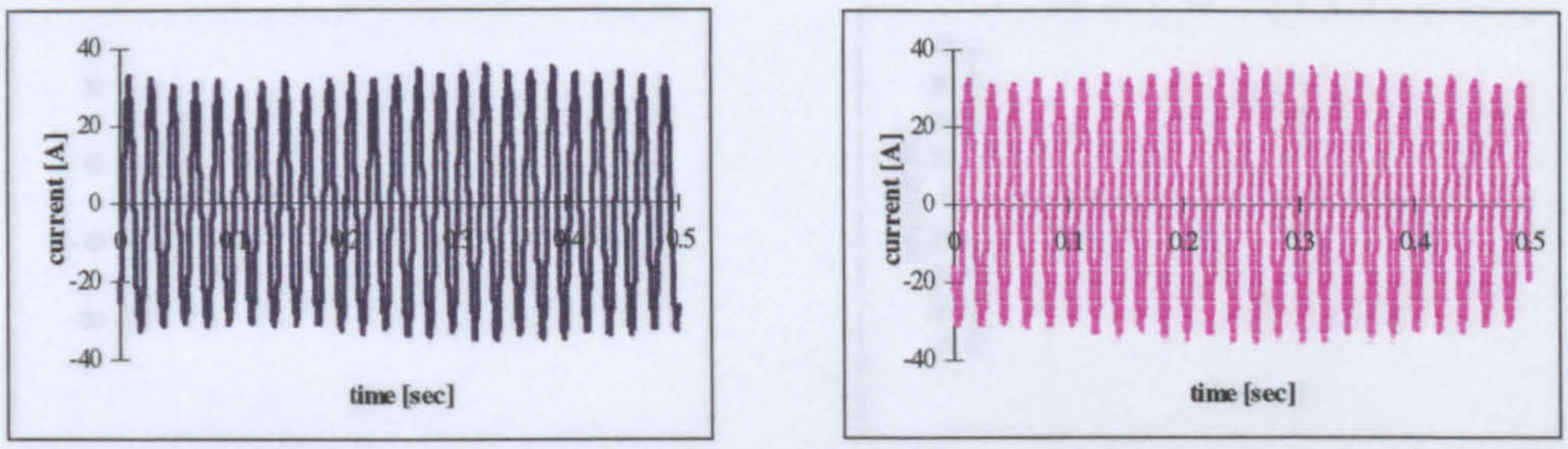

c) slip = 2%

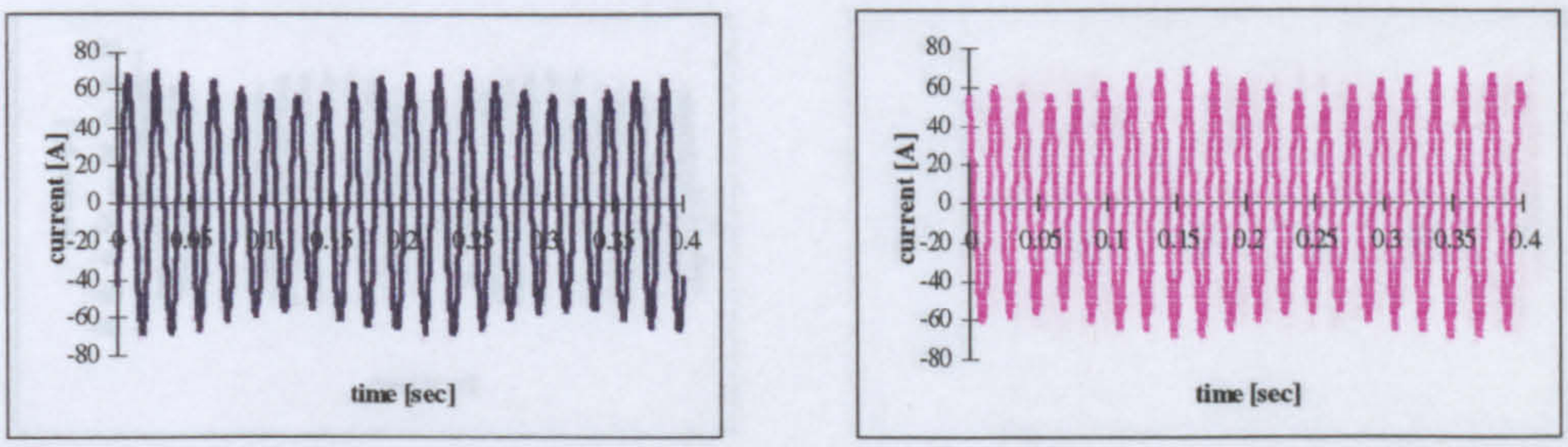

d) slip = 5%

Figure D.2 *Measured (left) and computed (right) stator current waveforms with four adjacent broken bars for different loads.*

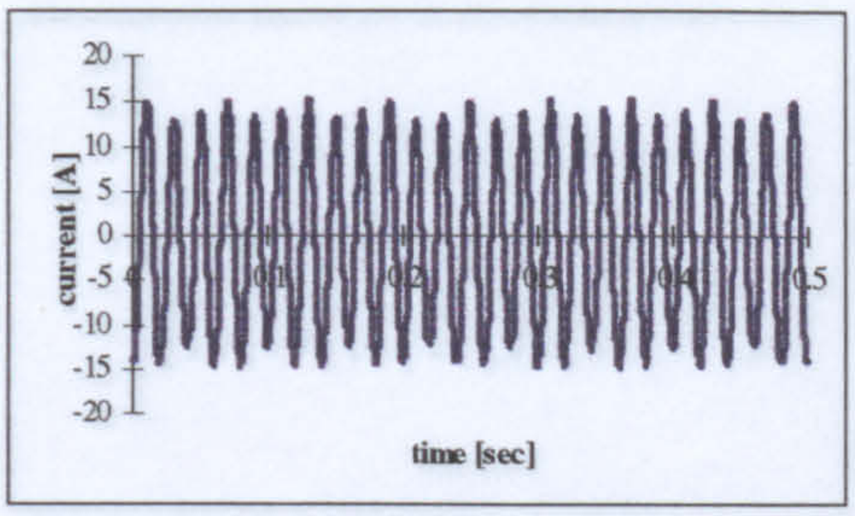

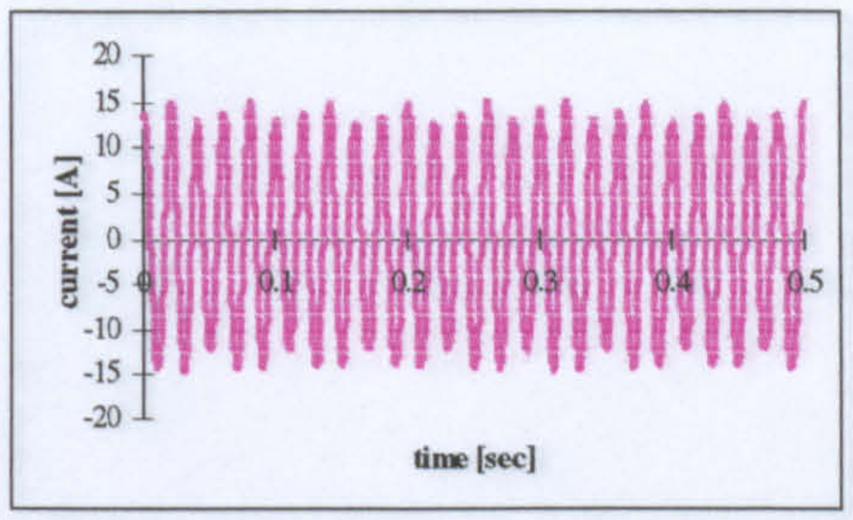

a) slip = 0%

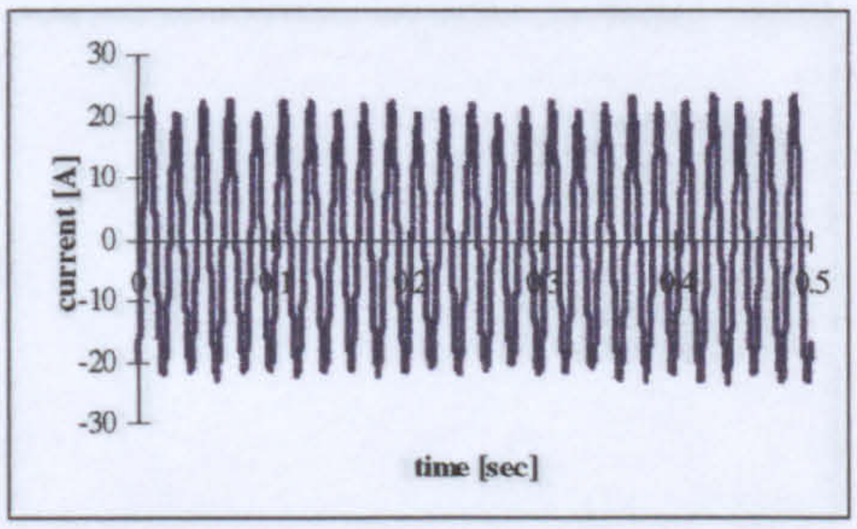

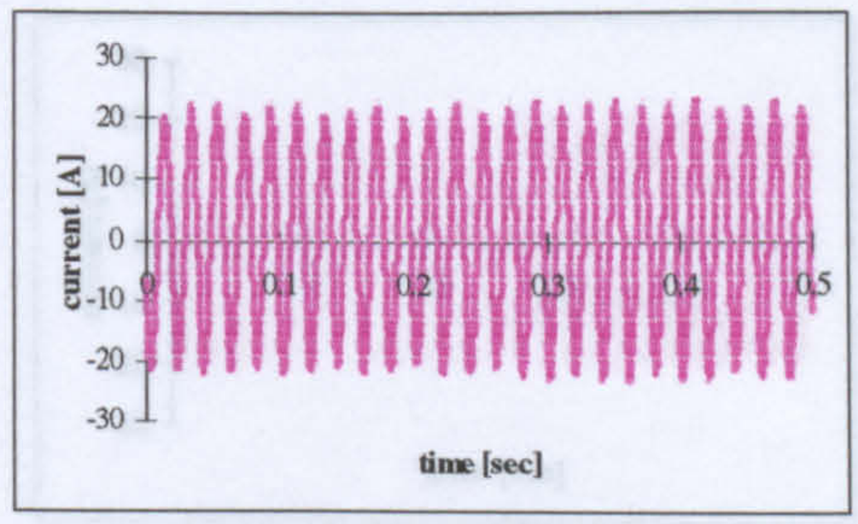

b) slip = 1%

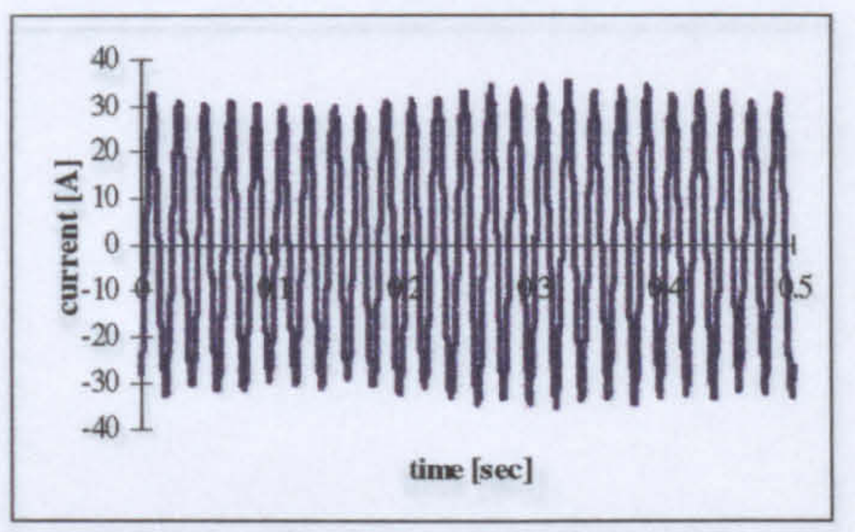

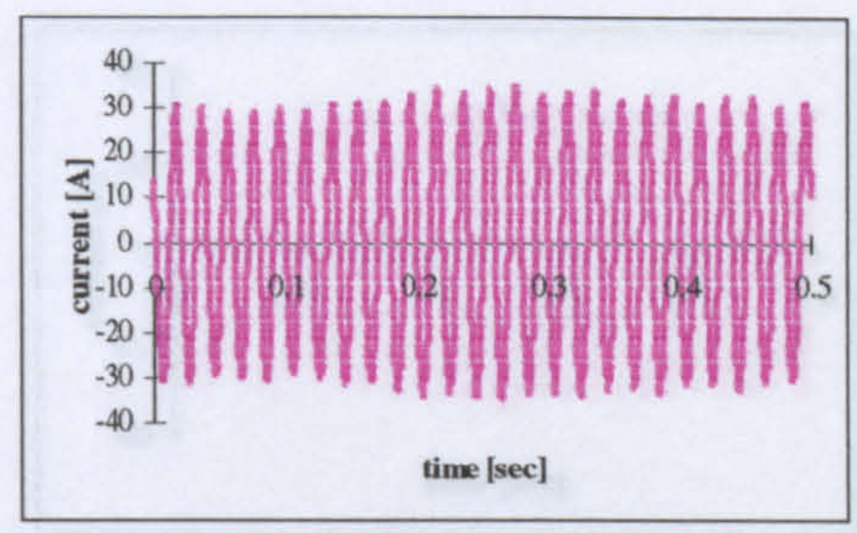

c) slip = 2%

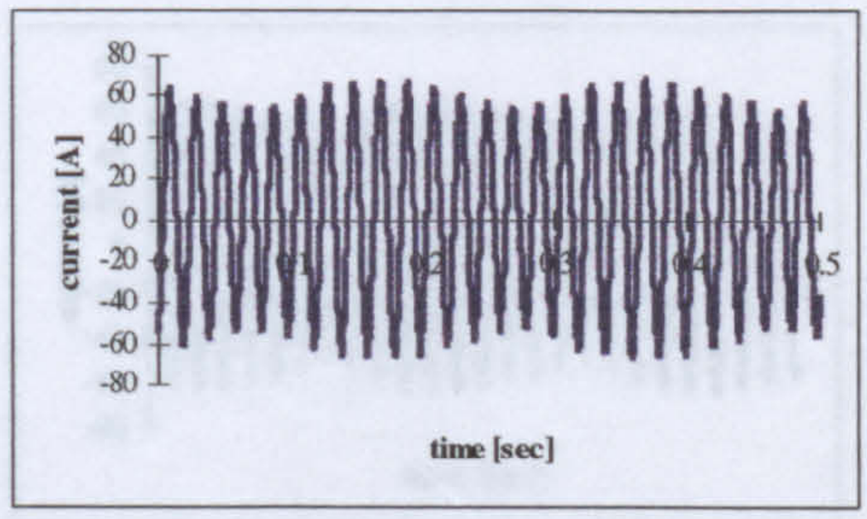

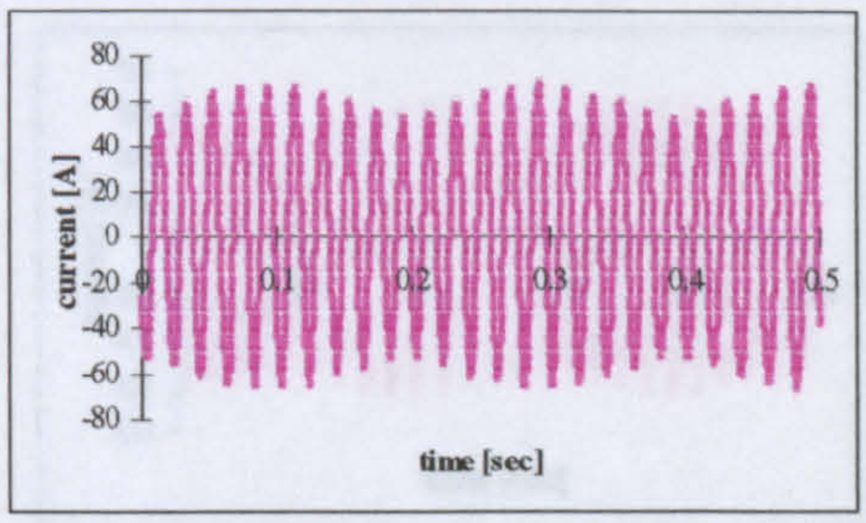

d) slip = 5%

Figure D.3 *Measured (left) and computed (right) stator current waveforms with five adjacent broken bars for different loads.*

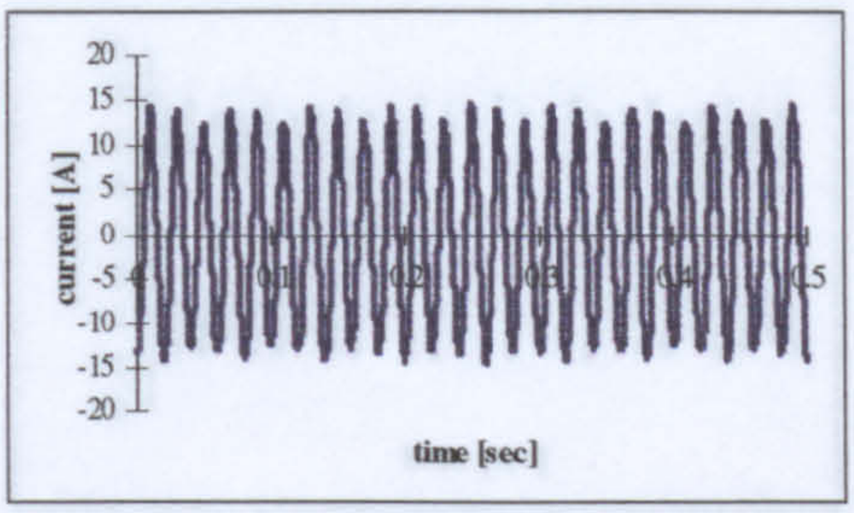

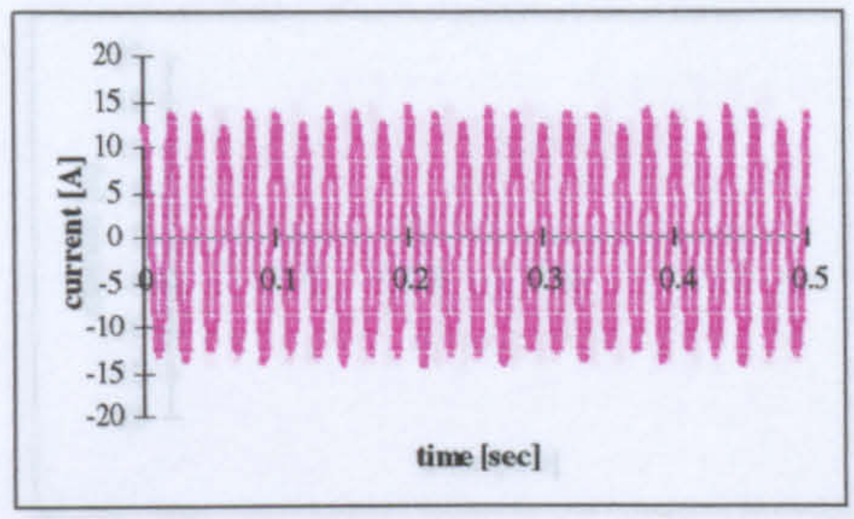

a) slip = 0%

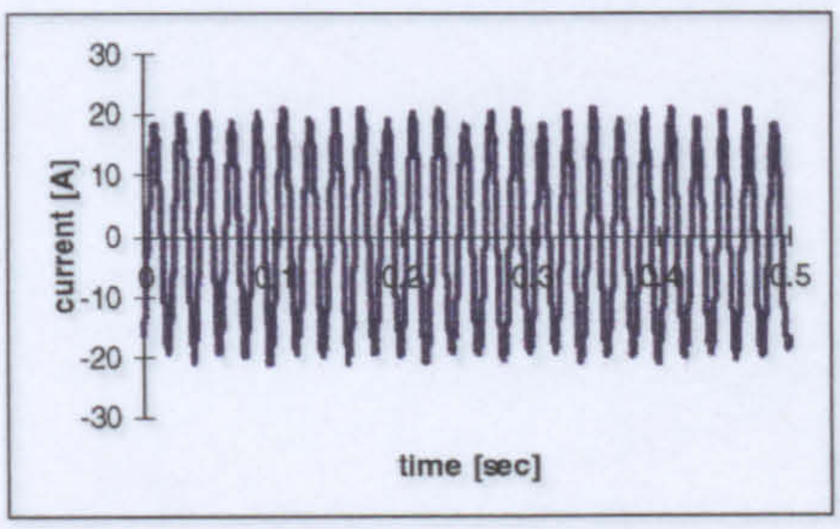

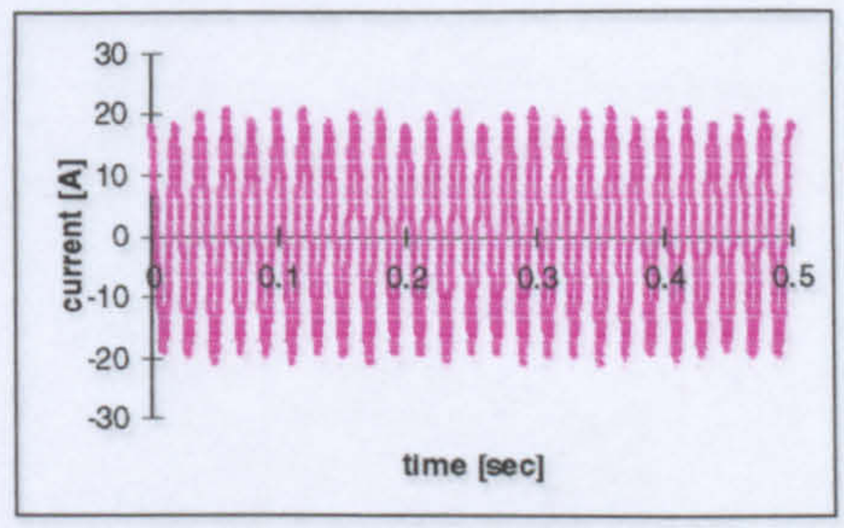

b) slip = 1%

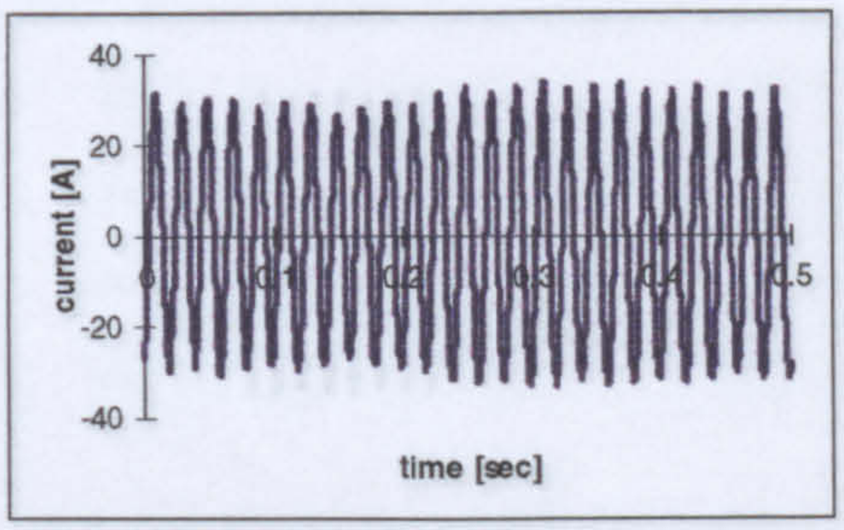

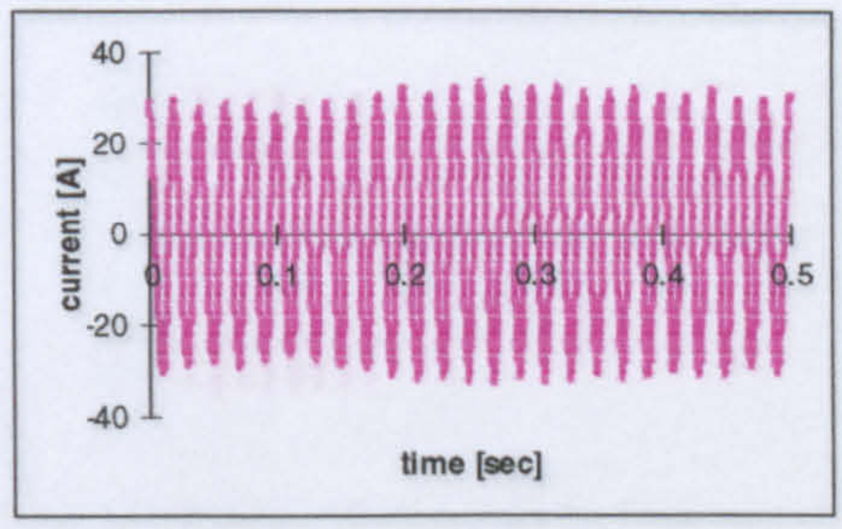

c) slip = 2%

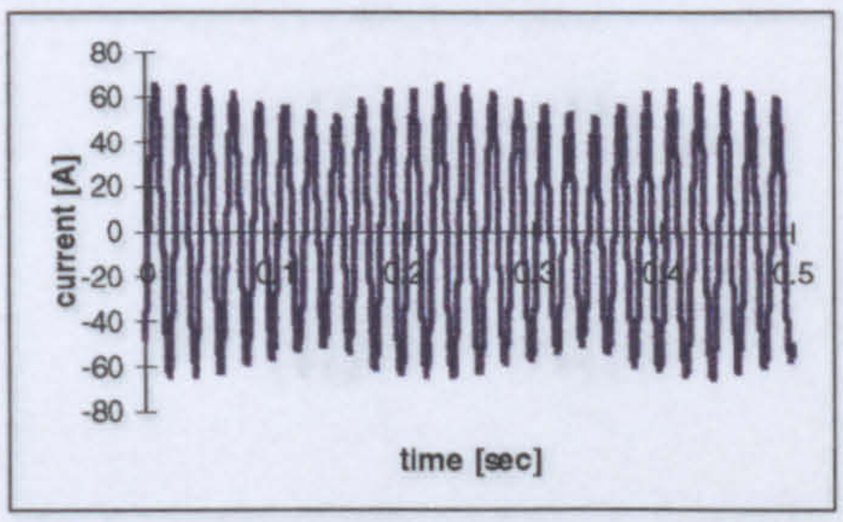

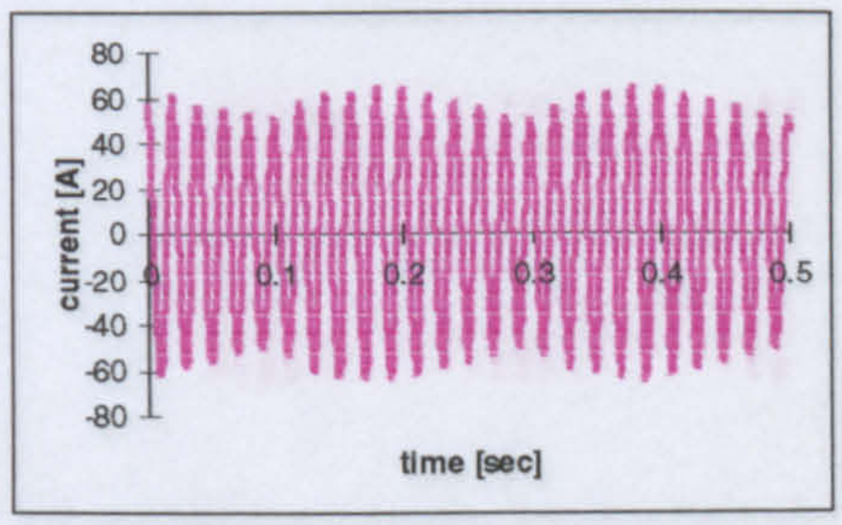

d) slip = 5%

Figure D.4 *Measured (left) and computed (right) stator current waveforms with six adjacent broken bars for different loads.*

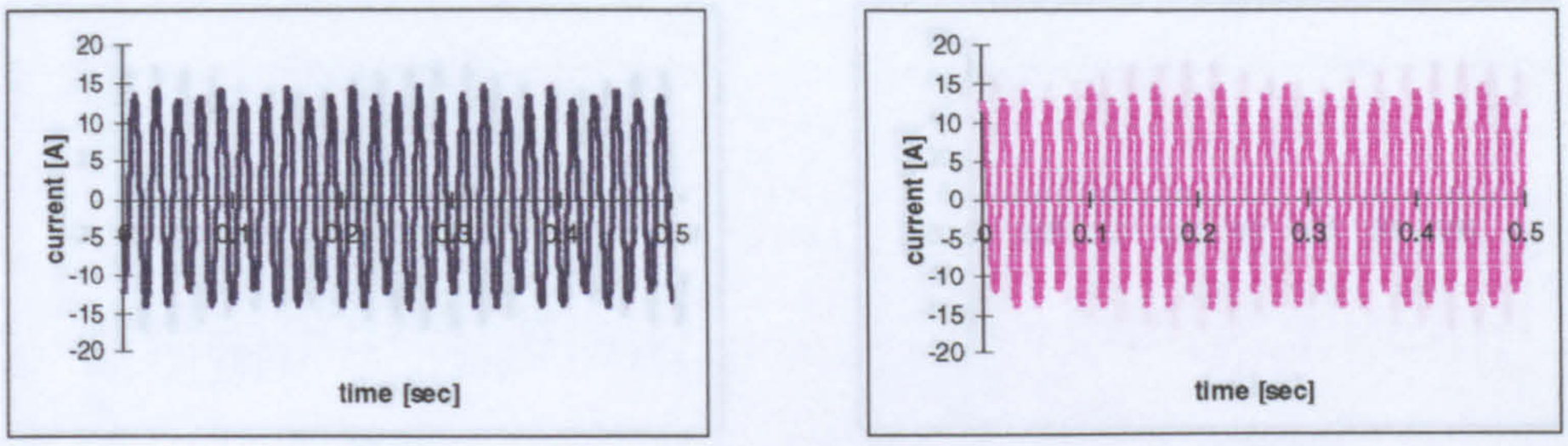

a) slip = 0%

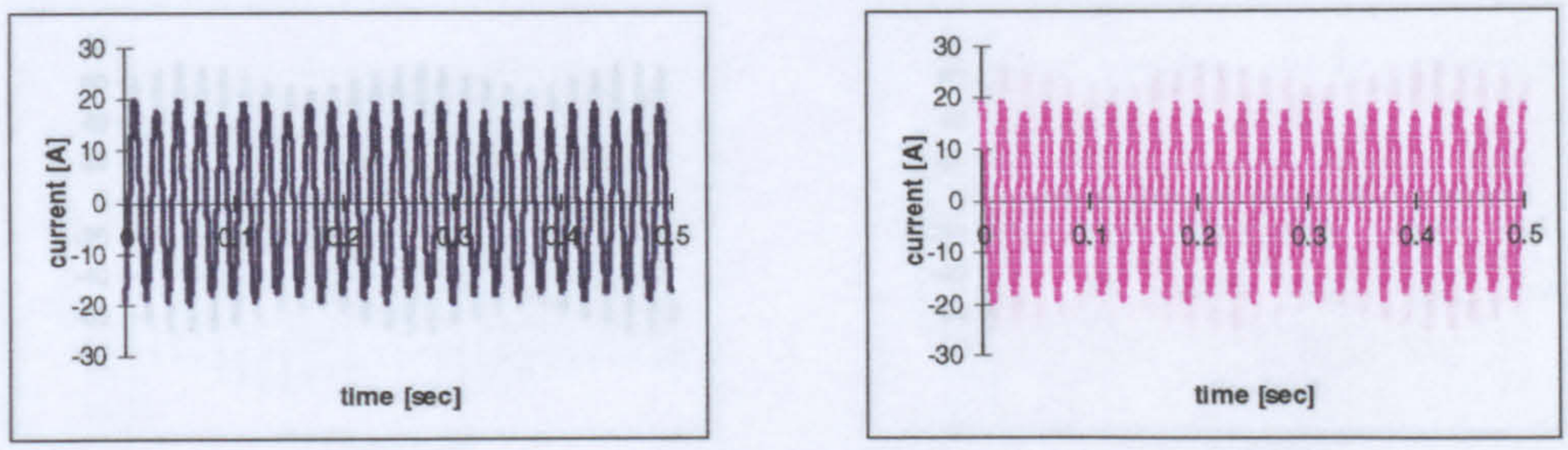

b) slip = 1%

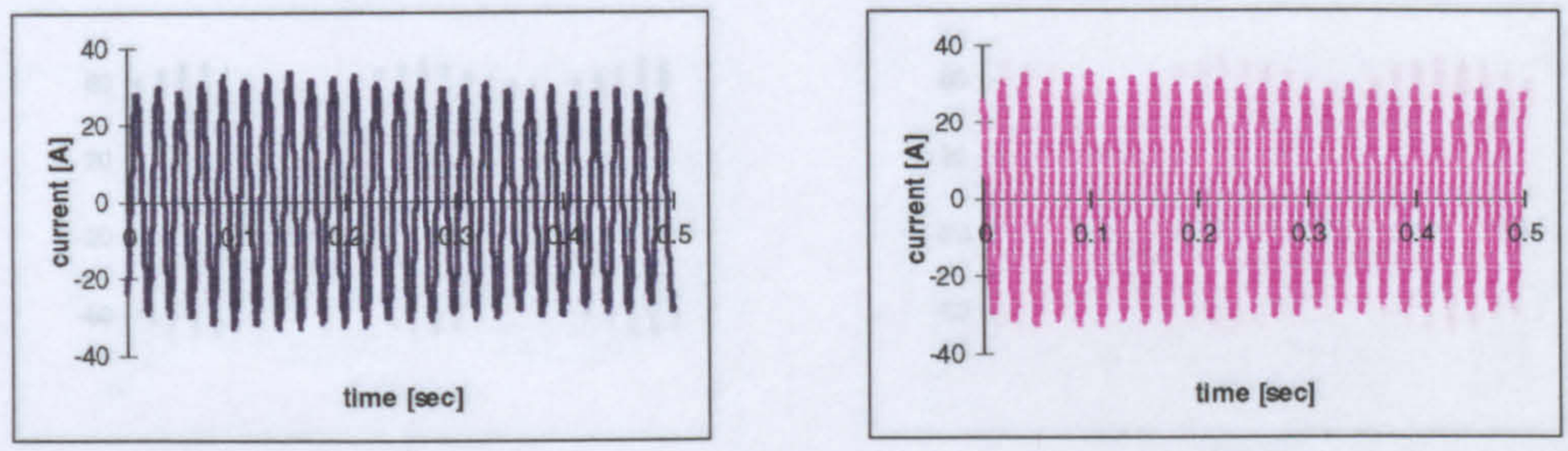

c) slip = 2%

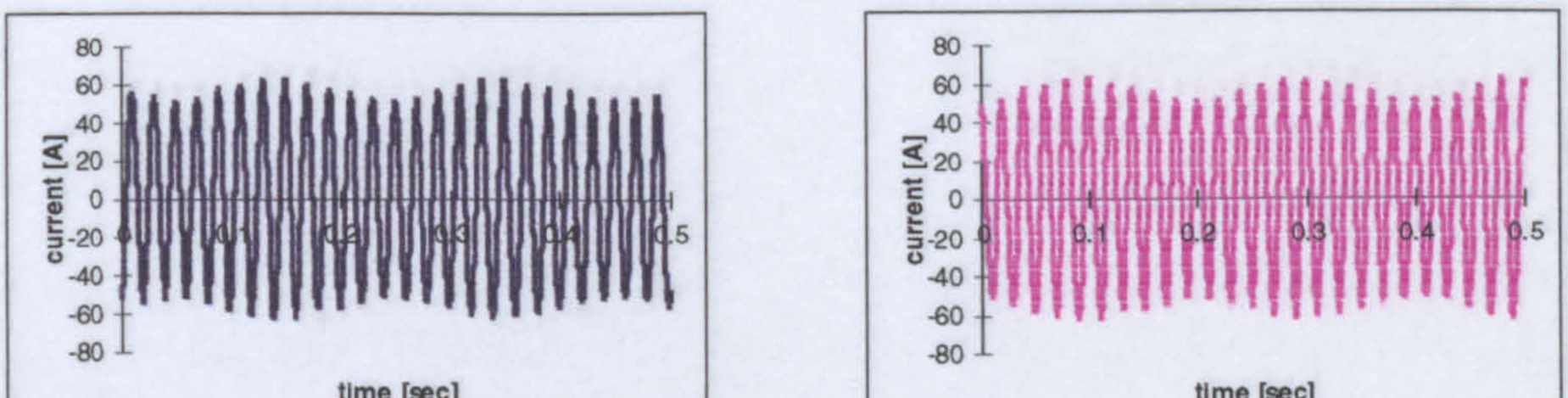

d) slip = 5%

Figure D.5 *Measured (left) and computed (right) stator current waveforms with seven adjacent broken bars for different loads.*

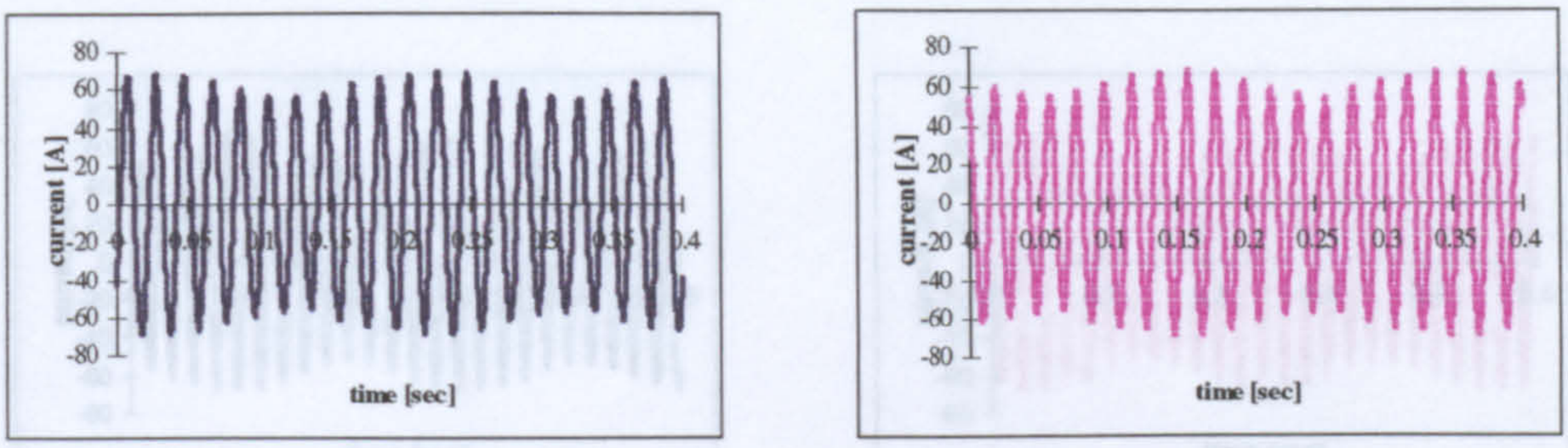

a) 4-0-0

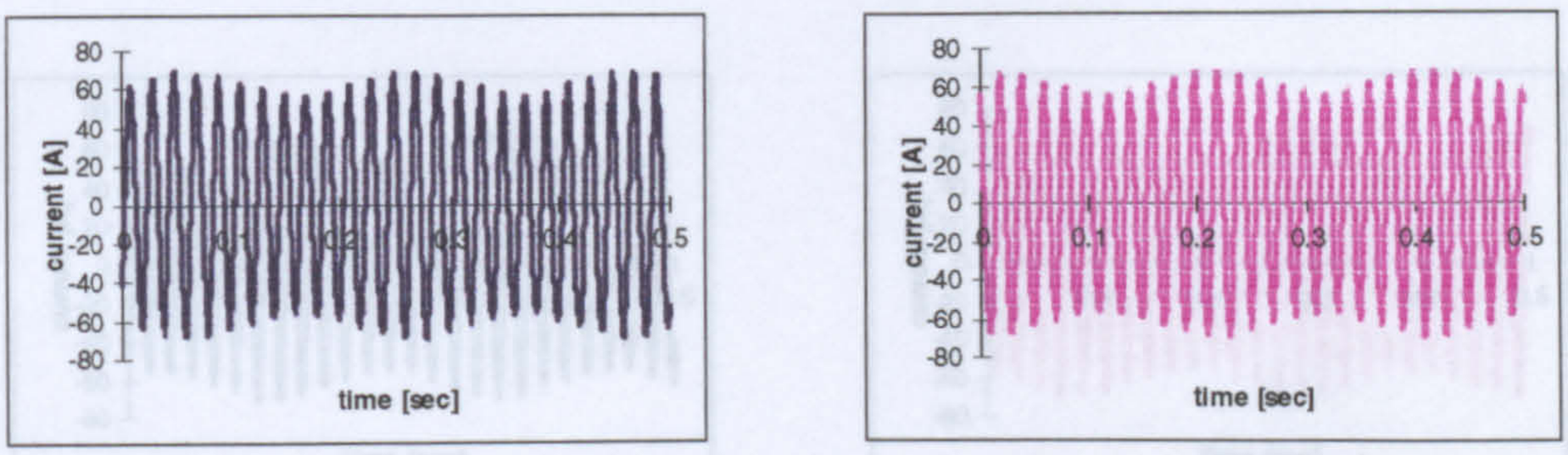

b) 2-2-0

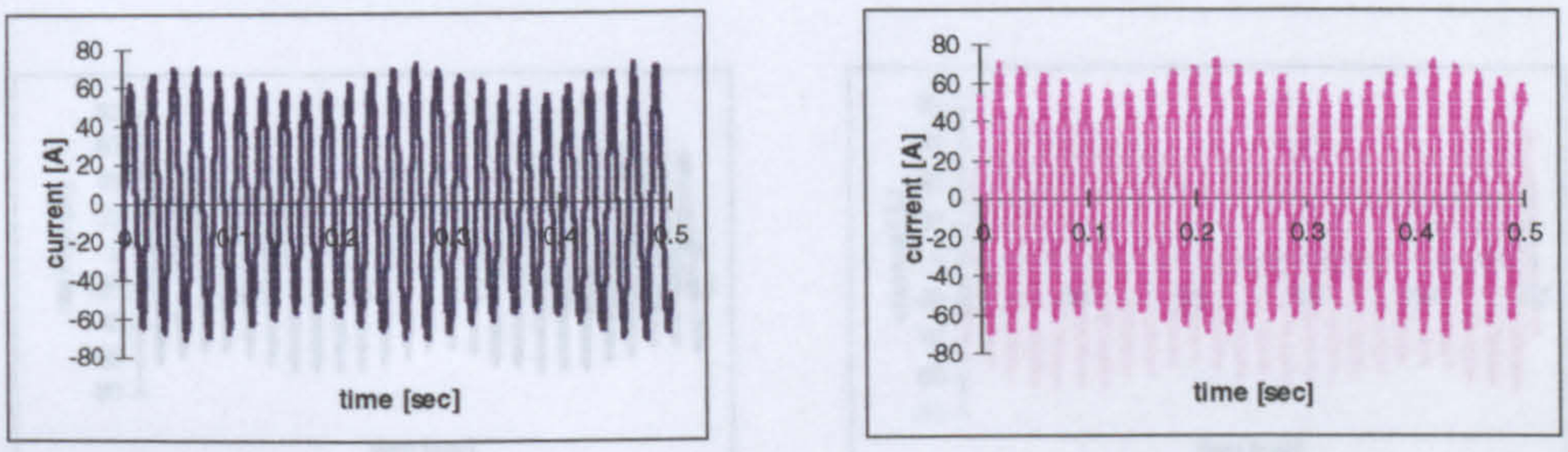

c) 2-1-1

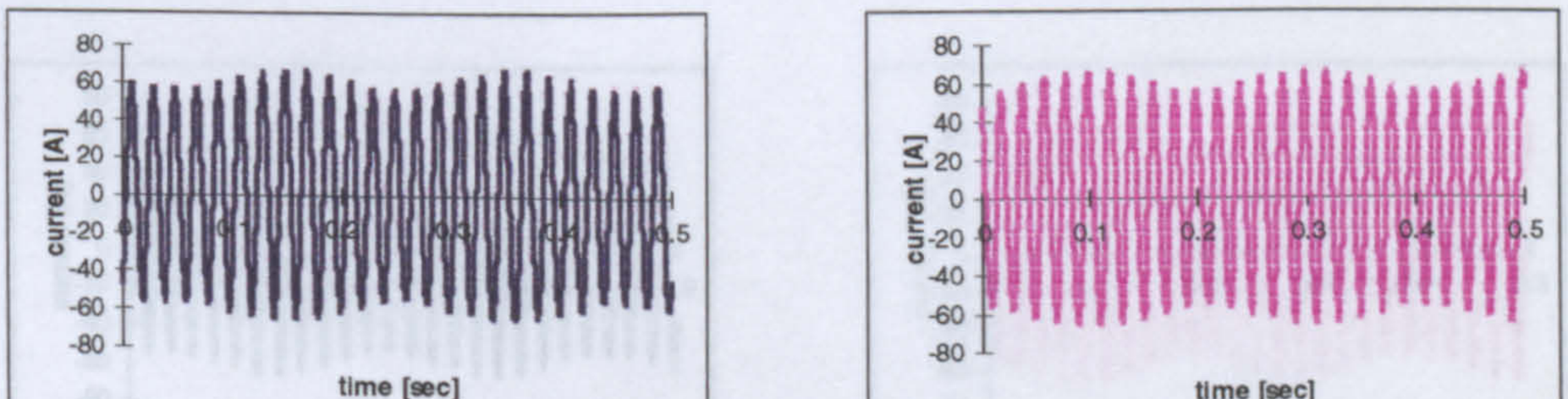

d) 3-1-0

Figure D.6 *Measured (left) and computed (right) stator current waveforms with four adjacent broken bars for different relative positions*

NB: The notation N1-N2-N3 means N1 broken bars under the first pole pair, N2 under the second one and N3 under the third pole pair.

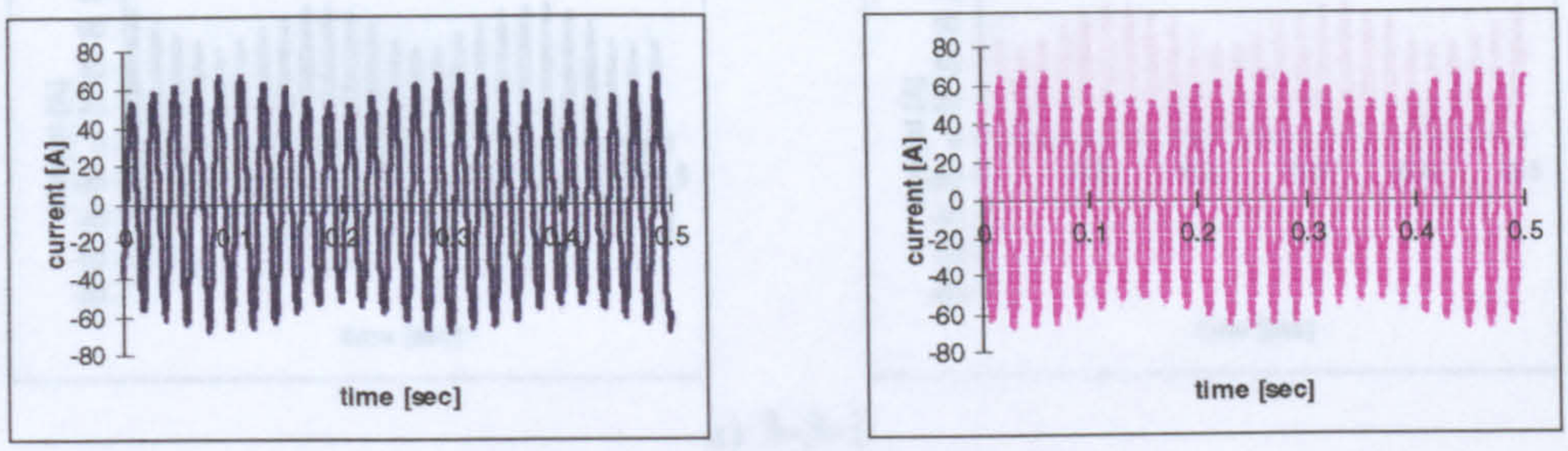

a) 3-1-1

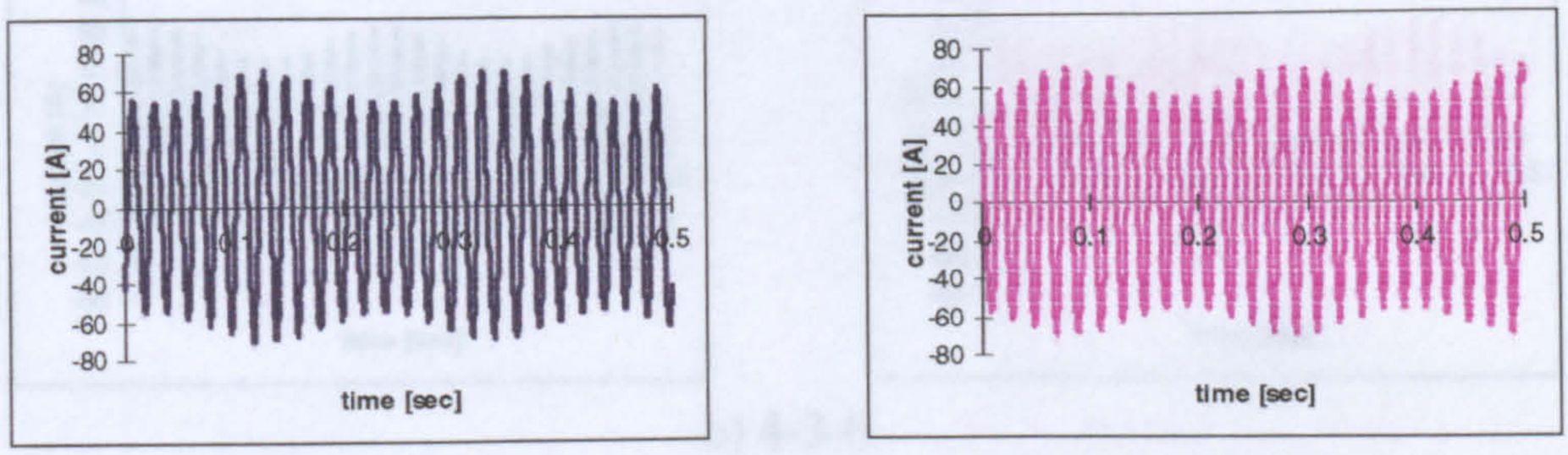

b) 2-2-1

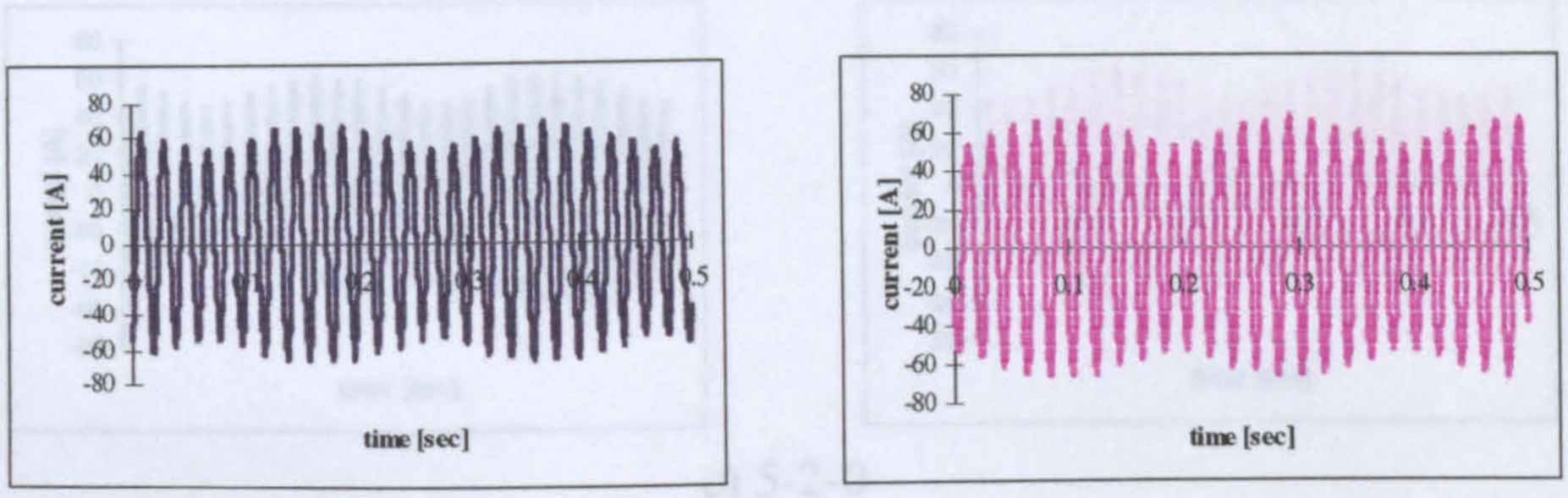

c) 5-0-0

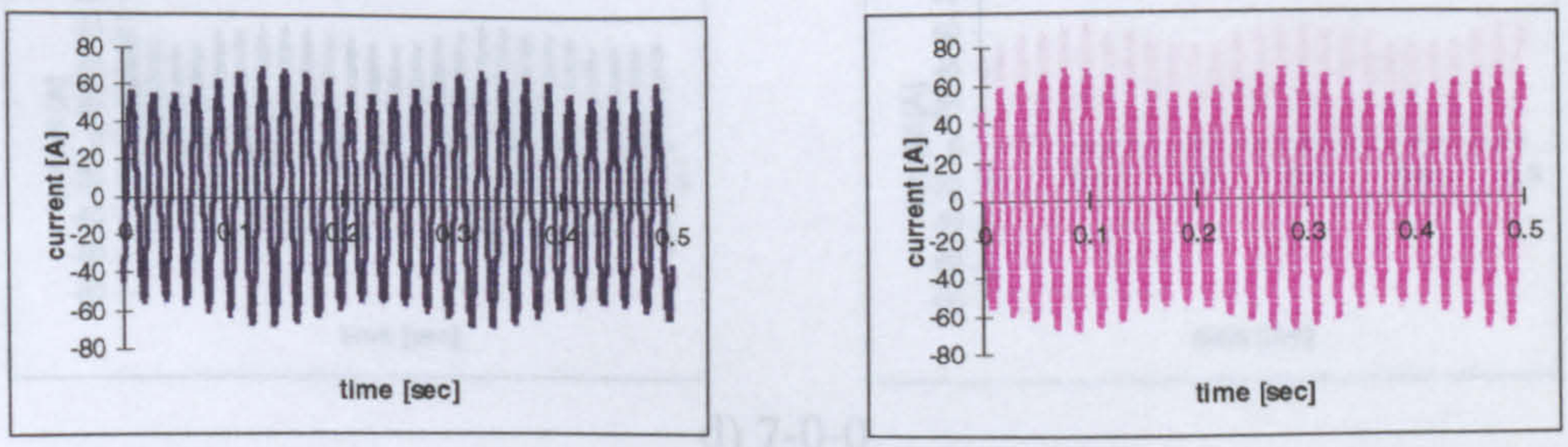

d) 3-2-0

Figure D.7 *Measured (left) and computed (right) stator current waveforms with five adjacent broken bars for different relative positions*

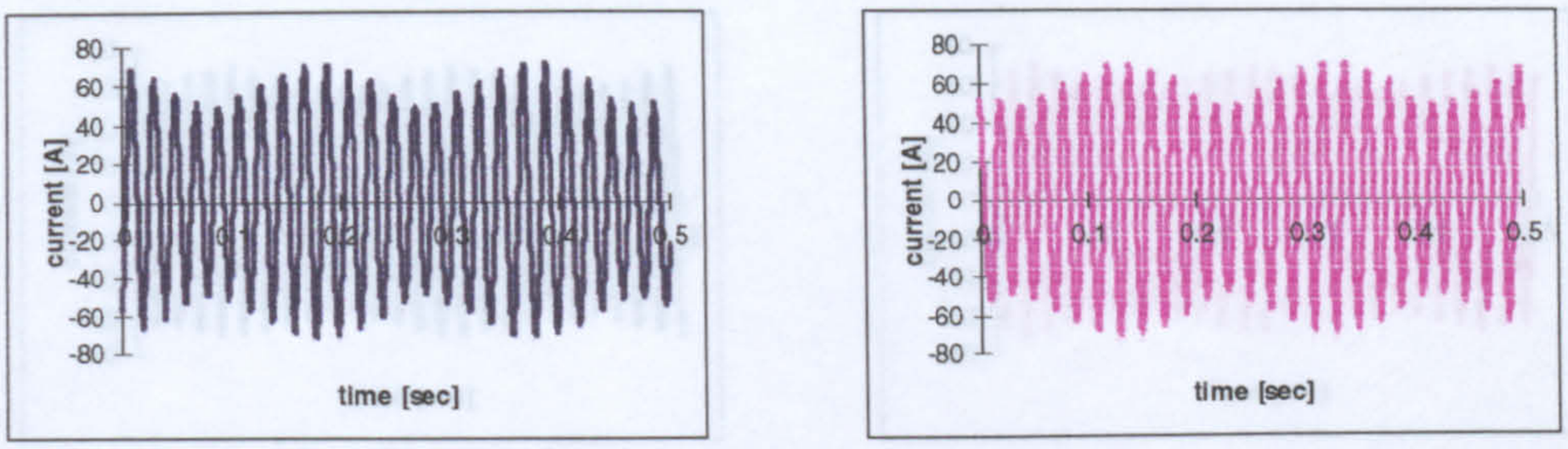

a) 3-3-1

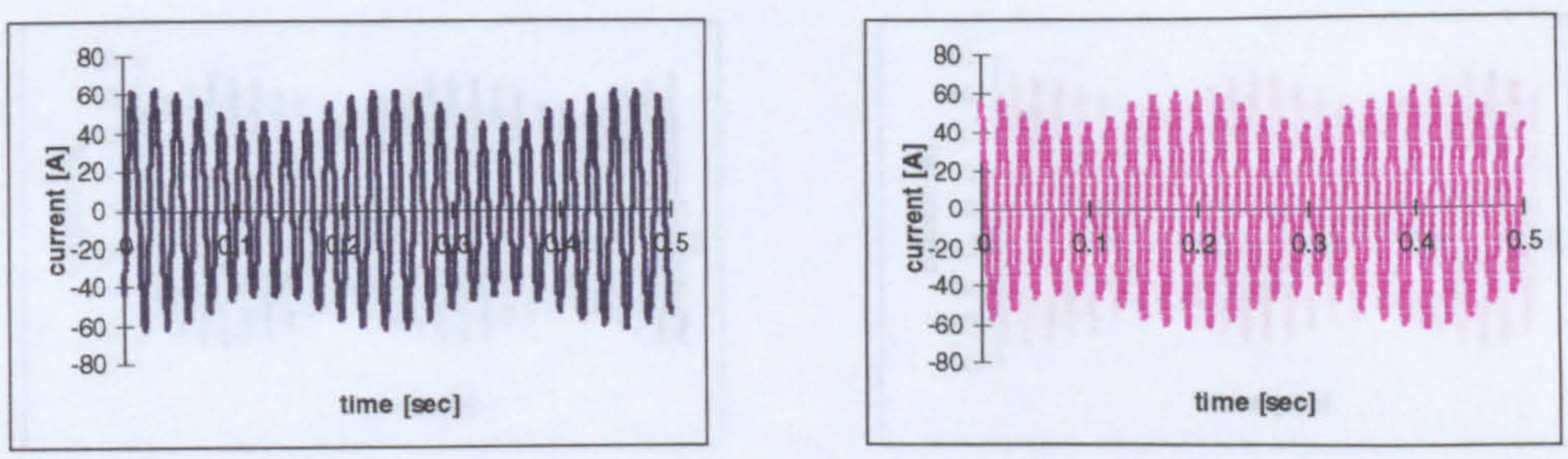

b) 4-3-0

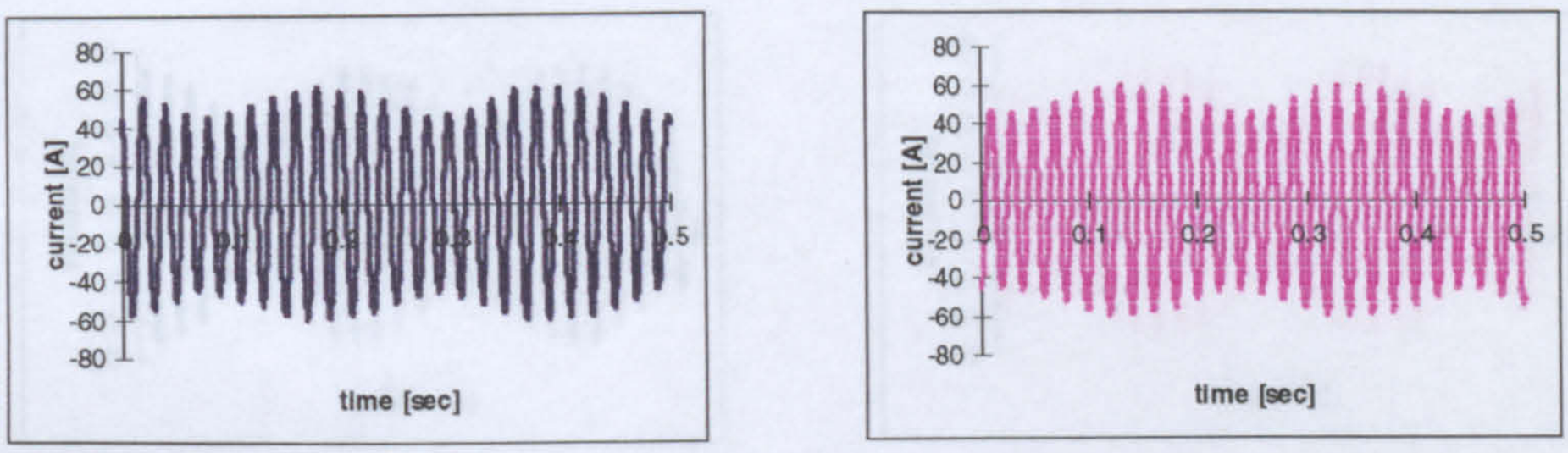

c) 5-2-0

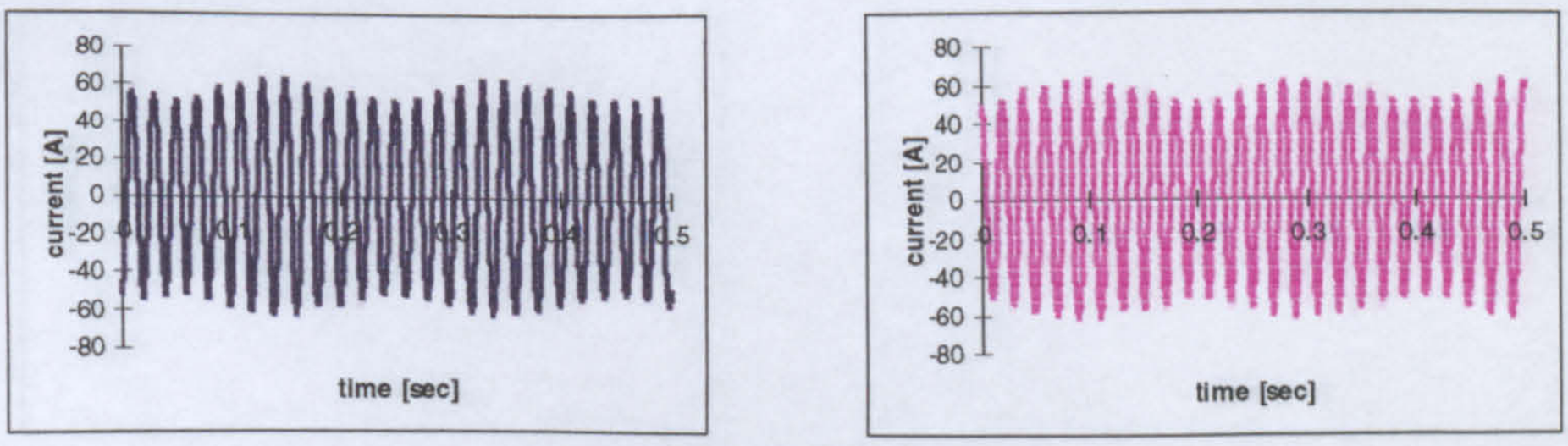

d) 7-0-0

Figure D.8 *Measured (left) and computed (right) stator current waveforms with seven adjacent broken bars for different relative positions*:

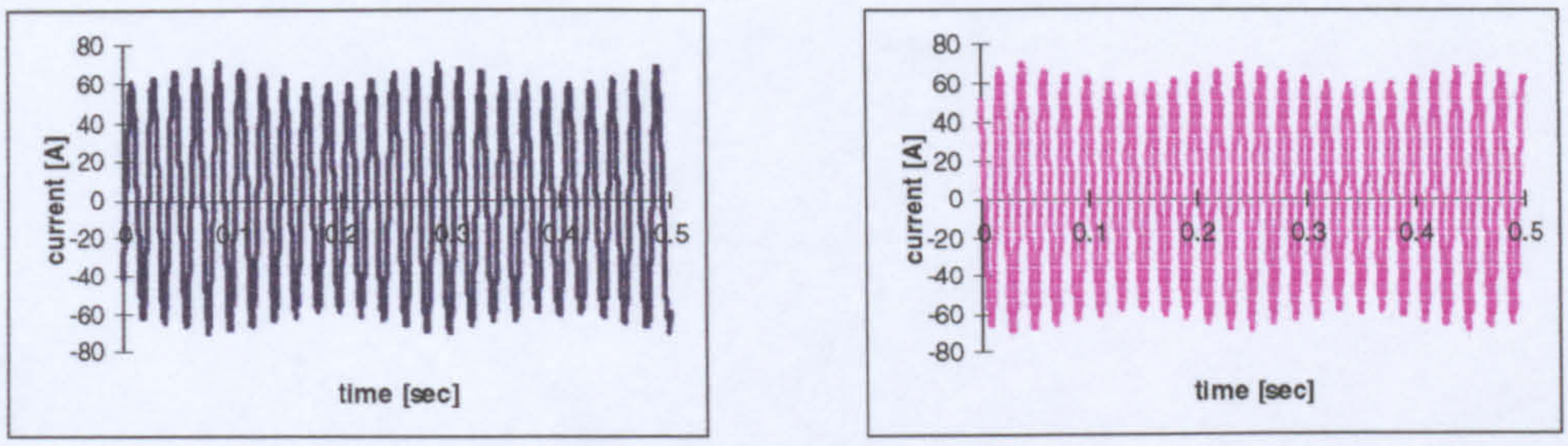

a) 1-1-1

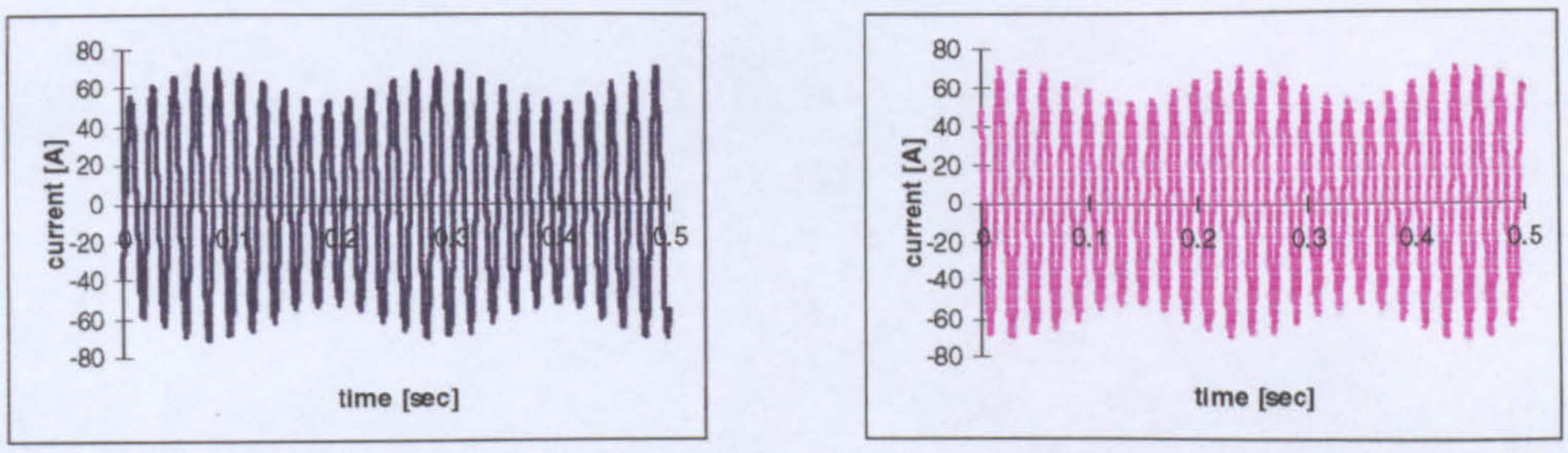

b) 2-2-2

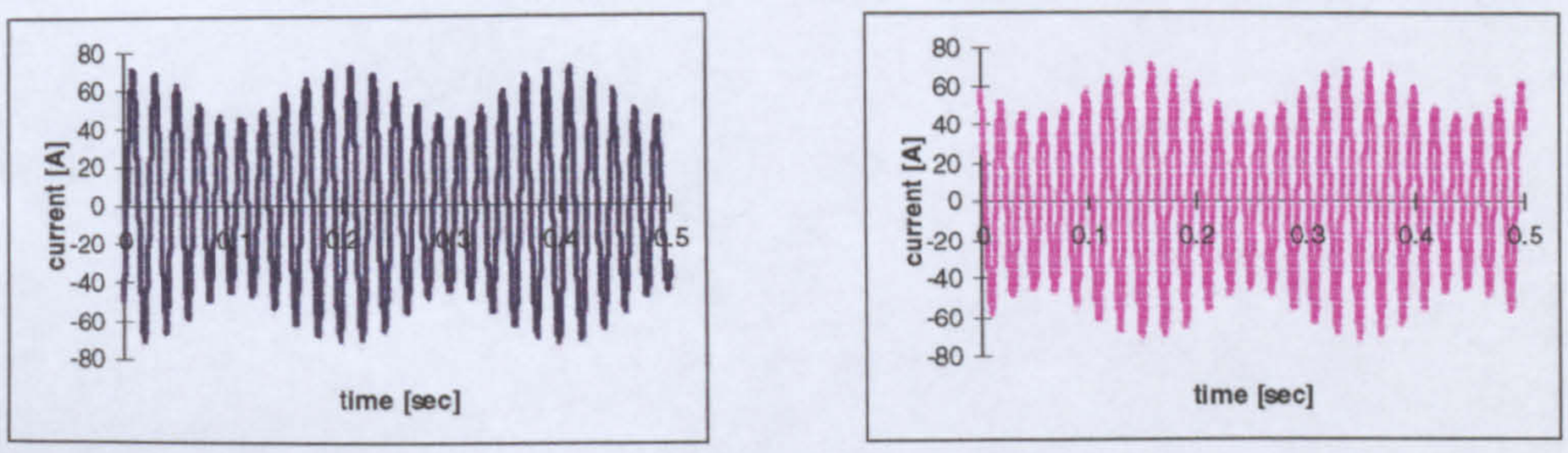

c) 3-3-3

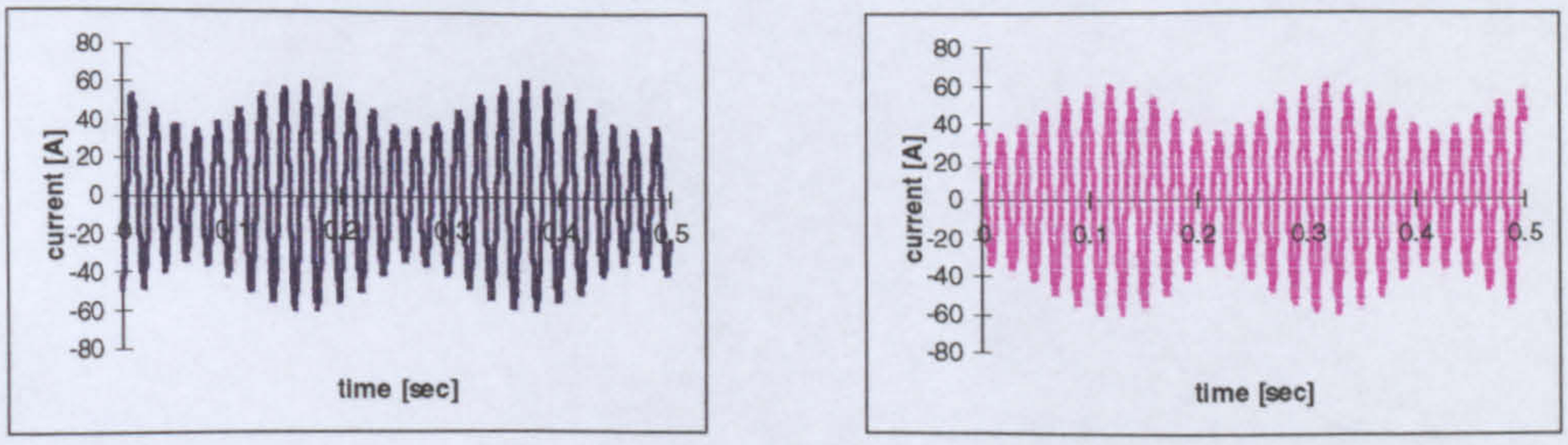

d) 4-4-4

Figure D.9 *Measured (left) and computed (right) stator current waveforms with one, two, three and four adjacent broken bars under each pole pair.*